POLITECNICO DI TORINO

Master’s Degree in Automotive Engineering

Geometric Definition of a New Electrical Cable Dashboard Layout

Supervisor:
Andrea TONOLI

Candidate:
Adem Berkay GENIS

Company Advisor:
Sabatino IANORA

ABSTRACT

The Cross-Car Beam (CCB) is one of the primary structural components of the automotive dashboard assembly, providing support for systems such as the steering column, HVAC unit, passenger airbag module, and electrical wiring harnesses. Conventional wiring harness layouts are generally routed externally around the Cross-Car Beam, which increases cable congestion and limits the available packaging volume within the dashboard region. As vehicle electrical systems become increasingly complex, improved packaging solutions are required to enhance space utilization and simplify harness integration.

This study proposes an internal wiring harness routing concept for the Cross-Car Beam by introducing routing openings within the beam structure and integrating cable guidance components, WAGO carrier mounting locations, and reinforcement structures. The objective of the proposed design is to improve packaging efficiency while maintaining acceptable structural and dynamic performance.

A three-dimensional CAD model of the proposed configuration was developed and evaluated using finite element analysis techniques. Three different configurations were investigated throughout the study: the original solid model, the optimized model containing routing openings, and the proposed model incorporating FeE420 reinforcement structures. Static structural analyses were performed under A-pillar loading and combined steering wheel, HVAC, and passenger airbag loading conditions. In addition, modal analyses were conducted to investigate the vibration characteristics and dynamic behavior of the three configurations.

The results demonstrated that the proposed internal routing concept significantly improved packaging capability and enabled more efficient utilization of the dashboard volume. Static analysis results indicated that the routing modifications did not introduce critical structural weaknesses under the investigated loading conditions. Although the routing openings reduced local stiffness and generated stress concentrations in the optimized configuration, the proposed reinforcement strategy effectively reduced tube stress levels and improved load distribution around the modified regions. Modal analysis results showed that the proposed model partially recovered the stiffness reduction caused by the routing openings while maintaining a more balanced strain energy distribution throughout the structure.

Overall, the proposed Cross-Car Beam design successfully achieved internal wiring harness integration while maintaining acceptable structural integrity and vibration performance. The developed design provides a practical solution for future automotive dashboard architectures requiring improved packaging efficiency and enhanced cable management capabilities.

Table of Contents

List of Abbreviations 5

List of Figures 6

List of Tables 11

Introduction 12

Chapter 1 – Cross-Car Beam Systems 13

1.1 Introduction to Cross-Car Beam Systems 13

Chapter 2 - Literature Review 15

2.1 Cross-Car Beam Systems in Automotive Design 15

2.2 Wiring Harness Routing Approaches 15

2.3 Packaging Optimization in Automotive Interiors 18

2.4 Finite Element Analysis in Automotive Engineering 21

Chapter 3 - Problem Definition 24

3.1 Limitations of Existing Design 24

3.2 Structural Optimization 30

3.3 Design Objectives and Engineering Requirements 35

3.4 Development of the Optimized Routing System 42

3.5 Cable Guide Processes and Harness Routing Configuration 48

3.6 Final Optimized Assembly Configuration 57

3.7 Air Duct – Cross-Car Beam Displacement, Area and, Volume Analysis 62

Chapter 4 - Materials and Methodology 69

4.1 Cad Modeling Procedure 69

4.2 Static Structural Preparation Crash Test (4000N) 80

4.3 Additional Crash Loading Scenarios (Steering Wheel, HVAC unit, Airbag Deployment) 84

4.4 Modal Analysis Preparation Processes 92

Chapter 5 - Results And Discussion 102

5.1 Static Structural Analysis Results 102

5.1.1 A-Pillar Loading Results (4000 N) 103

5.1.2 Additional Crash Loading Sceneroius Results (Steering Wheel, HVAC, Airbag Deployement) 119

5.2 Modal Analysis Results 129

5.2.1 Solid Model Modal Analysis Results 129

5.2.2 Optimized Model Modal Analysis Results 133

5.2.3 Proposed Model Modal Analysis Results 137

5.2.4 Comparison of Modal Analysis Results 141

Chapter 6 - Conclusions 143

6.1 Contributions of the Study 143

6.2 Recommendations for Future Work 144

REFERENCES 145

List of Abbreviations

DOF	**Degrees of Freedom**
HUD	**Head-up Display**
CAD	**Computer-Aided Design**
CAE	**Computer-Aided Engineering**
CCB	**Cross-Car Beam**
ECU	**Electronic Control Unit**
FEA	**Finite Element Analysis**
FEM	**Finite Element Method**
HVAC	**Heating, Ventilation and Air Conditioning**
Hz	**Hertz**
kg	**Kilogram**
MPa	**Megapascal**
mm	**Millimeter**
N	**Newton**
NVH	**Noise, Vibration and Harshness**
OEM	**Original Equipment Manufacturer**
RBE	**Rigid Body Element**
S&R	**Squeak and Rattle**

List of Figures

Figure 1.1 General Cross-Car Beam Structure 13
Figure 1.2 General Cross-Car Beam structure parts 14
Figure 1.3 Wiring harness routing layout inside the Cross-Car Beam 15
Figure 2.1 Wiring harness new layout 16
Figure 2.2 Wiring harness old layout 16
Figure 2.3 General Solution of Cross-Car Beam and wiring harness routing layout........ 17
Figure 2.4 Typical Dashboard wiring harness routing configuration 17
Figure 2.5 Conventional external wiring harness routing around the Cross-Car beam 18
Figure 2.6 Comparison between conventional and optimized packaging layouts 19
Figure 2.7 Internal wiring harness routing through the Cross-Car Beam 20
Figure 2.8 Isometric view of optimized packaging layout 20
Figure 2.9 Isometric view of Traditional packaging layout 21
Figure 2.10 Finite element mesh model of the Cross-Car Beam assembly 22
Figure 2.11 Von Mises contour obtained from finite element crash analysis 23
Figure 2.12 Modal analysis mode shapes of the Cross-Car Beam Structure 23
Figure 2.13 Modal analysis mode shapes of the Cross-Car Beam Structure 23
Figure 3.1 Conventional external wiring harness routing around the Cross-Car beam........ 25
Figure 3.2 Complex cable arrangement in the original dashboard configuration........ 25
Figure 3.3 Cross-Car Beam old version top-view four small openings........ 27
Figure 3.4 Cross-Car Beam old version isometric-view four small openings 27
Figure 3.5 Cross-Car Beam old version isometric-view four small openings 28
Figure 3.6 Cross-Car Beam new version front isometric-view four small openings........ 29
Figure 3.7 Cross-Car Beam new version back isometric-view four small openings 29
Figure 3.8 Cross-Car Beam new version sheet metal attached front isometric-view four openings........ 30
Figure 3.9 Cross-Car Beam new version sheet metal attached back isometric-view four openings 30
Figure 3.10 Packaging congestion caused by external harness routing in the original design 31
Figure 3.11 Internal routing and modular connector integration concept........ 32
Figure 3.12 Internal wiring harness routing through the hollow Cross-Car Beam structure........ 33
Figure 3.13 Cross-Car Beam proposed model sheet metal attached front isometric-view 34
Figure 3.14 Cross-Car Beam proposed model sheet metal attached back isometric-view........ 34
Figure 3.15 Cross-Car Beam proposed model sheet metal attached detailed view 35
Figure 3.16 Internal routing concept of the optimized Cross-Car Beam design 36
Figure 3.17 Modular connector integration and branch cable organization 36
Figure 3.18 Modular connector integration and branch cable organization 37
Figure 3.19 Modular connector integration and branch cable organization 1^{st} *opening* 37
Figure 3.20 Modular connector integration and branch cable organization second opening 38
Figure 3.21 Modular connector integration and branch cable organization third opening........ 38
Figure 3.22 Modular connector integration and branch cable organization fourth opening 39
Figure 3.23 Wago model re-pin de-pin type assembly of connectors 40
Figure 3.24 Wago model re-pin de-pin type connectors and cable layout........ 40
Figure 3.25 Reinforcement plate attached on opening........ 41
Figure 3.26 Cable Guide for routing main cable through the inside of the Cross-Car Beam 43
F Figure 3.27 Clip mechanisms for routing easily cable........ 43
Figure 3.28 Wago type connector system 43
Figure 3.29 Reinforcement plate made by sheet metal 44
Figure 3.30 Old solution for making connect main cables 45
Figure 3.31 New solution for making connect main cables........ 45
Figure 3.32 Wago carrier and clip mechanisms layout for routing cable management 46
Figure 3.33 Comparison between old and new layout........ 47
Figure 3.34 Cable guidance and rail system........ 48
Figure 3.35 Cable guidance – rail system and cable layout 48

Figure 3.36 Cable guidance – ground rubber support system layout 49
Figure 3.37 Ground rubber support system 49
Figure 3.38 Reinforcement plate structure 50
Figure 3.39 The hook for engaging with Wago carrier 50
Figure 3.40 Assembly of Wago carrier, hook and reinforcement plate structure 50
Figure 3.41 Wago distribution 51
Figure 3.42 Wago male connector 51
Figure 3.43 Wago female connector 51
Figure 3.44 Detailed view while making connection 53
Figure 3.45 Wago-mini distribution 54
Figure 3.46 Wago-mini male connector 54
Figure 3.47 Wago-mini female connector 54
Figure 3.48 New cable guidance general layout 55
Figure 3.49 New cable guidance layout 55
Figure 3.50 New plastic hook supporter 55
Figure 3.51 First Wago-mini carrier assembly detailed view 56
Figure 3.52 First Wago-mini carrier assembly with locking cap detailed view 56
Figure 3.53 Second Wago-mini carrier assembly detailed view 56
Figure 3.54 Third and fourth Wago-mini carrier assembly detailed view 57
Figure 3.55 Cross-Car Beam structure and new cable guidance layout iso-view 58
Figure 3.56 Cross-Car Beam structure and new cable guidance layout front-view 59
Figure 3.57 Cross-Car Beam structure and new cable guidance layout back-view 59
Figure 3.58 First Wago-mini connector detailed view 60
Figure 3.59 Second Wago-mini connector detailed view 60
Figure 3.60 Third Wago-mini connector detailed view 61
Figure 3.61 Fourth Wago-mini connector detailed view 61
Figure 3.62 Airduct, Cross-Car Beam Structure of solid model 62
Figure 3.63 Airduct, Cross-Car Beam Structure of optimized model 62
Figure 3.64 Airduct, Cross-Car Beam displacement of optimized model 63
Figure 3.65 Airduct, Cross-Car Beam displacement of solid model 63
Figure 3.66 Airduct, Cross-Car Beam displacement of optimized model 64
Figure 3.67 Airduct, Cross-Car Beam displacement of solid model 64
Figure 3.68 Airduct, Cross-Car Beam displacement of optimized model 65
Figure 3.69 Airduct, Cross-Car Beam displacement of solid model 65
Figure 3.70 Airduct, Cross-Car Beam displacement of solid model 66
Figure 3.71 Airduct, Cross-Car Beam displacement of solid model 66
Figure 3.72 Airduct, Cross-Car Beam the area of optimized model 67
Figure 3.73 Airduct, Cross-Car Beam the area of solid model 67
Figure 3.74 Airduct, Cross-Car Beam the area of optimized model 68
Figure 3.75 Airduct, Cross-Car Beam the area of solid model 68
Figure 4.1 Original solid Cross-Car Beam model used as the reference configuration 69
Figure 4.2 Optimized Cross-Car Beam model with routing openings for internal harness integration 70
Figure 4.3 Proposed Cross-Car Beam model with FeE420 reinforcement structure plates 70
Figure 4.4 Geometry simplification process applied on solid Cross-Car Beam model 71
Figure 4.5 Geometry simplification process applied on optimized Cross-Car Beam model 72
Figure 4.6 Geometry simplification process applied on proposed Cross-Car Beam model 72
Figure 4.7 Mesh-Mating operations on solid Cross-Car Beam model 73
Figure 4.8 Mesh-Mating operations on optimized Cross-Car Beam model 73
Figure 4.9 Mesh-Mating operations on proposed Cross-Car Beam model 74
Figure 4.10 Finite element mesh generated for solid Cross-Car Beam model 74
Figure 4.11 Finite element mesh generated for optimized Cross-Car Beam model 75
Figure 4.12 Finite element mesh generated for proposed Cross-Car Beam model 75
Figure 4.13 Finite element mesh generated for proposed Cross-Car Beam model 76

Figure 4.14 Material Assignment for solid Cross-Car Beam model (FeE340) Yield Strength 340 MPa 76
Figure 4.15 Material Assignment for solid Cross-Car Beam model (FeE420) Yield Strength 420 MPa 77
Figure 4.16 Material Assignment for optimized Cross-Car Beam model (FeE340) Yield Strength 340 MPa 77
Figure 4.17 Material Assignment for optimized Cross-Car Beam model (FeE420) Yield Strength 420 MPa 78
Figure 4.18 Material Assignment for proposed Cross-Car Beam model (FeE340) Yield Strength 340 MPa 78
Figure 4.19 Material Assignment for proposed Cross-Car Beam model (FeE420) Yield Strength 420 MPa 79
Figure 4.20 Material Assignment for proposed Cross-Car Beam model (FeE420) Yield Strength 420 MPa 79
Figure 4.21 RBE 3 configurations (pink) applied on solid Cross-Car Beam model 450mm distance from A-pillar 80
Figure 4.22 RBE 3 configurations (yellow) applied on optimized Cross-Car Beam model 450mm distance from A-pillar 80
Figure 4.23 RBE 3 configurations (orange) applied on proposed Cross-Car Beam model 450mm distance from A-pillar 81
Figure 4.24 4000 N applied on node by using RBE 3 connections on solid Cross-Car Beam model 82
Figure 4.25 4000 N applied on node by using RBE 3 connections on optimized Cross-Car Beam model 82
Figure 4.26 4000 N applied on node by using RBE 3 connections on proposed Cross-Car Beam model 82
Figure 4.27 Constraints are applied to the solid Cross-Car Beam marked as orange 83
Figure 4.28 Constraints are applied to the optimized Cross-Car Beam marked as orange 83
Figure 4.29 Constraints are applied to the proposed Cross-Car Beam marked as orange 84
Figure 4.30 RBE 2 applied for the Steering wheel column on solid Cross-Car Beam model 85
Figure 4.31 RBE 2 applied for the Steering wheel column on optimized Cross-Car Beam model 86
Figure 4.32 RBE 2 applied for the Steering wheel column on proposed Cross-Car Beam model 86
Figure 4.33 RBE 2 applied for the HVAC unit on solid Cross-Car Beam model marked as orange 87
Figure 4.34 RBE 2 applied for the HVAC unit on optimized Cross-Car Beam model marked as orange 87
Figure 4.35 RBE 2 applied for the HVAC unit on proposed Cross-Car Beam model marked as orange 88
Figure 4.36 RBE 2 applied for the Airbag unit on solid Cross-Car Beam model marked as orange 88
Figure 4.37 RBE 2 applied for the Airbag unit on optimized Cross-Car Beam model marked as orange 89
Figure 4.38 RBE 2 applied for the Airbag unit on proposed Cross-Car Beam model marked as orange 89
Figure 4.39 shows the forces applied on solid Cross-Car Beam model marked as orange 90
Figure 4.40 shows the forces applied on optimized Cross-Car Beam model marked as orange 90
Figure 4.41 shows the forces applied on proposed Cross-Car Beam model marked as orange 91
Figure 4.42 shows the constraints applied on solid Cross-Car Beam model marked as orange 91
Figure 4.43 shows the constraints applied on optimized Cross-Car Beam model marked as orange 92
Figure 4.44 shows the constraints applied on proposed Cross-Car Beam model marked as orange 92
Figure 4.45 Finite element mesh generated for the solid CCB model 93
Figure 4.46 Finite element mesh generated for the optimized CCB model 93
Figure 4.47 Finite element mesh generated for the proposed CCB model 94
Figure 4.48 Glue connections and mesh mating definitions applied to the solid CCB model marked as yellow 94
Figure 4.49 Glue connections and mesh mating definitions applied to the optimized CCB model marked as yellow 95
Figure 4.50 Glue connections and mesh mating definitions applied to the proposed CCB model marked as yellow 95
Figure 4.51 Refined mesh around routing openings and reinforcement structures 96
Figure 4.52 Material Assignment for solid Cross-Car Beam model (FeE420) Yield Strength 420 MPa............. 96
Figure 4.53 Material Assignment for solid Cross-Car Beam model (FeE340) Yield Strength 340 MPa............. 96
Figure 4.54 Material Assignment for optimized Cross-Car Beam model (FeE420) Yield Strength 420 MPa 97
Figure 4.55 Material Assignment for optimized Cross-Car Beam model (FeE340) Yield Strength 340 MPa 97
Figure 4.56 Material Assignment for proposed Cross-Car Beam model (FeE420) Yield Strength 420 MPa 97
Figure 4.57 Material Assignment for proposed Cross-Car Beam model (FeE340) Yield Strength 340 MPa 98
Figure 4.58 Material Assignment for proposed Cross-Car Beam model (FeE420) Yield Strength 420 MPa 98
Figure 4.59 Location of the 8 kg concentrated mass (CM) used in the solid CCB model 98
Figure 4.60 Location of the 8 kg concentrated mass (CM) used in the optimized CCB model.......................... 99

Figure 4.61 Location of the 8 kg concentrated mass (CM) used in the proposed CCB model 99
Figure 4.62 Boundary conditions applied to the solid CCB model 100
Figure 4.63 Boundary conditions applied to the optimized CCB model 100
Figure 4.64 Boundary conditions applied to the proposed CCB model 100
Figure 4.65 Final finite element model prepared for modal frequency extraction 8 modes are requested ... 101
Figure 4.66 Example of the result of model analysis of the first mode 101
Figure 4.67 Strain energy distribution obtained from modal analysis 102
Figure 5.1 Max displacement of solid CCB model (front-iso view) 104
Figure 5.2 Max displacement of solid CCB model (back-iso view) 104
Figure 5.3 Max displacement occurs A-pillar corner (detailed-view) 105
Figure 5.4 Max displacement of optimized CCB model (front-iso view) 106
Figure 5.5 Max displacement of optimized CCB model (back-iso view) 106
Figure 5.6 Max displacement occurs A-pillar corner (detailed-view) 107
Figure 5.7 Max displacement of proposed CCB model (front-iso view) 108
Figure 5.8 Max displacement of proposed CCB model (back-iso view) 108
Figure 5.9 Von Mises Stress distribution of the solid CCB model (front-iso view) 109
Figure 5.10 Von Mises Stress distribution of the solid CCB model (back-iso view) 110
Figure 5.11 Von Mises Stress distribution of the solid CCB model (detailed view) 110
Figure 5.12 Von Mises Stress distribution of the optimized CCB model (front-iso view) 111
Figure 5.13 Von Mises Stress distribution of the optimized CCB model (back-iso view) 112
Figure 5.14 Von Mises Stress distribution of the optimized CCB model (detailed view) 112
Figure 5.15 Von Mises Stress distribution of the proposed CCB model (front-iso view) 113
Figure 5.16 Von Mises Stress distribution of the proposed CCB model (back-iso view) 114
Figure 5.17 Von Mises Stress distribution of the proposed CCB model (detailed view) 114
Figure 5.18 Local tube Displacement of the solid CCB model 115
Figure 5.19 Local tube Von Mises stress of the solid CCB model 116
Figure 5.20 Local tube Displacement of the optimized CCB model 116
Figure 5.21 Local tube Von Mises stress of the optimized CCB model 117
Figure 5.22 Comparison of local tubes solid – optimized CCB model 117
Figure 5.23 Local tube Displacement of the proposed CCB model 118
Figure 5.24 Local tube Von Mises stress of the proposed CCB model 118
Figure 5.25 Total deformation of the solid CCB model 119
Figure 5.26 Total deformation of the optimized CCB model 120
Figure 5.27 Total deformation of the proposed CCB model 120
Figure 5.28 Von Mises stress distribution of the solid CCB model 122
Figure 5.29 Von Mises stress distribution of the optimized CCB model 122
Figure 5.30 Von Mises stress distribution of the proposed CCB model 123
Figure 5.31 Local tube deformation of the solid CCB model 125
Figure 5.32 Local tube Von mises stress distribution of the solid CCB model 125
Figure 5.33 Local tube deformation of the optimized CCB model 126
Figure 5.34 Local tube Von mises stress distribution of the optimized CCB model 127
Figure 5.35 Local tube deformation of the proposed CCB model 127
Figure 5.36 Local tube Von mises stress distribution of the proposed CCB model 128
Figure 5.37 Local tube Von mises stress distribution of the proposed CCB model detailed view 128
Figure 5.38 First vibration mode shape of the solid CCB model 130
Figure 5.39 Strain energy distribution of mode 1 for the solid CCB model 131
Figure 5.40 Second vibration mode shape of the solid CCB model 131
Figure 5.41 Strain energy distribution of mode 2 for the solid CCB model 132
Figure 5.42 Third vibration mode shape of the solid CCB model 132
Figure 5.43 Strain energy distribution of mode 3 for the solid CCB model 133
Figure 5.44 First vibration mode shape of the optimized CCB model 134
Figure 5.45 Strain energy distribution of mode 1 for the optimized CCB model 135
Figure 5.46 Second vibration mode shape of the optimized CCB model 135

Figure 5.47 Strain energy distribution of mode 2 for the optimized CCB model 136
Figure 5.48 Third vibration mode shape of the optimized CCB model 136
Figure 5.49 Strain energy distribution of mode 3 for the optimized CCB model 137
Figure 5.50 First vibration mode shape of the proposed CCB model 138
Figure 5.51 Strain energy distribution of mode 1 for the proposed CCB model 139
Figure 5.52 Second vibration mode shape of the proposed CCB model 139
Figure 5.53 Strain energy distribution of mode 2 for the proposed CCB model 140
Figure 5.54 Third vibration mode shape of the proposed CCB model 140
Figure 5.55 Strain energy distribution of mode 3 for the proposed CCB model 141

List of Tables

Table 3-1 Comparison of the displacement between Airduct – Cross Car Beam at the solid and optimized model ... 66
Table 3-2 Comparison of the area and volume between Airduct – Cross-Car Beam at the solid and optimized model ... 68
Table 5-1 Maximum and minimum displacements and stress points of the solid CCB model ... 105
Table 5-2 Maximum and minimum displacements and stress points of the optimized CCB model ... 107
Table 5-3 Maximum displacements comparison of three model and stress points of the proposed CCB model ... 109
Table 5-4 Von Mises stress points and materials of the solid CCB model ... 111
Table 5-5 Von Mises stress points and materials of the optimized CCB model ... 113
Table 5-6 Von Mises stress points and materials of the proposed CCB model ... 115
Table 5-7 General Comparison of three models (Displacement, Stress) ... 119
Table 5-8 Results table of the solid CCB model ... 121
Table 5-9 Results and comparison table of the solid - optimized CCB model ... 121
Table 5-10 Results table of the proposed CCB model ... 121
Table 5-11 Von mises stress results table of the solid CCB model ... 124
Table 5-12 Von mises stress results table of the optimized CCB model ... 124
Table 5-13 Von mises stress results table of the proposed CCB model ... 124
Table 5-14 Local tube Von Mises stress distribution and deformation results of the solid CCB model ... 126
Table 5-15 Local tube Von mises stress distribution and deformation results of the optimized CCB model 127
Table 5-16 Local tube Von mises stress distribution and deformation results of the proposed CCB model 129
Table 5-17 Natural Frequencies and Strain Energy values of the solid CCB model ... 130
Table 5-18 Natural Frequencies and Strain Energy values of the optimized CCB model ... 134
Table 5-19 Natural Frequencies and Strain Energy values of the proposed CCB model ... 137
Table 5-20 Natural Frequencies and Strain Energy values of the proposed CCB model ... 141
Table 5-21 Comparison of Strain Energy Values ... 142

Introduction

This research and development project was conducted within the engineering department of **TecnoCad Group**, a premier global partner in the automotive and commercial vehicle sectors. Founded in 1986 in Turin, Italy, TecnoCad is a cornerstone of the Piedmontese "Automotive Valley." Headquartered in the historic Mirafiori district, the company specializes in "Tecneering" a unique synergy between creative styling and rigorous mechanical engineering. Operating out of the renowned "Manta22" hub, TecnoCad manages the entire vehicle development lifecycle. This thesis applies TecnoCad’s industry-leading methodologies in packaging and structural optimization to the integration of the Cross Car Beam (CCB) and vehicle wiring systems.
In contemporary vehicle architecture, the cockpit module has transitioned from a basic structural interface into a high-density hub of electronic systems and safety technologies. At the center of this assembly is the **Cross Car Beam (CCB)**. Historically, the CCB functioned as a purely structural component, spanning the A-pillars to provide lateral stiffness and a mounting platform for the steering column.
However, modern consumer trends toward "Digital Cockpits" incorporating Head-Up Displays (HUD), expansive infotainment screens, and complex climate control units have made the packaging space behind the dashboard a premium commodity. The **wiring harness**, a bulky network of power and data cables, is a major contributor to this spatial congestion. Traditionally, these harnesses are routed externally along the CCB, which occupies critical volume and complicates the overall assembly process.
Standard external wiring harness layouts present several engineering and manufacturing challenges:
Spatial Inefficiency: External routing limits the available volume for larger HVAC units or advanced safety modules.
Assembly Complexity: The requirement for numerous external fasteners and clips increases manual labor time and the risk of mis-installation.
Physical Vulnerability: Cables mounted on the exterior of structural beams are more susceptible to pinching, heat exposure, and mechanical damage during the vehicle's lifecycle.

Weight Constraints: The additional brackets and protective cladding required for external routing add parasitic weight, contradicting modern lightweighting goals.

This research demonstrates that by utilizing **sheet metal reinforcement** around structural cut-outs, engineers can achieve significant packaging gains up to **40mm on the steering side** without compromising safety. The final design achieves a 71% reduction in strain energy for critical vibration modes compared to the baseline, providing a blueprint for more durable, lightweight, and space-efficient vehicle interiors

Chapter 1 – Cross-Car Beam Systems

1.1 Introduction to Cross-Car Beam Systems

The Cross-Car Beam (CCB) is one of the most important structural components located inside the dashboard system of modern vehicles. It extends across the width of the vehicle and connects the A-pillars, providing structural rigidity and support for several interior subsystems. The CCB acts as the primary support structure for the steering column, dashboard assembly, HVAC unit, passenger airbag module, infotainment system, and electrical wiring harnesses.

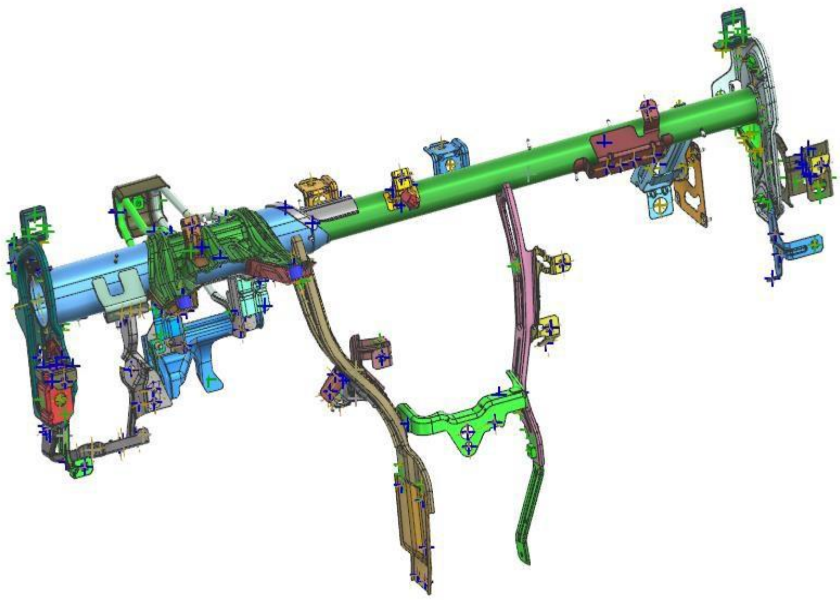

Figure 1.1 General Cross-Car Beam Structure

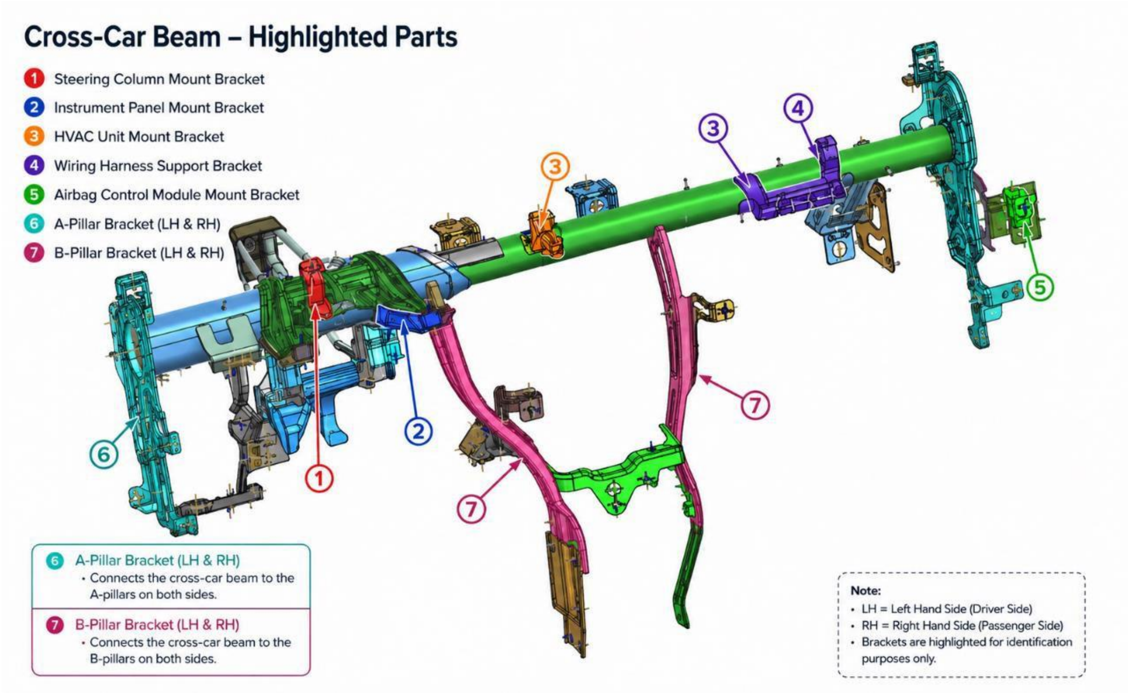

Figure 1.2 General Cross-Car Beam structure parts

Due to the increasing complexity of electrical systems in modern vehicles, especially electric vehicles, efficient integration of wiring harnesses inside the dashboard has become a major engineering challenge.

In conventional vehicle architectures, wiring harnesses are generally routed externally around the cross-car beam structure. However, this routing strategy causes several disadvantages, including reduced packaging space, cable congestion, increased assembly complexity, vibration-related wear, and difficult maintenance operations. As vehicle interior systems continue to grow in complexity, the need for optimized wiring harness integration has become increasingly important.

This thesis focuses on the optimization of wiring harness routing through the hollow section of the Cross-Car Beam. The proposed design aims to improve packaging efficiency, increase available dashboard space, reduce cable complexity, improve serviceability, and maintain structural integrity under crash and vibration loading conditions.

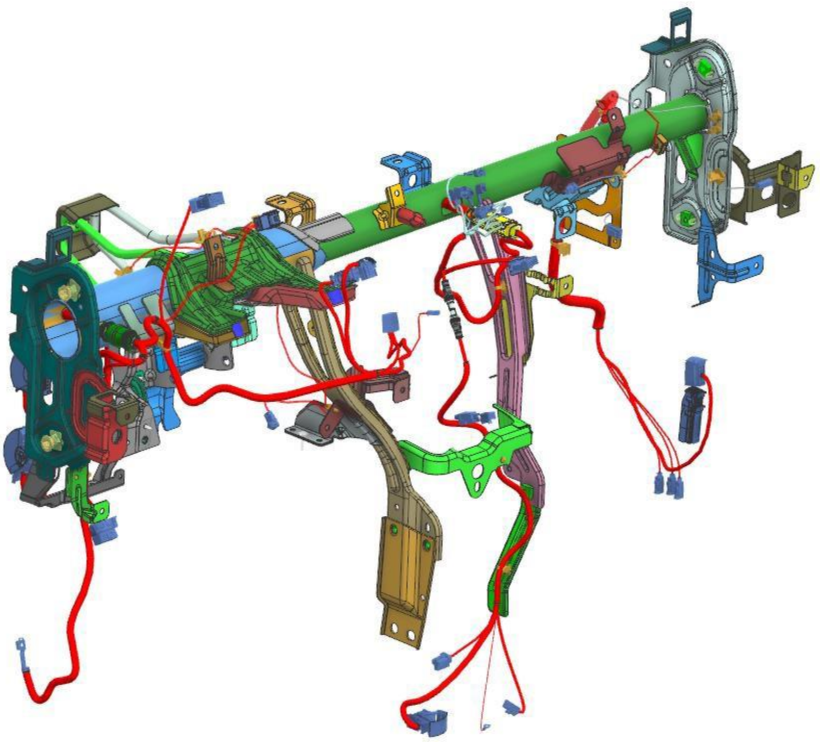

Figure 1.3 Wiring harness routing layout inside the Cross-Car Beam

Chapter 2 - Literature Review

2.1 Cross-Car Beam Systems in Automotive Design

Cross-Car Beam systems are widely used in modern automotive dashboard structures due to their ability to provide structural support while integrating multiple vehicle subsystems. The CCB distributes loads between the A-pillars and acts as the backbone of the dashboard assembly. Previous studies have shown that the CCB significantly contributes to steering column stability, passenger safety, and vibration control within the dashboard region.

Traditional Cross-Car Beam structures are manufactured using tubular steel or sheet metal assemblies due to their high stiffness-to-weight ratio. The beam must simultaneously satisfy packaging, safety, manufacturability, and NVH (Noise, Vibration, and Harshness) requirements.

2.2 Wiring Harness Routing Approaches

Wiring harness systems are responsible for distributing electrical power and communication signals between vehicle components. Conventional harness routing strategies generally position the harness externally around the Cross-Car Beam using clips, clamps, and brackets.

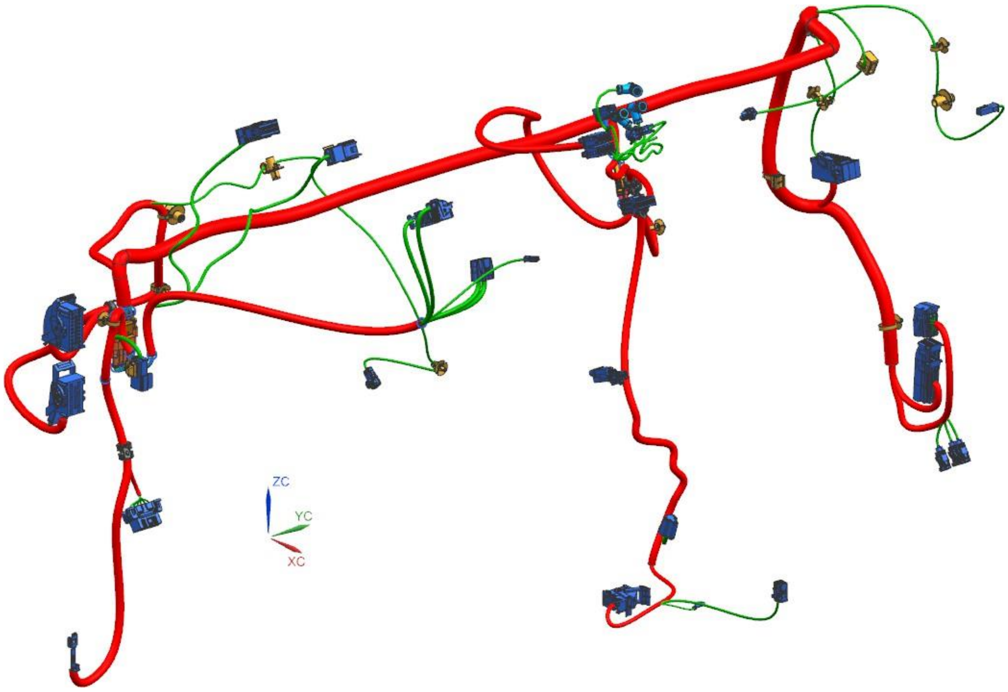

Figure 2.1 Wiring harness new layout

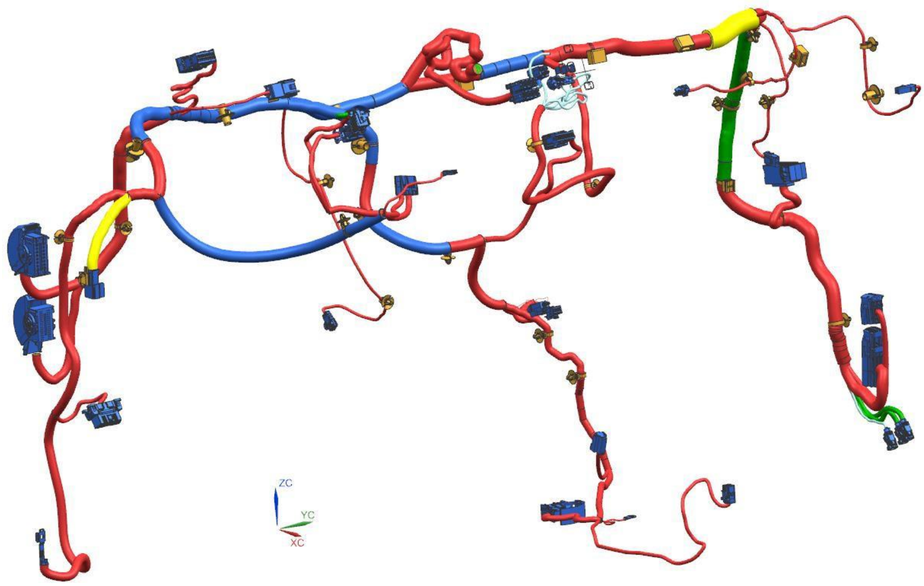

Figure 2.2 Wiring harness old layout

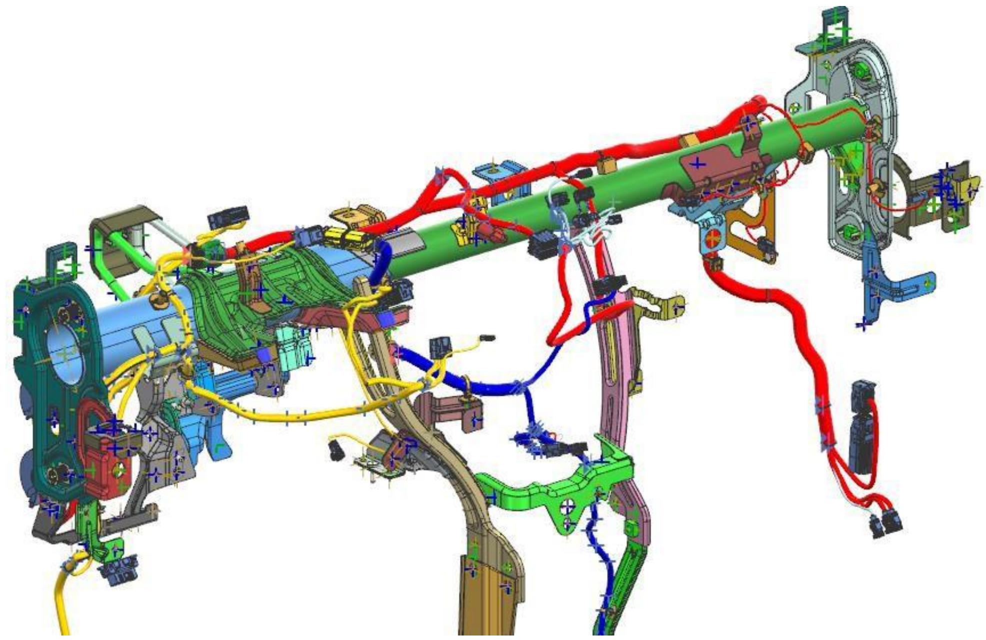

Figure 2.3 General Solution of Cross-Car Beam and wiring harness routing layout

Although this approach simplifies initial assembly, it creates several disadvantages related to packaging efficiency and cable protection.

External routing methods increase dashboard congestion and expose the harness to vibration, sharp edges, and thermal sources. In addition, larger wiring systems required in electric vehicles significantly increase routing complexity. Therefore, modular routing concepts and internal beam routing methods have become important research topics in recent automotive development.

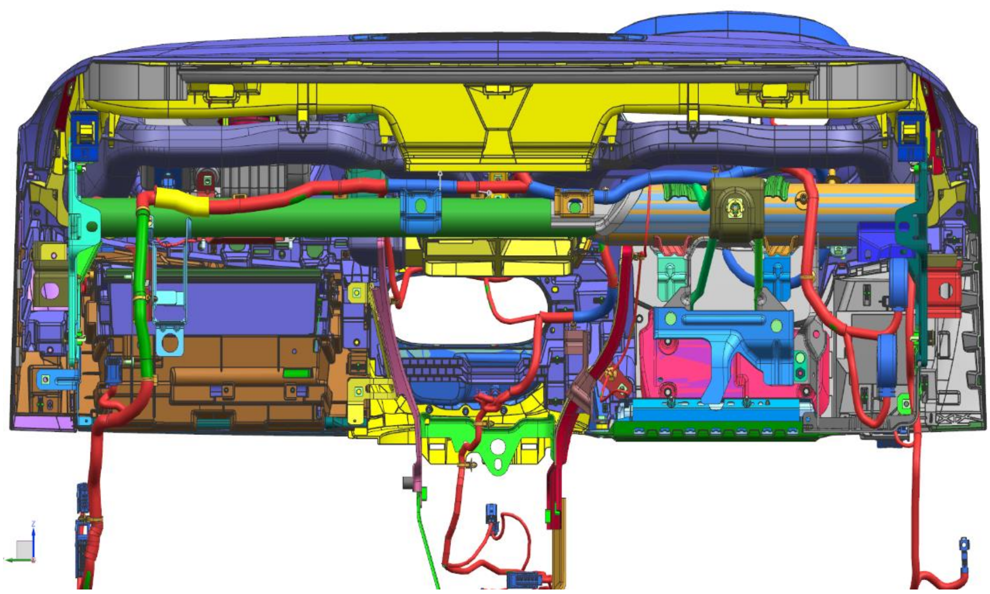

Figure 2.4 Typical Dashboard wiring harness routing configuration

2.3 Packaging Optimization in Automotive Interiors

Packaging optimization is one of the most critical engineering objectives in modern automotive interior design. As vehicle technologies continue to evolve, especially in electric and hybrid vehicles, the number of electronic systems integrated within the dashboard area has significantly increased [6][7].
The dashboard region is considered one of the most congested areas of a vehicle because it contains both structural and electrical subsystems simultaneously. Components such as infotainment systems, HVAC modules, airbags, wiring harnesses, and electronic control units must all be integrated into a limited packaging volume while maintaining passenger comfort and manufacturability [6].
Traditional wiring harness routing methods generally position cable bundles externally around the Cross-Car Beam structure using clips and brackets. Although this approach simplifies assembly accessibility, it occupies considerable dashboard space and increases cable congestion [8].

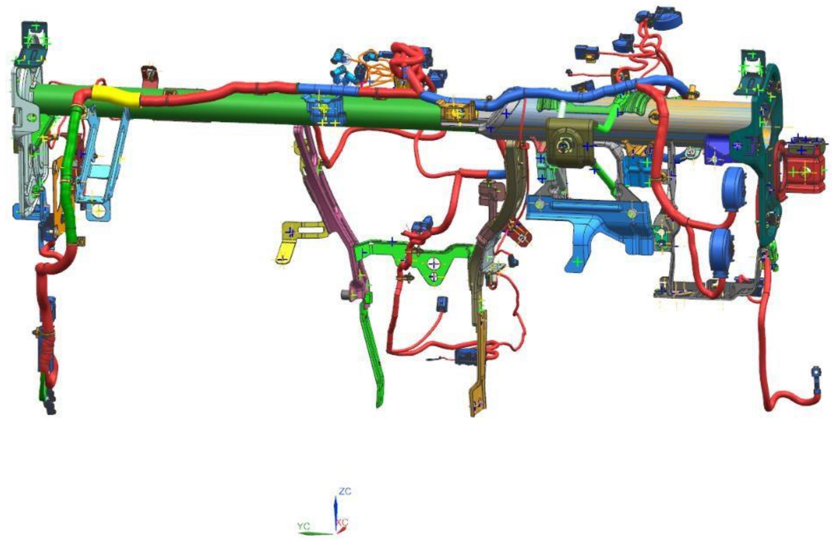

Figure 2.5 Conventional external wiring harness routing around the Cross-Car beam

Externally routed harnesses are also more vulnerable to vibration-induced wear, thermal exposure, and mechanical interaction with surrounding components. These factors may negatively affect durability and long-term reliability of the electrical system [8][9].
In recent automotive engineering studies, internal routing strategies have gained increasing attention due to their ability to improve packaging efficiency and simplify dashboard architecture. Routing the main wiring harness through the hollow section of the Cross-Car Beam allows engineers to utilize previously unused internal structural volume [7].

The increase in available packaging space provides several engineering advantages. Larger HVAC ducts can be integrated into the dashboard system, which improves airflow efficiency and reduces aero-acoustic noise within the cabin [9]. In addition, the freed packaging volume allows integration of larger infotainment systems and electronic modules without increasing overall dashboard dimensions [6].

Figure 2.6 Comparison between conventional and optimized packaging layouts

Another important advantage of packaging optimization is the improvement of assembly and serviceability processes. Modular routing concepts reduce cable complexity and allow independent disconnection of harness branches during maintenance operations [8].
From a structural perspective, packaging optimization must be carefully balanced with mechanical integrity. Introducing routing openings into the Cross-Car Beam may reduce local stiffness and create stress concentration regions. Therefore, reinforcement strategies are required to maintain crashworthiness while achieving packaging improvements.

In this study, packaging optimization is achieved by relocating the primary wiring harness inside the hollow Cross-Car Beam structure while using modular connectors and cable guide systems for branch integration. This approach improves dashboard space utilization, assembly flexibility, and cable protection simultaneously.

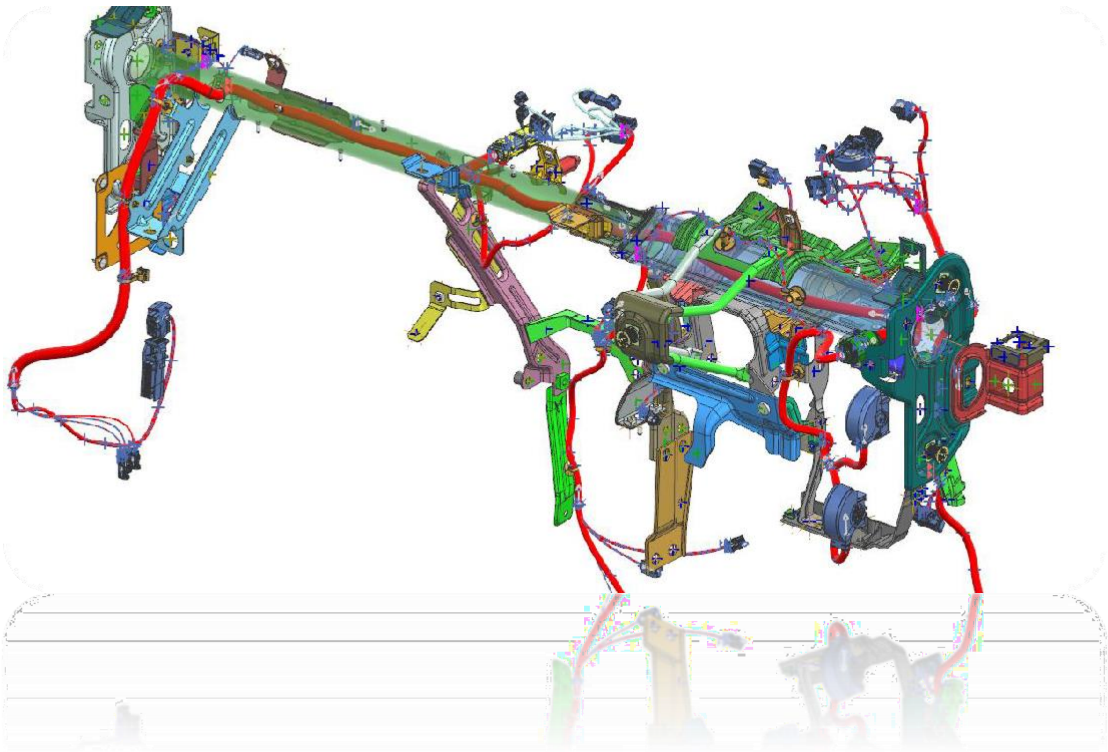

Figure 2.7 Internal wiring harness routing through the Cross-Car Beam

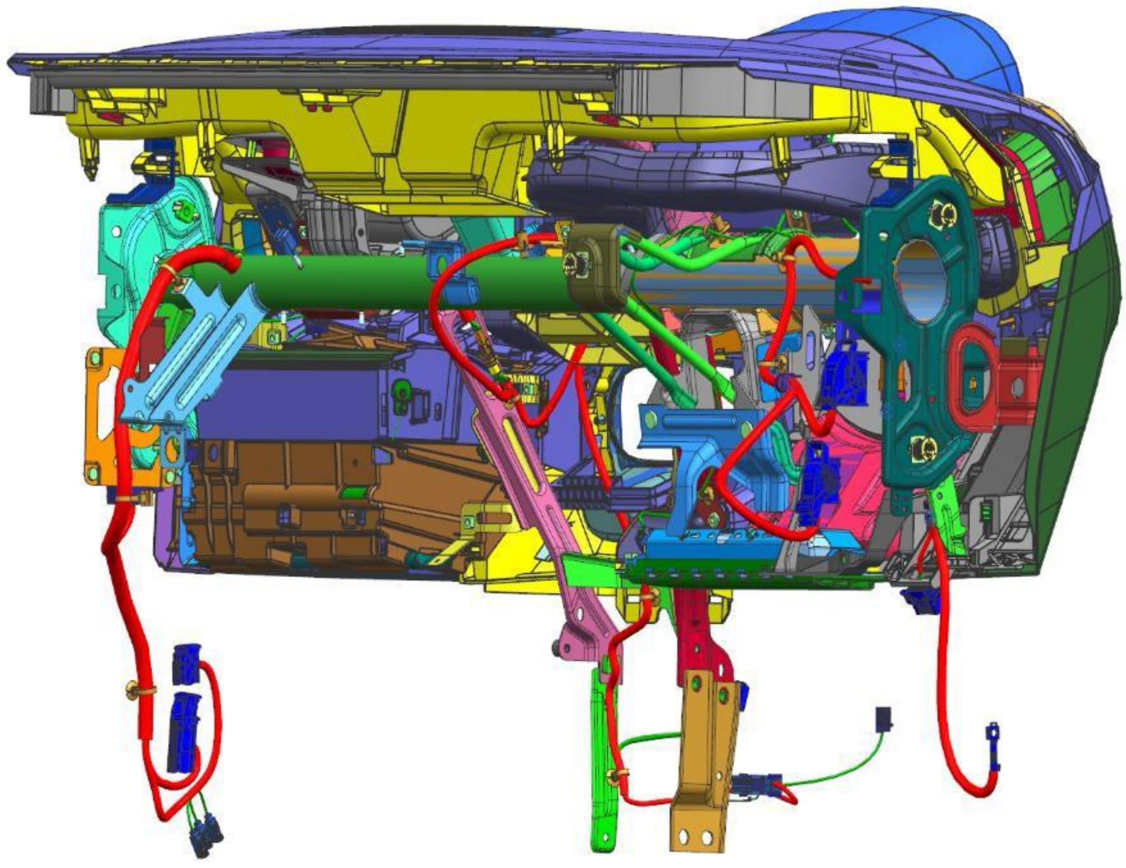

Figure 2.8 Isometric view of optimized packaging layout

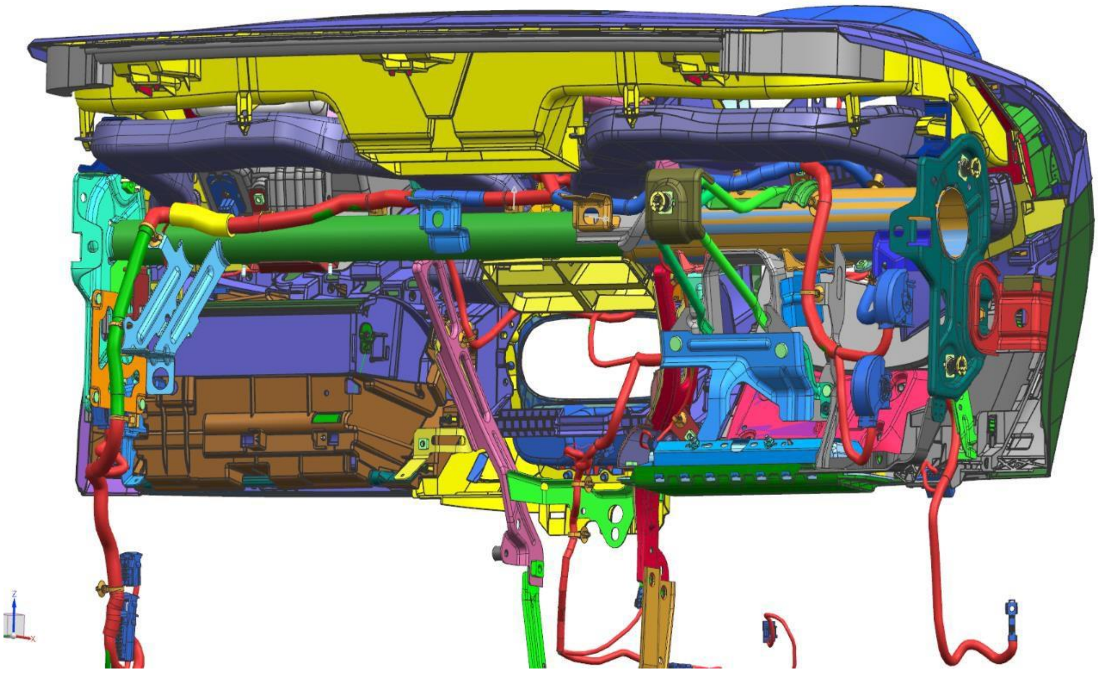

Figure 2.9 Isometric view of Traditional packaging layout

2.4 Finite Element Analysis in Automotive Engineering

Finite Element Analysis (FEA) is a numerical simulation method widely used in modern engineering to predict the structural, thermal, and dynamic behavior of components under different loading conditions [1][2]. The method is based on dividing a complex geometry into smaller interconnected elements, which are mathematically analyzed to approximate the behavior of the entire structure [1]. In automotive engineering, Finite Element Analysis has become one of the most important tools during the design and optimization stages of vehicle development. The automotive industry continuously demands lighter, safer, and more efficient vehicle structures while simultaneously reducing development time and manufacturing costs [3]. As a result, FEA allows engineers to evaluate multiple design concepts virtually before manufacturing physical prototypes. One of the major advantages of Finite Element Analysis is its ability to predict the behavior of complex structures under realistic operating conditions. Automotive components are subjected to static loads, vibration loads, thermal effects, fatigue loading, and crash impact forces during vehicle operation [2][3]. Performing physical tests for every design iteration would require significant time and financial resources. Therefore, numerical simulation methods provide a faster and more economical approach for evaluating structural performance. Finite Element Analysis is extensively used in many automotive applications, including chassis systems, dashboard assemblies, steering systems, suspension components, body structures, and crash safety systems [3]. Through FEA, engineers can identify stress concentration regions, evaluate displacement behavior, optimize material distribution, and improve overall structural performance [1]. The fundamental principle of Finite Element Analysis involves discretizing a complex geometry into smaller finite elements connected through nodes.

Figure 2.10 Finite element mesh model of the Cross-Car Beam assembly

Material properties such as elastic modulus, density, yield strength, and Poisson’s ratio are assigned to these elements in order to simulate realistic structural behavior [2]. Boundary conditions and external loads are then applied to the model to represent actual operating environments. One of the most important applications of FEA in automotive engineering is crash analysis. Vehicle safety regulations require structural components to withstand severe impact conditions while protecting occupants and maintaining structural integrity [5]. Crash simulations help engineers evaluate how forces are transferred through the vehicle structure during collision events and allow identification of critical stress concentration regions.

In crash analysis, stress distribution and displacement behavior are carefully examined to determine potential failure regions. Structural components experiencing stresses above the material yield strength may undergo permanent deformation or structural failure [1][5]. Therefore, finite element crash simulations are widely used to optimize structural geometry and improve load transfer paths.

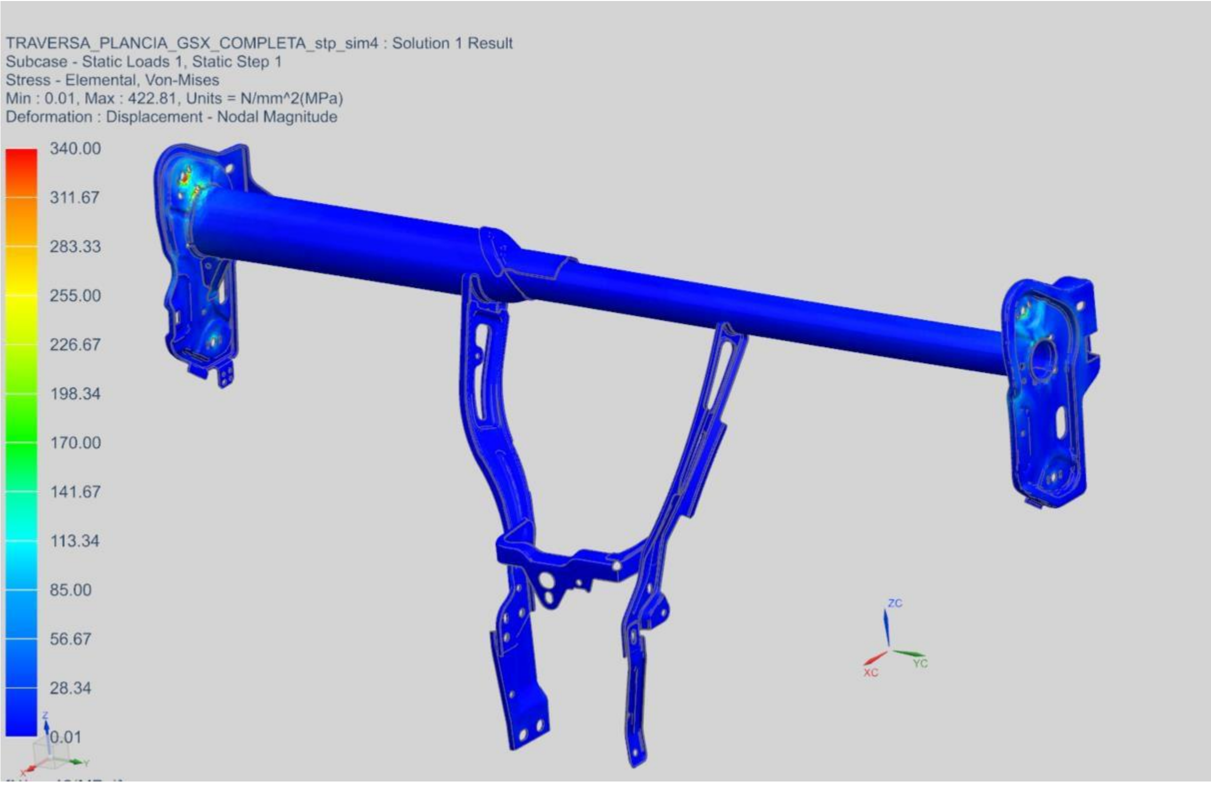

Figure 2.11 Von Mises contour obtained from finite element crash analysis

Another important application of FEA in automotive systems is modal analysis. Modal analysis is used to determine the natural frequencies and vibration mode shapes of a structure [4].

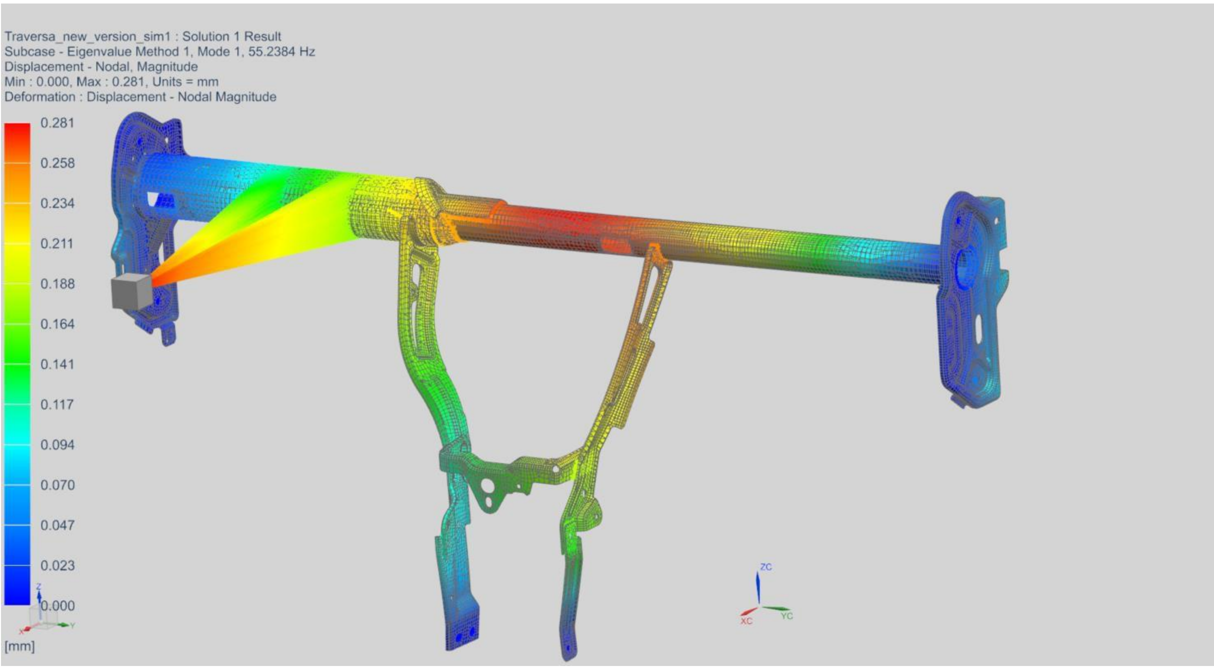

Figure 2.12 Modal analysis mode shapes of the Cross-Car Beam Structure

Every mechanical structure possesses natural frequencies at which resonance may occur if external excitation frequencies approach the structural natural frequency.
In vehicle interior systems, vibration behavior is particularly important because dashboard structures are continuously exposed to engine vibrations, road excitations, and aerodynamic disturbances. Excessive vibration may lead to squeak-and-rattle problems, passenger discomfort, and fatigue-related damage over time [4].
Modal analysis also provides strain energy distribution information, which helps engineers identify regions where vibration energy becomes concentrated within the structure. Areas with high localized strain energy are generally more susceptible to fatigue-related structural damage [4].

The Cross-Car Beam is a critical structural component within the dashboard assembly because it supports multiple subsystems simultaneously, including the steering column, HVAC system, passenger airbag, infotainment units, and electrical wiring harnesses. Since the beam experiences both static and dynamic loading conditions, Finite Element Analysis becomes essential for evaluating its structural behavior.

In this study, Finite Element Analysis is performed to investigate the structural performance of the original, optimized, and reinforced Cross-Car Beam configurations. Static crash analysis is conducted to evaluate displacement behavior, stress distribution, and structural integrity under crash-equivalent loading conditions, while modal analysis is performed to evaluate vibration characteristics and strain energy distribution.

Chapter 3 - Problem Definition

3.1 Limitations of Existing Design

The original Cross-Car Beam (CCB) configuration used a conventional external wiring harness routing strategy in which the main electrical cables and branch harnesses were positioned around the outer surfaces of the beam structure. This type of routing method is commonly used in automotive dashboard systems because it provides relatively direct accessibility during initial assembly and maintenance procedures. However, despite its simplicity, the conventional external routing configuration introduced several important packaging, structural, manufacturability, and durability-related disadvantages within the dashboard assembly.
One of the most significant limitations of the original design was the inefficient utilization of available packaging space inside the dashboard region. The dashboard area of a modern vehicle is one of the most congested zones because it contains multiple structural, mechanical, and electrical systems integrated within a highly restricted volume. Components such as HVAC ducts, infotainment displays, passenger airbags, steering systems, electronic control units, sensors, and wiring harnesses must all coexist within the same packaging environment.
In the original configuration, the main wiring harness and all branch cables were routed externally around the Cross-Car Beam.

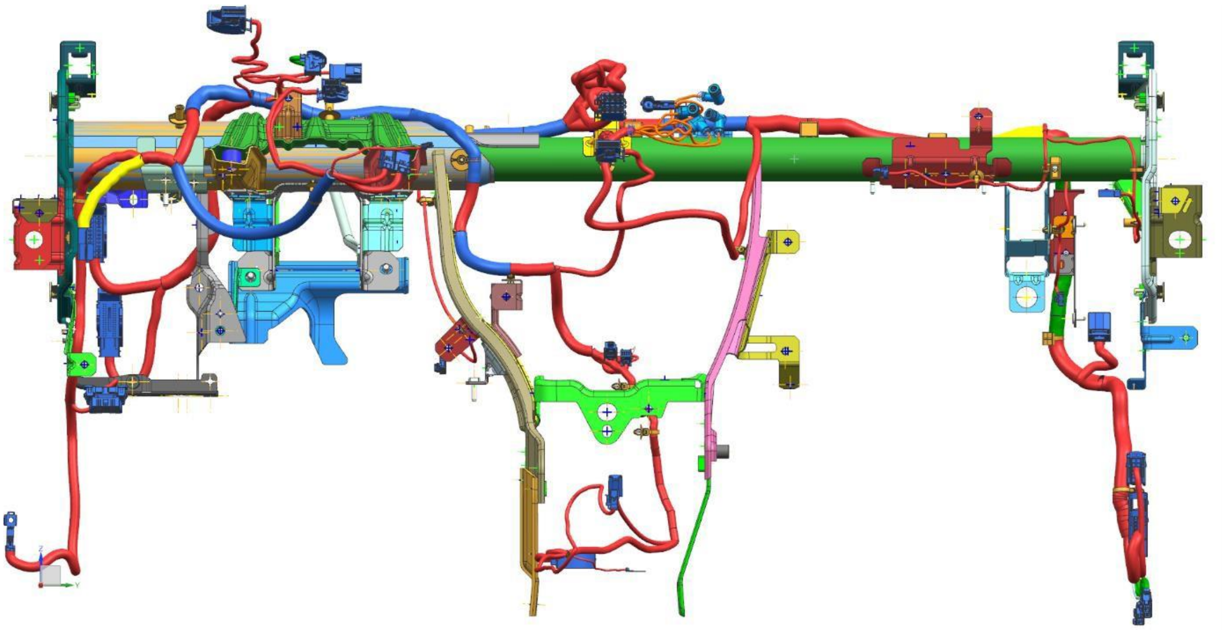

Figure 3.1 Conventional external wiring harness routing around the Cross-Car beam

As a result, a considerable amount of usable dashboard space became occupied by electrical routing components. The external harnesses reduced the available clearance between the dashboard trim and the beam structure, limiting the packaging flexibility of surrounding systems. This problem becomes even more critical in modern electric and hybrid vehicles because electrical architectures are continuously increasing in complexity. Advanced driver assistance systems (ADAS), digital cockpit technologies, larger infotainment screens, ambient lighting systems, and multiple communication networks require significantly larger and more complex wiring harnesses compared to conventional vehicles. Consequently, traditional external routing methods become increasingly inefficient as the number of electrical systems grows. Another major limitation of the original design was the complexity of the cable layout.

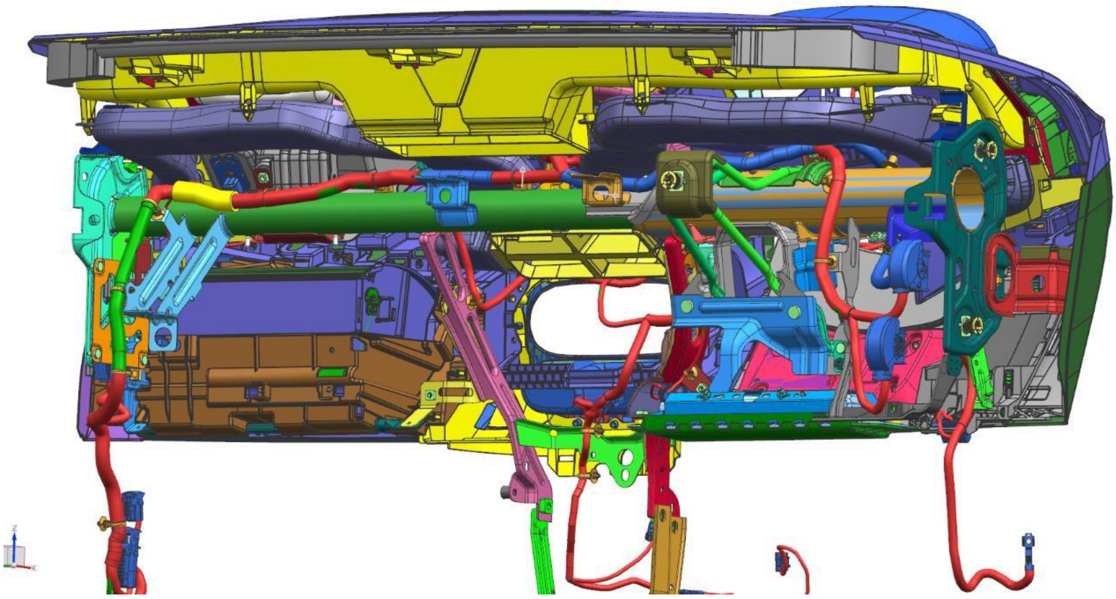

Figure 3.2 Complex cable arrangement in the original dashboard configuration

Since all electrical branches were routed externally around the beam structure, the dashboard assembly became highly congested with intersecting cable paths and multiple connection points. The branch cables occupied different regions around the beam and interacted closely with neighboring dashboard components. This routing complexity created several engineering disadvantages. First, the assembly process became more difficult because operators were required to manually guide multiple branch cables through narrow packaging regions during installation. The presence of numerous external branches increased assembly time and reduced manufacturing efficiency. Second, the congested cable arrangement increased the possibility of cable interference during both assembly and vehicle operation. External harnesses could potentially interact with HVAC ducts, steering column components, brackets, clips, and surrounding dashboard elements. Such interactions may result in cable misalignment, local deformation, or long-term durability problems. The external routing strategy also negatively affected serviceability and maintenance accessibility. During repair or replacement procedures, accessing individual harness branches often required partial removal of dashboard components. Since multiple cable branches were bundled externally around the beam, maintenance operations became more time-consuming and complicated. Another important limitation of the original design was the increased vulnerability of the external harnesses to mechanical and environmental damage. Vehicle dashboard systems are continuously exposed to dynamic operating conditions, including road-induced vibrations, engine excitations, thermal fluctuations, and structural movement during vehicle operation. Under such conditions, externally routed harnesses may experience repeated contact with sharp edges, mounting brackets, fasteners, or moving mechanical components. Long-term vibration exposure can gradually damage cable insulation through abrasion and frictional wear. In addition, repeated dynamic loading may loosen connectors or create squeak-and-rattle (S&R) problems within the dashboard structure. Thermal exposure represented another critical concern in the original design.

Because the external harnesses were positioned near HVAC ducts and electronic components, the cables were subjected to elevated thermal conditions during vehicle operation. Continuous thermal exposure may accelerate aging of insulation materials and reduce the long-term reliability of the electrical system. From a structural perspective, the original Cross-Car Beam geometry also presented important limitations regarding internal routing capability. The beam structure originally contained only four relatively small openings that were insufficient for routing large electrical harnesses through the hollow section of the beam.

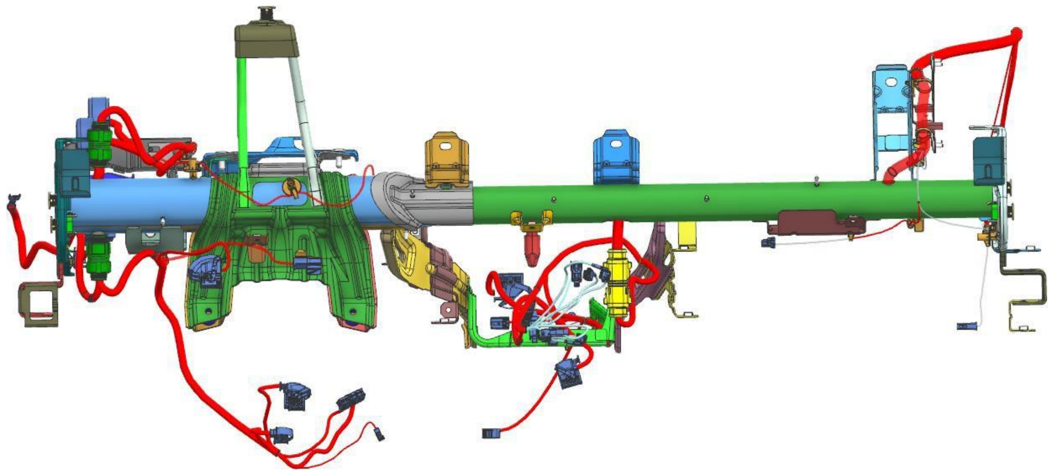

Figure 3.3 Cross-Car Beam old version top-view four small openings

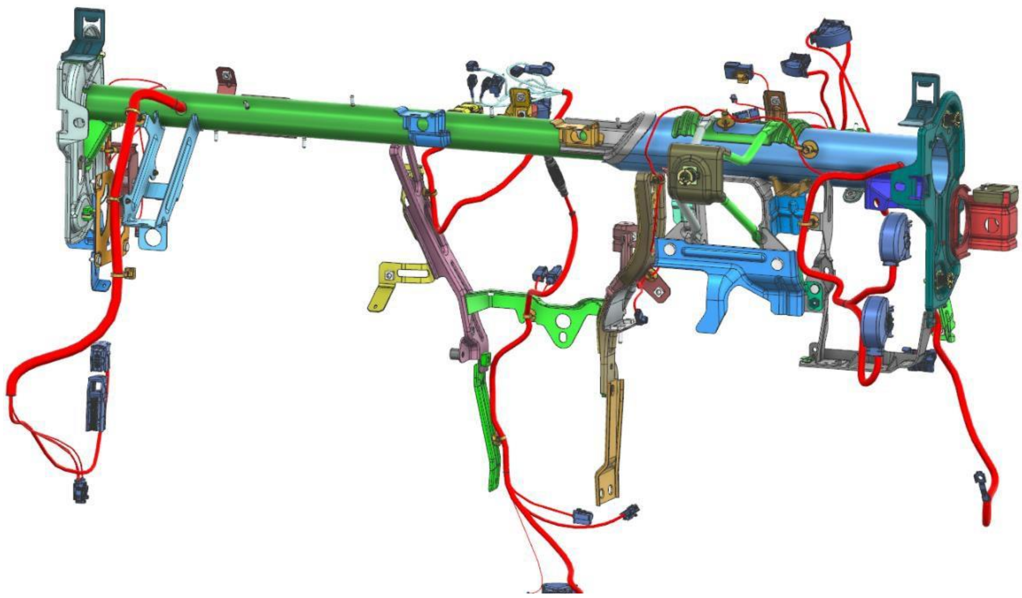

Figure 3.4 Cross-Car Beam old version isometric-view four small openings

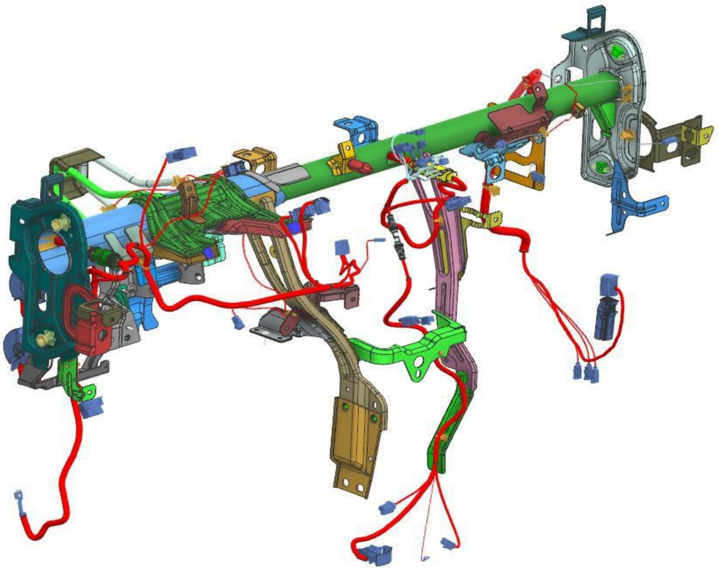

Figure 3.5 Cross-Car Beam old version isometric-view four small openings

As wiring systems continue to increase in size due to modern vehicle electronics, the original opening dimensions could not accommodate the required cable bundles effectively. The limited opening size restricted internal routing possibilities and prevented efficient utilization of the hollow beam volume.

In addition to packaging limitations, the original routing configuration also reduced the overall visual organization of the dashboard assembly. The large number of externally visible cable branches created more complicated and less organized architecture, making the assembly appear cluttered and increasing routing management difficulty.

Because of these limitations, a new routing concept became necessary to improve packaging efficiency, reduce cable complexity, increase serviceability, and provide better protection for the wiring harness system. However, implementing internal routing through the Cross-Car Beam required modifications to the beam geometry, including enlargement of the existing openings.

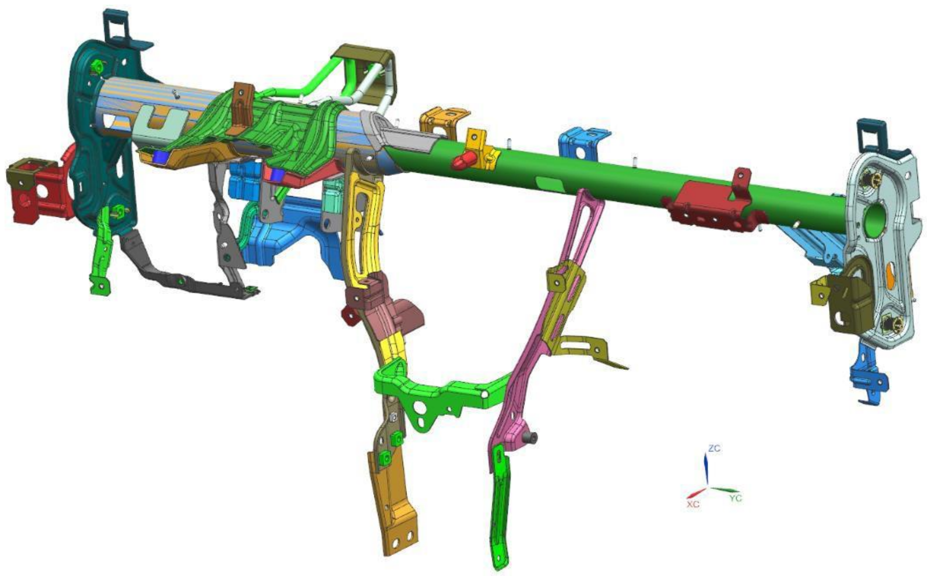

Figure 3.6 Cross-Car Beam new version front isometric-view four small openings

Figure 3.7 Cross-Car Beam new version back isometric-view four small openings

Although enlarging the openings improves cable routing capability and internal packaging efficiency, such modifications may also influence structural behavior. Introducing larger openings into a load-carrying structural component may reduce local stiffness, alter load transfer paths, and create stress concentration regions around the modified areas. Therefore, the development of the optimized Cross-Car Beam required a balanced engineering approach that could simultaneously satisfy packaging, manufacturability, structural integrity, crashworthiness, and durability requirements.

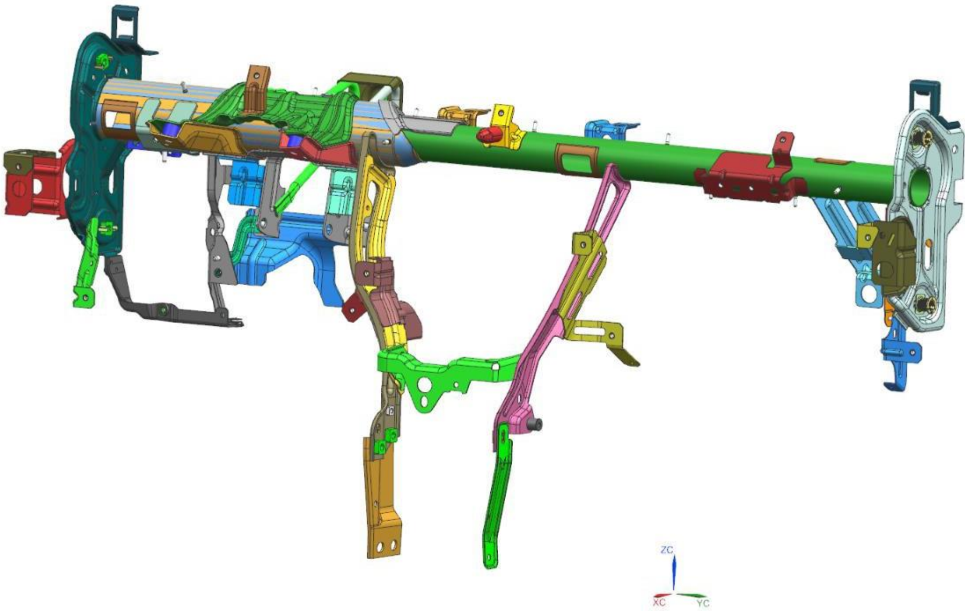

Figure 3.8 Cross-Car Beam new version sheet metal attached front isometric-view four openings

Figure 3.9 Cross-Car Beam new version sheet metal attached back isometric-view four openings

3.2 Structural Optimization

The limitations identified in the original Cross-Car Beam configuration demonstrated the necessity for a new engineering approach capable of improving both packaging efficiency and structural functionality within the dashboard assembly. As modern vehicles continue to incorporate increasingly complex electrical and electronic systems, conventional external harness routing strategies become progressively insufficient in terms of space utilization, manufacturability, durability, and system organization.

One of the primary motivations for optimization was the need to increase available packaging space inside the dashboard region. In modern automotive interiors, the dashboard area must accommodate many integrated subsystems within a highly restricted volume. Components such as HVAC ducts, infotainment displays, steering systems, passenger airbags, electronic control units, sensors, wiring harnesses, and support brackets all compete for limited packaging space. In the original design, the externally routed harness occupied a significant amount of usable volume around the Cross-Car Beam. This congestion restricted the available clearance between the dashboard trim and structural components, limiting the flexibility of interior packaging design. As electrical systems continue to increase in size and complexity, maintaining the conventional external routing approach would further intensify dashboard congestion and assembly difficulties.

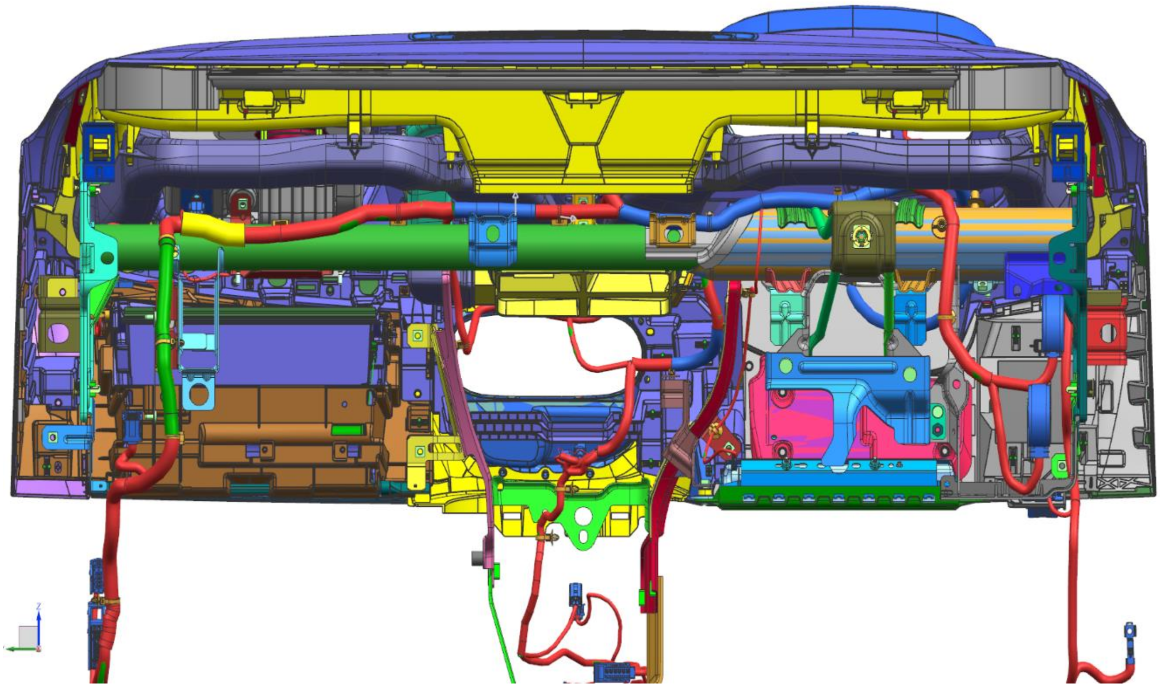

Figure 3.10 Packaging congestion caused by external harness routing in the original design

Another major motivation for optimization was the reduction of cable complexity and improvement of assembly organization. The original routing configuration contained numerous externally positioned branch cables distributed around the beam structure. This arrangement created complicated routing paths that increased manufacturing difficulty and reduced assembly efficiency. During production processes, operators were required to manually guide and position multiple branch cables around narrow dashboard regions. Such operations increased assembly time and raised the possibility of installation errors, cable interference, and connector misalignment. Therefore, a more organized and modular routing strategy became necessary to simplify manufacturing operations. The optimization process also aimed to improve the serviceability and maintainability of the dashboard electrical system. In conventional external routing systems, maintenance operations often require removal of multiple surrounding components in order to access individual harness branches. This increases repair time and complicates maintenance procedures.

A modular internal routing concept allows individual cable branches to be disconnected independently through connector systems, significantly improving accessibility during servicing operations. Therefore, optimization of the routing configuration contributes not only to manufacturing efficiency but also to long-term maintenance performance.

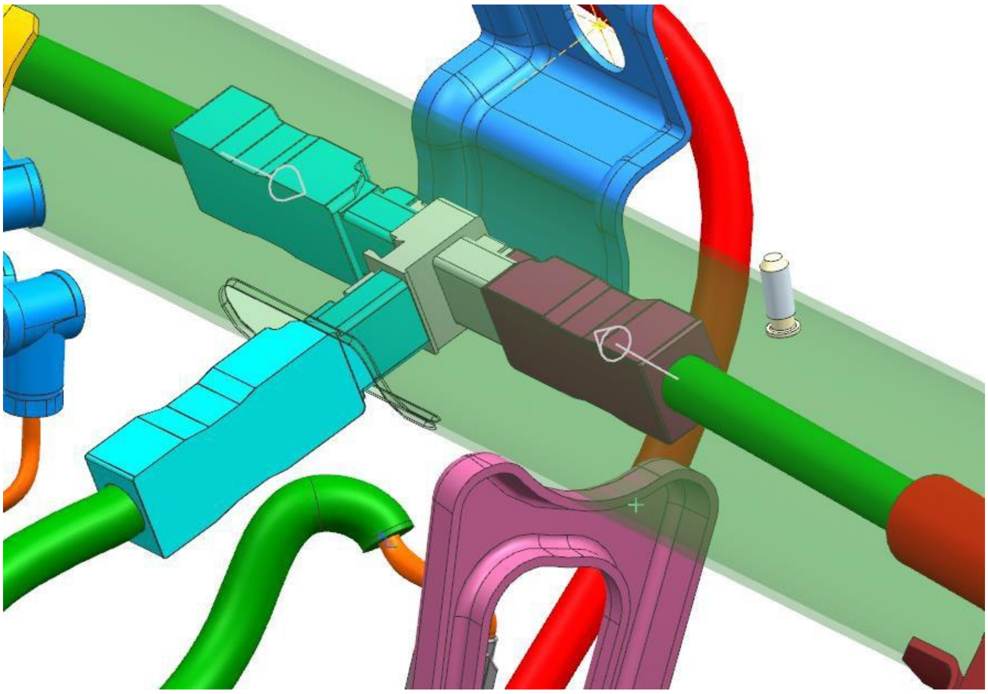

Figure 3.11 Internal routing and modular connector integration concept

Another important factor driving the optimization process was the need to improve protection of the wiring harness system against mechanical and environmental effects. External harnesses are continuously exposed to vibration, friction, thermal loading, and accidental contact with surrounding components during vehicle operation. Long-term exposure to such conditions may lead to abrasion of cable insulation, connector loosening, squeak-and-rattle problems, and electrical reliability issues. In addition, cables positioned close to HVAC ducts and thermal sources may experience elevated temperatures that accelerate material aging. By relocating the main wiring harness inside the hollow Cross-Car Beam structure, the beam itself can act as a protective enclosure for the electrical system. Internal routing significantly reduces direct exposure of the harness to external mechanical interactions and vibration-related damage.

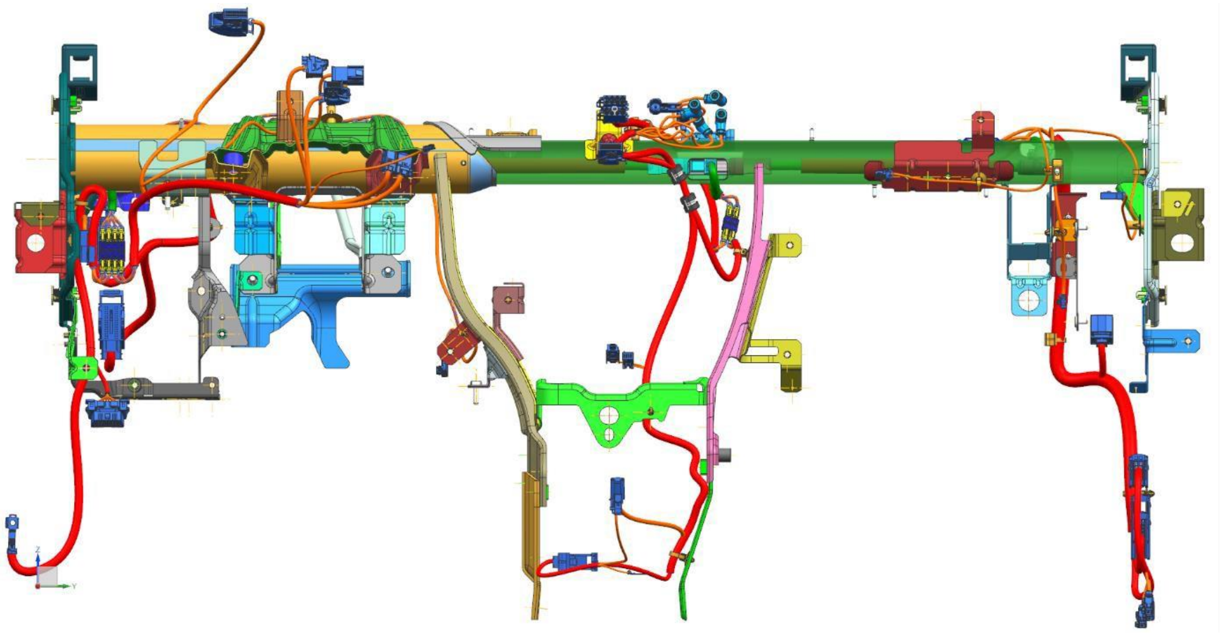

Figure 3.12 Internal wiring harness routing through the hollow Cross-Car Beam structure

Despite these packaging and protection advantages, introducing internal routing into the Cross-Car Beam also creates important structural challenges. The original beam geometry was not designed to accommodate large internal cable bundles. Therefore, enlargement of the existing beam openings became necessary in order to allow passage of the wiring harness through the hollow section. However, modifications to structural components may significantly influence load transfer behavior and stiffness characteristics. The Cross-Car Beam is a critical load-carrying component responsible for supporting the steering column, dashboard assembly, HVAC system, passenger airbag module, and additional interior subsystems. Enlarging the beam openings introduces geometric discontinuities into the structure, which may reduce local stiffness and create stress concentration regions around the modified areas. Such stress concentrations may negatively affect crashworthiness and long-term durability performance if not properly addressed. Another important consideration during the optimization process was vibration behavior. Structural modifications that reduce stiffness may alter the natural frequencies and vibration modes of the Cross-Car Beam assembly. If the modified structure becomes more susceptible to resonance under operational excitation frequencies, excessive vibration amplitudes and fatigue-related problems may occur. Therefore, the optimization process required a balanced engineering approach capable of simultaneously satisfying multiple performance criteria. The new design needs to; improve dashboard packaging efficiency, reduce external cable congestion, simplify assembly operations, improve maintenance accessibility, protect the wiring harness system, maintain structural stiffness, preserve crashworthiness, and ensure acceptable vibration performance. To achieve these objectives, the proposed design introduces an internal wiring harness routing strategy combined with modular connector systems, cable guide mechanisms, and reinforcement structures around the modified beam openings.

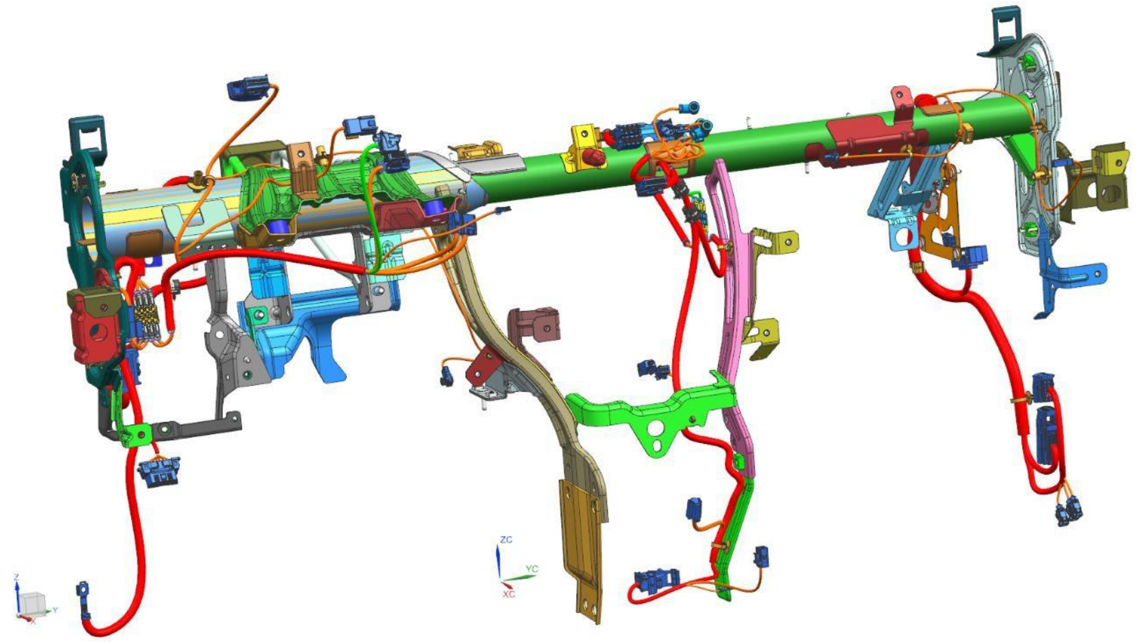

Figure 3.13 Cross-Car Beam proposed model sheet metal attached front isometric-view

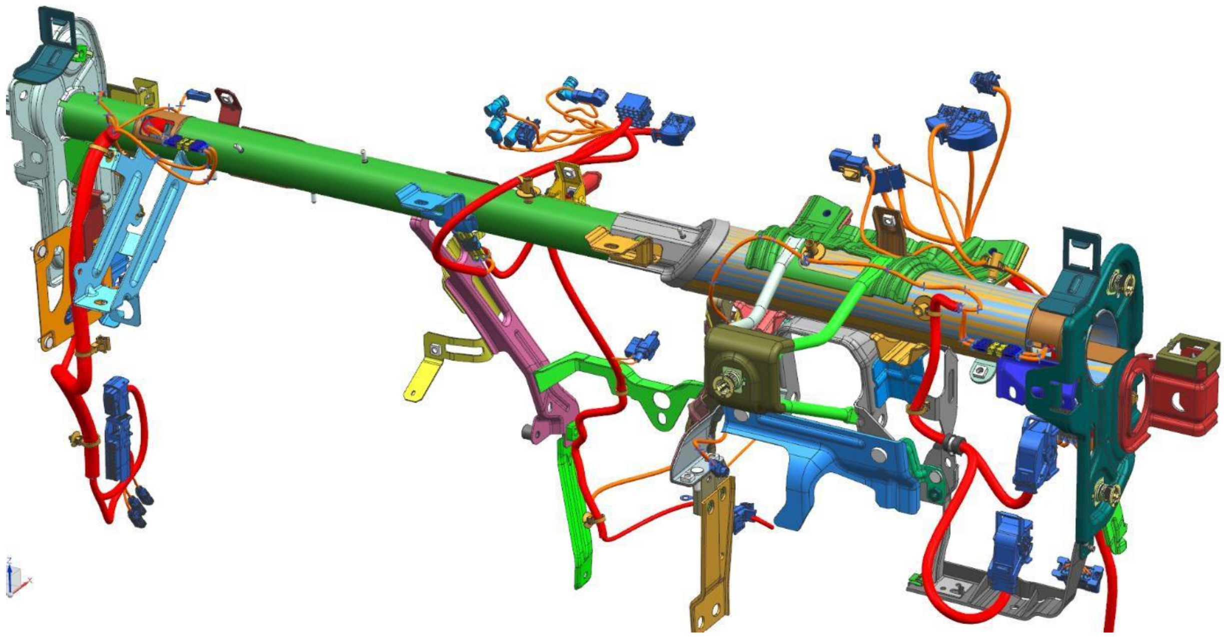

Figure 3.14 Cross-Car Beam proposed model sheet metal attached back isometric-view

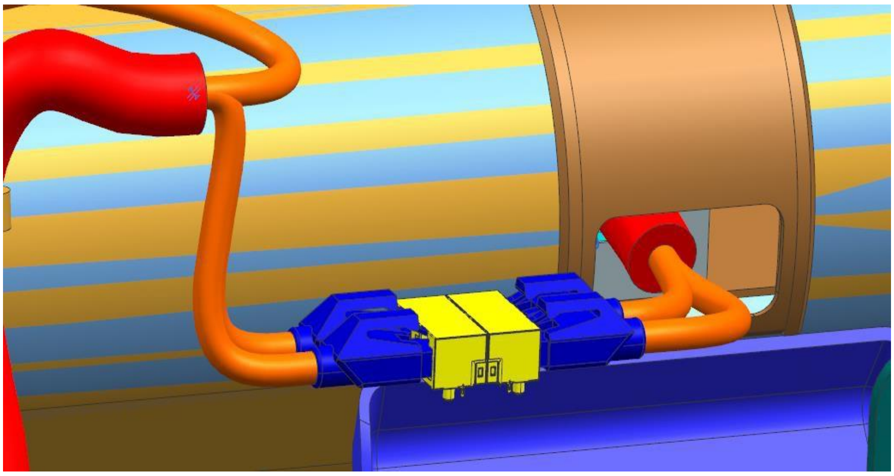

Figure 3.15 Cross-Car Beam proposed model sheet metal attached detailed view

The optimization process presented in this thesis therefore represents a multidisciplinary engineering approach integrating packaging design, structural engineering, manufacturability considerations, crash analysis, and vibration analysis into a single integrated dashboard architecture.

3.3 Design Objectives and Engineering Requirements

Following the identification of the limitations associated with the original Cross-Car Beam configuration, a comprehensive set of design objectives and engineering requirements was established to guide the development of the optimized dashboard architecture. The primary goal of the optimization process was not only to improve wiring harness routing capability, but also to achieve a balanced engineering solution capable of simultaneously satisfying packaging, structural, manufacturability, durability, and serviceability requirements.

In modern automotive engineering, component optimization must consider multiple performance criteria simultaneously because modifications introduced to improve one parameter may negatively affect another. For example, increasing the size of routing openings inside the Cross-Car Beam may improve packaging efficiency and internal routing capability, but at the same time may reduce local structural stiffness and increase stress concentration levels. Therefore, the design process required a multidisciplinary engineering approach capable of balancing conflicting design requirements.

One of the most important objectives of the proposed design was the improvement of dashboard packaging efficiency. In the original configuration, the externally routed wiring harness occupied a considerable amount of space around the Cross-Car Beam and reduced the available volume for surrounding dashboard components. As electrical systems become larger and more complex in modern vehicles, the need for efficient utilization of dashboard packaging space becomes increasingly critical.

The optimized design therefore aimed to relocate the primary wiring harness inside the hollow Cross-Car Beam structure in order to free external dashboard space and reduce cable congestion. By utilizing the unused internal volume of the beam, the proposed routing concept allows improved integration of HVAC ducts, infotainment systems, airbag modules, and additional electronic components.

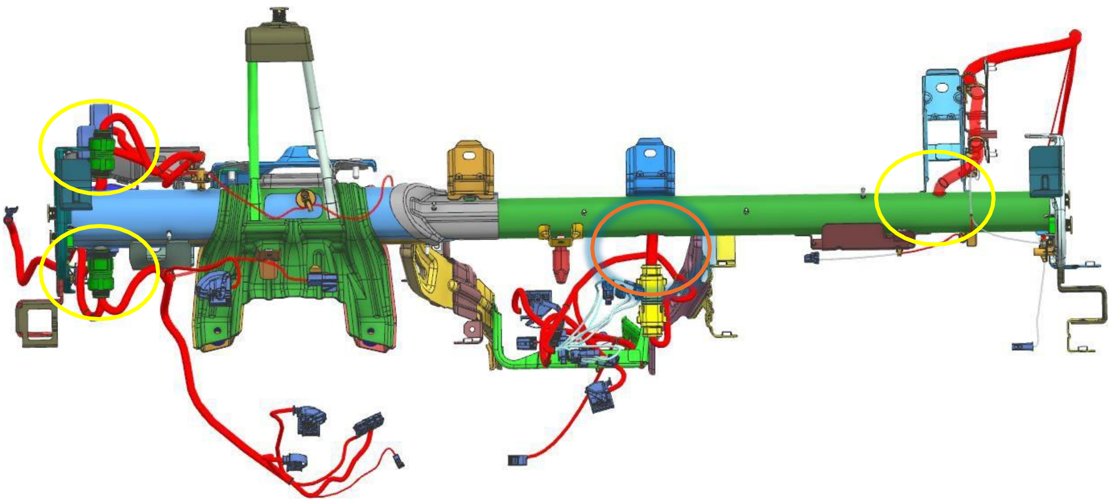

Figure 3.16 Internal routing concept of the optimized Cross-Car Beam design

Another important design objective was the reduction of cable complexity and improvement of system organization. Conventional external routing methods often produce highly congested cable arrangements containing multiple intersecting branches and connection points around the dashboard structure. Such configurations increase assembly difficulty, reduce accessibility, and complicate maintenance operations.

The optimized design therefore aimed to introduce a more modular harness architecture in which the primary cable bundle remains inside the beam while branch cables are connected externally through modular connector systems. This approach reduces external cable occupation and improves the overall organization of the dashboard electrical system.

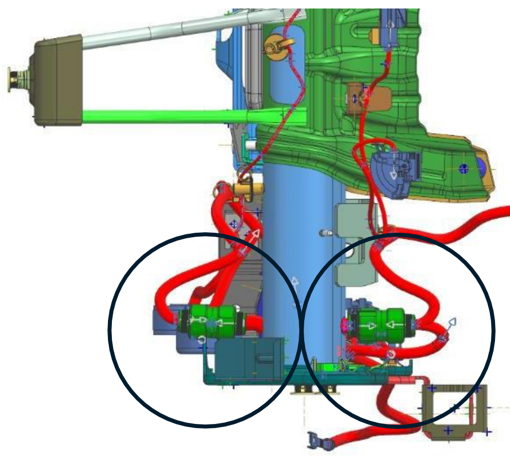

Figure 3.17 Modular connector integration and branch cable organization

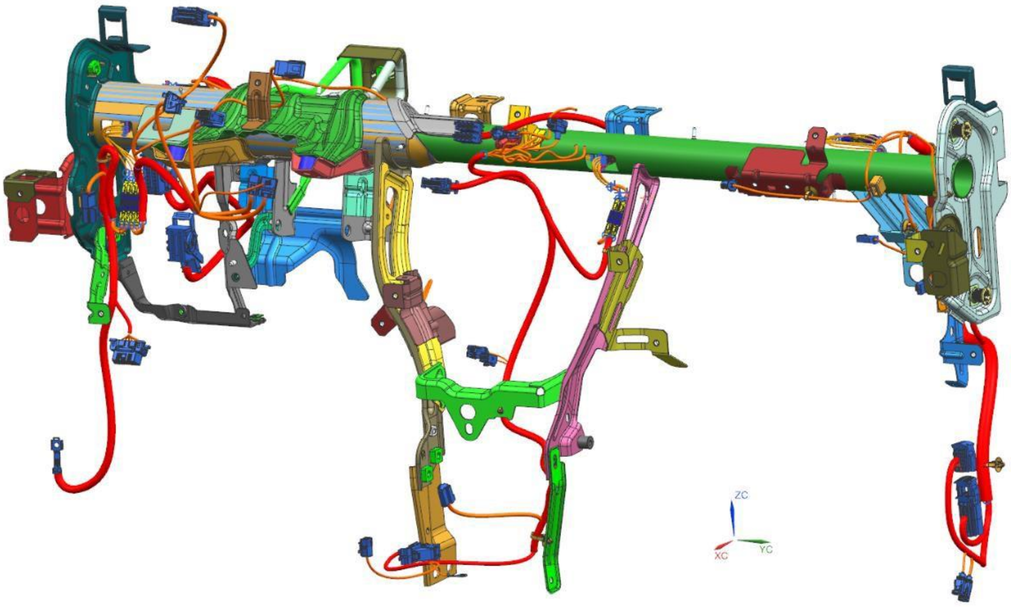

Figure 3.18 Modular connector integration and branch cable organization

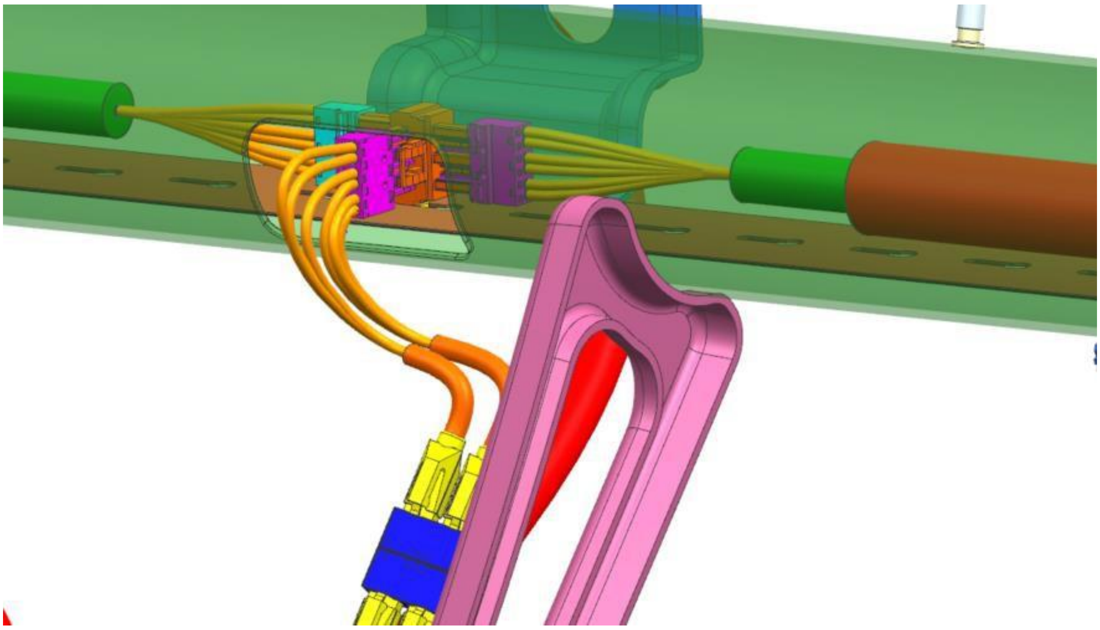

Figure 3.19 Modular connector integration and branch cable organization 1st opening

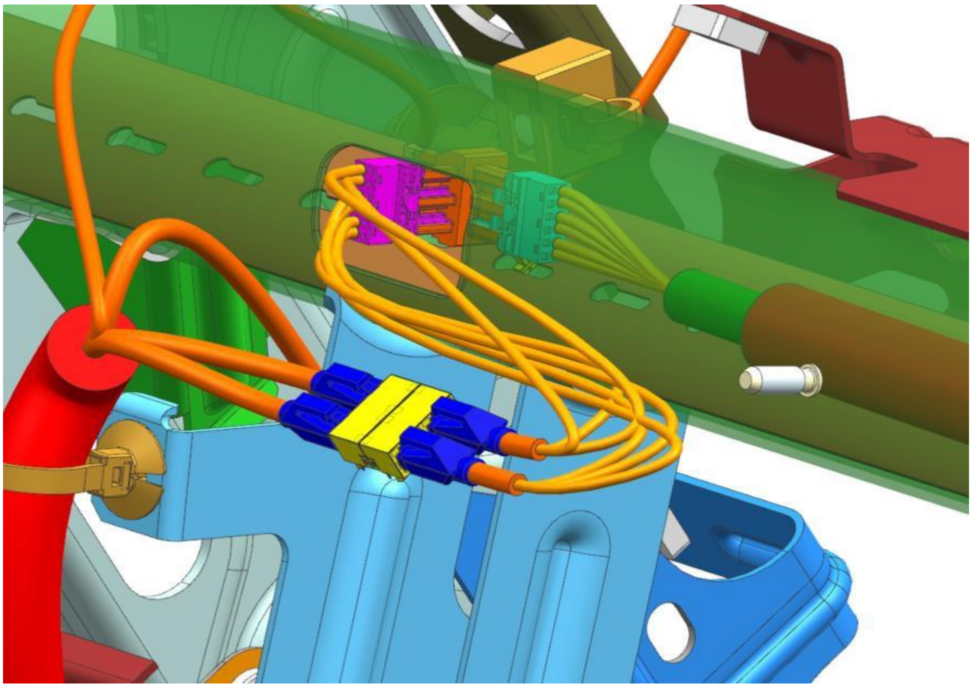

Figure 3.20 Modular connector integration and branch cable organization second opening

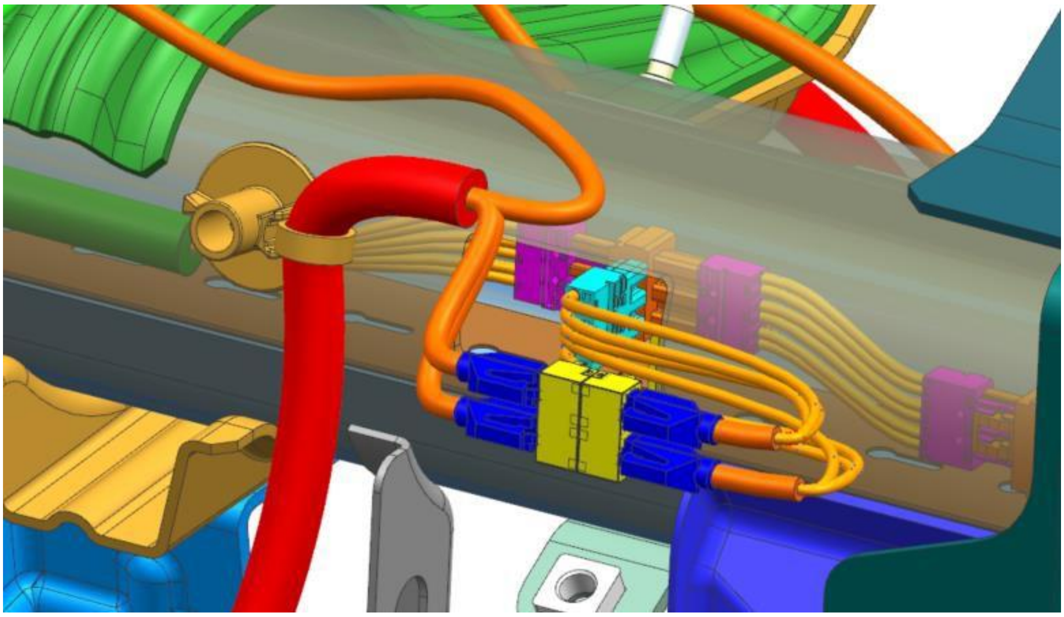

Figure 3.21 Modular connector integration and branch cable organization third opening

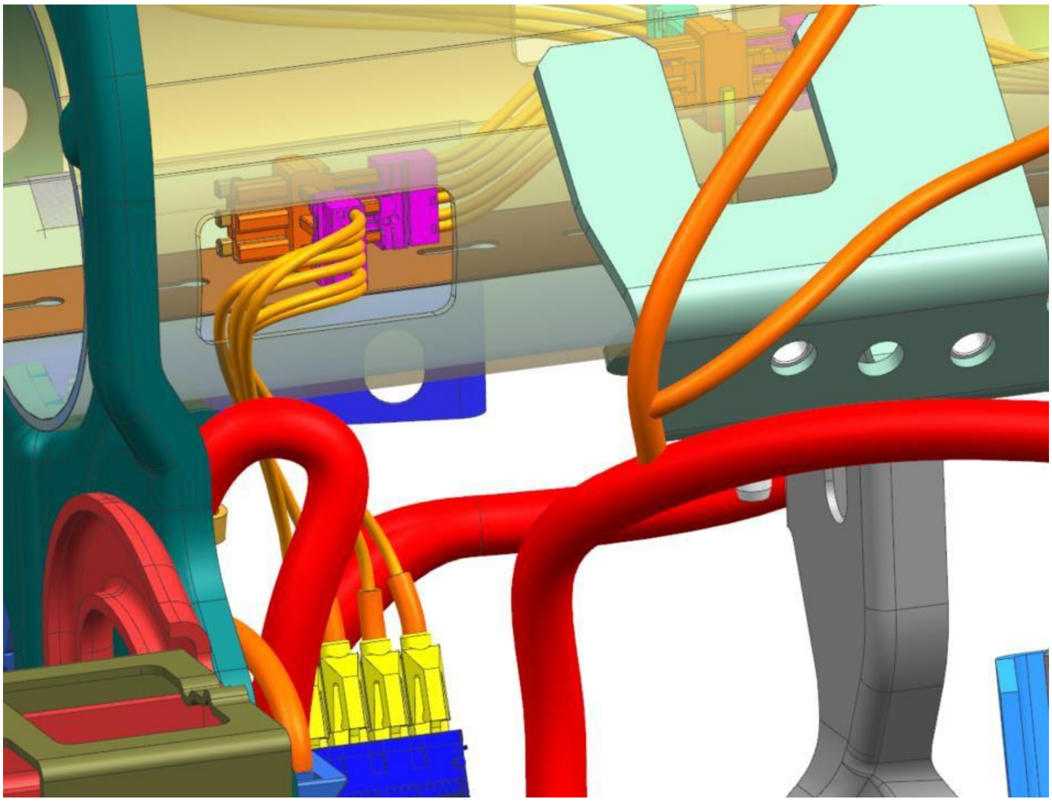

Figure 3.22 Modular connector integration and branch cable organization fourth opening

Improvement of assembly efficiency and manufacturability also represented major engineering objectives during the development process. In mass-production automotive manufacturing, assembly simplicity and repeatability are extremely important because even small reductions in assembly time can significantly affect manufacturing cost and production efficiency.

In the original configuration, assembly operators were required to manually position multiple external cable branches around narrow dashboard regions. This increased installation complexity and raised the possibility of routing errors or cable interference. Therefore, the optimized system aimed to simplify installation procedures by introducing cable guides, modular connectors, clips, and guided routing mechanisms.

The cable guide system was specifically designed to improve insertion and extraction of the wiring harness during assembly and maintenance operations. Adjustable alignment features and modular branch connections were integrated into the design to increase assembly flexibility and reduce operator difficulty.

Another major engineering objective was the improvement of serviceability and maintenance accessibility. Vehicle electrical systems frequently require inspection, repair, or replacement during the service life of the vehicle. In conventional external routing systems, accessing individual cable branches may require removal of surrounding dashboard components, significantly increasing maintenance time and labor cost.

The optimized design therefore focused on improving modularity through the use of re-pin and de-pin capable connector systems. By dividing the harness into smaller modular branches connected through standardized interfaces, maintenance operations can be performed more efficiently without requiring complete disassembly of the dashboard assembly.

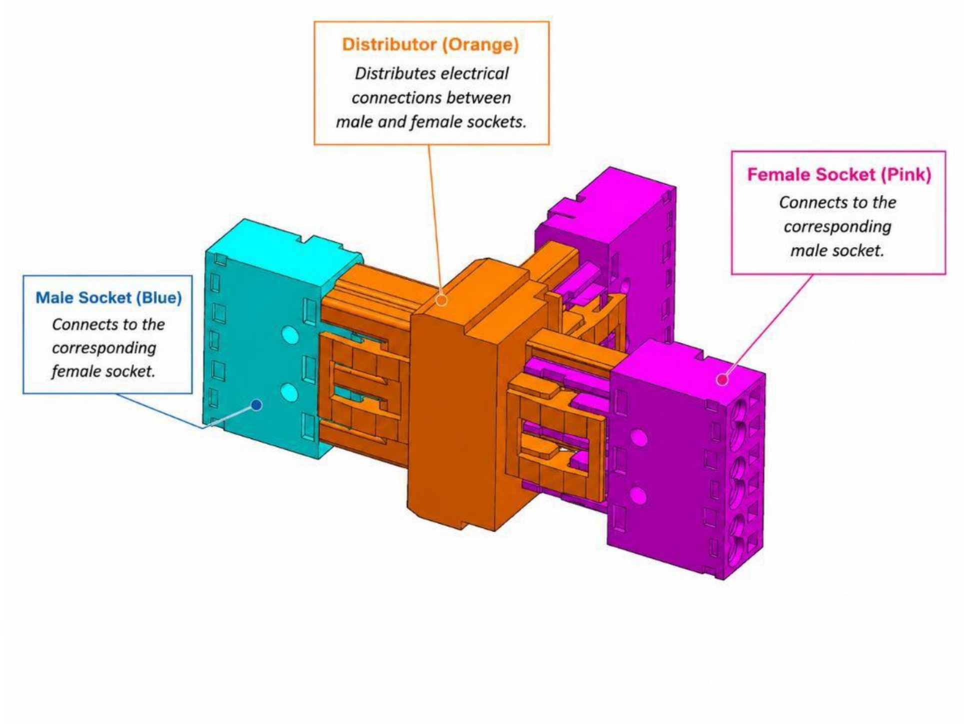

Figure 3.23 Wago model re-pin de-pin type assembly of connectors

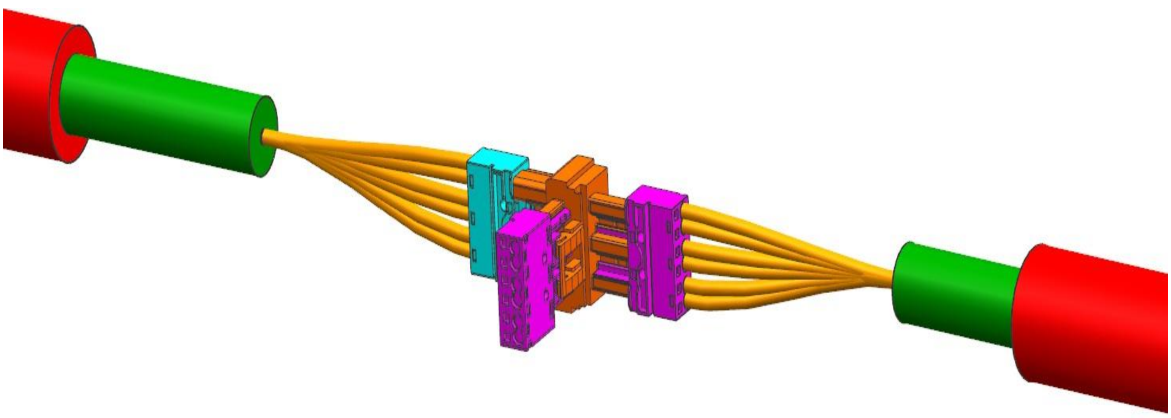

Figure 3.24 Wago model re-pin de-pin type connectors and cable layout

Here can be seen from **Figure 3.24** red cable refers to “main cable” and others which are green and orange represents to “mini electrical cables”

Protection of the wiring harness system against mechanical and environmental effects was also considered a critical engineering requirement. During vehicle operation, dashboard structures are continuously exposed to vibration, thermal loading, structural movement, and road-induced dynamic excitation.

Externally routed cables are more vulnerable to friction, abrasion, thermal exposure, and accidental contact with surrounding components. Long-term exposure to such conditions may damage cable insulation, reduce connector reliability, and increase the risk of electrical failure.

By routing the primary harness inside the hollow Cross-Car Beam structure, the beam itself acts as a protective enclosure that shields the electrical system from external mechanical interaction. This internal routing concept significantly improves cable protection and reduces the likelihood of vibration-induced wear or accidental damage.

Despite the numerous packaging and assembly advantages of internal routing, structural integrity remained one of the most critical engineering requirements throughout the optimization process. The Cross-Car Beam is a load-carrying structural component responsible for supporting major dashboard subsystems including the steering column, HVAC unit, airbag module, and dashboard assembly.

Therefore, any geometric modification introduced to improve routing capability must preserve sufficient stiffness and crashworthiness performance. Enlarging the beam openings to accommodate the internal wiring harness may create local stress concentration regions and alter load transfer paths within the structure.

To address these concerns, reinforcement strategies were integrated into the optimized design. Sheet metal reinforcement plates were introduced around the modified beam openings in order to restore local stiffness and improve structural stability under loading conditions.

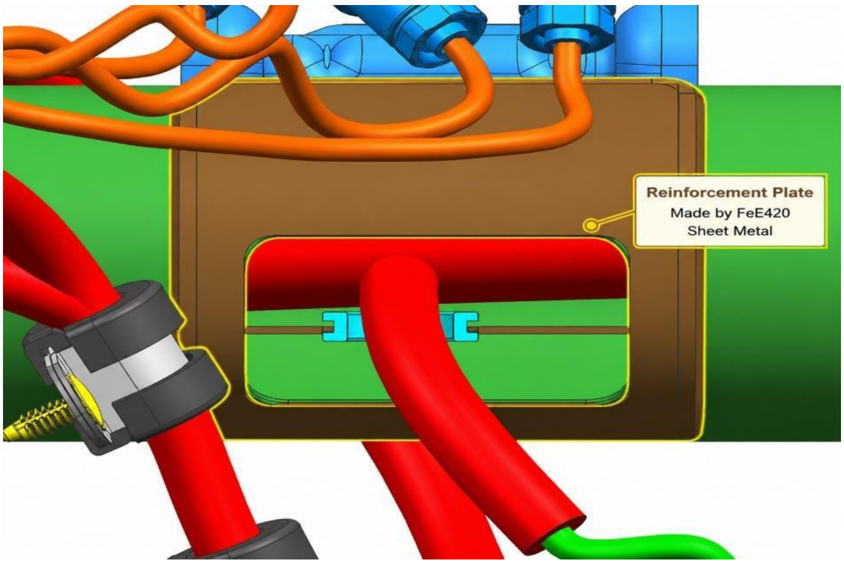

Figure 3.25 Reinforcement plate attached on opening

Another important engineering requirement involved vibration and dynamic behavior. Structural modifications affecting stiffness may alter the natural frequencies and vibration characteristics of the dashboard assembly. Excessive vibration or resonance may lead to squeak-and-rattle problems, passenger discomfort, connector loosening, and fatigue-related structural damage.

Therefore, the optimized design needed to maintain acceptable modal behavior while simultaneously improving packaging efficiency. Modal analysis and strain energy evaluation were therefore incorporated into the engineering validation process in order to ensure balanced dynamic performance.

Weight optimization also represented an important design consideration. Modern automotive engineering continuously seeks to reduce vehicle mass in order to improve fuel efficiency, reduce emissions, and increase electric vehicle range. Although reinforcement structures were required around the modified openings, the optimized design aimed to maintain a lightweight architecture while preserving structural integrity
Consequently, the final design objectives of this study can be summarized as follows: Improve dashboard packaging efficiency, Increase available HVAC and infotainment space, reduce external cable congestion, simplify assembly operations, improve serviceability and maintenance accessibility, protect the wiring harness from mechanical damage, maintain structural stiffness and crashworthiness, preserve acceptable vibration performance, and achieve an efficient lightweight design.

The proposed Cross-Car Beam optimization presented in this thesis was therefore developed as a multidisciplinary engineering solution integrating packaging design, structural engineering, vibration analysis, manufacturability considerations, and electrical system integration into a unified dashboard architecture.

3.4 Development of the Optimized Routing System

The development of the optimized routing system focused on transforming the conventional external wiring harness configuration into a more compact, organized, and internally integrated dashboard architecture. The optimization process included modification of the Cross-Car Beam geometry together with the development of additional routing components such as cable guides, clip mechanisms, Wago carrier structures, and reinforcement elements.

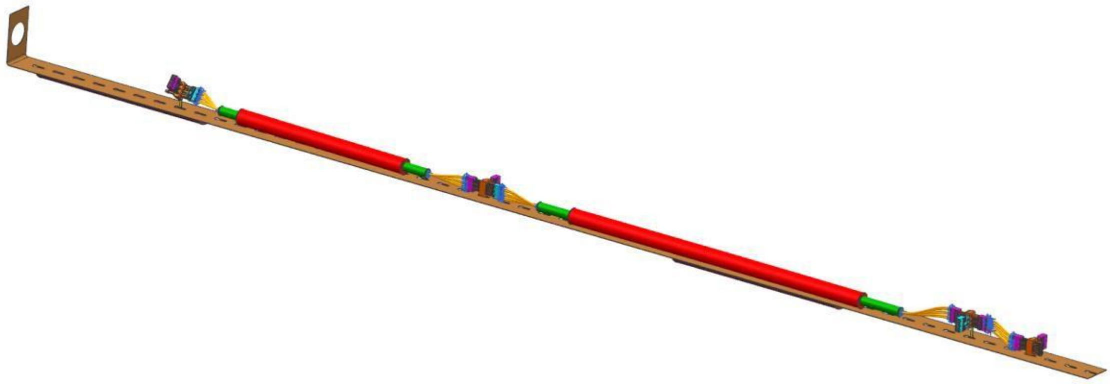

Figure 3.26 Cable Guide for routing main cable through the inside of the Cross-Car Beam

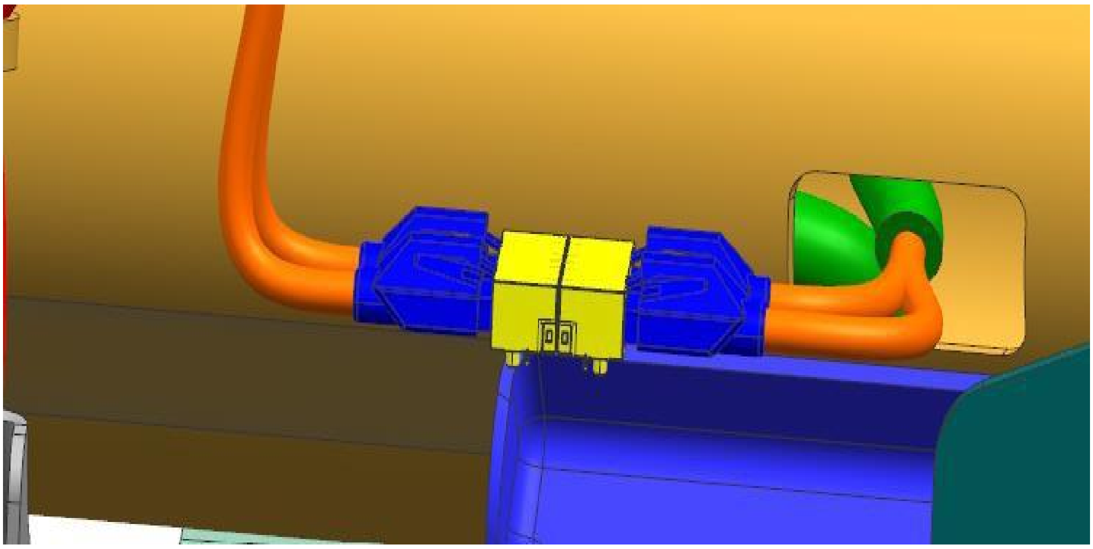

F Figure 3.27 Clip mechanisms for routing easily cable

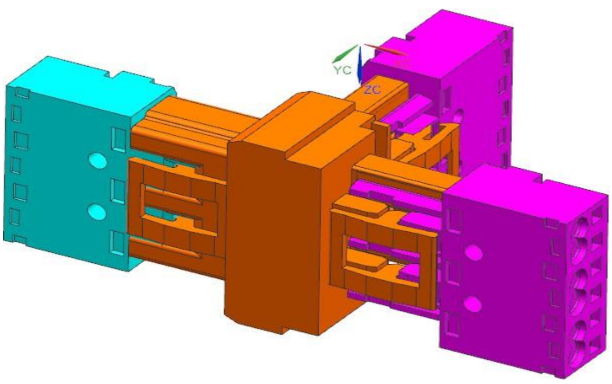

Figure 3.28 Wago type connector system

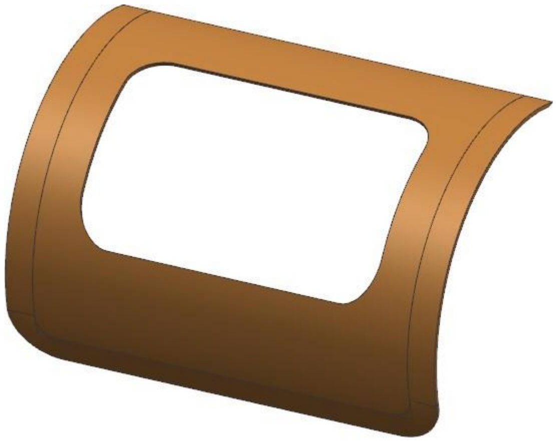

Figure 3.29 Reinforcement plate made by sheet metal

The primary objective of the redesigned routing system was to improve packaging efficiency inside the dashboard assembly while simultaneously simplifying cable organization and improving protection of the electrical harness system. Instead of distributing the wiring harness externally around the beam structure, the optimized configuration aimed to relocate the primary harness inside the hollow Cross-Car Beam.

To support this routing concept, the geometry of the original beam structure was modified by enlarging selected routing openings. The original openings were insufficient for large cable bundle integration and limited the possibility of internal routing. Therefore, the opening dimensions were redesigned according to the required harness diameter and branch routing directions.

The center opening region of the beam was mainly developed for the passage of the primary harness bundle through the tubular structure. Additional routing openings were also positioned near the left-hand and right-hand sides of the beam to allow branch cable distribution toward surrounding dashboard systems.

The left-side routing region was developed near the green connector location to support branch cable integration and improve accessibility during assembly procedures. Another routing region was positioned near the rear side of the tube where the red cable exists, allowing continuation of the harness toward additional vehicle subsystems.

Although the enlarged openings improved routing capability, the internal movement of the harness inside the beam created the need for a dedicated cable management system. Therefore, a cable guide mechanism was developed in order to control harness positioning during insertion, operation, and maintenance procedures.

The cable guide system was designed to support the primary harness during insertion through the beam openings while preventing uncontrolled movement inside the hollow structure.

The guide geometry provided a controlled routing path that minimized direct contact between the cable bundle and the internal beam surfaces.

Compared to the original external routing configuration, the cable guide significantly improved harness organization and simplified installation procedures. Instead of manually positioning multiple external branches around surrounding dashboard components, the optimized system allowed a more direct and organized internal insertion process.

Another important component integrated into the optimized routing system was the clip mechanism. In the original design, branch cables were attached externally using conventional fixing methods that occupied additional dashboard space and increased assembly complexity.

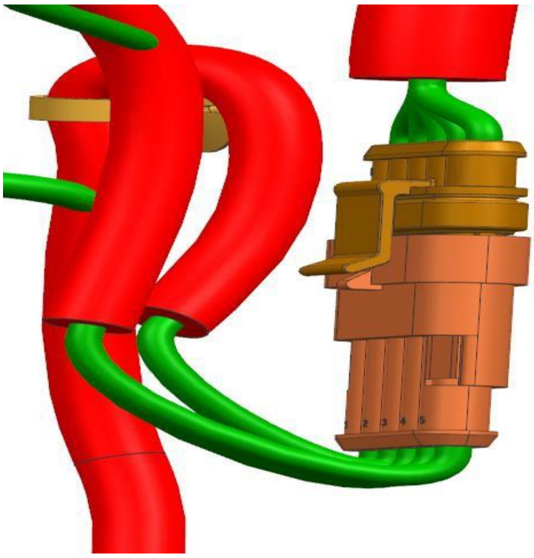

Figure 3.30 Old solution for making connect main cables

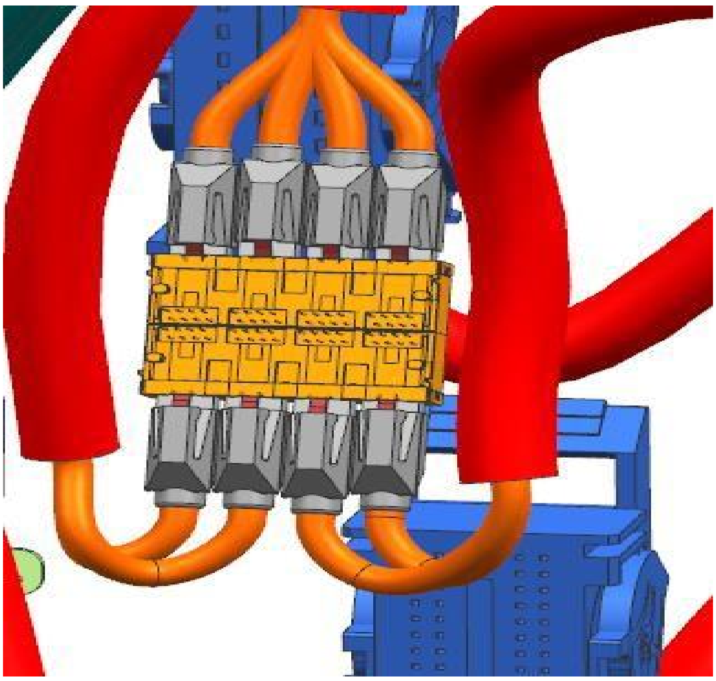

Figure 3.31 New solution for making connect main cables

Thanks to the by using clip mechanisms this solution allows us to make connect or disconnect easily of main cables otherwise that would be take time operation by using screwdriver to extract mini cables from connector.

The redesigned clip system provided more compact attachment points for branch cable management while improving positioning stability during vehicle operation. The clips also reduced uncontrolled cable movement generated by vibration and dynamic loading conditions

Special attention was also given to simplifying branch cable integration through the development of modular connector architecture. The optimized system incorporated male and female socket configurations together with a Wago carrier structure to improve modularity and simplify assembly operations.

The Wago carrier system functioned as a central distribution structure for the electrical connections inside the dashboard assembly. Instead of routing multiple independent branch cables externally, the modular carrier allowed organized connection of electrical branches through standardized interfaces.

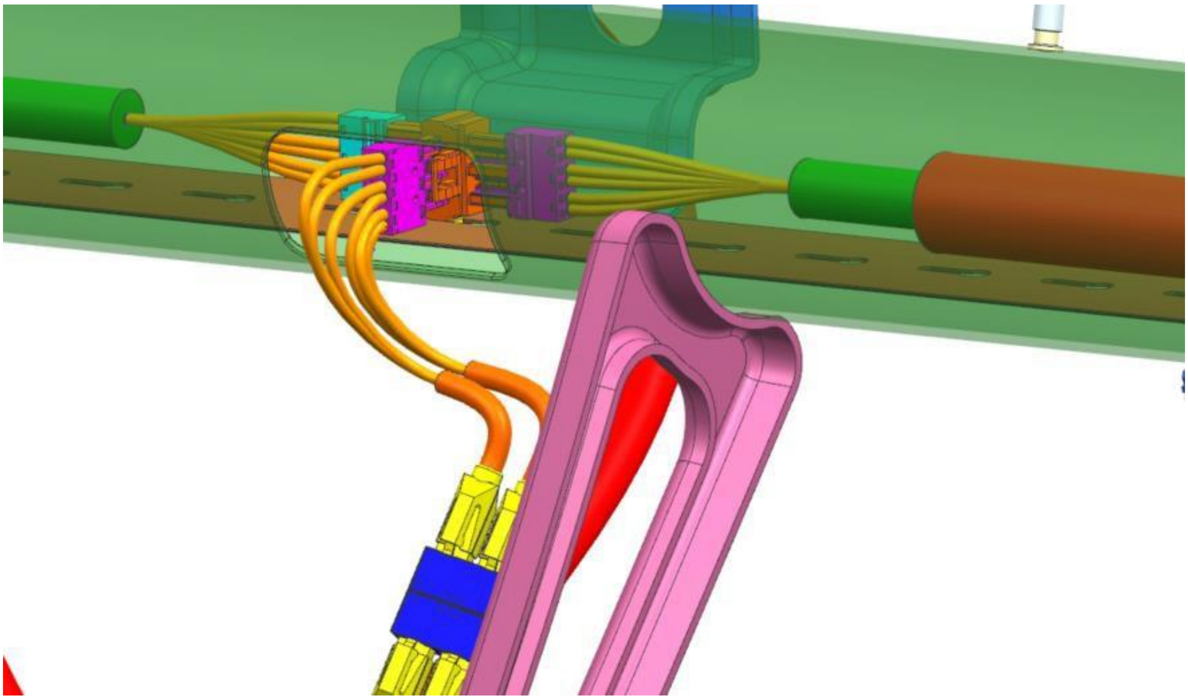

Figure 3.32 Wago carrier and clip mechanisms layout for routing cable management

The modular connector concept also improved serviceability and maintenance accessibility. During repair procedures, individual branch connections could be disconnected independently without requiring complete removal of the main harness assembly. This reduced maintenance complexity and improved accessibility inside the dashboard structure.

Another major advantage of the Wago carrier configuration was the improvement of cable organization around the branch connection regions.

The distributor system reduced cable congestion and created a more compact electrical architecture inside the dashboard assembly.

Because the enlargement of the beam openings introduced structural discontinuities into the tubular beam structure, reinforcement elements were required around the modified regions. Therefore, reinforcement plates manufactured from FeE420 sheet metal were integrated around the critical opening areas.

The reinforcement structures were developed to improve local stiffness and reduce stress concentration effects generated by the enlarged openings. Particular attention was given to the center opening region because this area experienced the largest geometric modification within the beam structure.

The reinforcement plate geometry was designed according to the shape of the modified openings while maintaining compatibility with the internal routing configuration. The reinforcement structures improved structural stability without significantly reducing the available internal routing volume.

Throughout the development process, multiple CAD iterations were evaluated in order to achieve a balanced relationship between routing capability, packaging efficiency, assembly accessibility, structural stiffness, and manufacturability.

The final optimized routing system successfully integrated internal harness routing, modular connector distribution, cable guidance mechanisms, clip systems, and reinforcement structures into a unified dashboard support architecture.

Compared to the original configuration, the optimized design provided improved packaging efficiency, better cable organization, simplified assembly operations, enhanced serviceability, increased routing protection, and improved dashboard space utilization.

Figure 3.33 Comparison between old and new layout

3.5 Cable Guide Processes and Harness Routing Configuration

As for cable guide development, there were made some strategies to carry cable layout easily through inside of the beam. The one that is cable guide + rail system

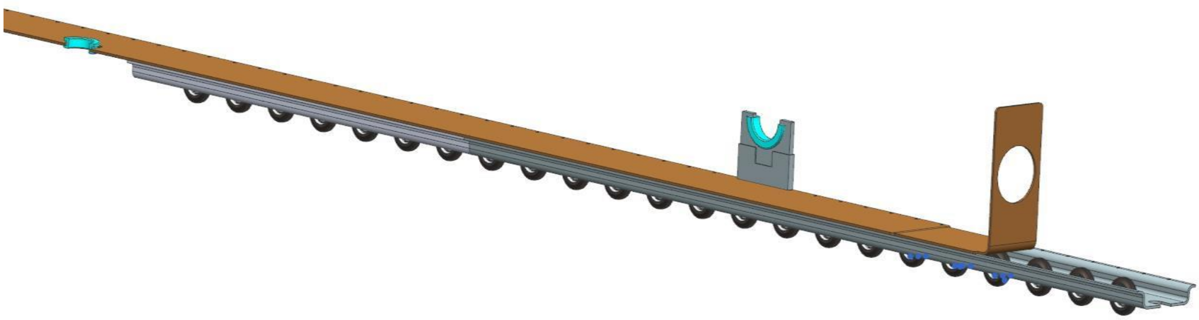

Figure 3.34 Cable guidance and rail system

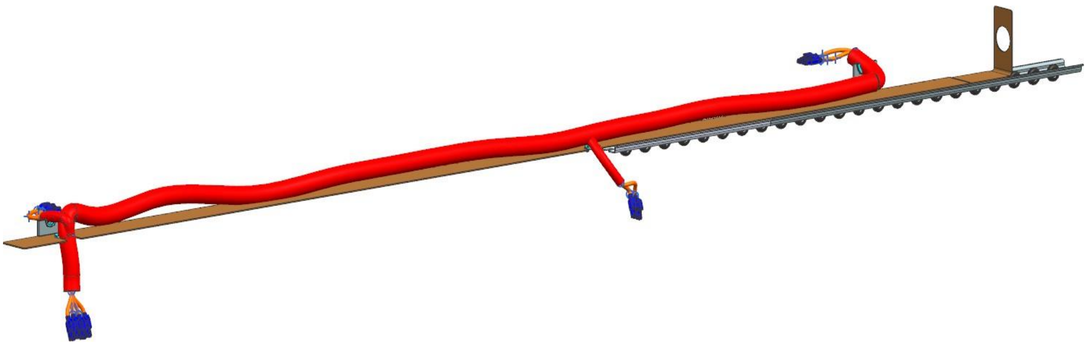

Figure 3.35 Cable guidance – rail system and cable layout

Figure 3.35 illustrates the preparation of the main wiring harness before installation inside the Cross-Car Beam (CCB). Owing to the developed cable guide system, each branch of the harness corresponds to a specific exit point of the CCB, allowing the branch cables to be extracted more easily during assembly and maintenance operations. This routing concept improves cable organization and simplifies harness distribution inside the dashboard structure. However, the efficiency of the system strongly depends on the availability and positioning of dedicated exit openings on the Cross-Car Beam. During the initial design stage, a rail-based guiding system was also considered as a possible solution for supporting the harness during routing operations. Although the rail system provided controlled cable movement, there was concern regarding possible contact between the rail mechanism and the inner surface of the Cross-Car Beam during installation or operational vibration conditions. Such contact could potentially lead to local deformation, vibration-related wear, or undesirable interaction with the beam structure over time. Therefore, an improved routing configuration was developed in order to eliminate these risks and provide a safer and more reliable cable guidance mechanism. The following figure presents the newly developed routing configuration and the updated cable guide design integrated into the optimized Cross-Car Beam structure.

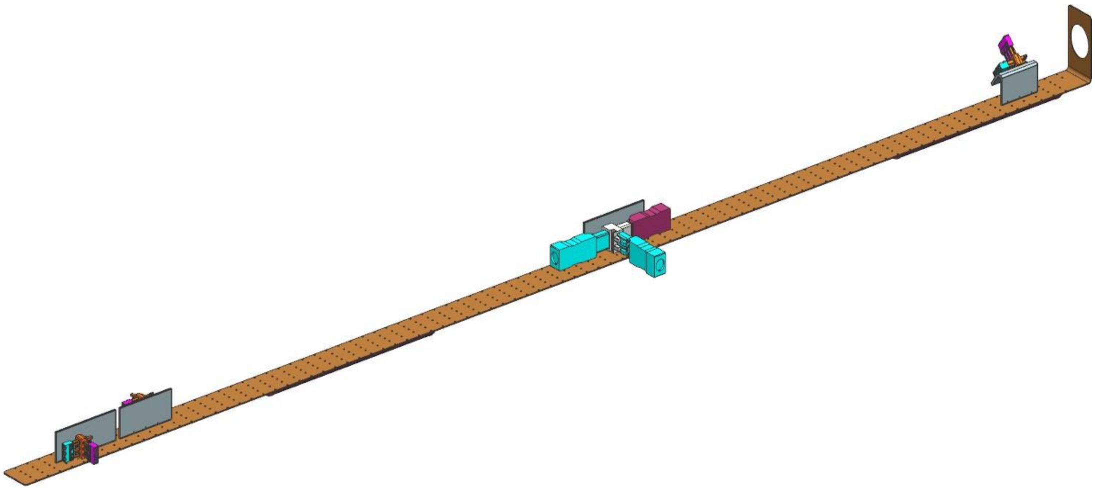

Figure 3.36 Cable guidance – ground rubber support system layout

Figure 3.37 Ground rubber support system

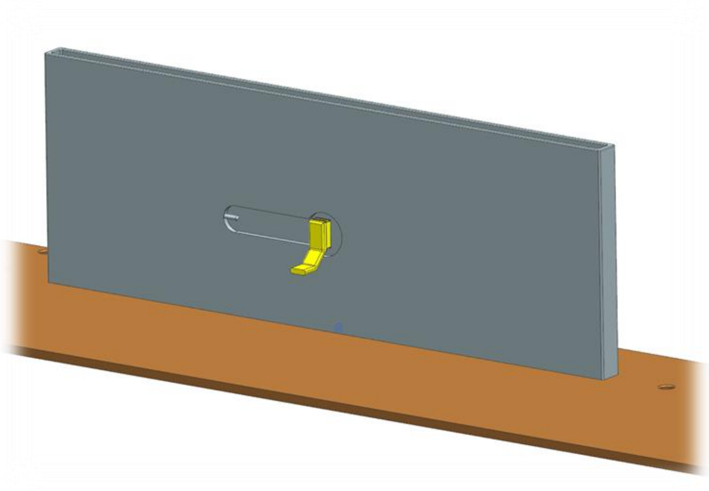

Figure 3.38 Reinforcement plate structure

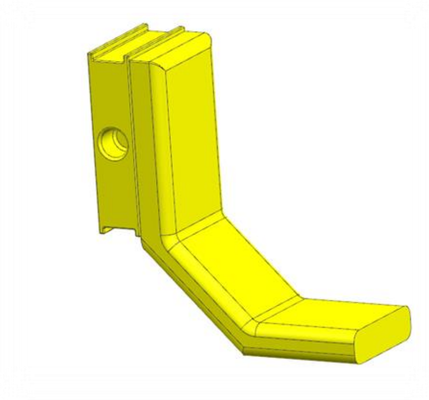

Figure 3.39 The hook for engaging with Wago carrier

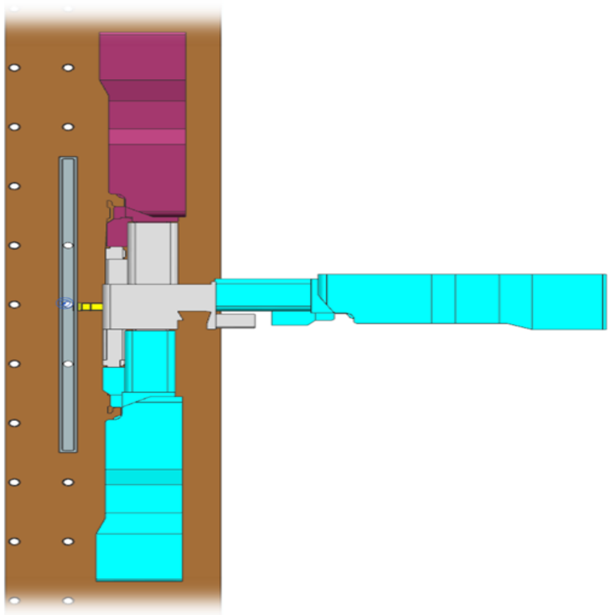

Figure 3.40 Assembly of Wago carrier, hook and reinforcement plate structure

New Figures present the newly developed routing configuration and the updated cable guidance concept integrated into the optimized Cross-Car Beam structure. As shown in **Figure 3.44**, the Wago connection system was successfully integrated into the routing architecture in order to improve modularity and simplify branch cable management.

Figure 3.41 Wago distribution

Figure 3.42 Wago male connector

Figure 3.43 Wago female connector

In addition to the Wago integration, two important design improvements were introduced into the new configuration: the ground rubber support system and the reinforcement plate structure engaged with the Wago connections. The first improvement involved replacement of the previously considered rail-based support system with a ground rubber solution positioned beneath the Cross-Car Beam. As discussed previously, the rail system could potentially create direct contact with the beam structure during routing operations or vibration conditions. Such interaction might result in local deformation, unwanted vibration effects, or surface wear on the Cross-Car Beam. To eliminate these risks, a ground rubber support element was introduced beneath the beam structure. The rubber component provides controlled support for the routing system while minimizing direct rigid contact between the cable guidance components and the Cross-Car Beam. This solution improves vibration isolation and reduces the possibility of local structural deformation during operation. The second major improvement was related to stabilization of the Wago connection system during cable assembly operations. As previously mentioned, the main wiring harness is prepared before installation inside the Cross-Car Beam. However, several branch cables are connected externally through the designated exit points located along the beam structure. During these connection procedures, assembly forces are applied to the Wago connections while attaching or removing branch cables. Under such loading conditions, the Wago carrier system may potentially slide toward the left-hand or right-hand side of the structure. This undesired movement could complicate assembly procedures, reduce positioning accuracy, and increase installation time. In order to prevent such displacement, a dedicated reinforcement plate was developed and integrated with the Wago carrier structure. The reinforcement plate was designed to stabilize the Wago connections during cable installation and extraction operations. By restricting unwanted movement of the carrier system, the reinforcement structure improves assembly stability and provides a more reliable connection interface during maintenance and routing procedures. In addition to improving operational stability, the reinforcement plate also contributes to improved structural rigidity around the connection region. The integrated design therefore enhances both mechanical support and assembly efficiency within the optimized routing configuration.

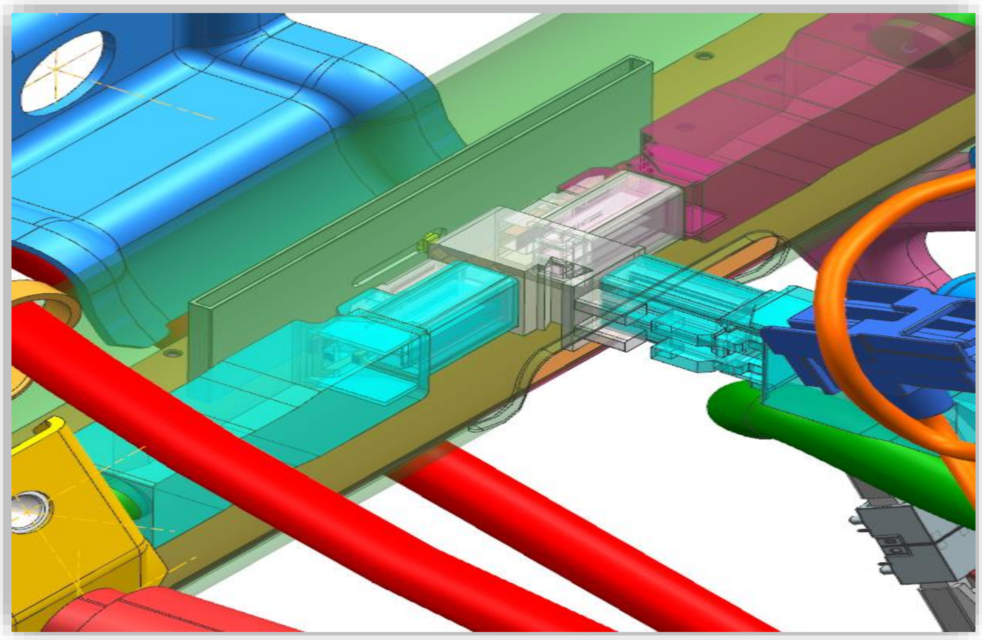

Figure 3.44 Detailed view while making connection

As can be seen in **Figure 3.44**, during these operations the blue male connector is attached from the outside of the CCB because it remains fixed thanks to the reinforcement plate structure and screw hole, and the Wago carrier does not slide to the right or left after assembly. The Wago carrier can be easily removed from the reinforcement plate structure by using the blue connector and can be removed by simply sliding it to the right after assembly, because we designed a hook for such easy removal. However, while this system was indeed feasible in terms of being used globally and for duration, the problem still lay with the reinforcement plate structure; because this structure was made of sheet metal, the risk of any local deformation in the CCB during the orientation process reappeared. Therefore, we redesigned this system to prevent any local deformation from metal part also to avoid leakage at the connection entry points by using plastic hook supports and locking caps respectively, switched from the Wago connector to the Wago-mini connector for space saving, and additionally changed the cable guidance layout. Some figures illustrating these changes are shown below.

Figure 3.45 Wago-mini distribution

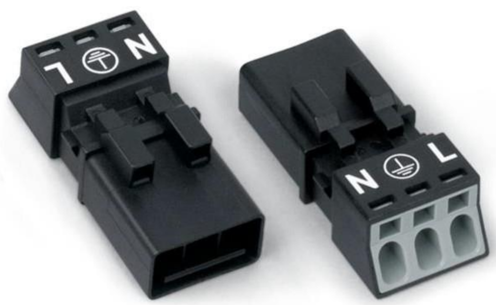

Figure 3.46 Wago-mini male connector

Figure 3.47 Wago-mini female connector

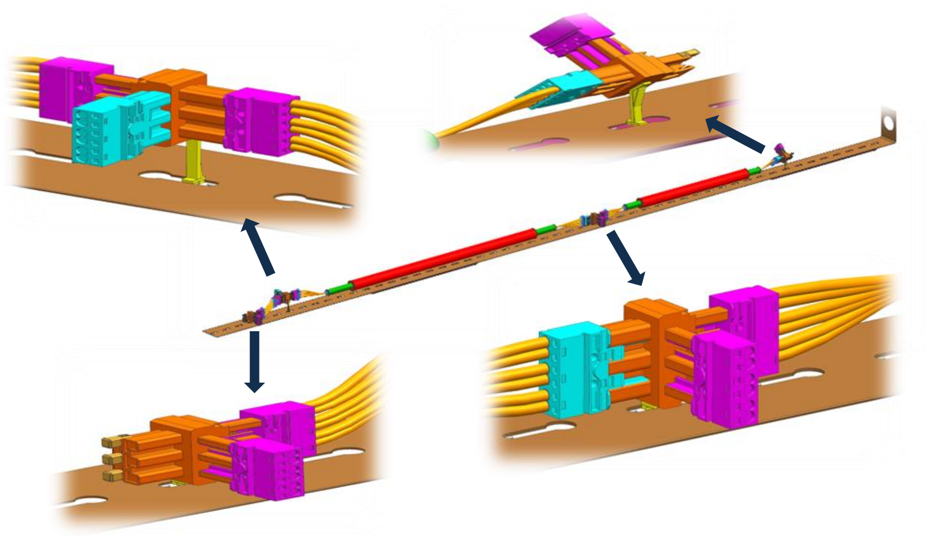

Figure 3.48 New cable guidance general layout

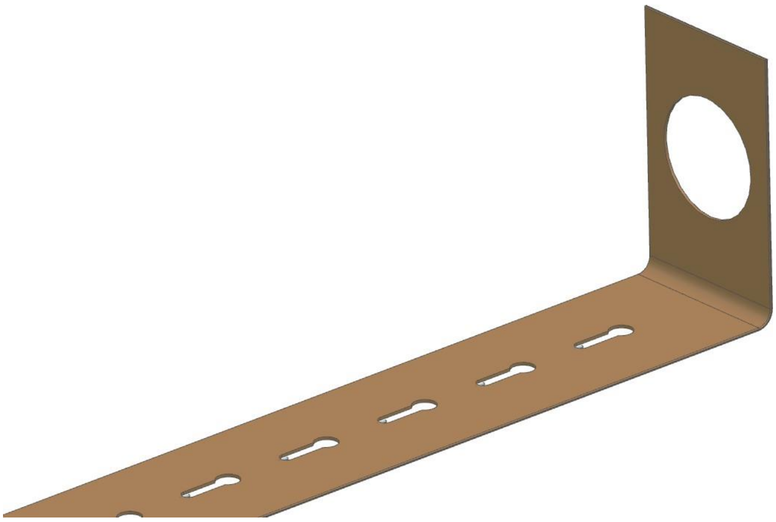

Figure 3.49 New cable guidance layout

Figure 3.50 New plastic hook supporter

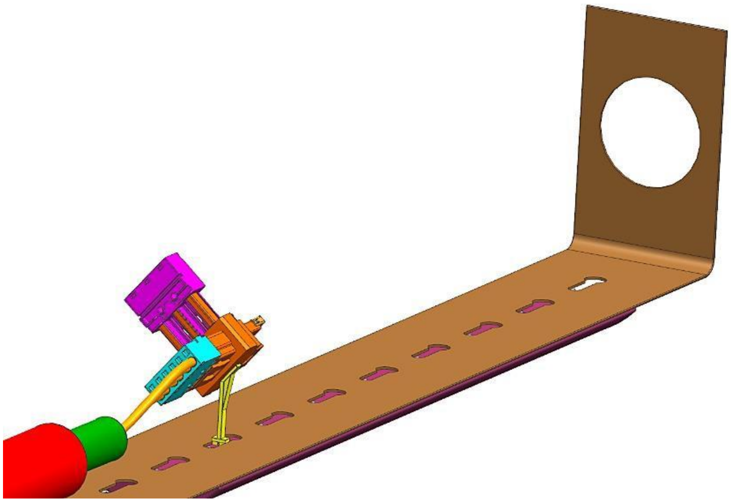

Figure 3.51 First Wago-mini carrier assembly detailed view

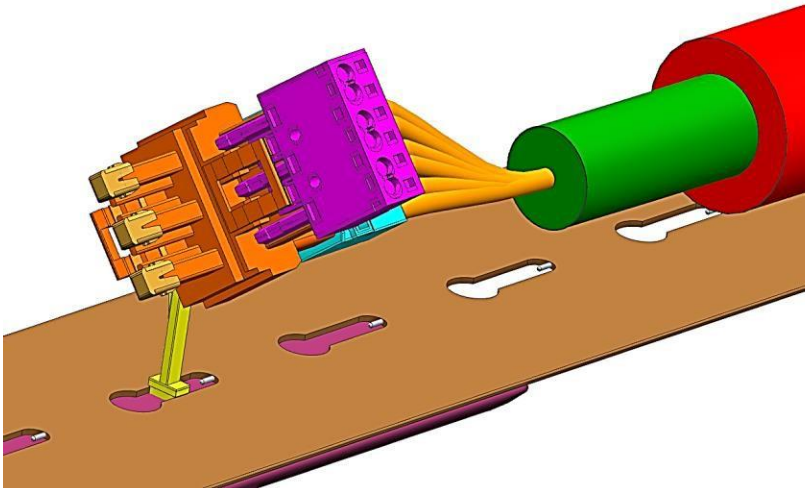

Figure 3.52 First Wago-mini carrier assembly with locking cap detailed view

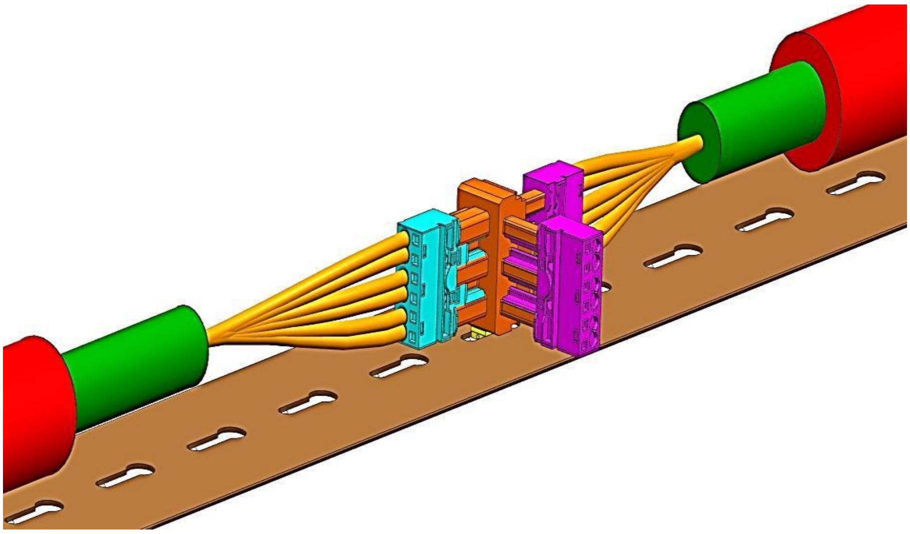

Figure 3.53 Second Wago-mini carrier assembly detailed view

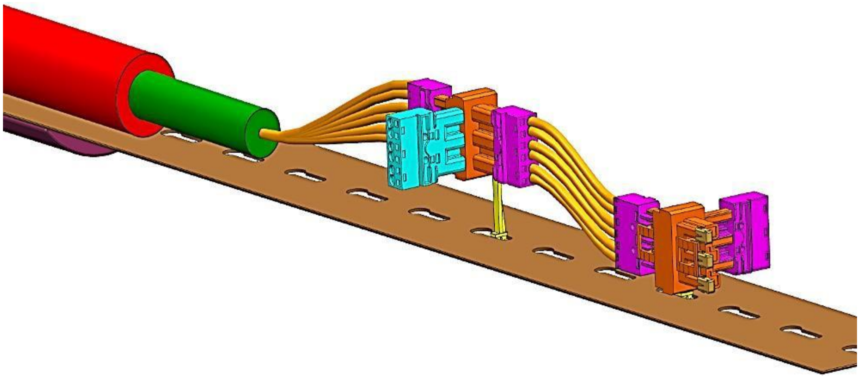

Figure 3.54 Third and fourth Wago-mini carrier assembly detailed view

3.6 Final Optimized Assembly Configuration

The final optimized assembly configuration represents the complete integration of the redesigned Cross-Car Beam structure, internal wiring harness routing system, cable guide mechanism, modular connector architecture, reinforcement structures, and Wago-mini carrier system into a unified dashboard support assembly.

The objective of the final configuration was to combine all previously developed optimization components into a compact and functional routing architecture capable of improving packaging efficiency, cable organization, assembly accessibility, and structural stability simultaneously.

In the final assembly, the primary wiring harness was successfully relocated inside the hollow Cross-Car Beam structure through the enlarged routing openings developed during the optimization process. The internal routing path allowed the main cable bundle to travel through the beam while branch cables were distributed externally through dedicated exit regions.

The center opening region functioned as the primary transition area for the main harness insertion into the beam structure. Additional routing openings located near the left-hand and right-hand sides of the beam enabled controlled branch distribution toward surrounding dashboard systems.

The optimized cable guide system was fully integrated into the final assembly in order to control harness positioning and simplify installation procedures. The guide structure supported the harness during insertion and extraction operations while preventing excessive movement inside the hollow beam section.

Compared to the original external routing configuration, the final assembly significantly improved organization of the electrical architecture inside the dashboard system. The internal routing concept reduced cable congestion around surrounding components and created additional packaging space for HVAC ducts, infotainment systems, and electronic modules.

Another major improvement achieved in the final assembly was the integration of the modular Wago-mini connection system. The Wago-mini carrier, together with the male and female socket structures, provided a compact and organized interface for branch cable distribution.
The modular connector system simplified assembly and maintenance operations by allowing individual branch connections to be connected or disconnected independently. This improved accessibility and reduced the complexity of service procedures within the dashboard assembly.
The ground rubber support system was also incorporated beneath the Cross-Car Beam in order to reduce direct rigid contact between the routing components and the beam structure. This configuration minimized the possibility of local deformation and improved vibration isolation during operational loading conditions.

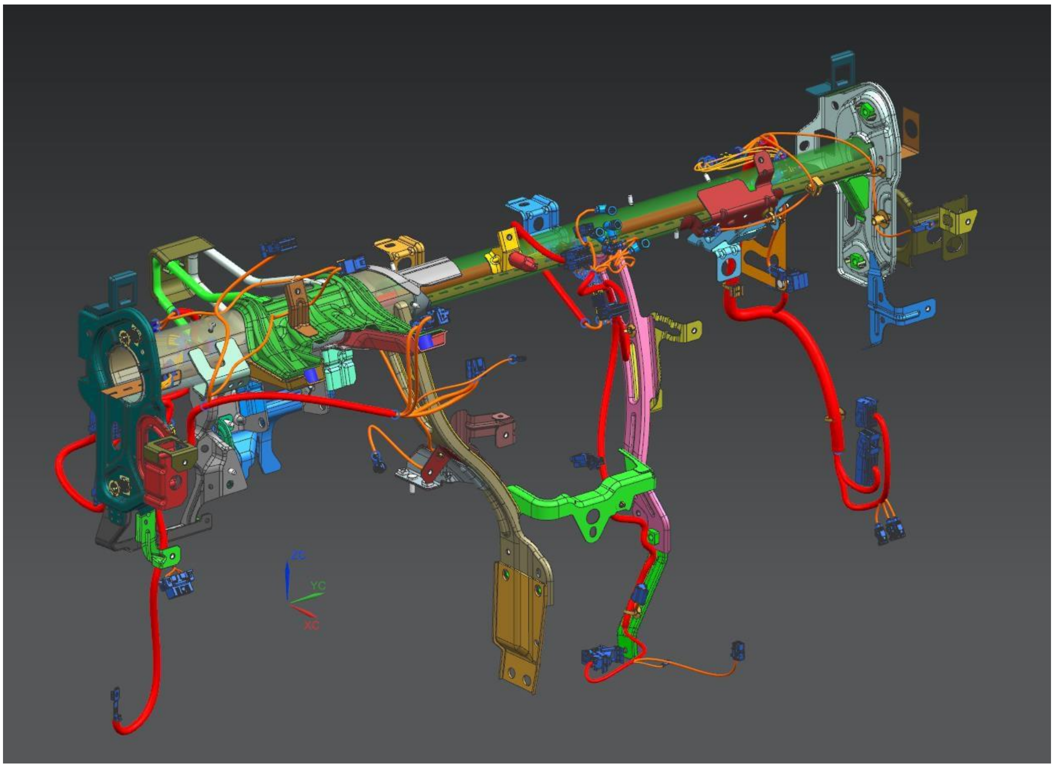

Figure 3.55 Cross-Car Beam structure and new cable guidance layout iso-view

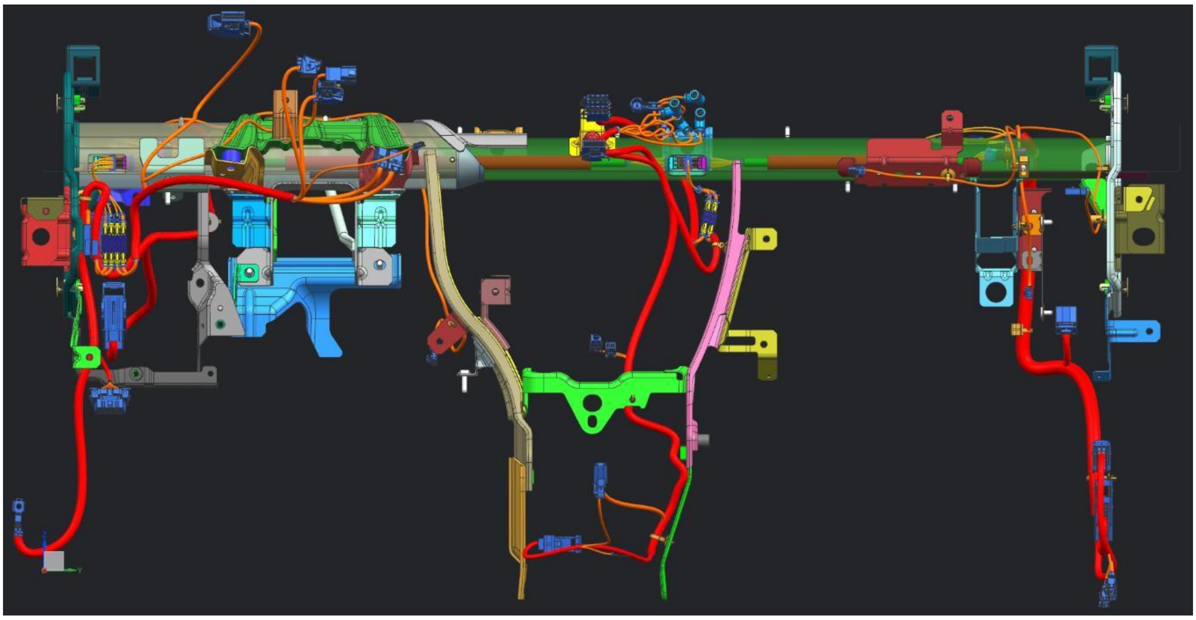

Figure 3.56 Cross-Car Beam structure and new cable guidance layout front-view

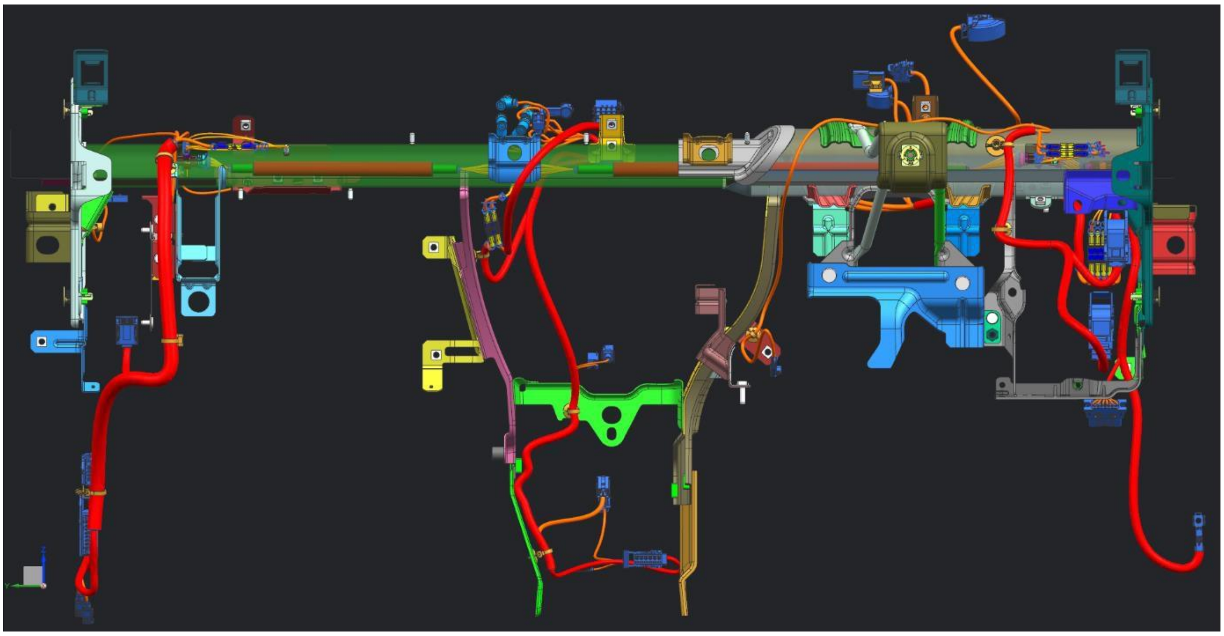

Figure 3.57 Cross-Car Beam structure and new cable guidance layout back-view

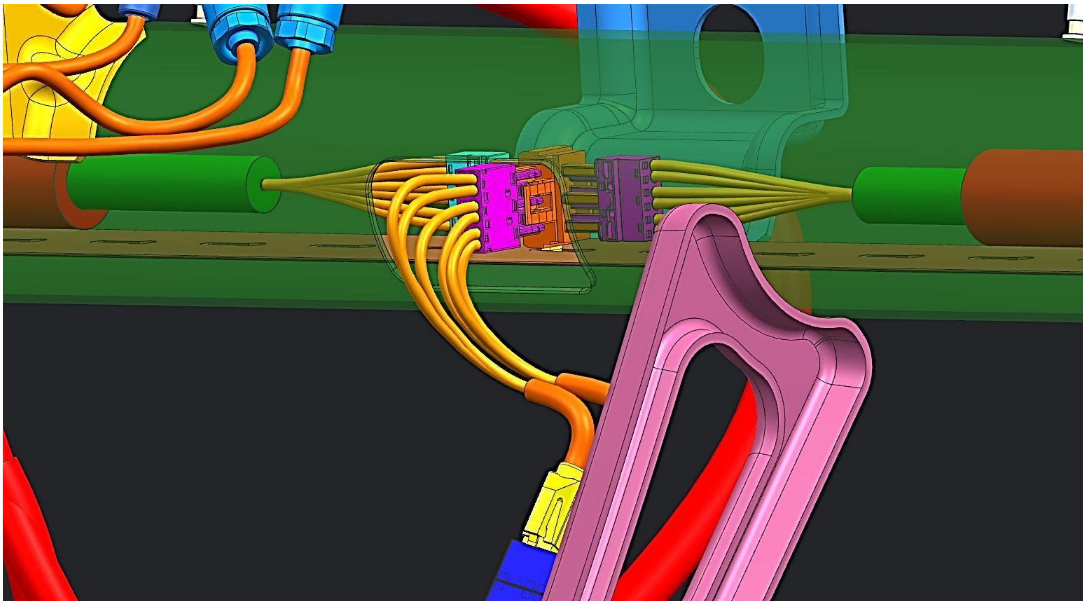

Figure 3.58 First Wago-mini connector detailed view

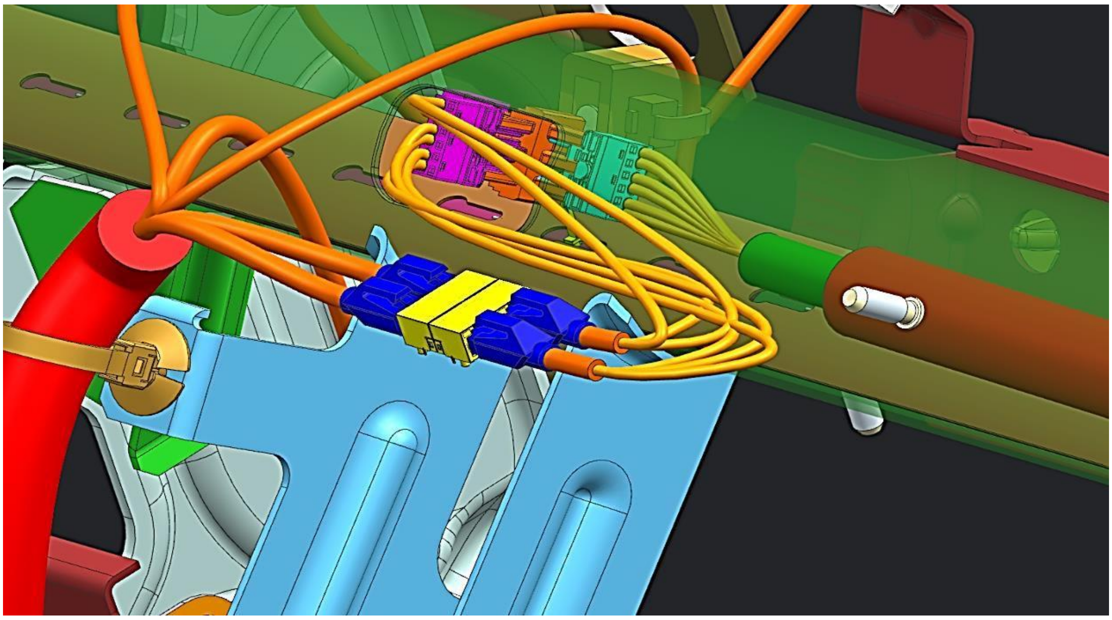

Figure 3.59 Second Wago-mini connector detailed view

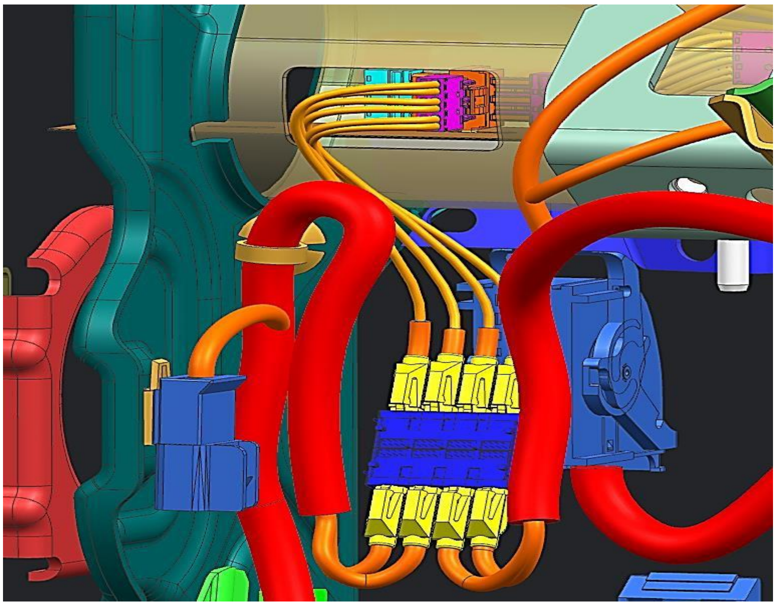

Figure 3.60 Third Wago-mini connector detailed view

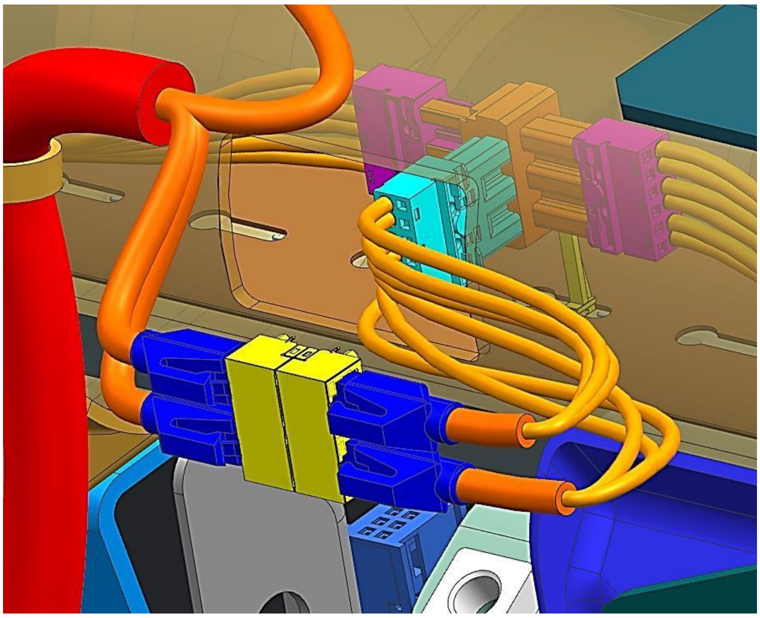

Figure 3.61 Fourth Wago-mini connector detailed view

3.7 Air Duct – Cross-Car Beam Displacement, Area and, Volume Analysis

We previously saw the differences between the original and optimized versions. Now, we will examine in detail how much space we have gained in terms of measurement, area and volume; we will also look at the cross-sectional view. This progress is most important because we are changing the geometry of the CCB because we want to both improve the space and reduce complexity and analyze the robustness of the CCB after modification. But for now, we will focus on how much space we have gained thanks to the modified version.

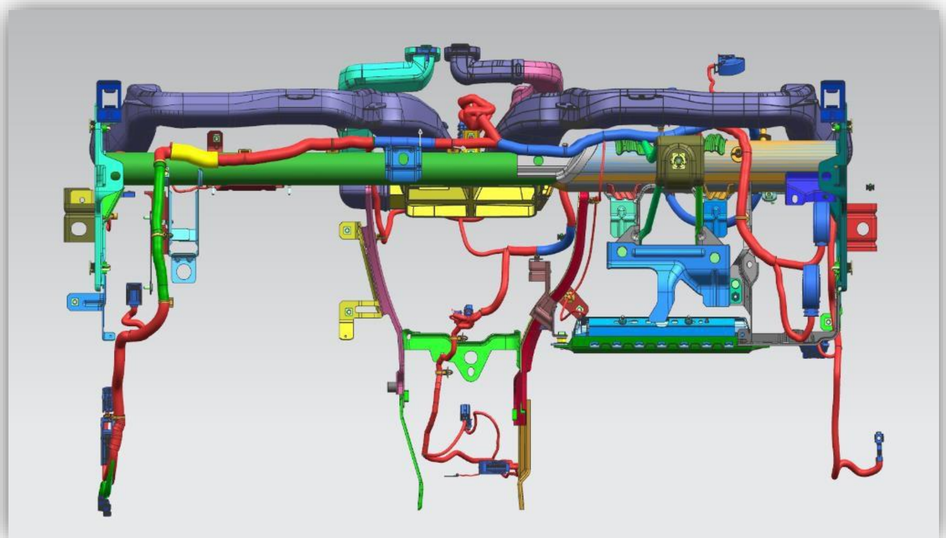

Figure 3.62 Airduct, Cross-Car Beam Structure of solid model

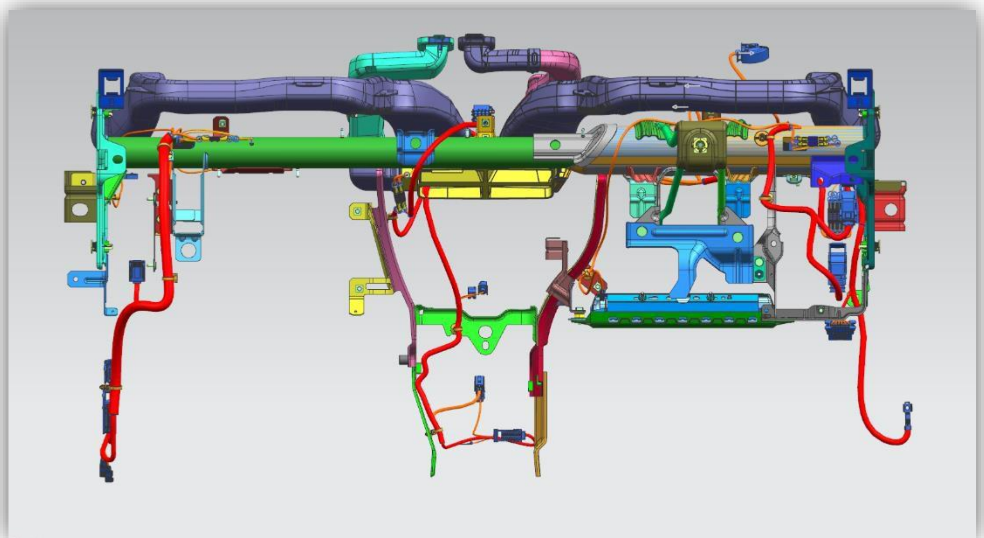

Figure 3.63 Airduct, Cross-Car Beam Structure of optimized model

First consideration will be related to the displacement between Airduct and Cross-Car Beam structure of solid and optimized model

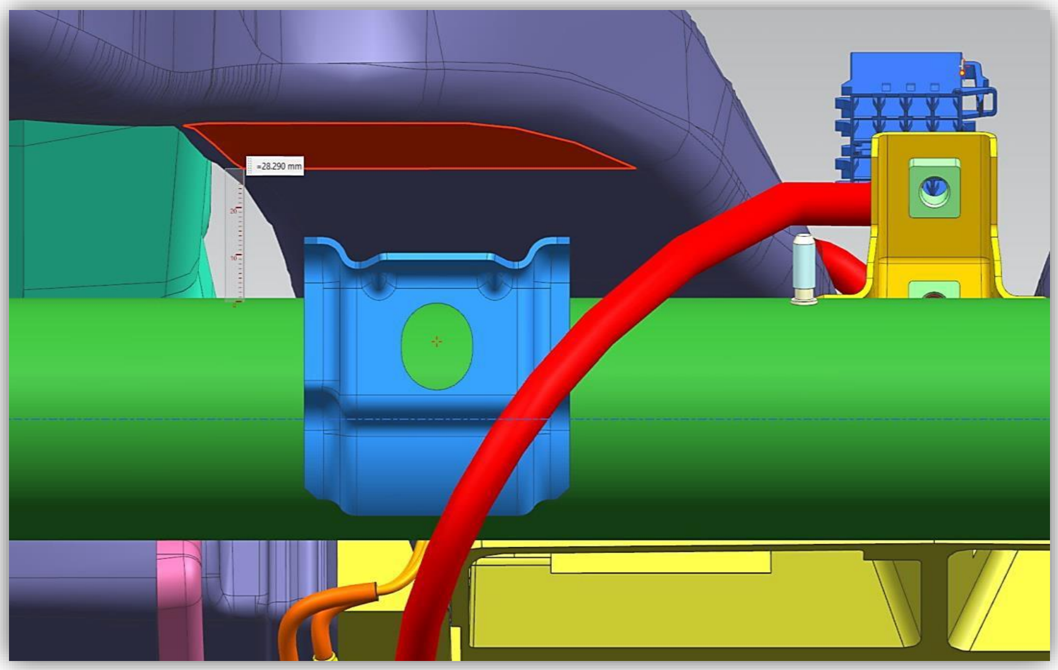

Figure 3.64 Airduct, Cross-Car Beam displacement of optimized model

can be seen that from **figure 3.64** the value is **28.290 mm**

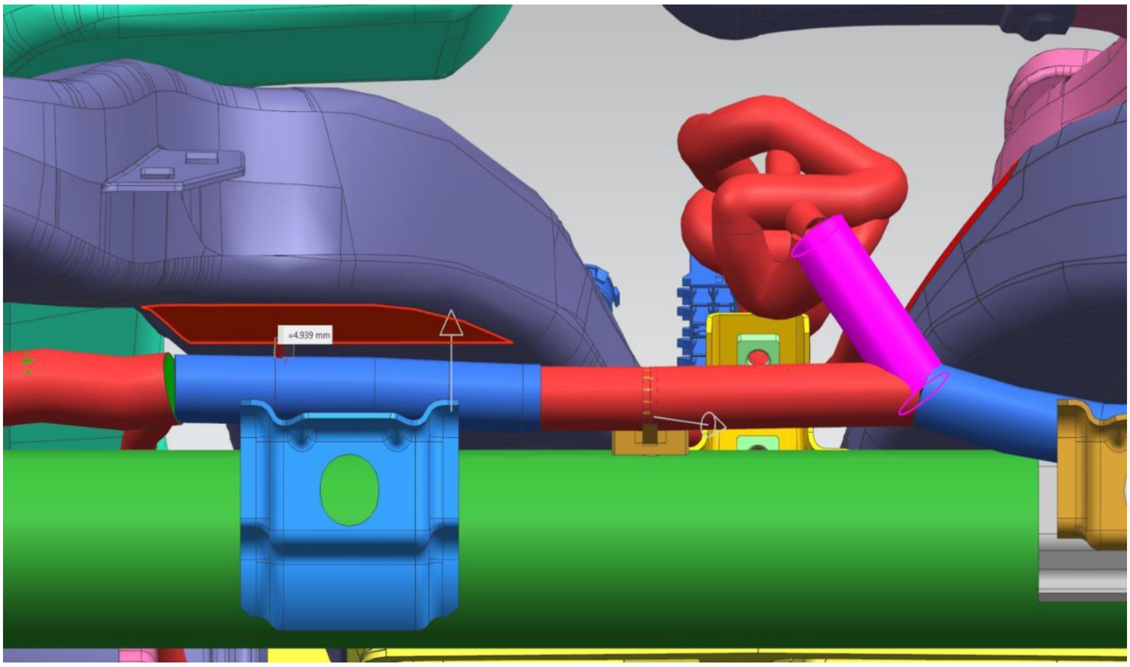

Figure 3.65 Airduct, Cross-Car Beam displacement of solid model

However, here displacement is **4.939 mm** compared to optimized model we have less space.

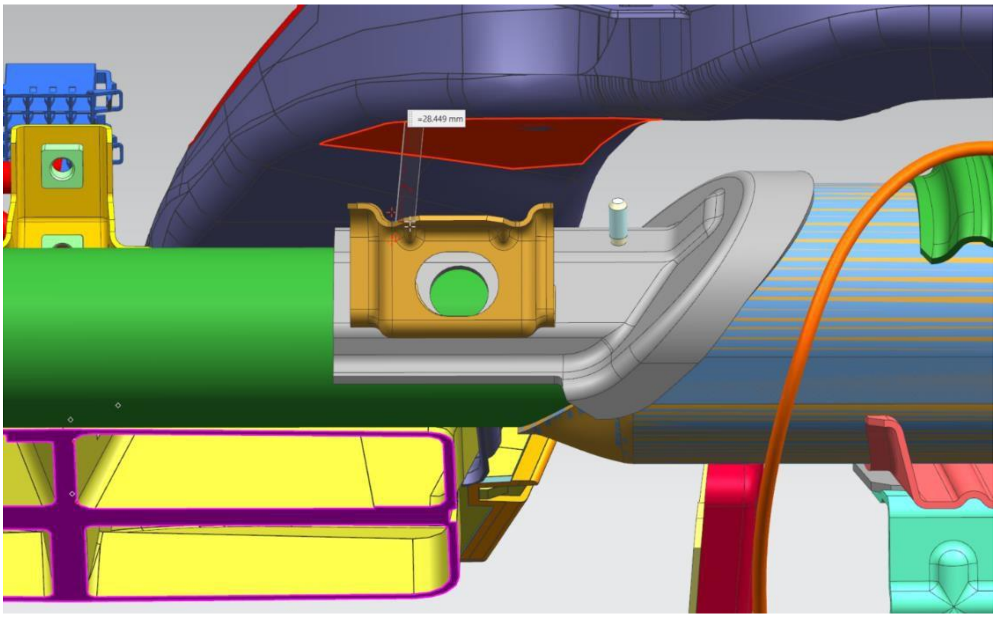

Figure 3.66 Airduct, Cross-Car Beam displacement of optimized model

Here in the optimized model displacement is **28.449 mm**

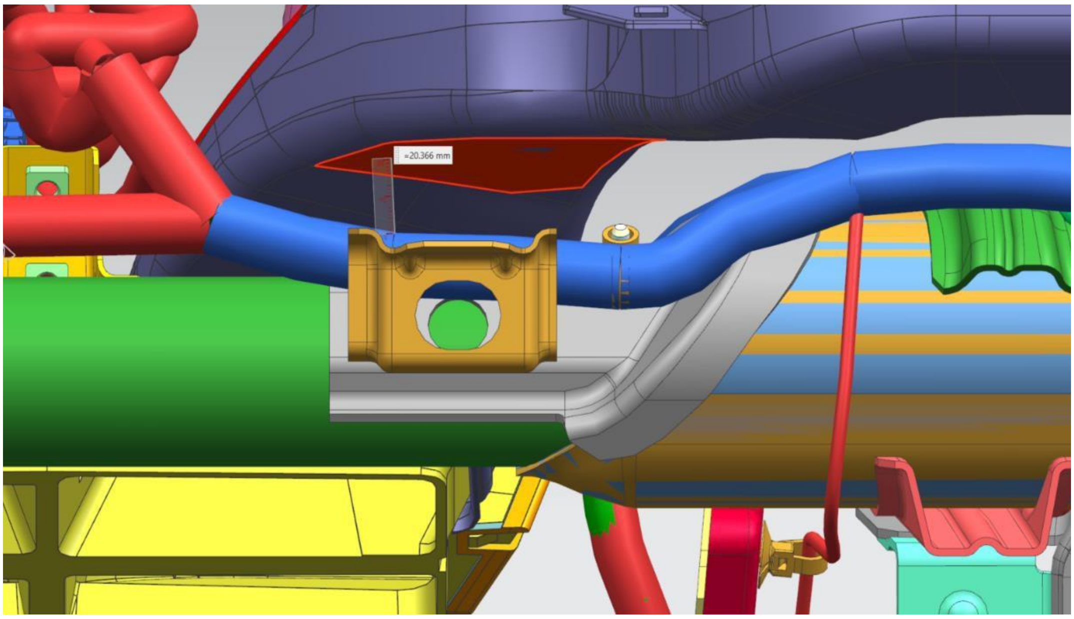

Figure 3.67 Airduct, Cross-Car Beam displacement of solid model

Here in the solid model displacement is **20.366 mm**

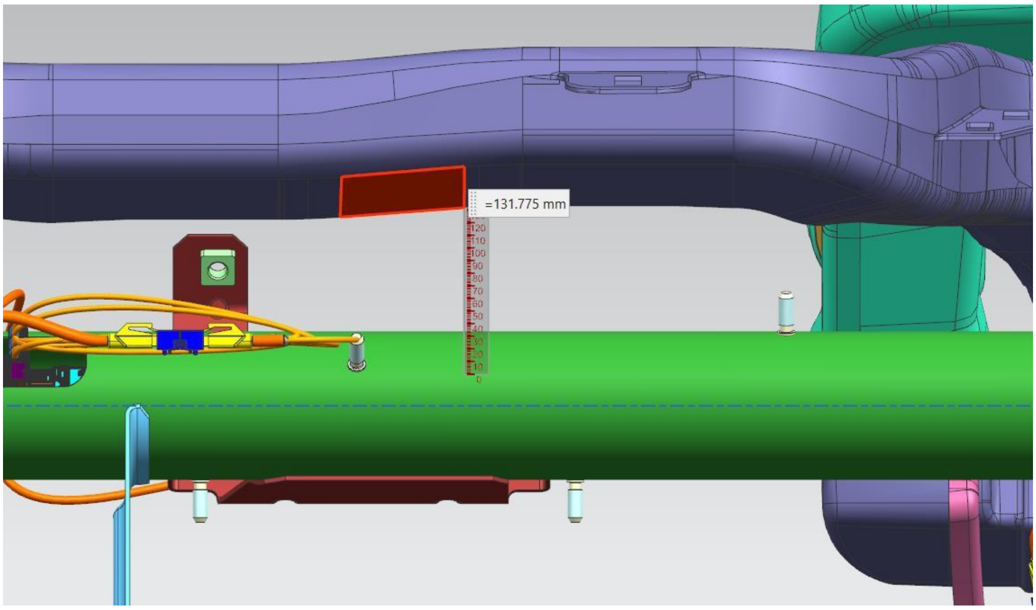

Figure 3.68 Airduct, Cross-Car Beam displacement of optimized model

Here we have **131.775 mm** space in optimized model

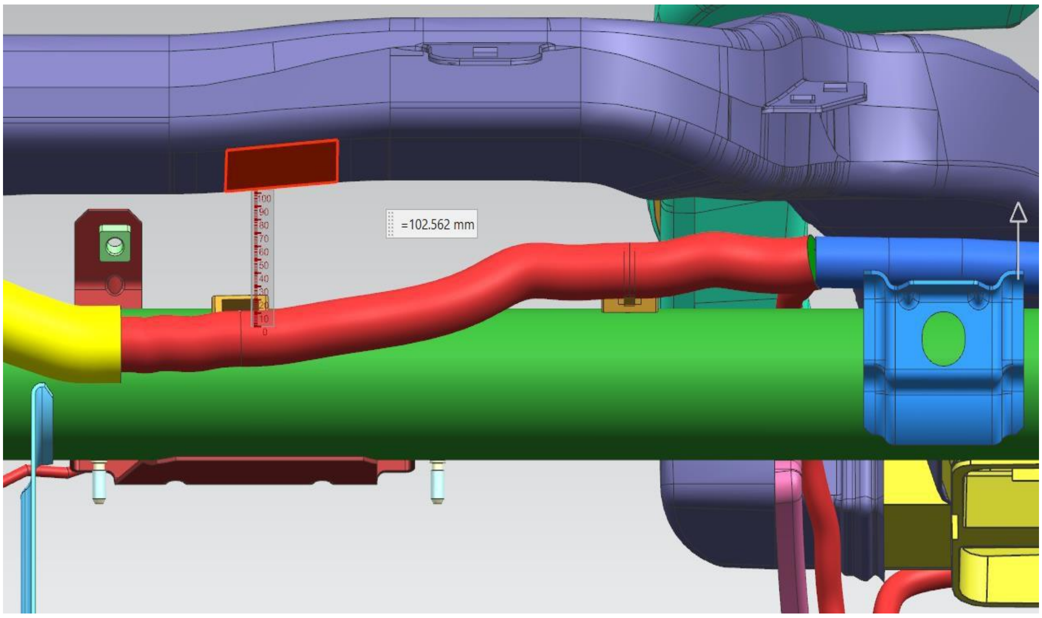

Figure 3.69 Airduct, Cross-Car Beam displacement of solid model

However, the solid model we have **102.562 mm** space between Airduct and CCB

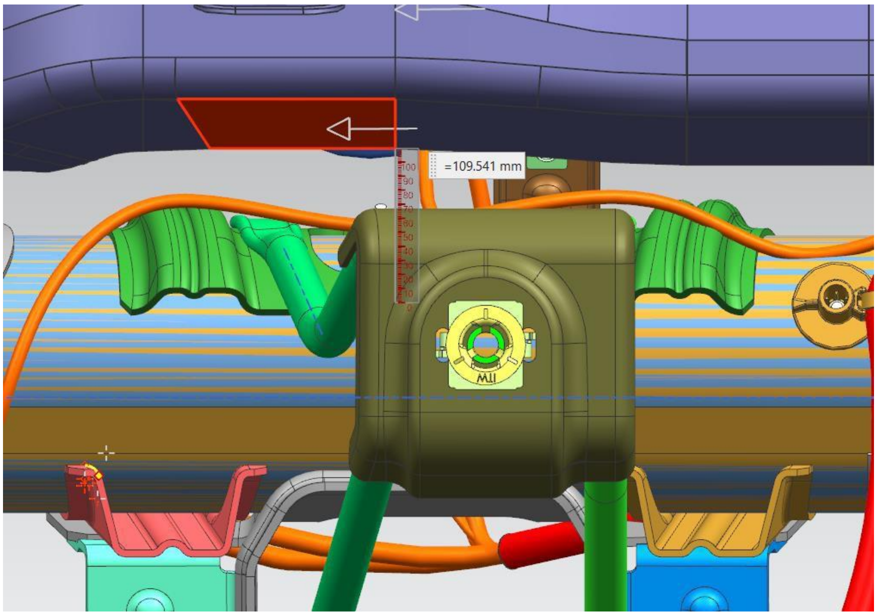

Figure 3.70 Airduct, Cross-Car Beam displacement of solid model

The optimized model space between Airduct and CCB where steering wheel side is 109.541mm.

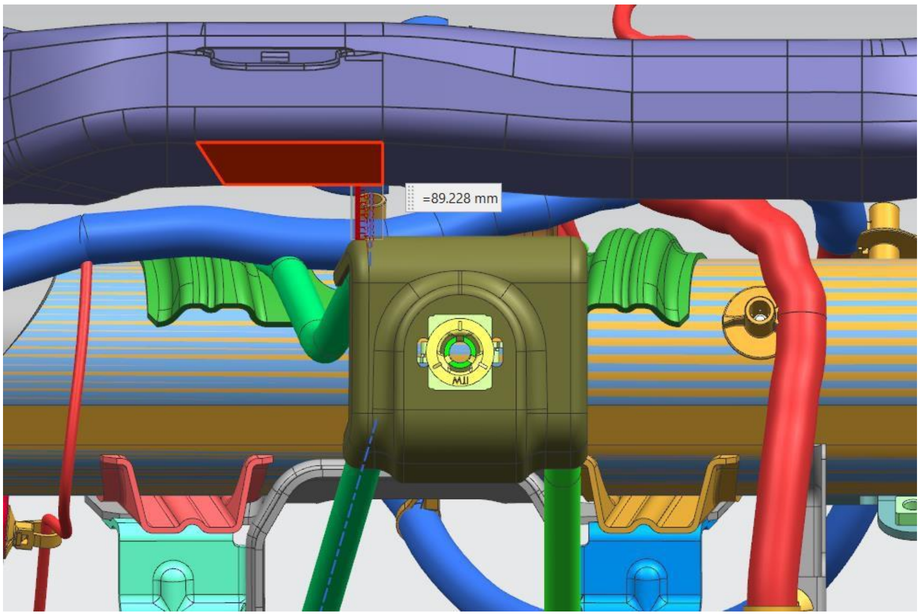

Figure 3.71 Airduct, Cross-Car Beam displacement of solid model

The solid model, space between Airduct and CCB where steering wheel side is **89.228 mm.**

Table 3-1 Comparison of the displacement between Airduct – Cross Car Beam at the solid and optimized model

Measurement Point	Solid Model (mm)	Optimized Model (mm)	Difference(mm)	Change (%)
Point 1	4.939	28.290	+23.351	+472.8 %
Point 2	20.366	28.449	+8.083	+39.7%
Point 3	102.562	131.775	+29.213	+28.5%
Point 4	89.228	109.541	+20.313	+22.8%

Now, we will look at other important criteria such as the area and volume comparison that occupied on the dashboard of optimized and solid model.

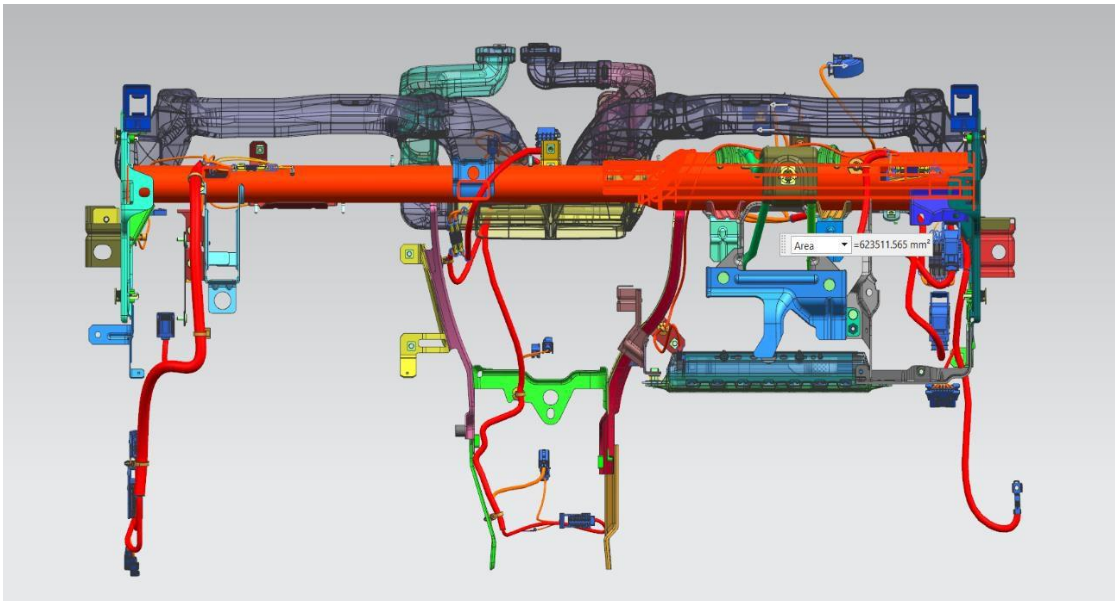

Figure 3.72 Airduct, Cross-Car Beam the area of optimized model

Here the area that occupied by the optimized model is **623511.565 mm^2**

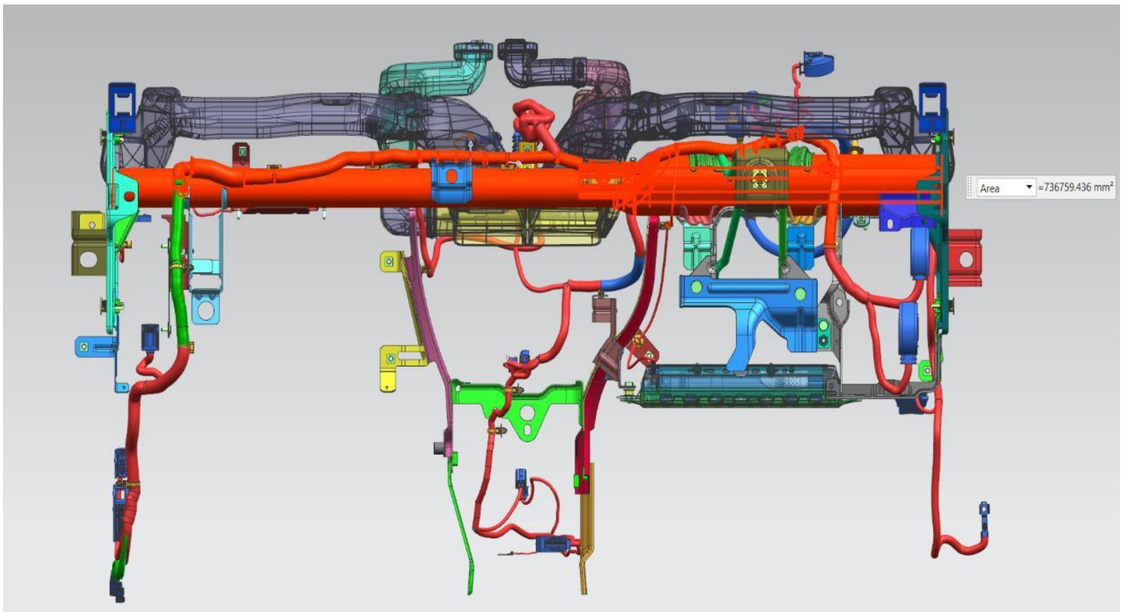

Figure 3.73 Airduct, Cross-Car Beam the area of solid model

However, can be seen that from **Figure 3.73** much more space occupied by the solid model because of the cables are **736759.436 mm^2.**

As for volume comparison;

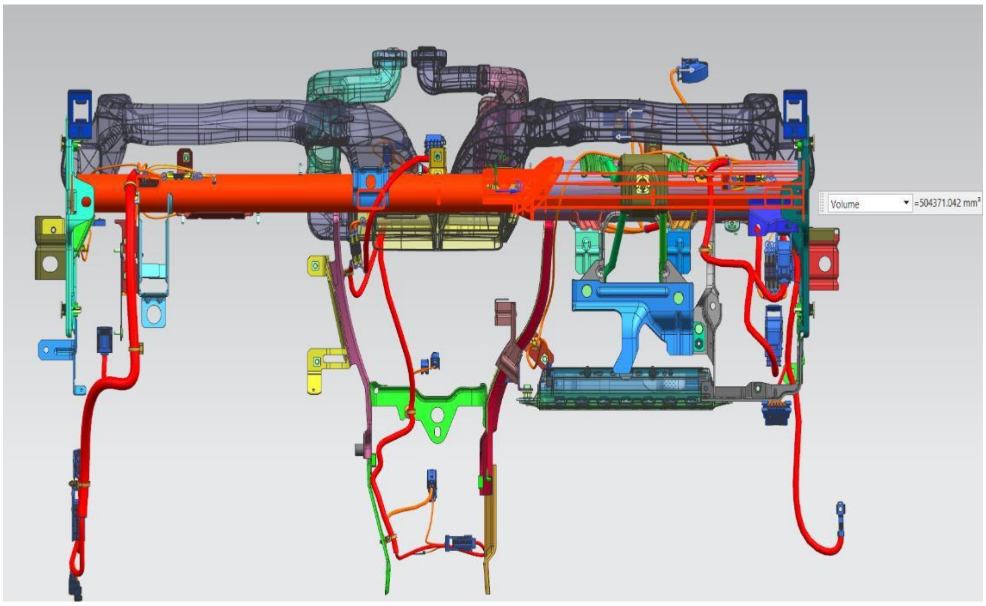

Figure 3.74 Airduct, Cross-Car Beam the area of optimized model

The optimized model volume that is occupied by Cross-Car Beam is **504371.042 mm^3**

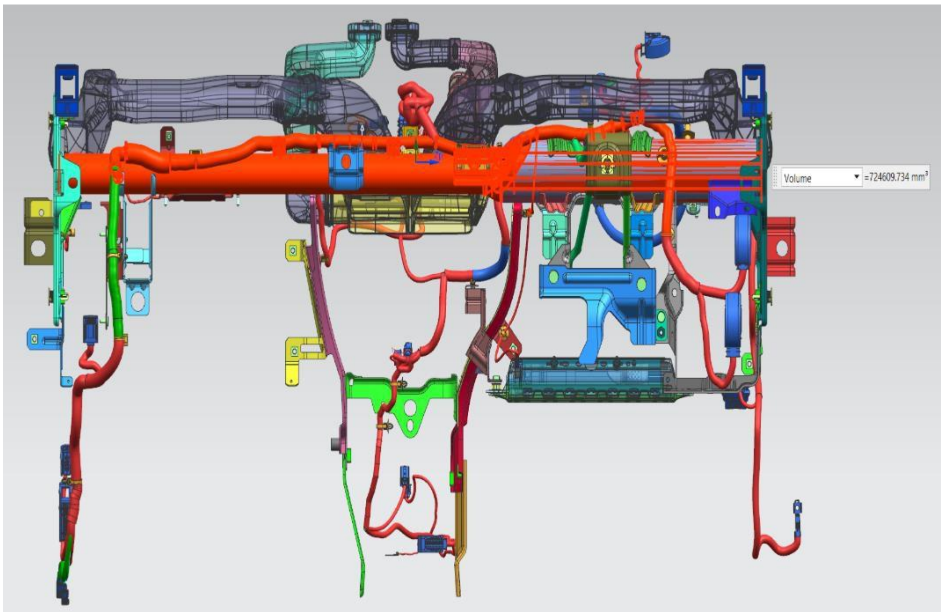

Figure 3.75 Airduct, Cross-Car Beam the area of solid model

As we expected, the solid model will occupy much more space compared to optimized model because existing of cables were located on Cross-Car beam and value is **724609.734 mm^3**

Table 3-2 Comparison of the area and volume between Airduct – Cross-Car Beam at the solid and optimized model

Metric	Solid Model	Optimized Model	Reduction (Saved)	Change (%)
Surface Area (mm^2)	736,759.436	623,511.565	-113,247.871	-15.37 %
Volume (mm^3)	724,609.734	504,371.042	-220,238.692	-30.40 %

Chapter 4 - Materials and Methodology

4.1 Cad Modeling Procedure

Prior to the finite element analysis process, three different Cross-Car Beam (CCB) configurations were prepared and optimized within the CAD and preprocessing environments. The purpose of preparing multiple models was to evaluate the structural influence of the routing openings and reinforcement structures on the mechanical behavior of the Cross-Car Beam assembly.
The first model represented the original solid Cross-Car Beam configuration without any routing openings or structural modifications. This model was considered the reference configuration because it preserved the original tubular beam geometry and structural continuity.

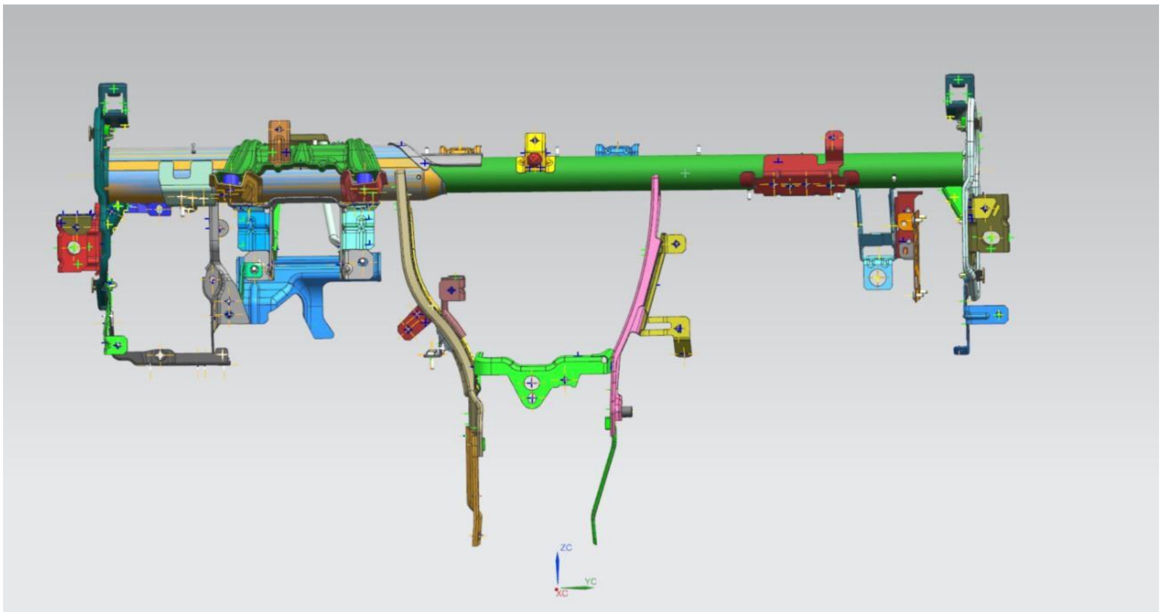

Figure 4.1 Original solid Cross-Car Beam model used as the reference configuration

The solid model was primarily used to establish the baseline structural performance of the Cross-Car Beam under identical loading and boundary conditions. Stress distribution, displacement behavior, and modal characteristics obtained from this configuration were later compared with the modified models.
The second model represented the optimized Cross-Car Beam containing the enlarged routing openings developed for internal wiring harness integration. In this configuration, the beam geometry was modified according to the proposed internal routing concept, and multiple openings were introduced into the tubular structure to allow passage of the wiring harness.

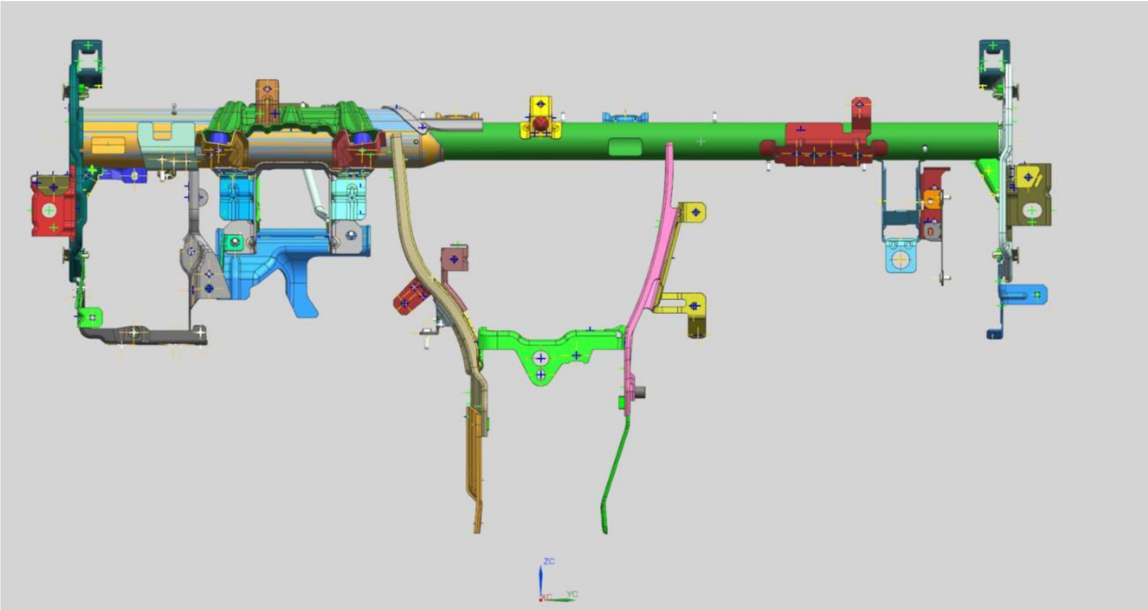

Figure 4.2 Optimized Cross-Car Beam model with routing openings for internal harness integration

These openings were positioned at the center, left-hand, and right-hand regions of the beam according to the routing layout developed during the optimization stage. Although the modified openings improved packaging efficiency and enabled internal cable routing, they also introduced geometric discontinuities into the structure.
As a result, this second model was expected to exhibit different stress concentration behavior and stiffness characteristics compared to the original solid configuration. Therefore, analysis of the optimized hole configuration was necessary to evaluate the structural influence of the routing modifications.
The third model represented the final proposed Cross-Car Beam configuration including both the routing openings and the reinforcement plate structures manufactured from FeE420 steel. In this model, reinforcement plates were integrated around the critical opening regions to improve local stiffness and reduce stress concentration effects caused by the enlarged holes.

Figure 4.3 Proposed Cross-Car Beam model with FeE420 reinforcement structure plates

The reinforcement structures were particularly important around the center routing opening because this region experienced the largest geometric modification within the beam structure. The reinforcement plates were also designed to stabilize the Wago-mini connection system during cable connection operations.
Comparison of the three configurations allowed detailed evaluation of the structural effectiveness of the proposed reinforcement strategy. The analysis process therefore made it possible to investigate the structural behavior of the original solid beam, the stiffness reduction caused by the routing openings, and the structural recovery achieved through reinforcement integration.
After preparation of the CAD geometries, all three models were transferred into the finite element preprocessing environment for geometry simplification and cleanup operations. Since production CAD models generally contain excessive geometric detail, simplification procedures were necessary to improve mesh quality and reduce computational cost during numerical analysis.
During the simplification stage, non-critical geometric features such as small fillets, cosmetic details, minor holes, embossed surfaces, and unnecessary assembly details were removed from the models.

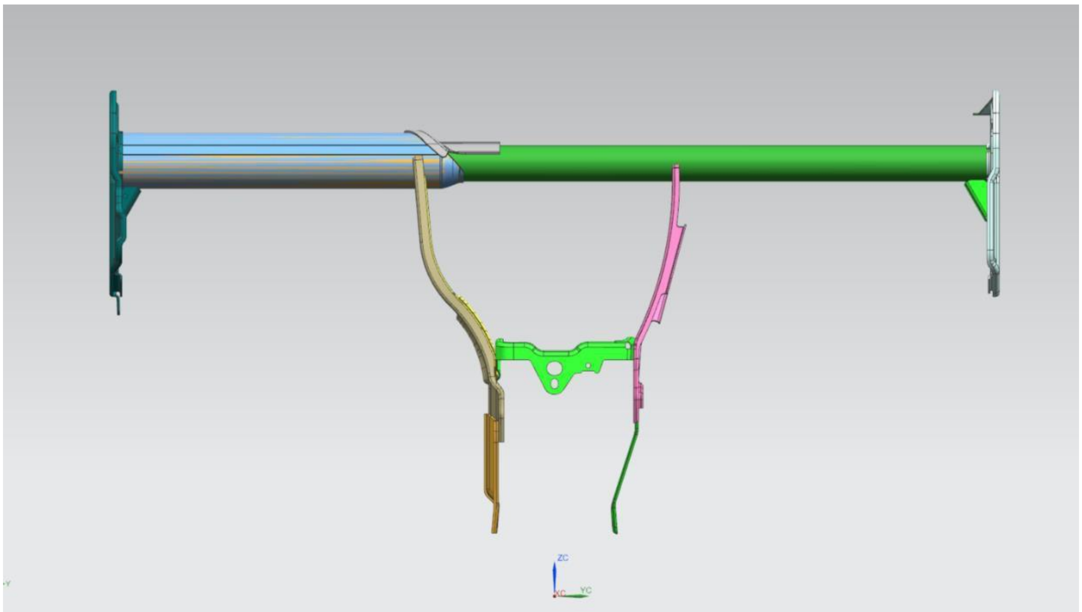

Figure 4.4 Geometry simplification process applied on solid Cross-Car Beam model

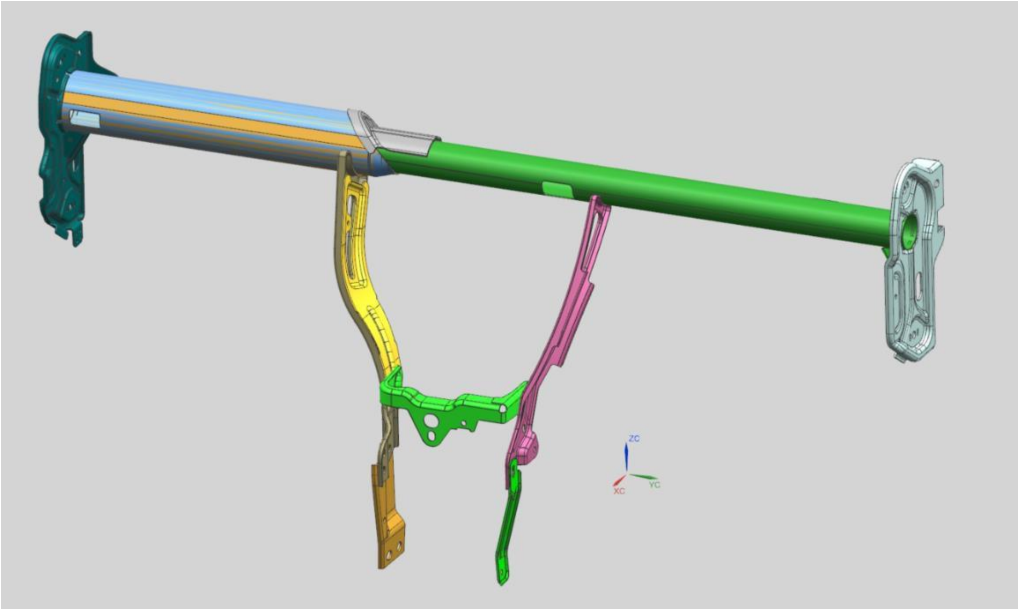

Figure 4.5 Geometry simplification process applied on optimized Cross-Car Beam model

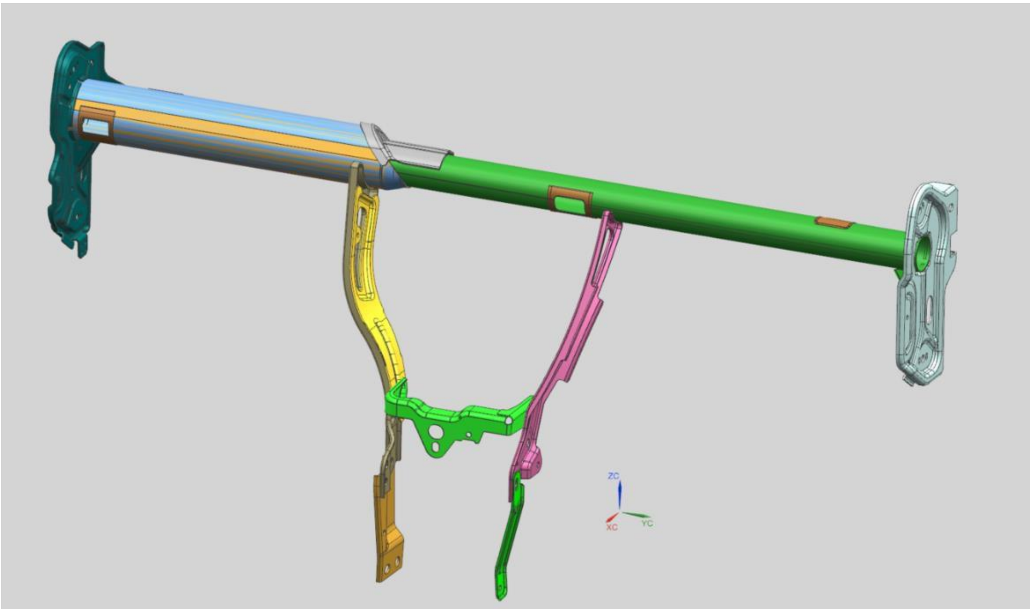

Figure 4.6 Geometry simplification process applied on proposed Cross-Car Beam model

However, all structurally significant regions including routing openings, reinforcement areas, mounting interfaces, and load transfer regions were preserved.
Following geometry simplification, glue and mesh mating operations were applied between contacting structural components to ensure proper connectivity during finite element calculations.

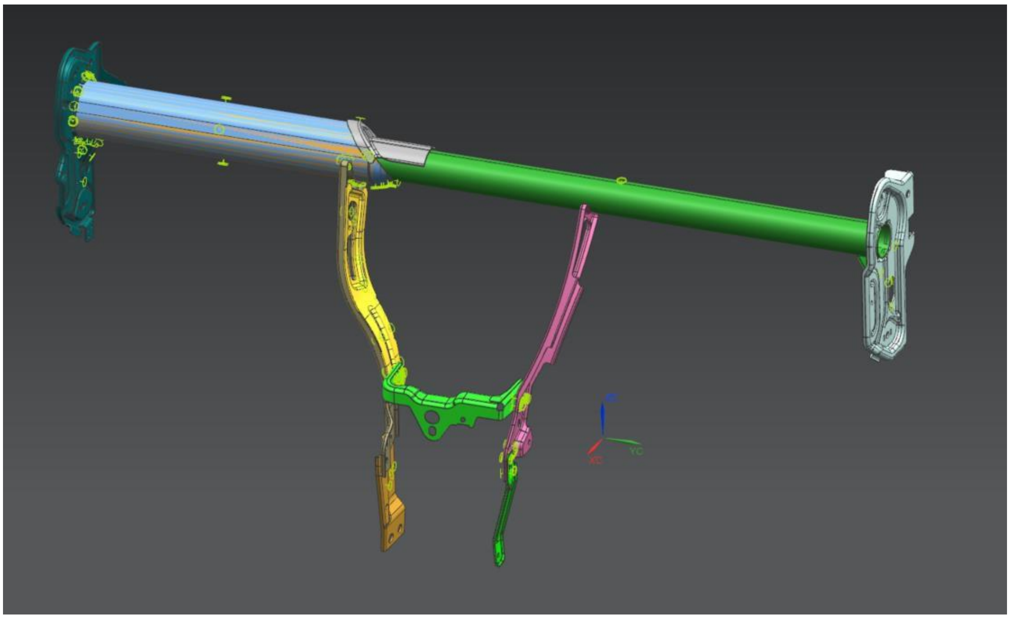

Figure 4.7 Mesh-Mating operations on solid Cross-Car Beam model

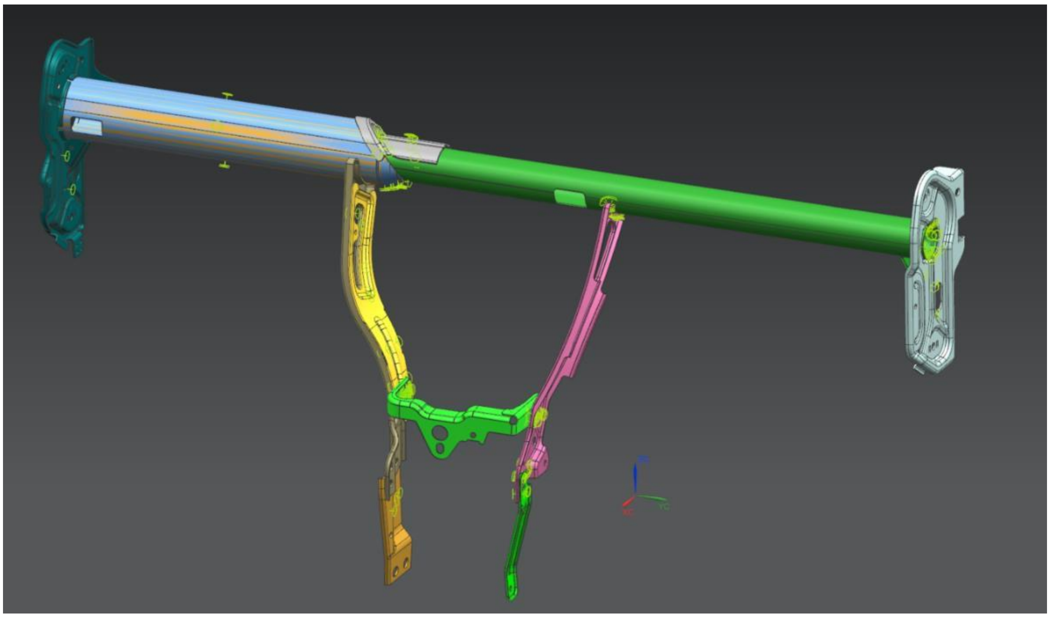

Figure 4.8 Mesh-Mating operations on optimized Cross-Car Beam model

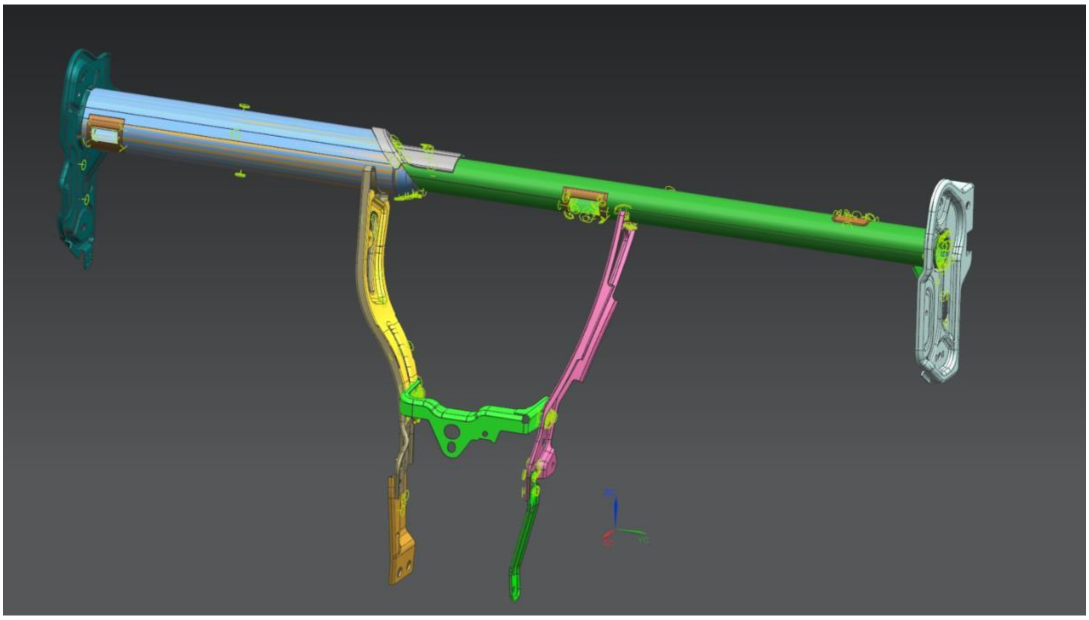

Figure 4.9 Mesh-Mating operations on proposed Cross-Car Beam model

These operations were especially important for the reinforced model because the reinforcement plates and the Cross-Car Beam structure needed to behave as a connected assembly under loading conditions.
The glue connections provided continuous load transfer between contacting surfaces and prevented separation of adjacent structural regions during analysis. Proper mesh mating also improved numerical stability and ensured accurate stress transfer between connected components.
After completion of the connectivity definitions, mesh generation procedures were performed for all three configurations. The meshing process divided the geometries into finite elements suitable for numerical calculation.

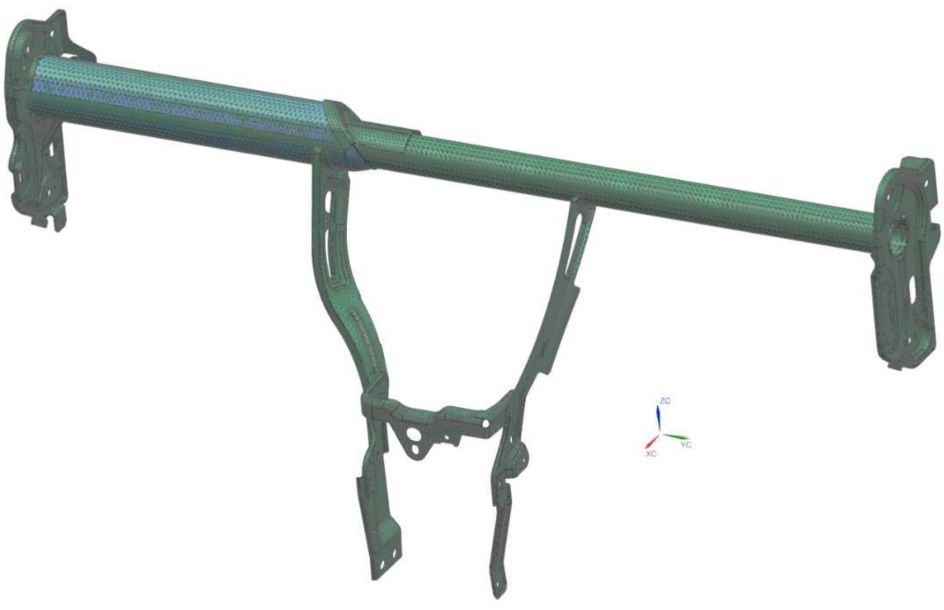

Figure 4.10 Finite element mesh generated for solid Cross-Car Beam model

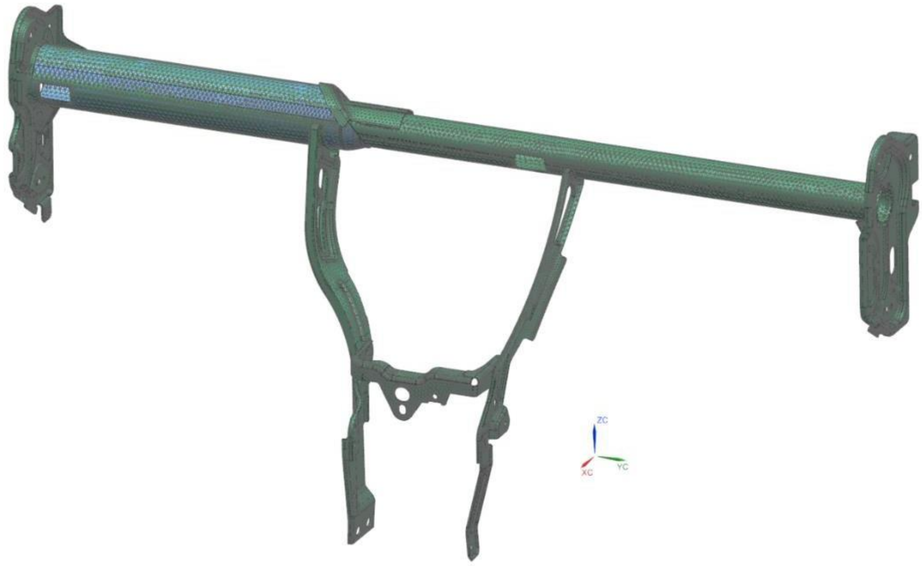

Figure 4.11 Finite element mesh generated for optimized Cross-Car Beam model

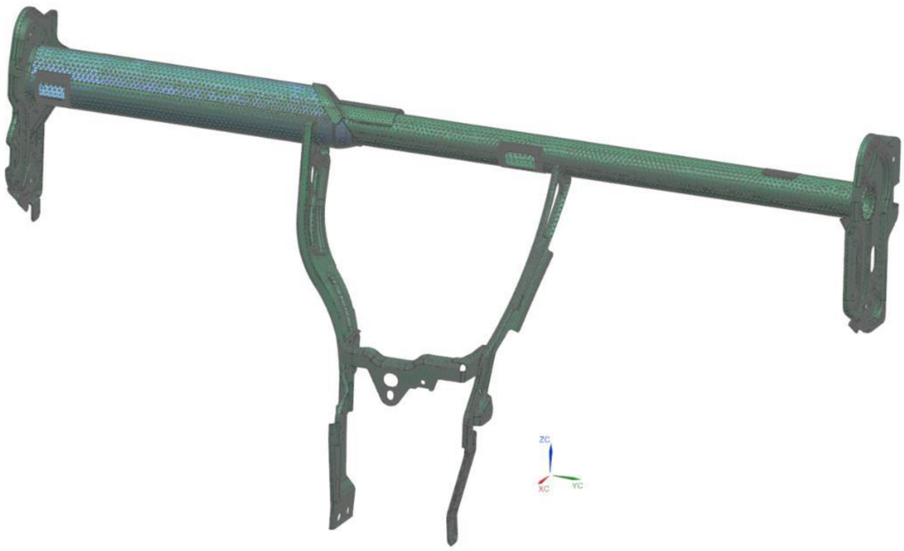

Figure 4.12 Finite element mesh generated for proposed Cross-Car Beam model

Special attention was given to the mesh density around the routing openings and reinforcement plate regions because these areas were expected to experience localized stress concentrations during loading conditions. Therefore, finer mesh structures were generated around the modified openings to improve stress distribution accuracy.

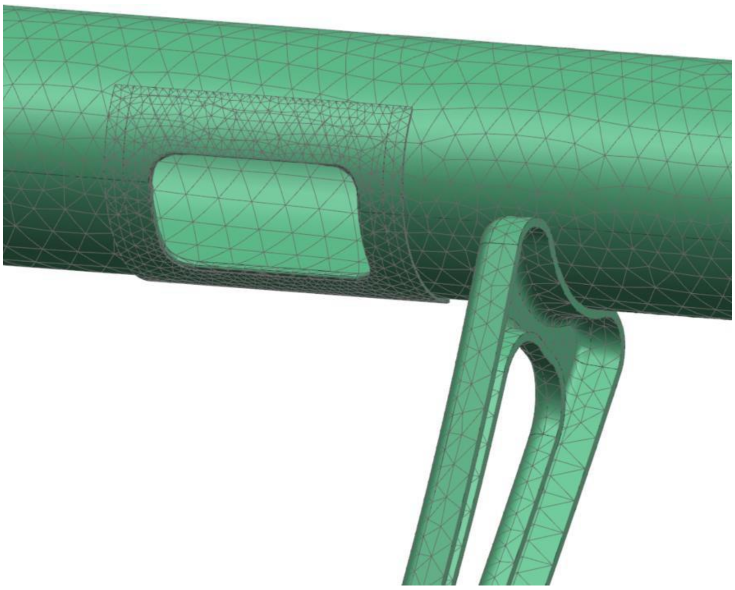

Figure 4.13 Finite element mesh generated for proposed Cross-Car Beam model

The remaining regions of the Cross-Car Beam assembly were meshed using relatively coarser element sizes to reduce computational time while maintaining acceptable solution accuracy. After the mesh generation stage, material properties were assigned to each structural component according to the physical materials used in the design. The main Cross-Car Beam structure was assigned to its corresponding steel material properties, while the reinforcement plates were defined using FeE420 steel material parameters.
Material properties including Young's modulus, Poisson's ratio, density, and yield strength were defined within the finite element software environment to simulate realistic structural behavior during static and modal analyses.

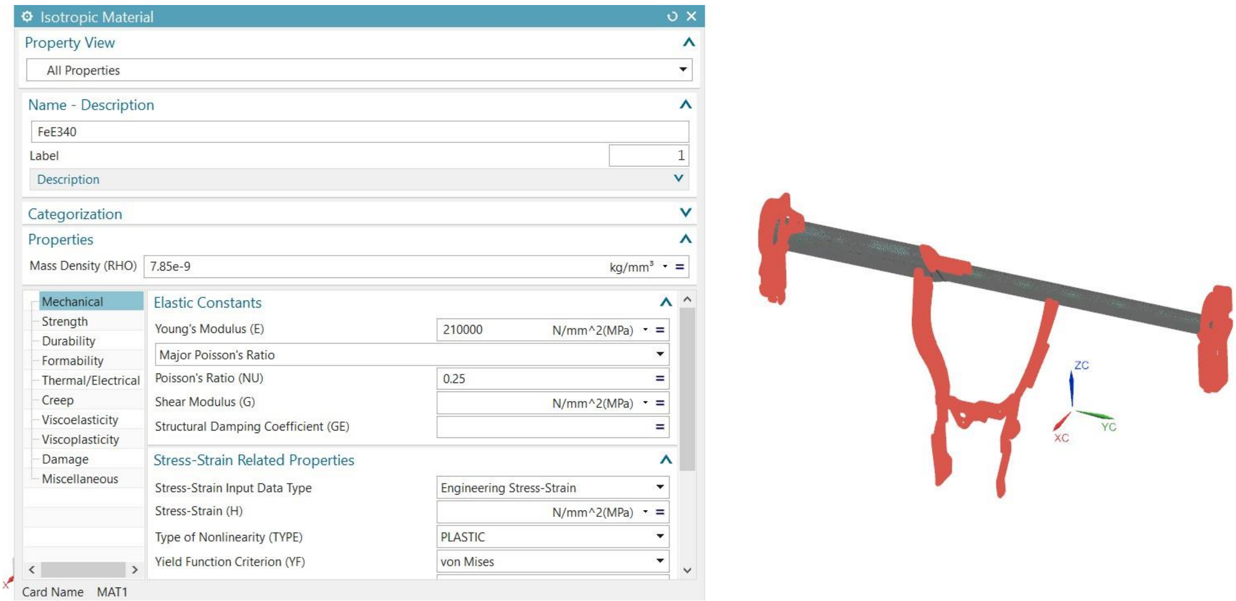

Figure 4.14 Material Assignment for solid Cross-Car Beam model (FeE340) Yield Strength 340 MPa

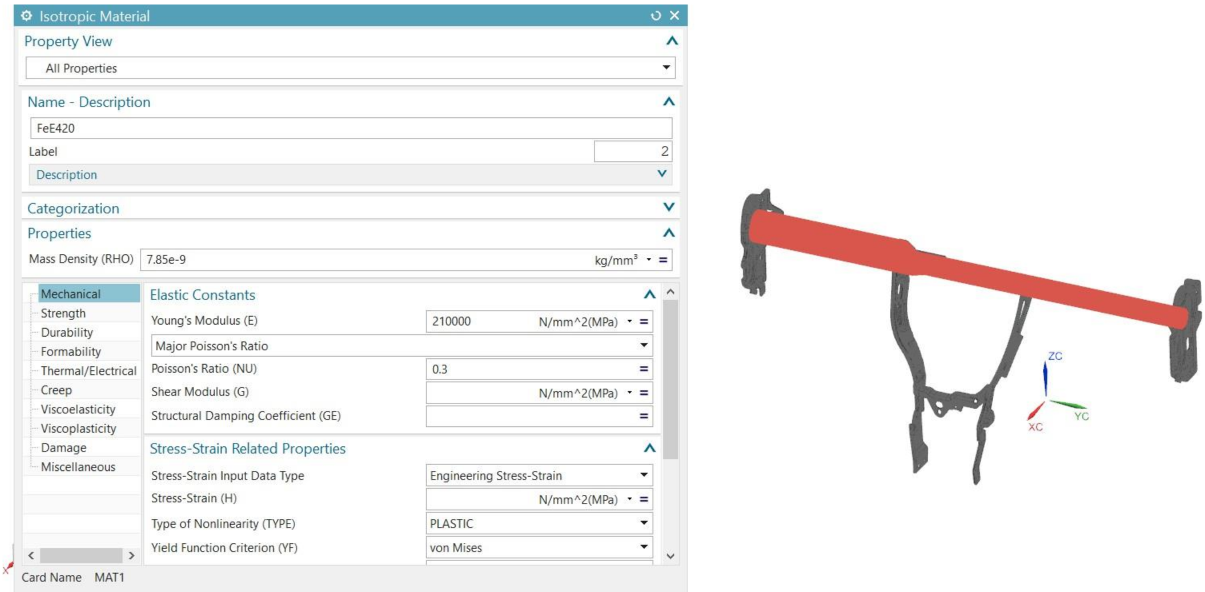

Figure 4.15 Material Assignment for solid Cross-Car Beam model (FeE420) Yield Strength 420 MPa

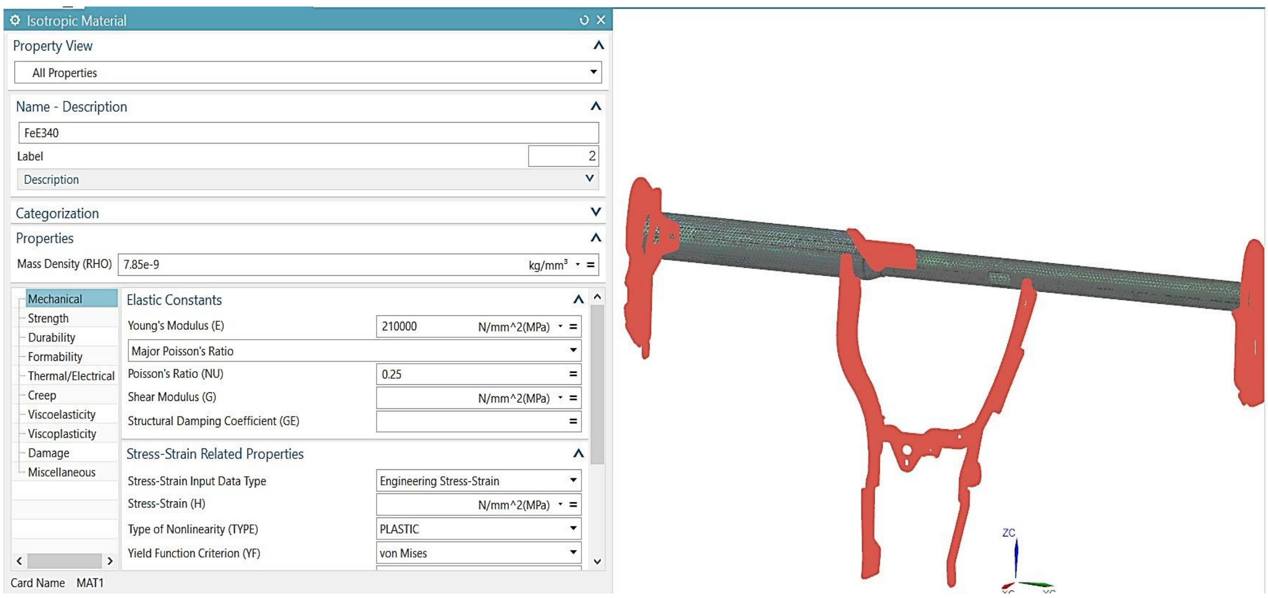

Figure 4.16 Material Assignment for optimized Cross-Car Beam model (FeE340) Yield Strength 340 MPa

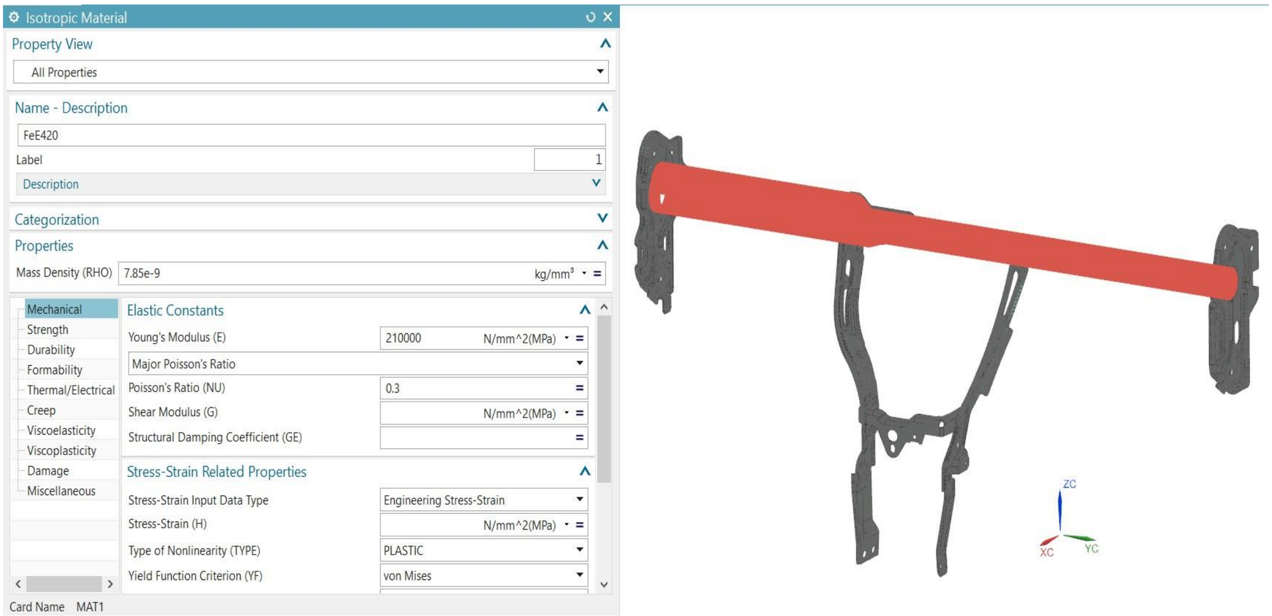

Figure 4.17 Material Assignment for optimized Cross-Car Beam model (FeE420) Yield Strength 420 MPa

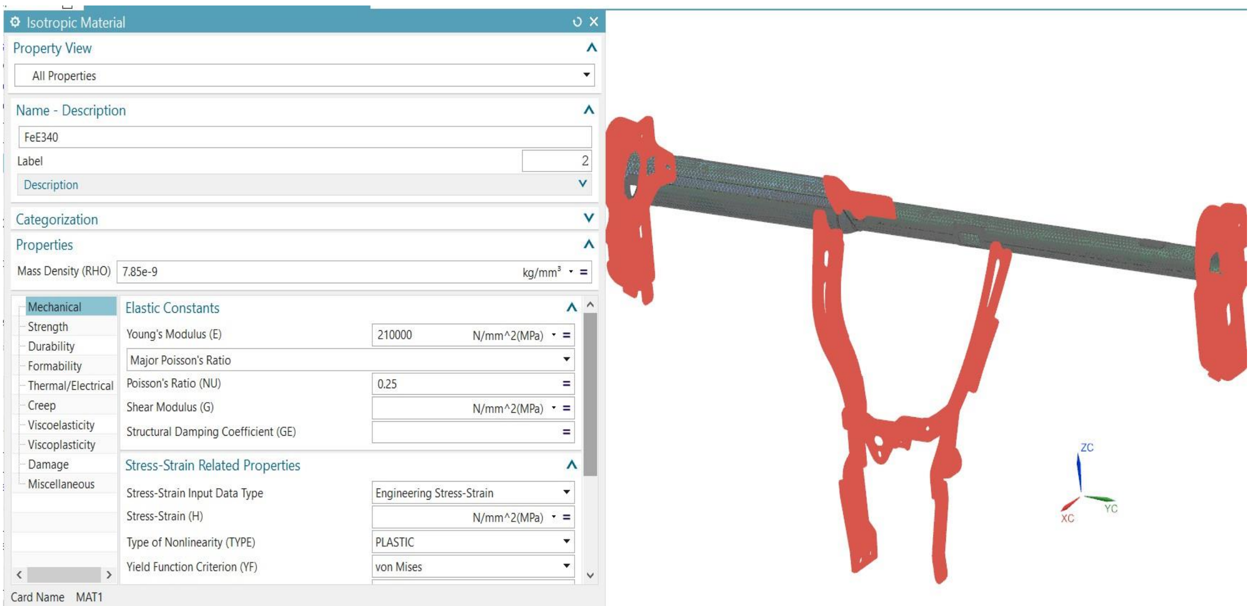

Figure 4.18 Material Assignment for proposed Cross-Car Beam model (FeE340) Yield Strength 340 MPa

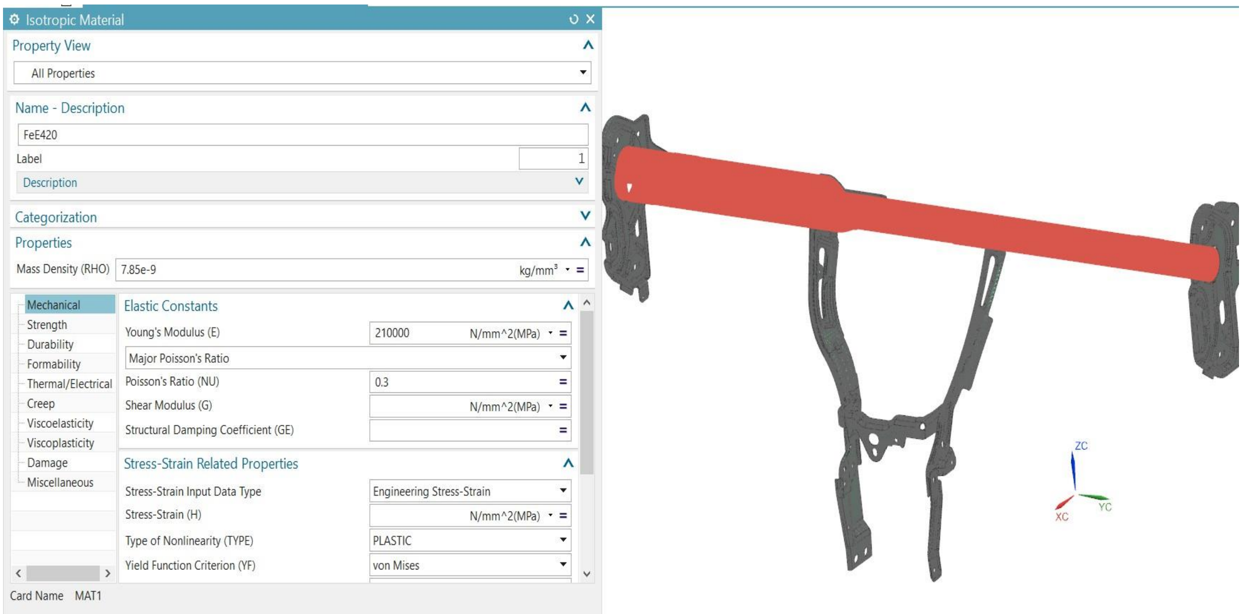

Figure 4.19 Material Assignment for proposed Cross-Car Beam model (FeE420) Yield Strength 420 MPa

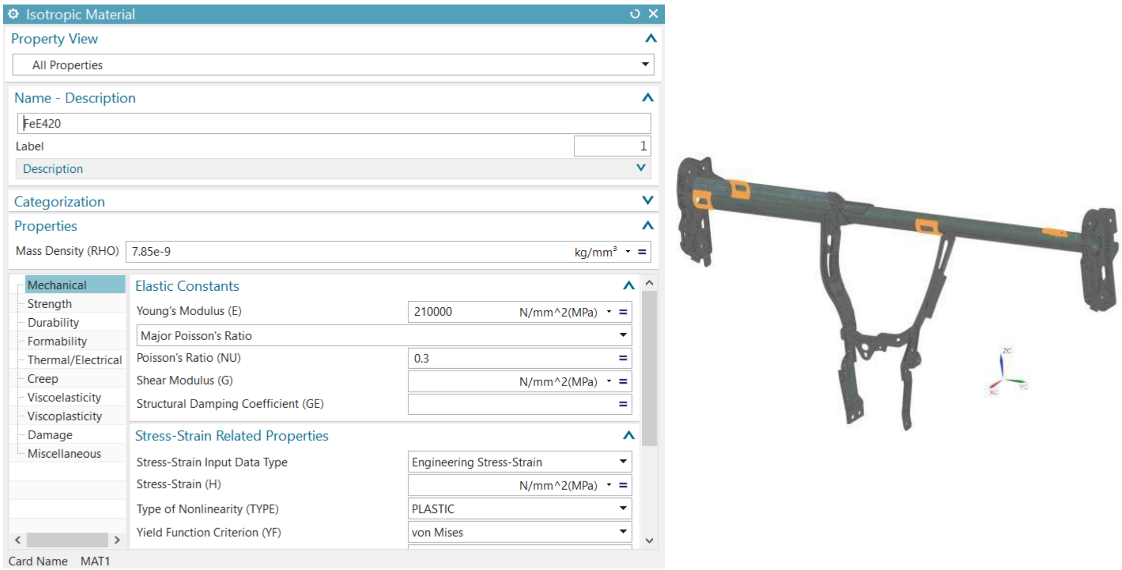

Figure 4.20 Material Assignment for proposed Cross-Car Beam model (FeE420) Yield Strength 420 MPa

After completion of geometry preparation, connectivity definition, mesh generation, and material assignment procedures, the finite element models became ready for application of boundary conditions and structural analysis operations.

4.2 Static Structural Preparation Crash Test (4000N)

Before performing the static structural analysis, the finite element models were prepared within the analysis environment to ensure accurate simulation of the structural behavior of the Cross-Car Beam (CCB) assembly under crash-equivalent loading conditions.
The static structural analysis was conducted using three different Cross-Car Beam configurations prepared during the CAD modeling stage.

Figure 4.21 RBE 3 configurations (pink) applied on solid Cross-Car Beam model 450mm distance from A-pillar

Figure 4.22 RBE 3 configurations (yellow) applied on optimized Cross-Car Beam model 450mm distance from A-pillar

Figure 4.23 RBE 3 configurations (orange) applied on proposed Cross-Car Beam model 450mm distance from A-pillar

The first configuration represented the original solid Cross-Car Beam without routing openings. The second configuration represented the optimized model containing enlarged routing holes developed for internal wiring harness integration. The third configuration represented the final proposed model including FeE420 reinforcement plates integrated around the modified opening regions.

The purpose of analyzing these three configurations was to evaluate the influence of the routing openings and reinforcement structures on the stress distribution, deformation behavior, and stiffness characteristics of the Cross-Car Beam assembly.

Prior to the analysis process, all models were imported into the finite element preprocessing environment where connectivity definitions, constraint conditions, load applications, and mesh interactions were prepared.

Since the Cross-Car Beam assembly consists of multiple connected structural components, proper load transfer between the regions was essential for achieving reliable numerical results.

Therefore, RBE3 elements were introduced at selected connection locations in order to distribute applied forces and constraint conditions more realistically across the structural regions.

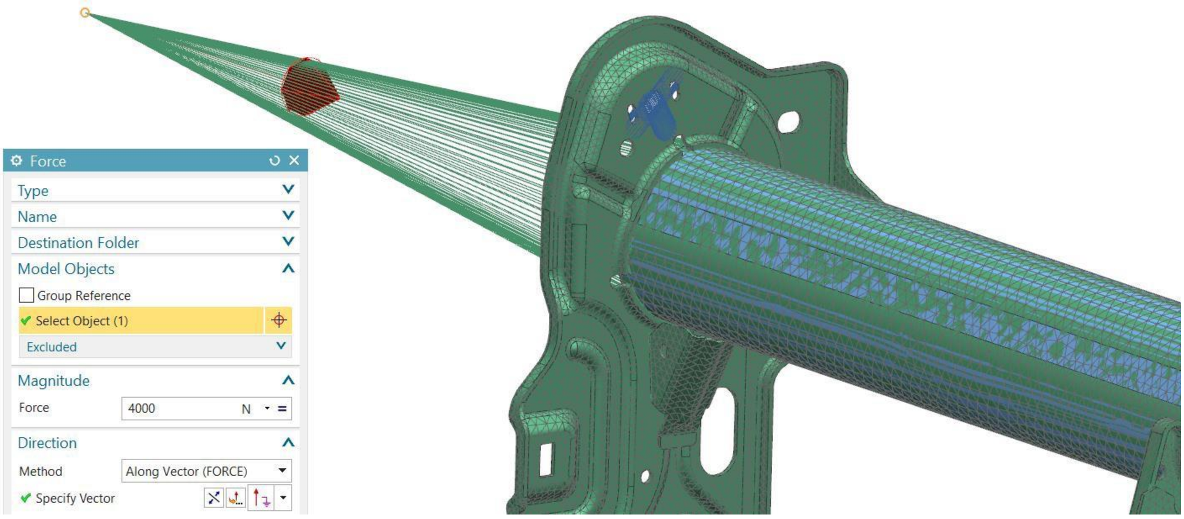

Figure 4.24 4000 N applied on node by using RBE 3 connections on solid Cross-Car Beam model

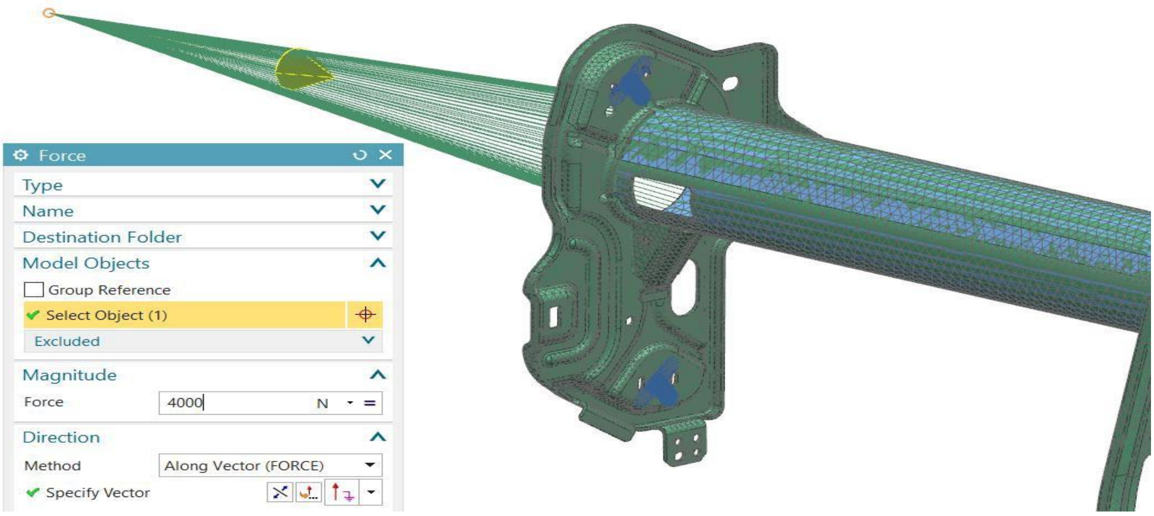

Figure 4.25 4000 N applied on node by using RBE 3 connections on optimized Cross-Car Beam model

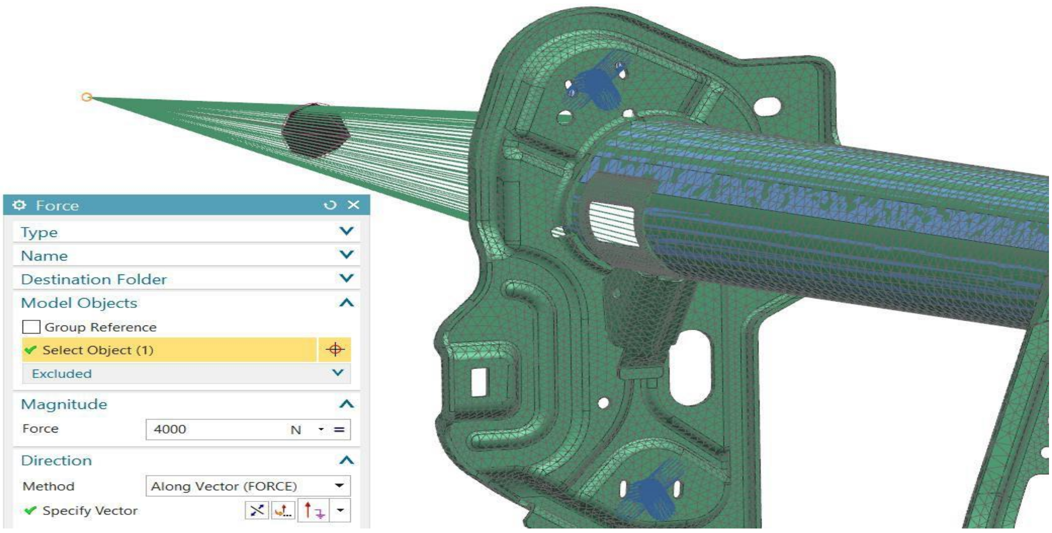

Figure 4.26 4000 N applied on node by using RBE 3 connections on proposed Cross-Car Beam model

The RBE3 connections were mainly used to transfer loading conditions from the A-pillar connection regions to the Cross-Car Beam structure while minimizing unrealistic local stiffness effects. Compared to rigid body constraints, the RBE3 formulation allowed distributed force transfer without excessively stiffening the structural model.
Boundary conditions were defined according to the mounting locations of the Cross-Car Beam inside the vehicle body structure. The support regions connected to the dashboard mounting interfaces were constrained to restrict translational and rotational motion during the analysis.

Figure 4.27 Constraints are applied to the solid Cross-Car Beam marked as orange

Figure 4.28 Constraints are applied to the optimized Cross-Car Beam marked as orange

Figure 4.29 Constraints are applied to the proposed Cross-Car Beam marked as orange

A crash-equivalent load of 4000 N was applied from the A-pillar region to simulate structural loading transferred to the dashboard support system during crash-related conditions.
The loading direction was selected according to the expected force transfer path between the A-pillar and the Cross-Car Beam assembly. The applied load represented concentrated structural loading acting on the beam structure during vehicle operation and crash events. The same boundary conditions, loading conditions, and RBE3 definitions were applied consistently to all three models to ensure accurate comparison of their structural behavior. Particular attention was given to the routing opening regions because these areas were expected to experience elevated stress concentration due to the geometric discontinuities introduced during the optimization process.
The reinforced model was also closely evaluated to investigate the effectiveness of the FeE420 reinforcement plates in improving local stiffness and reducing stress accumulation around the modified openings.
Following completion of the connectivity definitions and loading setup procedures, the finite element models became ready for mesh generation and static structural solution procedures.

4.3 Additional Crash Loading Scenarios (Steering Wheel, HVAC unit, Airbag Deployment)

In addition to the 4000 N A-pillar loading condition, additional crash-related loading scenarios were evaluated to investigate the structural behavior of the Cross-Car Beam (CCB) assembly under different operational and impact conditions. Since the Cross-Car Beam functions as the primary support structure for several critical dashboard subsystems, multiple loading cases were required to assess the structural reliability of the optimized design comprehensively.

The additional loading scenarios considered in this study included steering wheel displacement loading (8kg*35*gravity), HVAC unit loading (10kg*35*gravity), and passenger airbag deployment loading conditions (2.5kg*35*gravity). These loading cases were selected because they represent major structural interactions acting on the Cross-Car Beam during crash events and vehicle operation.

The analyses were conducted using the same three configurations previously prepared for the A-pillar crash analysis: The original solid Cross-Car Beam model, the optimized model containing enlarged routing openings, and the proposed reinforced model including FeE420 reinforcement plates.

Similarly, the same material definitions used in the previous crash analysis were maintained throughout all loading scenarios to ensure consistency between the simulations. The material properties assigned to the Cross-Car Beam structure and the FeE420 reinforcement plates remained unchanged during the steering wheel, HVAC, and airbag deployment analyses.

For all loading cases, the same mesh configuration, glue connections, and boundary condition methodology were also preserved to achieve reliable comparison between the three models, the only differences are proceeded RBE 2 configurations. The first additional loading condition focused on steering wheel displacement behavior. During frontal crash events, significant forces may be transferred through the steering column support structure toward the Cross-Car Beam assembly.

To simulate this condition, a steering wheel displacement load of 350 mm in the X-direction was applied through the steering column mounting region.

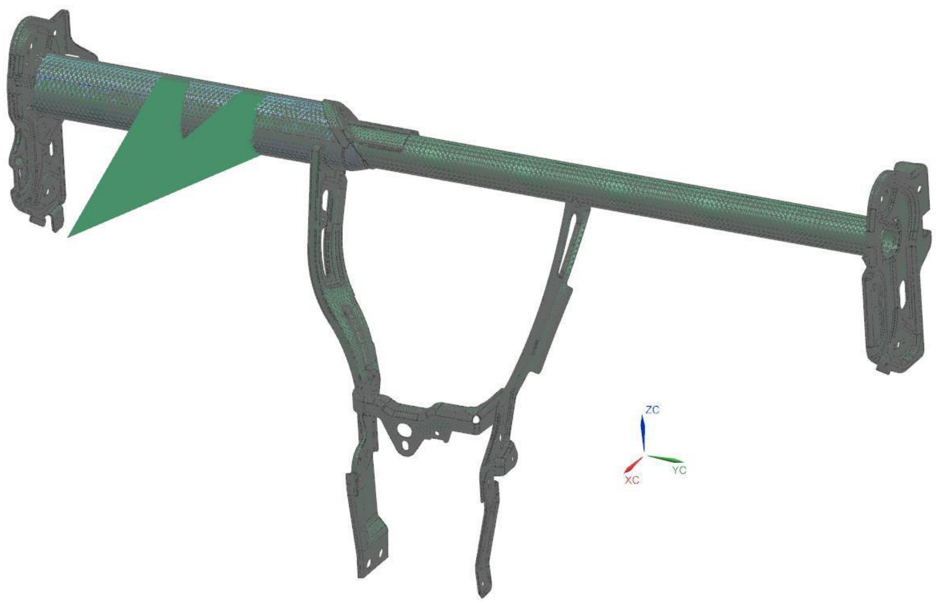

Figure 4.30 RBE 2 applied for the Steering wheel column on solid Cross-Car Beam model

Figure 4.31 RBE 2 applied for the Steering wheel column on optimized Cross-Car Beam model

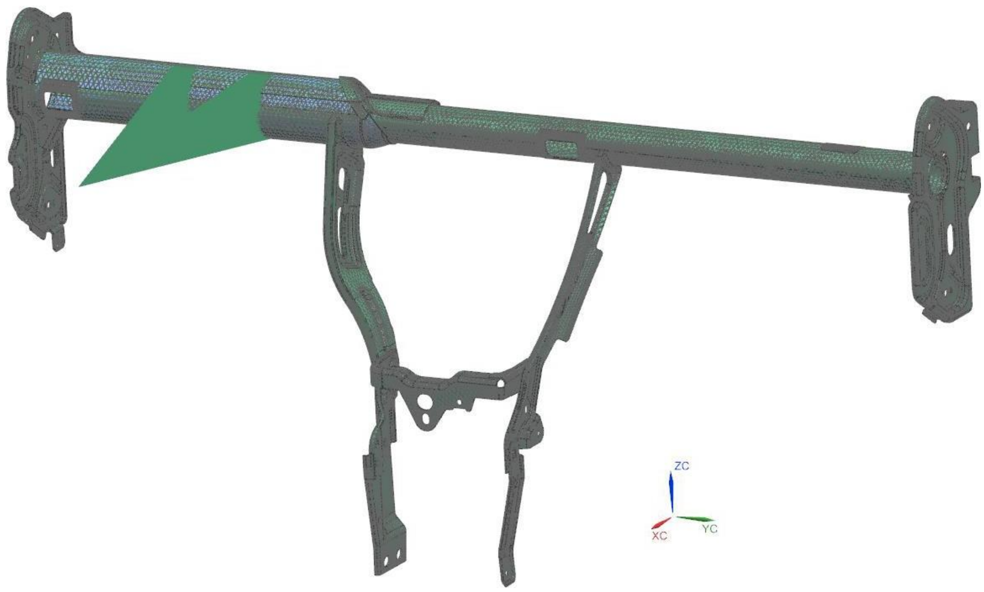

Figure 4.32 RBE 2 applied for the Steering wheel column on proposed Cross-Car Beam model

This displacement-based loading condition was used to evaluate the deformation response and structural stability of the dashboard support structure under severe steering system movement.
Attention was given to the stress distribution around the steering column support interfaces and the modified routing opening regions because these areas may experience localized stress concentration under steering-related loading conditions.
Another loading scenario involved the HVAC support structure integrated into the dashboard assembly. The HVAC module represents one of the largest subsystems mounted on the Cross-Car Beam and may transfer structural loads to the beam during crash and operational conditions.

Therefore, HVAC-related loading conditions were applied to the HVAC mounting interfaces to investigate the stiffness behavior and load transfer capability of the optimized Cross-Car Beam structure around the HVAC integration regions.

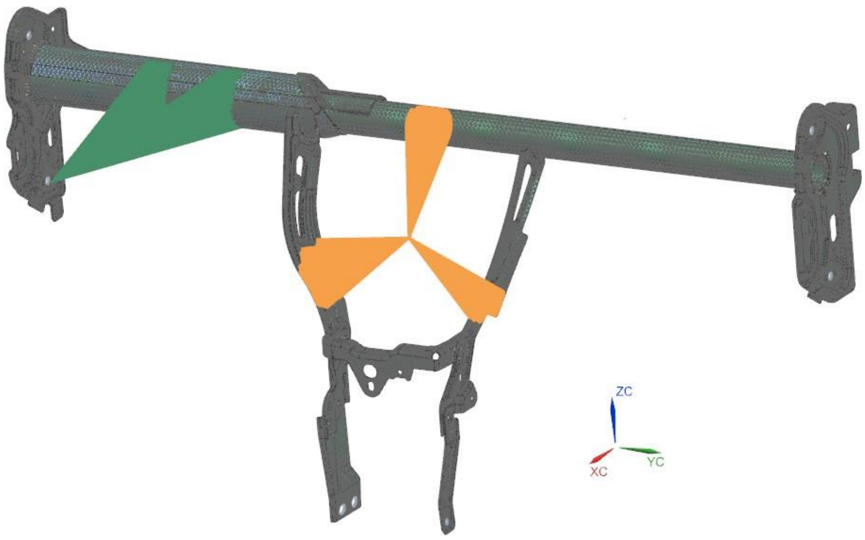

Figure 4.33 RBE 2 applied for the HVAC unit on solid Cross-Car Beam model marked as orange

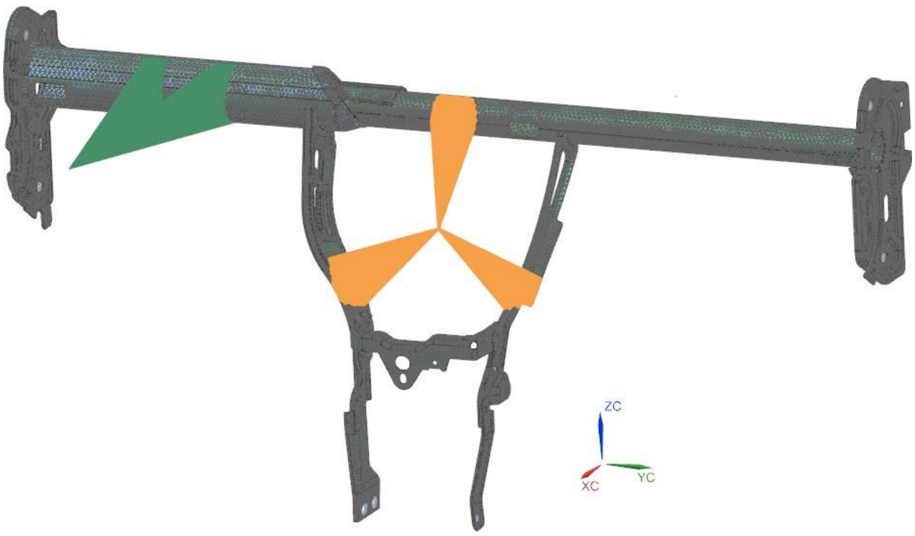

Figure 4.34 RBE 2 applied for the HVAC unit on optimized Cross-Car Beam model marked as orange

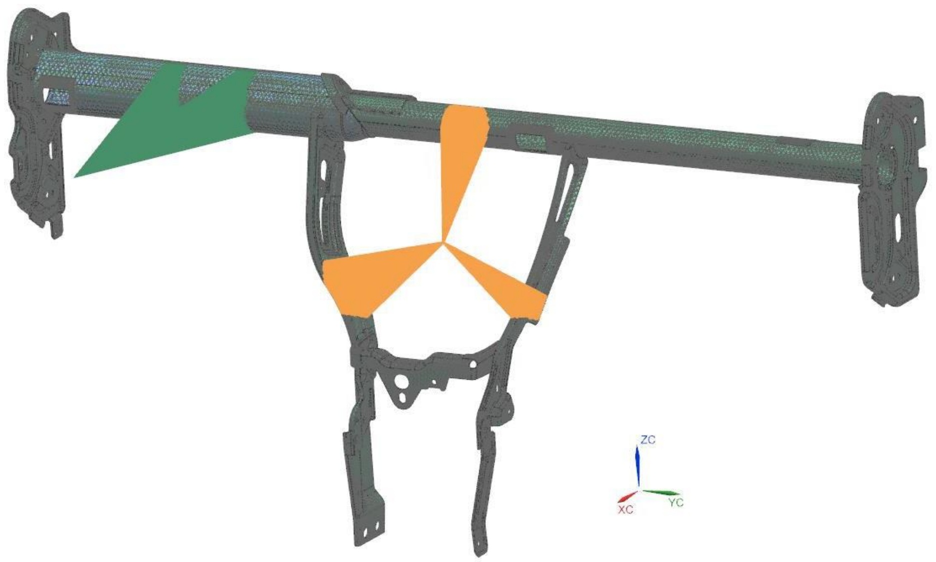

Figure 4.35 RBE 2 applied for the HVAC unit on proposed Cross-Car Beam model marked as orange

The final additional crash scenario involved passenger airbag deployment loading. During deployment, the passenger airbag system generates rapid reaction forces that are transferred directly through the dashboard support assembly.
To represent this condition, displacement loading corresponding to airbag deployment behavior was applied with 60 mm displacement in the X-direction and 80 mm displacement in the Z-direction at the airbag mounting region.

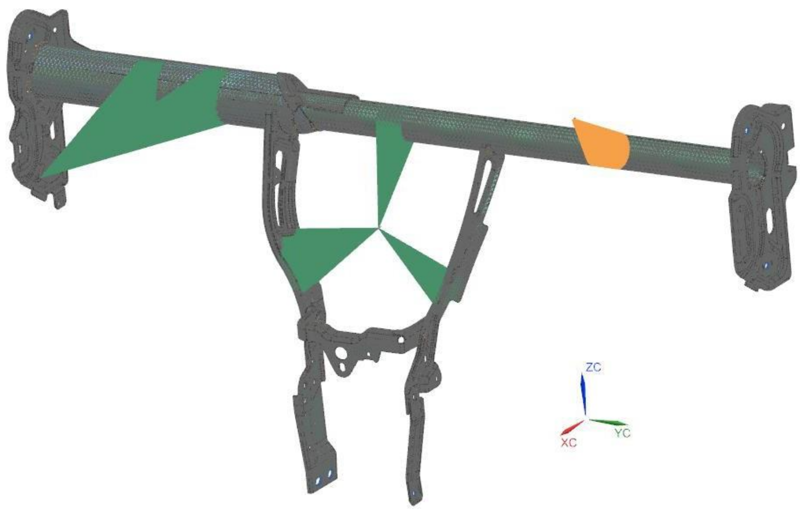

Figure 4.36 RBE 2 applied for the Airbag unit on solid Cross-Car Beam model marked as orange

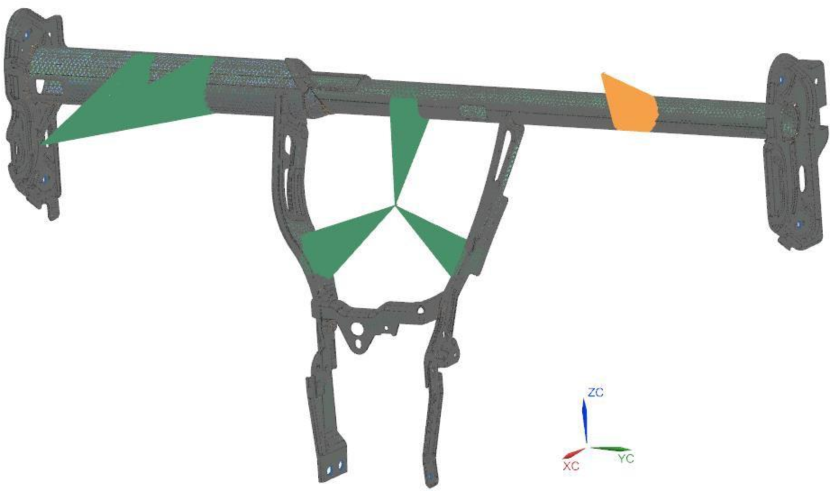

Figure 4.37 RBE 2 applied for the Airbag unit on optimized Cross-Car Beam model marked as orange

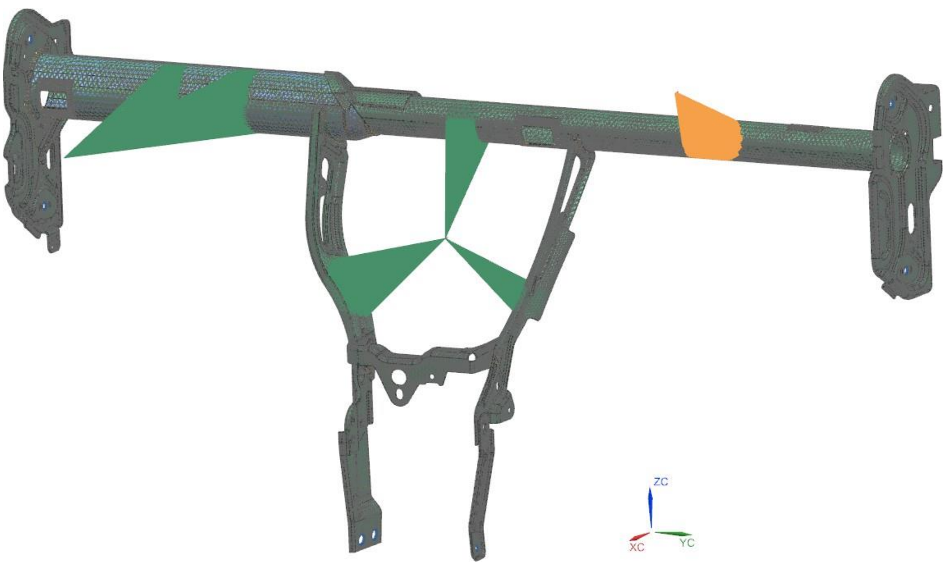

Figure 4.38 RBE 2 applied for the Airbag unit on proposed Cross-Car Beam model marked as orange

This loading condition was used to evaluate the structural response of the Cross-Car Beam assembly during airbag activation and to investigate the influence of the routing openings and reinforcement structures on the stability of the airbag support area.
Special attention was given to the reinforced model because the FeE420 reinforcement plates were expected to improve local stiffness around the modified opening regions and reduce stress concentration effects under multidirectional loading conditions.

The results obtained from the steering wheel displacement loading, HVAC loading, and airbag deployment loading scenarios were later compared between the three Cross-Car Beam configurations to evaluate the structural effectiveness of the optimized

routing architecture under different crash-related conditions.
Through these multiple loading evaluations, the structural reliability and crash performance of the optimized Cross-Car Beam assembly could be assessed more comprehensively under realistic automotive operating environments.

The steering column, HVAC unit, and airbag unit are subjected to forces of 2746.8 N, 3433.5 N, and 858.4 N, respectively.

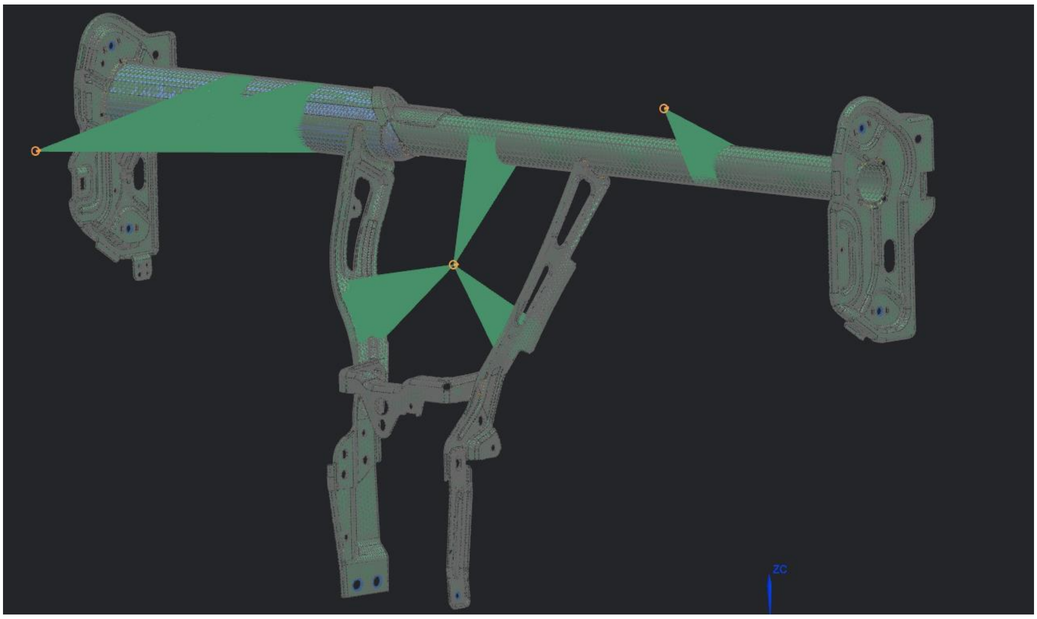

Figure 4.39 shows the forces applied on solid Cross-Car Beam model marked as orange

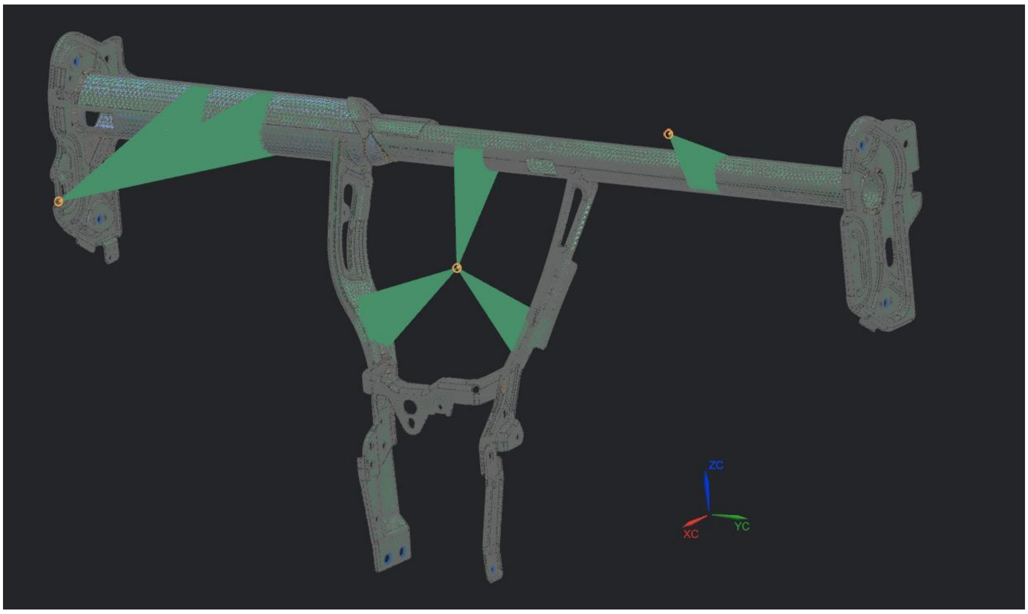

Figure 4.40 shows the forces applied on optimized Cross-Car Beam model marked as orange

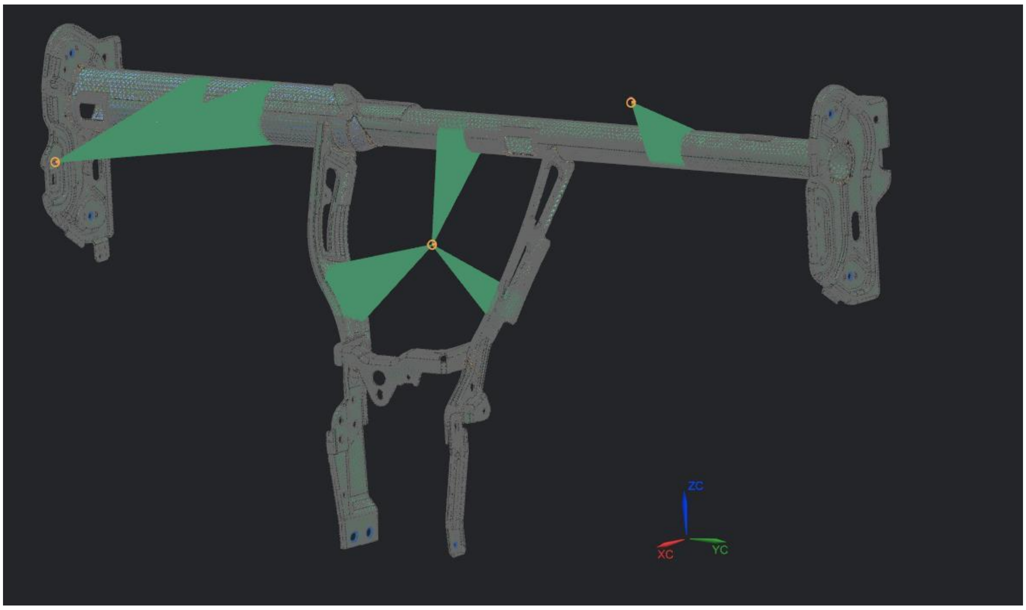

Figure 4.41 shows the forces applied on proposed Cross-Car Beam model marked as orange

The final preparation process includes the constraints applied to the three models; a fixed constraint approach has been considered.

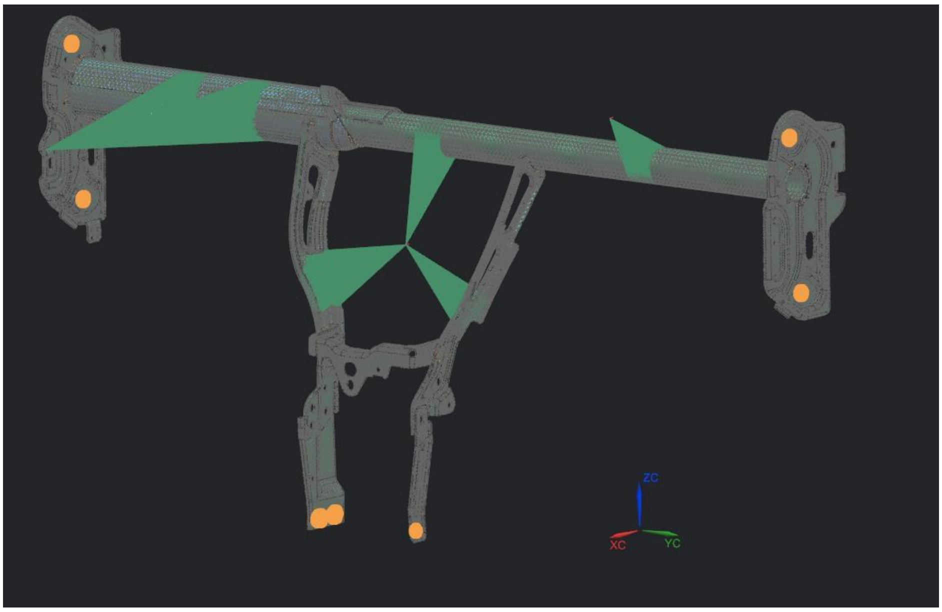

Figure 4.42 shows the constraints applied on solid Cross-Car Beam model marked as orange

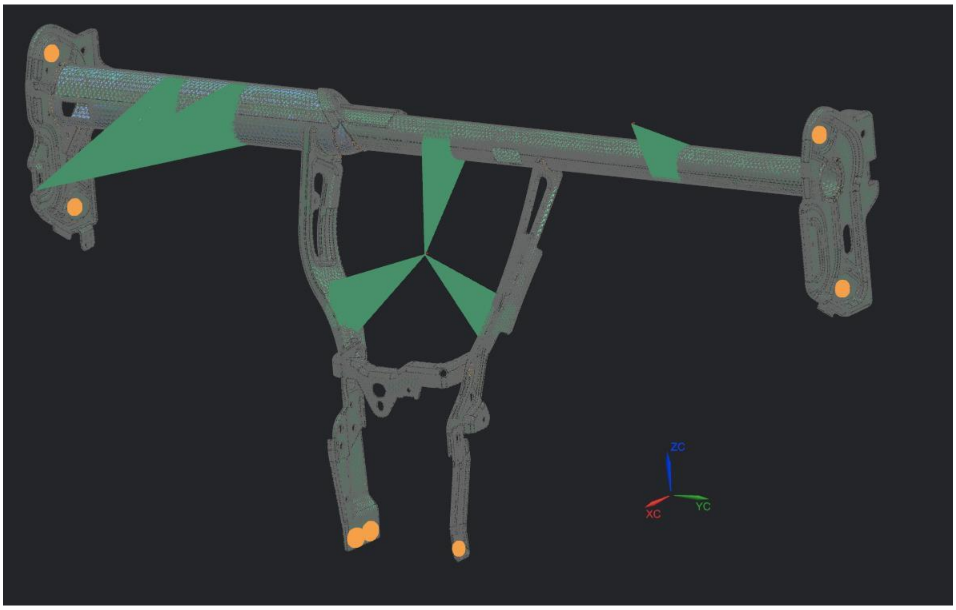

Figure 4.43 shows the constraints applied on optimized Cross-Car Beam model marked as orange

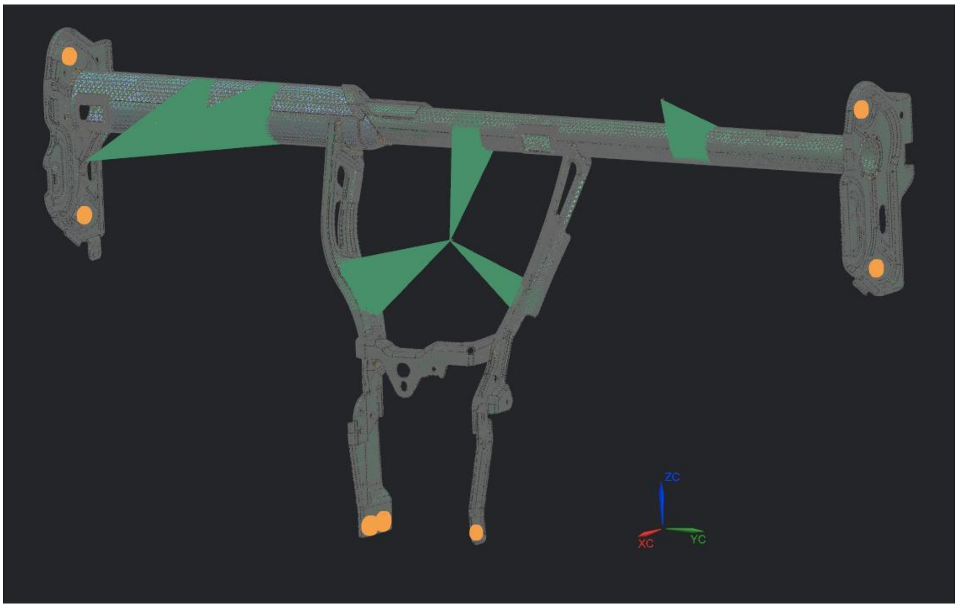

Figure 4.44 shows the constraints applied on proposed Cross-Car Beam model marked as orange

4.4 Modal Analysis Preparation Processes

Modal analysis was performed to investigate the dynamic characteristics of the Cross-Car Beam (CCB) assembly and to evaluate its vibration behavior under free vibration conditions. The analysis was conducted using the same three configurations previously developed for the static structural analyses: the original solid Cross-Car Beam model, the optimized model containing routing openings, and the proposed reinforced model incorporating FeE420 reinforcement plates around the modified opening regions.

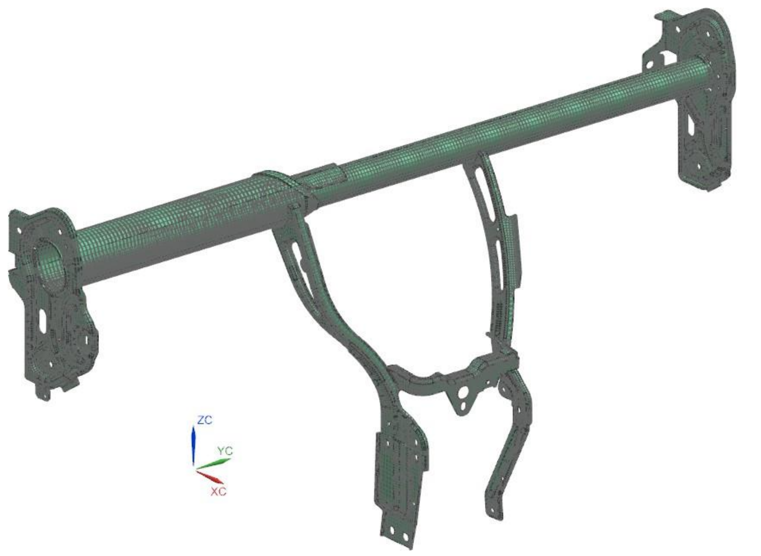

Figure 4.45 Finite element mesh generated for the solid CCB model

Figure 4.46 Finite element mesh generated for the optimized CCB model

Figure 4.47 Finite element mesh generated for the proposed CCB model

Before performing the modal analysis, all models underwent the same geometry preparation procedures described in the previous sections. Geometry simplification operations were applied to remove non-critical features while preserving all structural regions that could influence the dynamic response of the assembly. Particular attention was given to the routing openings, reinforcement structures, mounting interfaces, and load transfer regions.

Following geometry preparation, glue connections and mesh mating definitions were assigned between the contacting components of the assembly.

Figure 4.48 Glue connections and mesh mating definitions applied to the solid CCB model marked as yellow

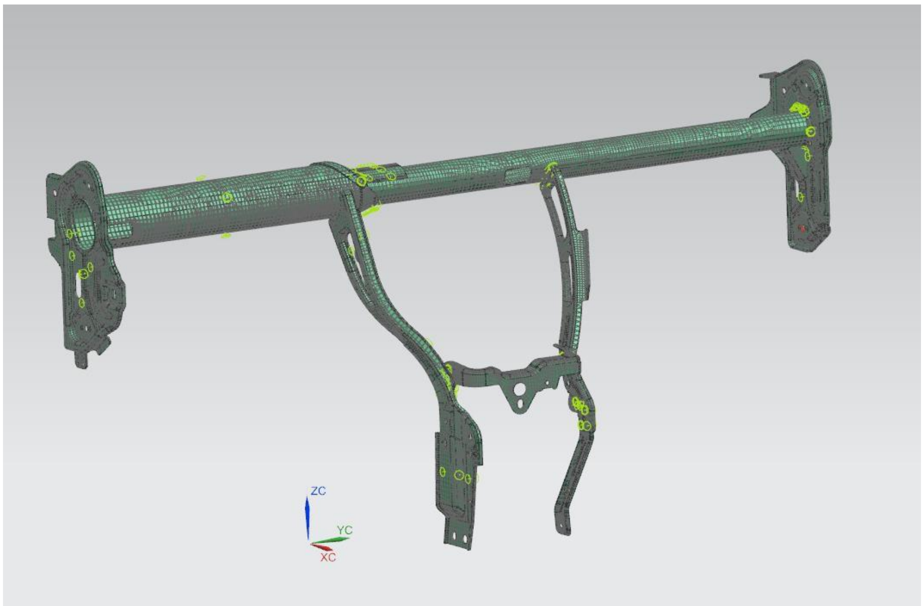

Figure 4.49 Glue connections and mesh mating definitions applied to the optimized CCB model marked as yellow

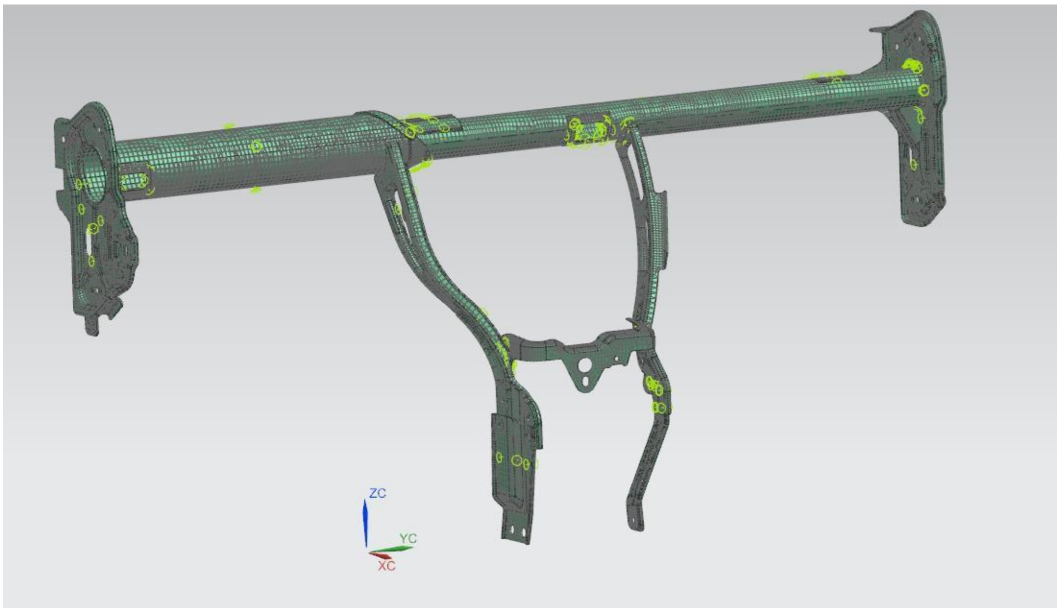

Figure 4.50 Glue connections and mesh mating definitions applied to the proposed CCB model marked as yellow

These connectivity definitions ensured proper force and displacement transfer between adjacent structural parts and allowed the assembly to behave as a continuous structure during vibration analysis.
The same finite element mesh used in the static structural analyses was maintained throughout the modal analysis procedure. Mesh refinement was applied around the routing openings and reinforcement plate regions because these areas were expected to exhibit significant local deformation during vibration.

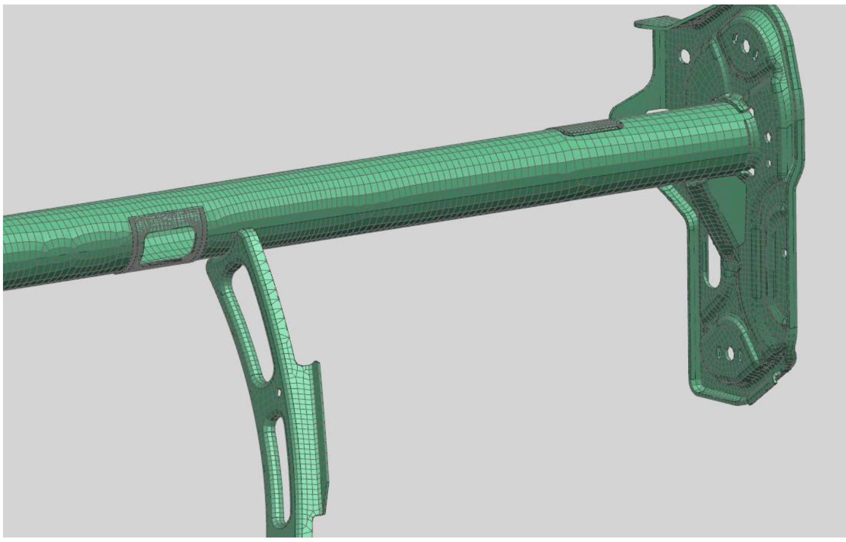

Figure 4.51 Refined mesh around routing openings and reinforcement structures

Maintaining a consistent mesh configuration also ensured direct comparison between static and modal analysis results.
The material properties assigned to the models remained identical to those used in the previous analyses. The Cross-Car Beam and reinforcement structures were modeled using linear elastic material behavior with the corresponding density, Young's modulus, and Poisson's ratio values defined in the material database.

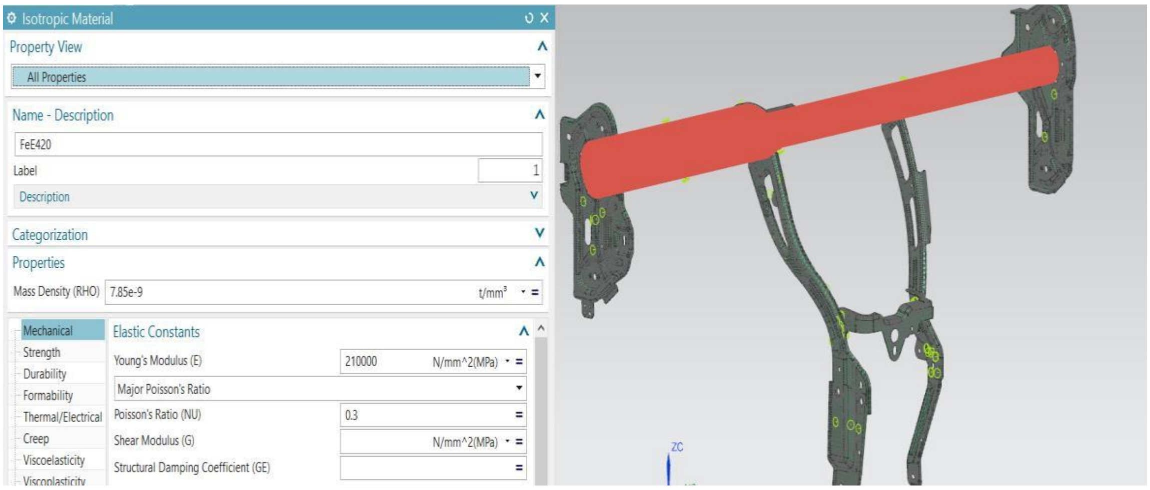

Figure 4.52 Material Assignment for solid Cross-Car Beam model (FeE420) Yield Strength 420 MPa

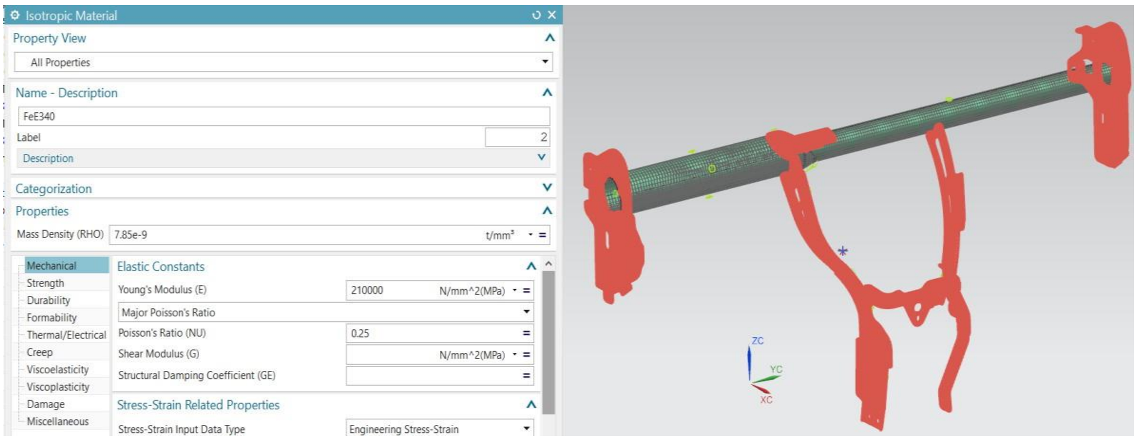

Figure 4.53 Material Assignment for solid Cross-Car Beam model (FeE340) Yield Strength 340 MPa

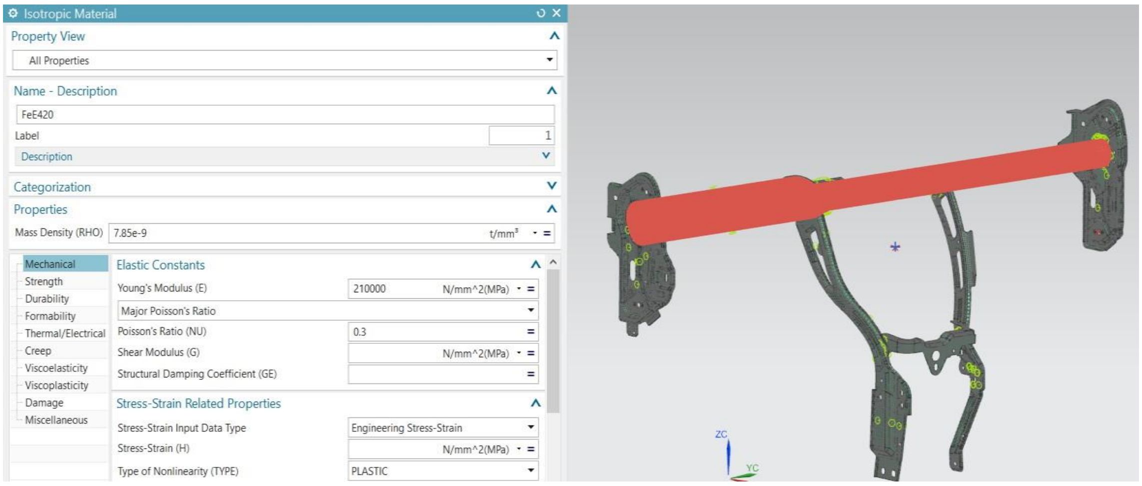

Figure 4.54 Material Assignment for optimized Cross-Car Beam model (FeE420) Yield Strength 420 MPa

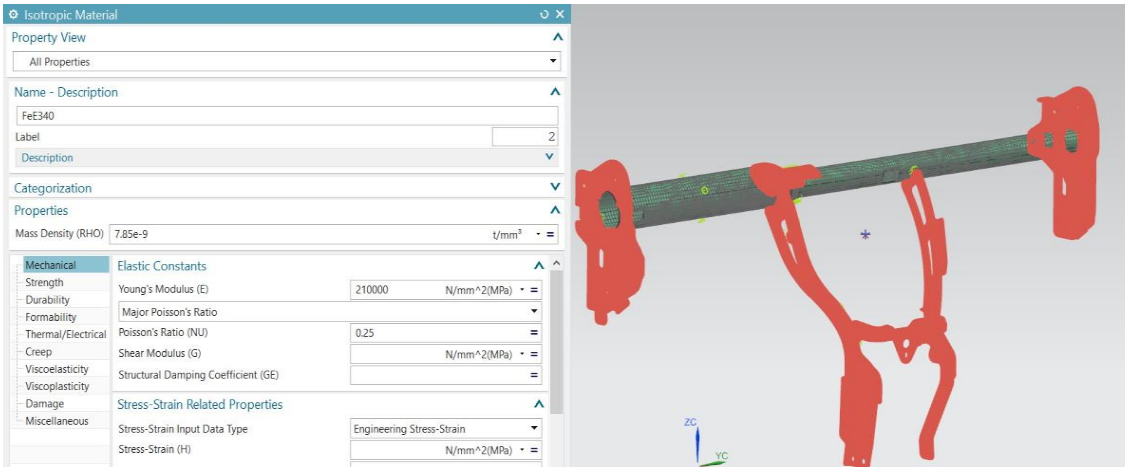

Figure 4.55 Material Assignment for optimized Cross-Car Beam model (FeE340) Yield Strength 340 MPa

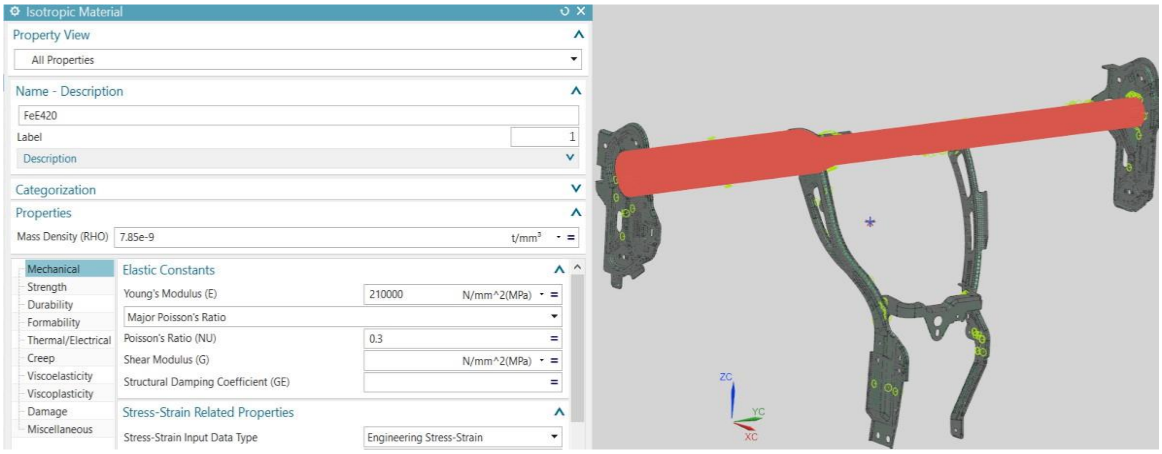

Figure 4.56 Material Assignment for proposed Cross-Car Beam model (FeE420) Yield Strength 420 MPa

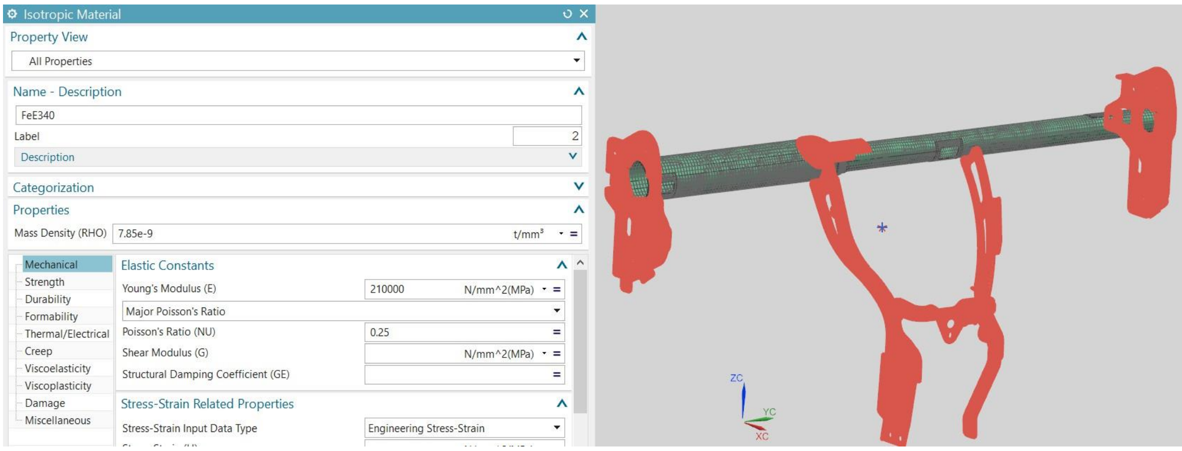

Figure 4.57 Material Assignment for proposed Cross-Car Beam model (FeE340) Yield Strength 340 MPa

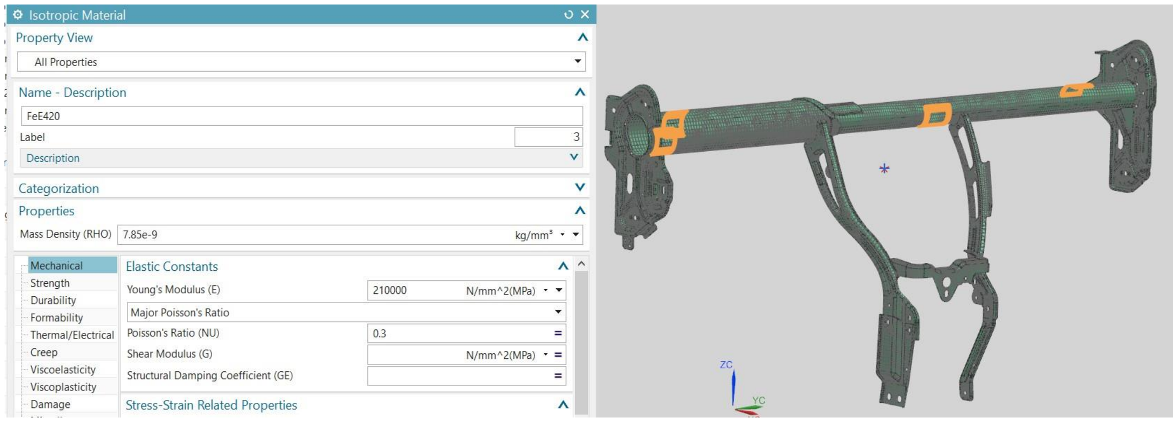

Figure 4.58 Material Assignment for proposed Cross-Car Beam model (FeE420) Yield Strength 420 MPa

To represent the mass contribution of dashboard subsystems mounted on the Cross-Car Beam, concentrated mass elements were introduced at specific locations of the assembly. A concentrated mass of **8 kg** was applied to the appropriate mounting region to represent the attached component and its influence on the dynamic behavior of the structure.

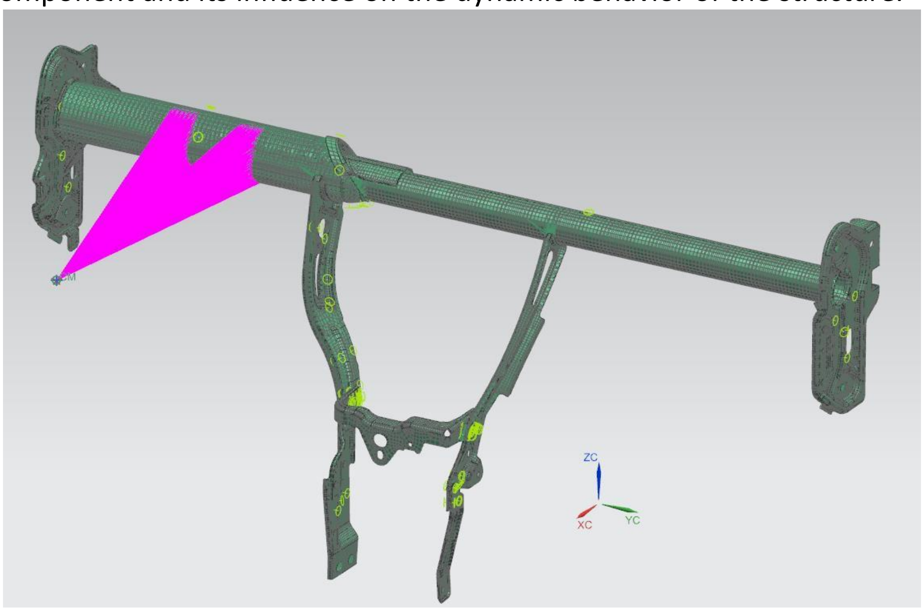

Figure 4.59 Location of the 8 kg concentrated mass (CM) used in the solid CCB model

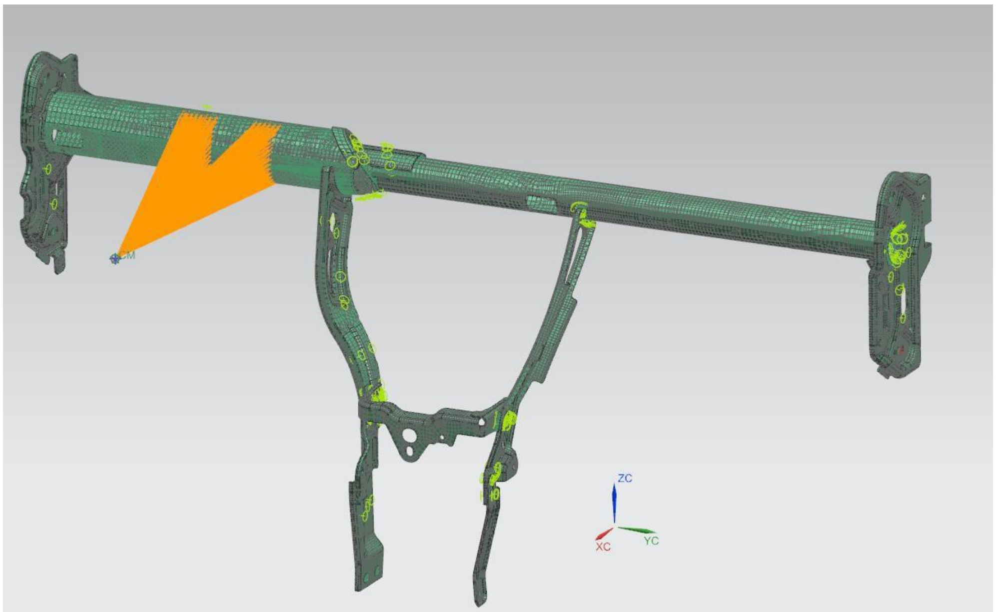

Figure 4.60 Location of the 8 kg concentrated mass (CM) used in the optimized CCB model

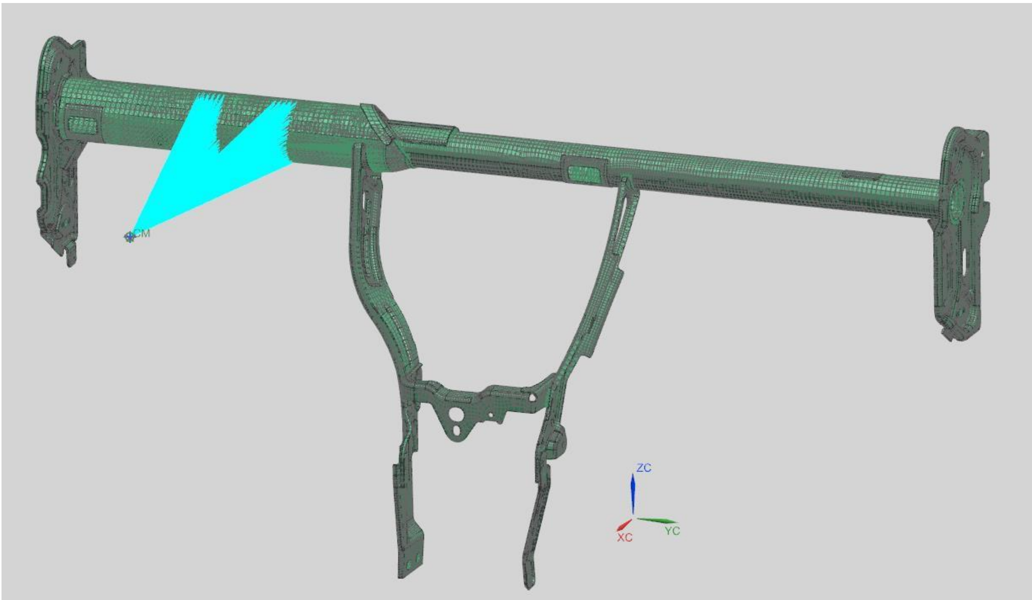

Figure 4.61 Location of the 8 kg concentrated mass (CM) used in the proposed CCB model

The inclusion of concentrated masses allowed the modal analysis to more accurately represent the actual operational conditions of the dashboard assembly.
Boundary conditions were defined according to the mounting locations of the Cross-Car Beam within the vehicle structure. The attachment points connecting the beam to the vehicle body were constrained to simulate realistic support conditions during vehicle operation.

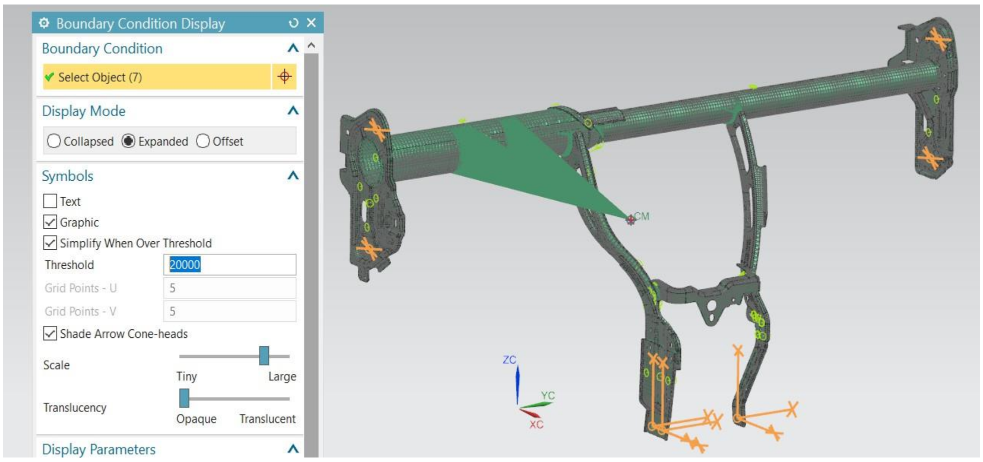

Figure 4.62 Boundary conditions applied to the solid CCB model

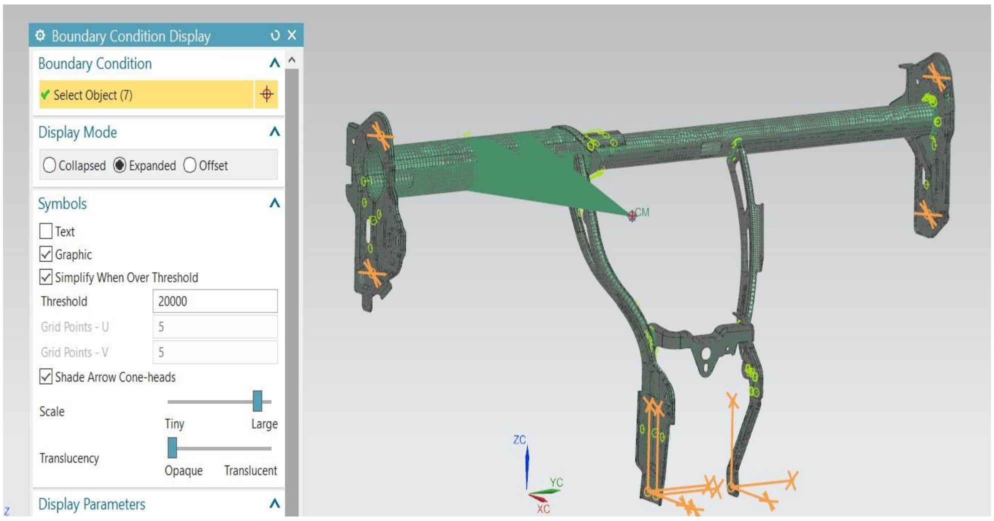

Figure 4.63 Boundary conditions applied to the optimized CCB model

Figure 4.64 Boundary conditions applied to the proposed CCB model

The same boundary conditions were applied to all three configurations to ensure consistency throughout the analysis.
Unlike static structural analysis, no external forces or displacements were applied during the modal analysis. The objective of the procedure was to determine the inherent dynamic properties of the structure by extracting its natural frequencies and corresponding mode shapes.

The modal solver calculated the vibration characteristics of the assembly by solving the eigenvalue problem associated with the global mass and stiffness matrices of the finite element model. Several vibration modes were extracted to investigate the dynamic response of the Cross-Car Beam over a range of frequencies relevant to automotive applications.

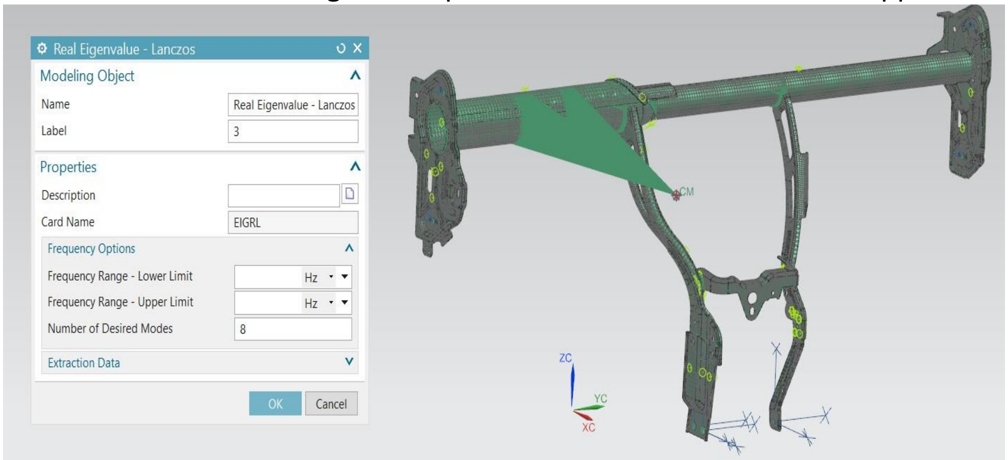

Figure 4.65 Final finite element model prepared for modal frequency extraction 8 modes are requested

In addition to natural frequency extraction, mode shape visualization and strain energy distribution were also evaluated. The mode shapes provide information regarding the deformation patterns associated with each vibration mode, while strain energy distribution helps identify the structural regions that contribute most significantly to the vibration behavior of the assembly.

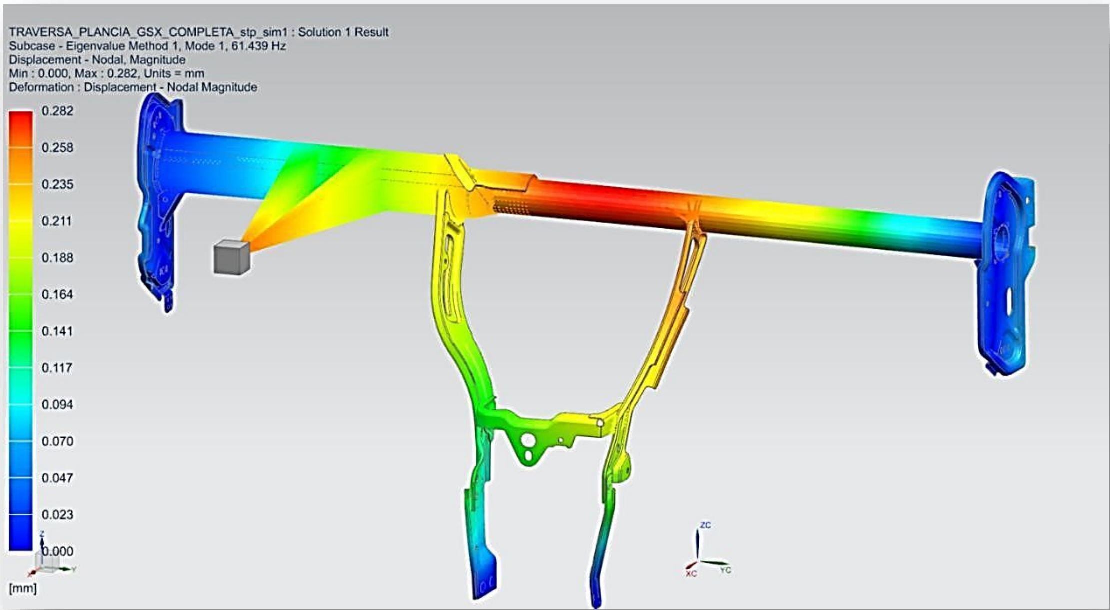

Figure 4.66 Example of the result of model analysis of the first mode

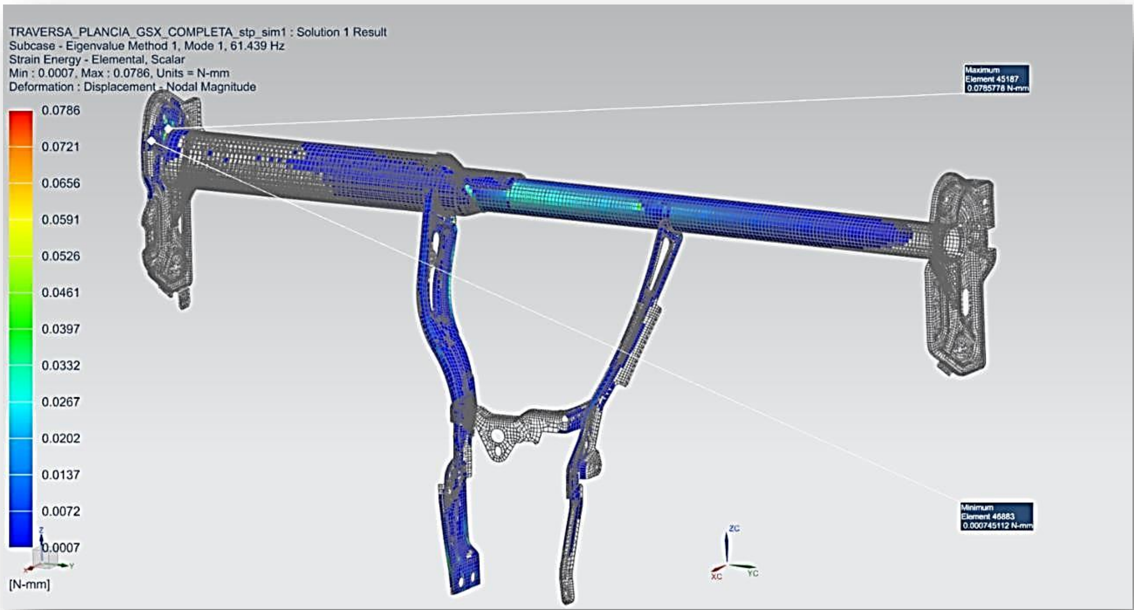

Figure 4.67 Strain energy distribution obtained from modal analysis

The same modeling procedure, material definitions, mesh configuration, concentrated mass representation, and boundary conditions were applied consistently to all three Cross-Car Beam configurations. This approach ensured that any differences observed during the modal analysis could be directly associated with the routing modifications and reinforcement structures introduced during the design optimization process.

Chapter 5 - Results And Discussion

5.1 Static Structural Analysis Results

Static structural analyses were conducted to evaluate the mechanical performance of the Cross-Car Beam (CCB) assembly under different crash-related loading conditions. The primary objective of these analyses was to investigate the influence of the routing modifications and reinforcement structures on the stress distribution, deformation behavior, and overall structural integrity of the assembly.
Three different Cross-Car Beam configurations were evaluated throughout the study.
The first configuration represented the original solid model without any routing modifications. The second configuration corresponded to the optimized model containing routing openings developed for internal wiring harness integration. The third configuration represented the proposed reinforced model, in which FeE420 reinforcement plates were incorporated around the modified opening regions.
All analyses were performed using identical material properties, mesh configurations, glue connections, mesh mating definitions, and boundary conditions in order to ensure a consistent comparison between the three models. This approach allowed the observed differences in structural behavior to be directly associated with the geometric modifications introduced during the optimization process.
The static structural assessment consisted of two main loading scenarios. The first loading case involved a 4000 N force applied from the A-pillar region to simulate structural loading

transferred through the vehicle body during crash conditions. The second loading case represented a combined crash scenario incorporating the effects of the steering wheel assembly, HVAC unit, and passenger airbag system under a 35g acceleration condition.
For each loading scenario, the structural response of the Cross-Car Beam assembly was evaluated using total deformation and von Mises stress distributions. In addition, stress concentrations occurring within the main tube structure were examined separately in order to assess the influence of the routing openings and reinforcement plates on the load transfer mechanism of the beam.
The obtained results provide a comprehensive comparison of the three configurations and enable evaluation of the structural feasibility of the proposed internal routing concept. The following sections present the detailed results and interpretations obtained from each loading scenario.

5.1.1 A-Pillar Loading Results (4000 N)

A static structural analysis was performed by applying a concentrated force of 4000 N at the A-pillar attachment region of the Cross-Car Beam assembly. This loading condition was selected to simulate the force transfer that may occur between the vehicle body structure and the dashboard support system during crash-related events. The primary objective of this analysis was to evaluate the structural response of the original, optimized, and reinforced Cross-Car Beam configurations under identical loading conditions and to determine the influence of the routing modifications on the overall structural performance.
The evaluation focused on two primary output parameters: total deformation and von Mises stress distribution. Total deformation was used to assess the global stiffness characteristics of the assembly, while von Mises stress was used to identify critical regions susceptible to yielding and structural failure. In addition, local stress levels within the main tube structure were separately evaluated because the tube represents the principal load-carrying component of the Cross-Car Beam assembly.
After solving the finite element model, deformation contours were first examined for all three configurations. The results indicated that the maximum displacement values remained relatively small despite the applied loading. The original solid model exhibited a maximum global displacement of approximately 0.546 mm. The highest deformation occurred near the outer attachment regions of the A/B pillar interfaces, while the central tube structure remained relatively stable. The low bracket structures also experienced limited movement, with deformation values remaining close to 0.1 mm. These observations indicate that the original Cross-Car Beam configuration possesses sufficient global stiffness under the investigated loading condition.

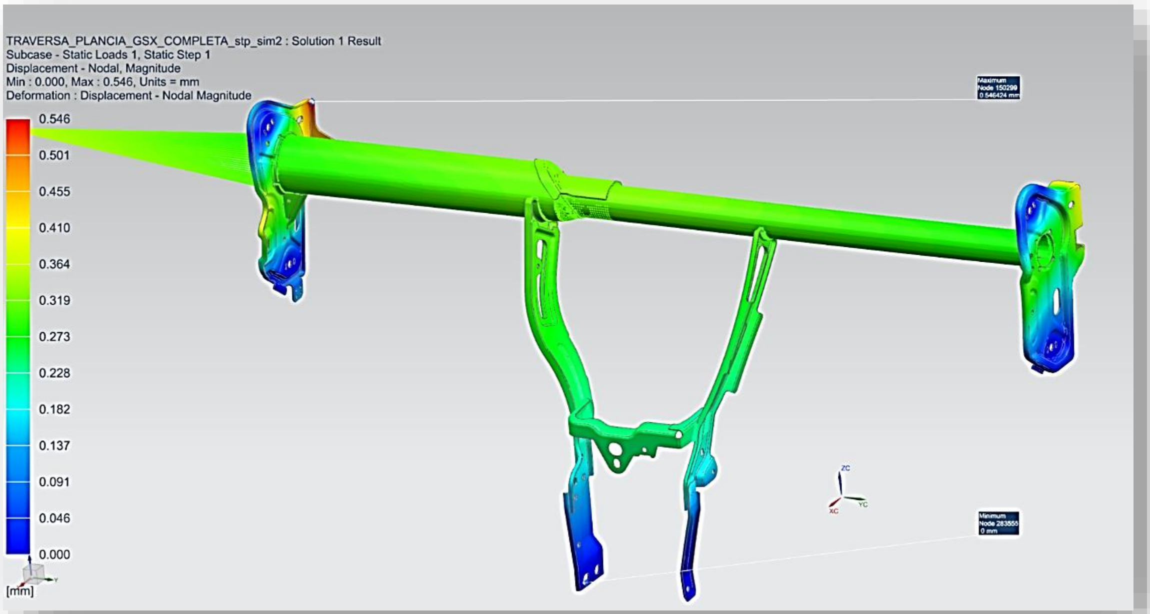

Figure 5.1 Max displacement of solid CCB model (front-iso view)

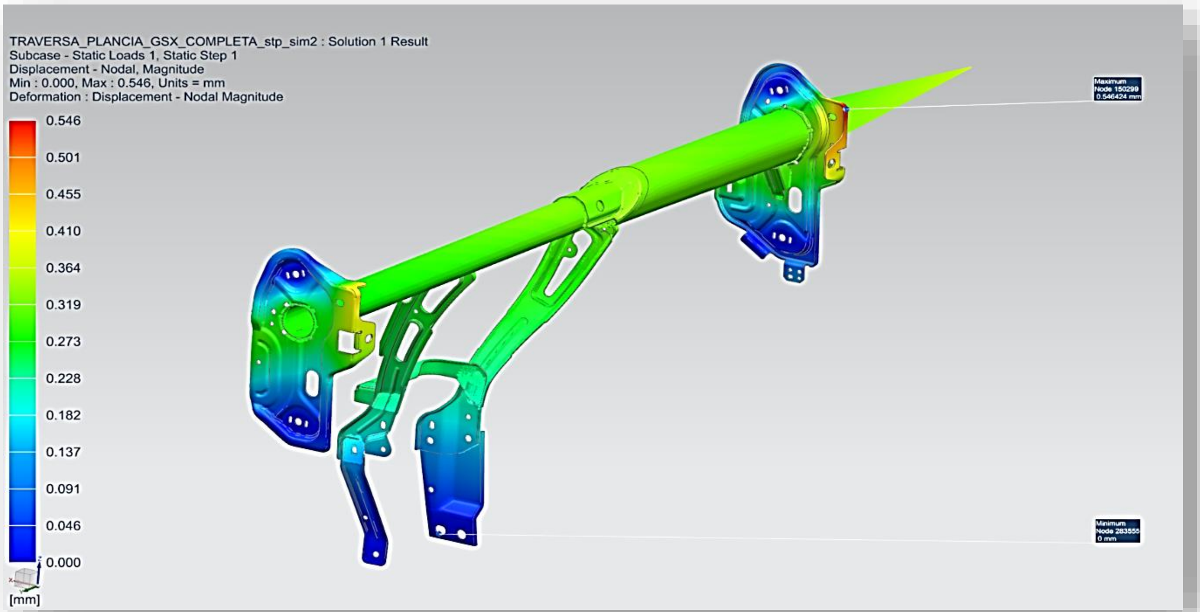

Figure 5.2 Max displacement of solid CCB model (back-iso view)

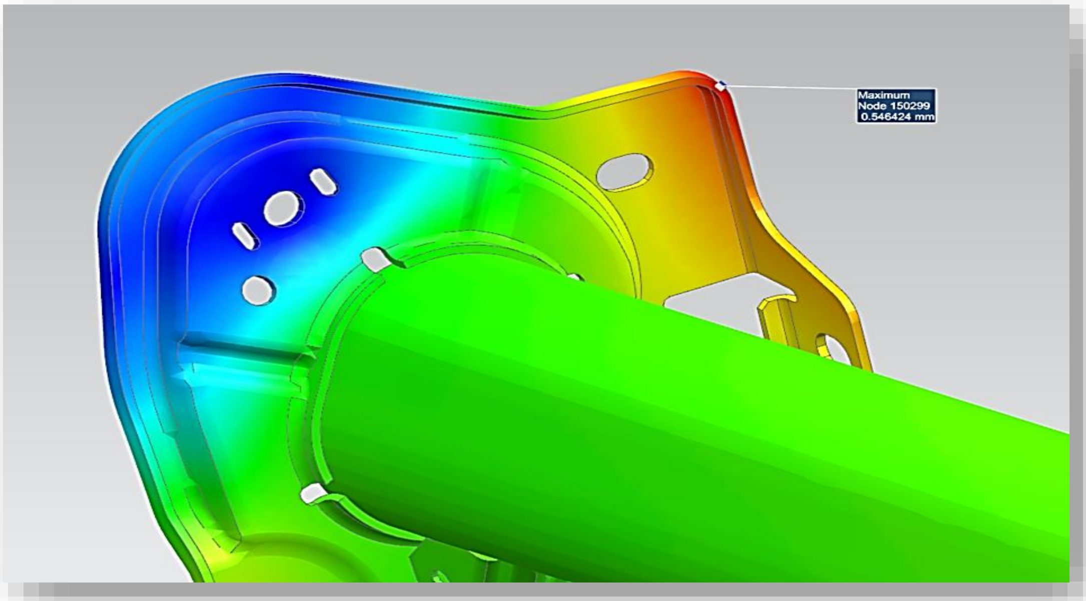

Figure 5.3 Max displacement occurs A-pillar corner (detailed-view)

Table 5-1 Maximum and minimum displacements and stress points of the solid CCB model

Component	Material	Max Displacement (mm)	Remarks
Tube (Main Beam)	FeE420	~0.350 mm	High stiffness observed.
A/B Pillars	FeE340	**0.546 mm (Max)**	Peak displacement at the outer edges.
Low Brackets	FeE340	~0.100 mm	Stable, minimal movement.
Global Result	-	**0.546 mm**	Within acceptable limits for stiffness.

The optimized model produced a maximum displacement of approximately 0.531 mm, which is slightly lower than the value obtained for the solid model. Although routing openings were introduced into the main tube structure, the reduction in displacement suggests that the modified geometry did not negatively affect the global stiffness of the assembly. A possible explanation for this behavior is that the opening geometry altered the stiffness distribution within the beam and improved the effectiveness of the load transfer path. Furthermore, the flanged regions surrounding the openings contributed additional local rigidity, compensating for the material removed from the tube wall.

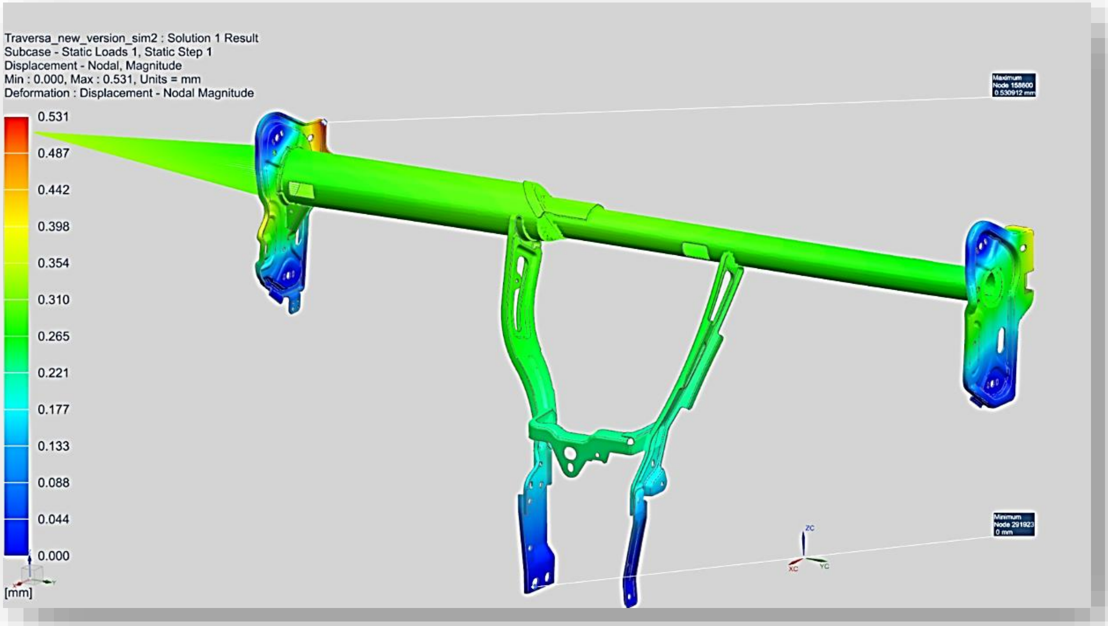

Figure 5.4 Max displacement of optimized CCB model (front-iso view)

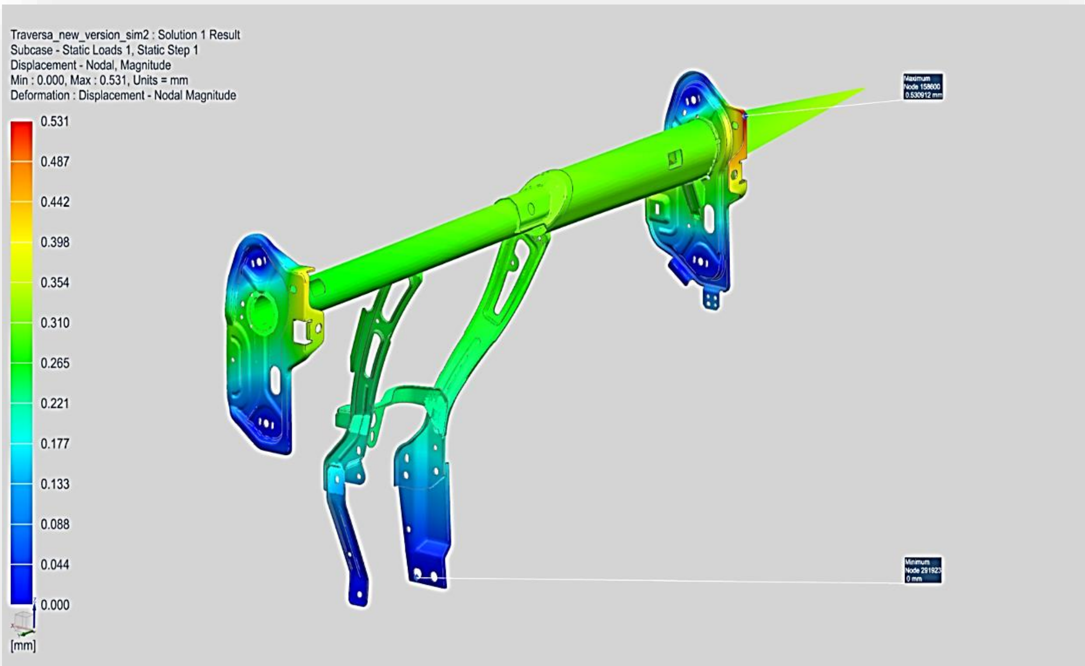

Figure 5.5 Max displacement of optimized CCB model (back-iso view)

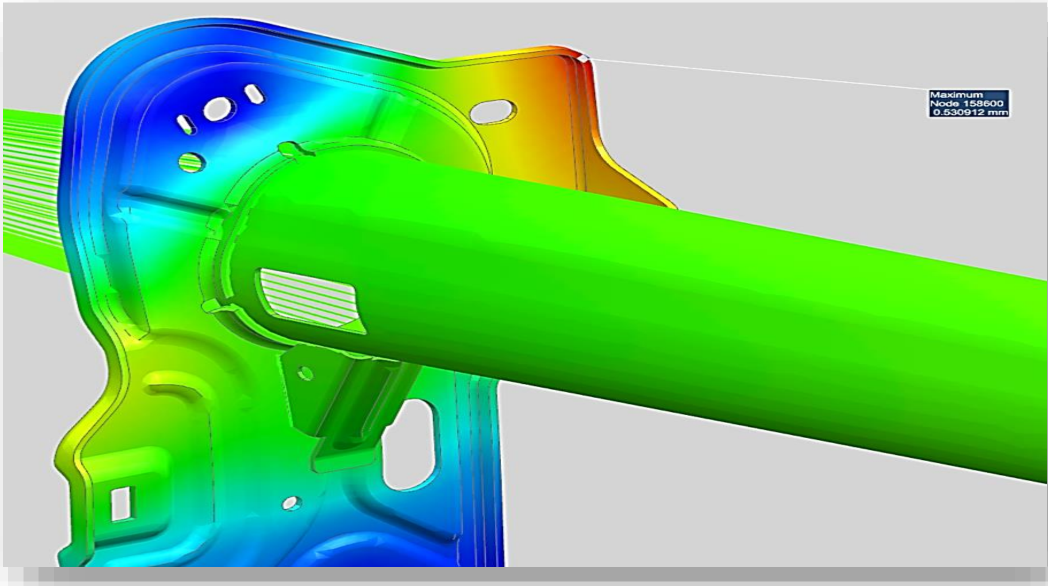

Figure 5.6 Max displacement occurs A-pillar corner (detailed-view)

Table 5-2 Maximum and minimum displacements and stress points of the optimized CCB model

Component	Material	Max Displacement (mm)	Status
Tube (Main Beam)	FeE420	0.332 mm	**Passed**
A/B Pillars	FeE340	**0.531 mm (Max)**	**Passed**
Low Brackets	FeE340	0.088 mm	**Passed**
Global Result	-	**0.531 mm**	**Acceptable**

The reinforced configuration exhibited the lowest displacement value, approximately 0.524 mm. The addition of FeE420 reinforcement plates around the routing openings increased local stiffness and reduced deformation in the modified regions. Although the improvement compared with the optimized model was relatively small, the results indicate that the reinforcement strategy successfully compensated for any stiffness reduction associated with the routing modifications.

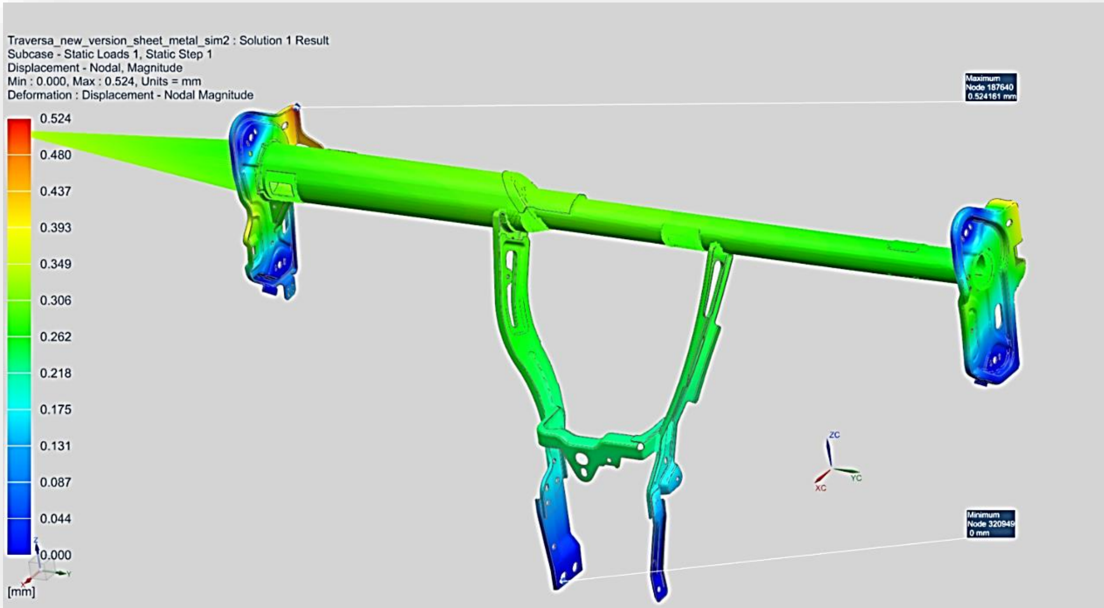

Figure 5.7 Max displacement of proposed CCB model (front-iso view)

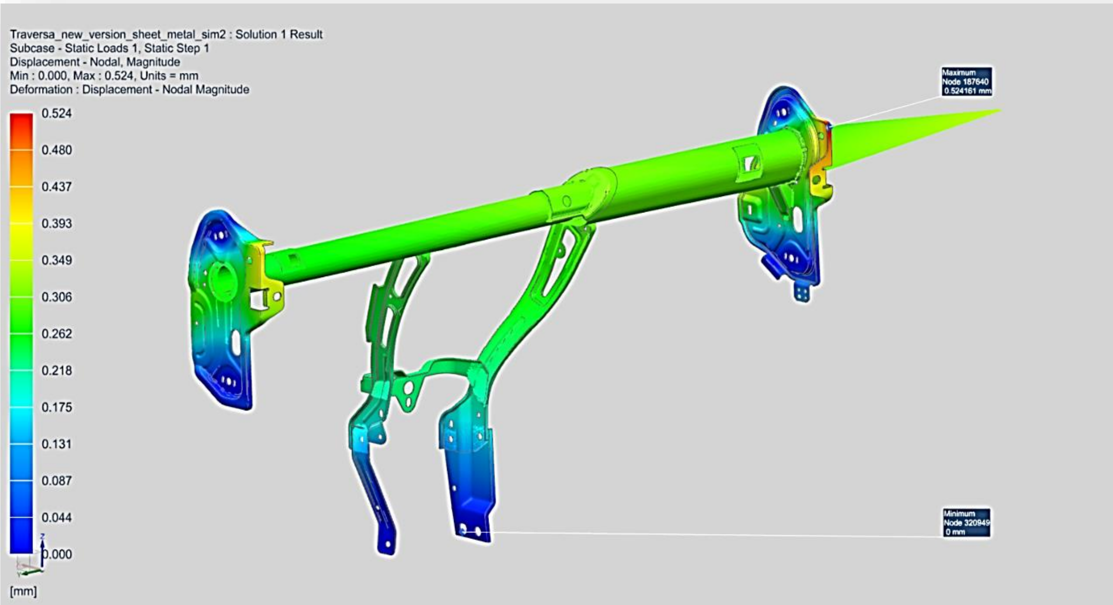

Figure 5.8 Max displacement of proposed CCB model (back-iso view)

Table 5-3 Maximum displacements comparison of three model and stress points of the proposed CCB model

Parameter	Standard Model (Full Tube)	Windowed Model (Lightweight)	Reinforced Model (Sheet Metal)
Max Displacement	~0.546 mm	~0.531 mm	**0.524 mm**
Global Stiffness	Baseline (High)	Reduced (Flexible)	**Restored (Optimized)**
Weight Status	Heavy	Lightest	**Lightweight + High Strength**
Node Location	Center of Tube	Center of Tube	**Node 187640**
Performance Verdict	Safe	Marginal (Vibration Risk)	**Excellent (Approved)**

Following the deformation evaluation, the von Mises stress distributions were examined. The highest stress levels in all three configurations were observed near the pillar attachment regions and bracket interfaces, where the external load was transferred into the structure. These locations are characterized by geometric discontinuities, mounting holes, and abrupt stiffness transitions, all of which contribute to local stress concentration.
The solid model exhibited a maximum stress value of approximately 422.7 MPa. The critical stress region was located near the attachment interface, where the local stress exceeded the yield strength of the FeE340 material used in the bracket region. Although the majority of the structure remained within acceptable stress limits, the localized hotspot indicates a potential yielding risk under severe loading conditions.

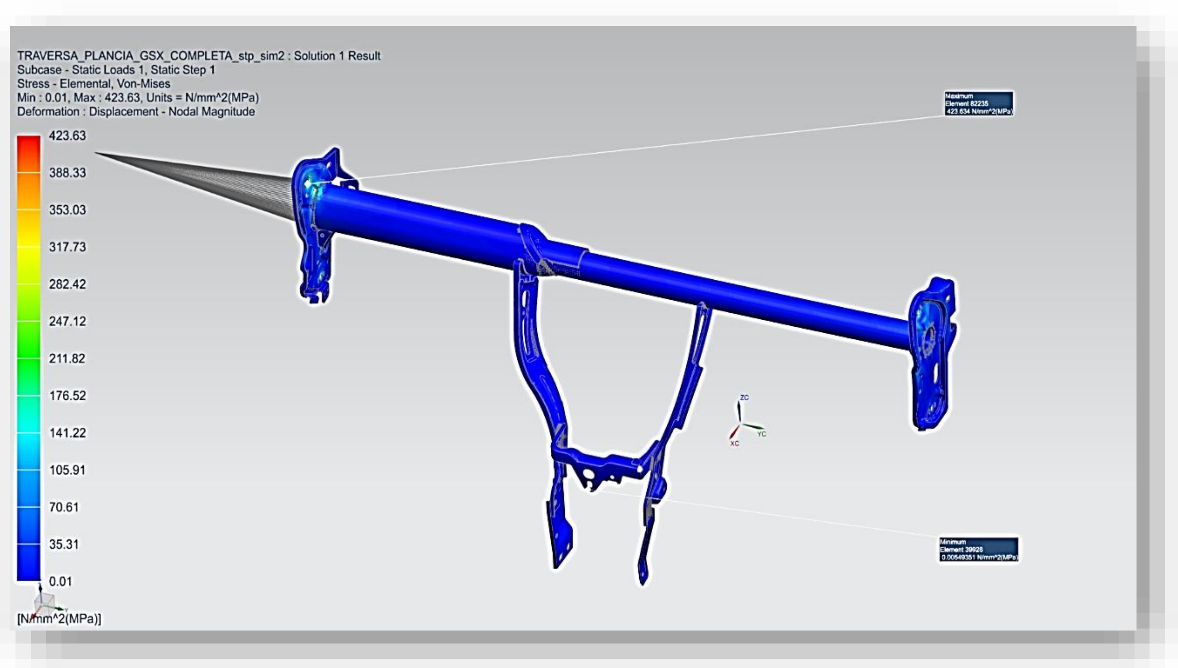

Figure 5.9 Von Mises Stress distribution of the solid CCB model (front-iso view)

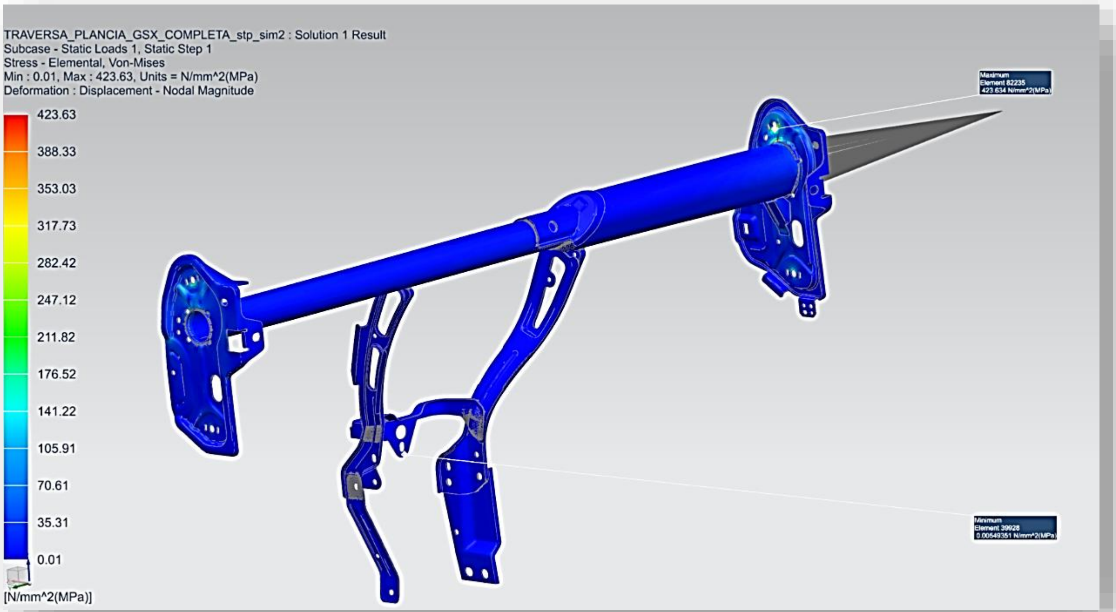

Figure 5.10 Von Mises Stress distribution of the solid CCB model (back-iso view)

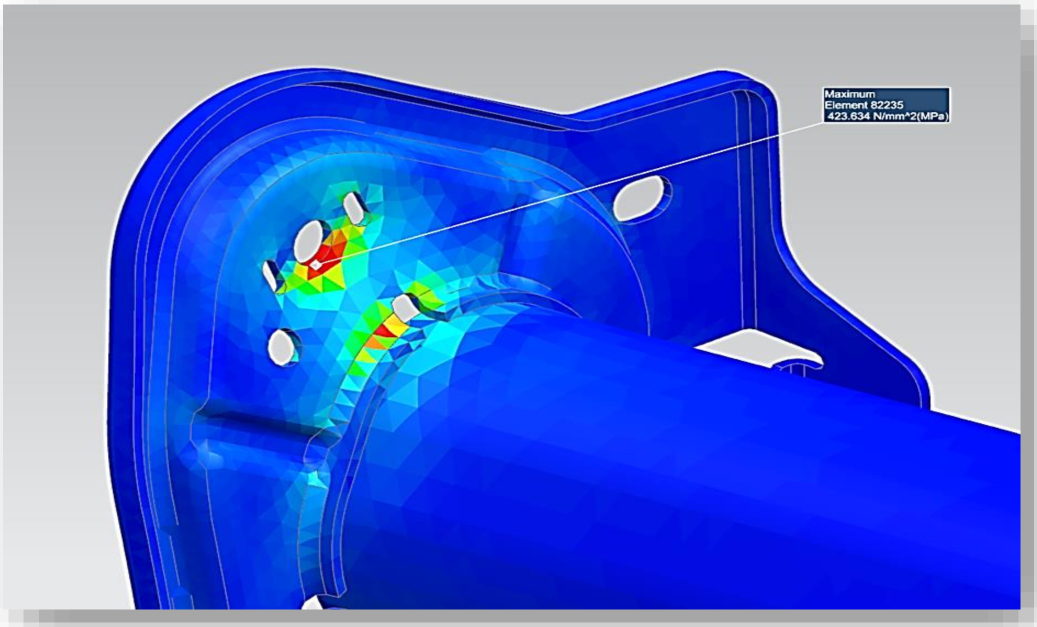

Figure 5.11 Von Mises Stress distribution of the solid CCB model (detailed view)

Table 5-4 Von Mises stress points and materials of the solid CCB model

Component	Material	Yield Strength (MPa)	Max Stress (MPa)	Status (Safety)
Tube (Main Beam)	FeE420	420 MPa	~120 MPa	**Safe**
A/B Pillars (General)	FeE340	340 MPa	~280 MPa	**Safe**
Critical Hotspot (Hole)	FeE340	340 MPa	**423.63 MPa**	**FAILURE / YIELDING**

The optimized model reduced the maximum stress value to approximately 405.74 MPa. At first glance, this result may appear counterintuitive because material was removed from the beam through the introduction of routing openings. However, the stress reduction can be explained by changes in the load transfer mechanism. In the original design, stresses remained concentrated within a relatively small structural region. After introducing the openings, the load path was redistributed around the opening boundaries and surrounding flanged regions, producing a more distributed stress field. As a result, peak von Mises stress values decreased despite the reduction in material volume.

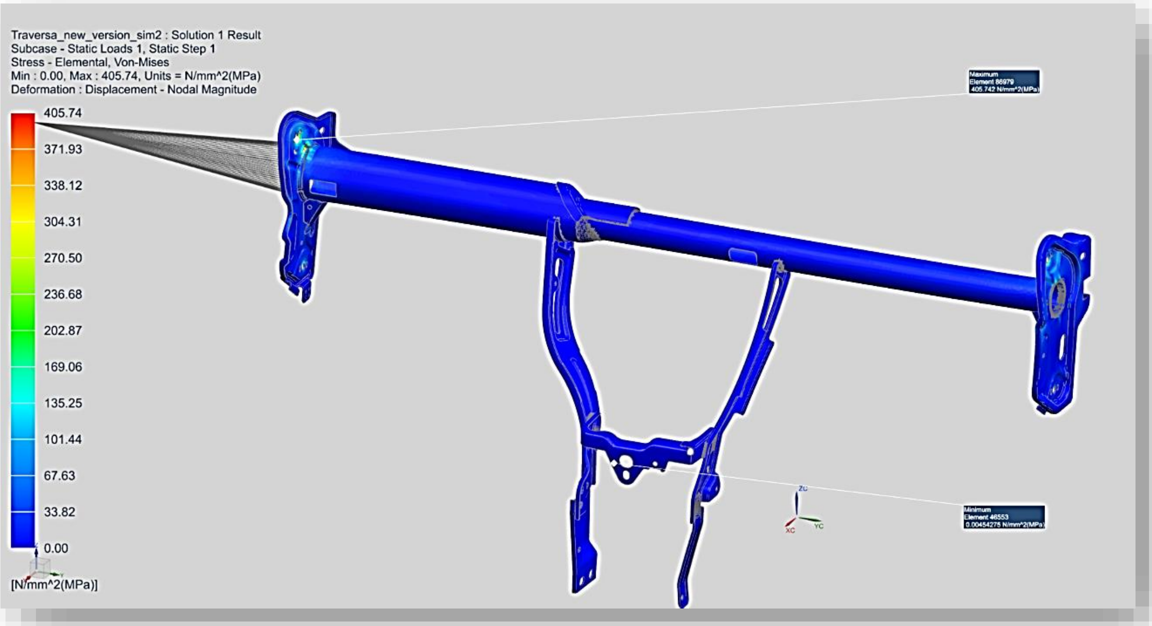

Figure 5.12 Von Mises Stress distribution of the optimized CCB model (front-iso view)

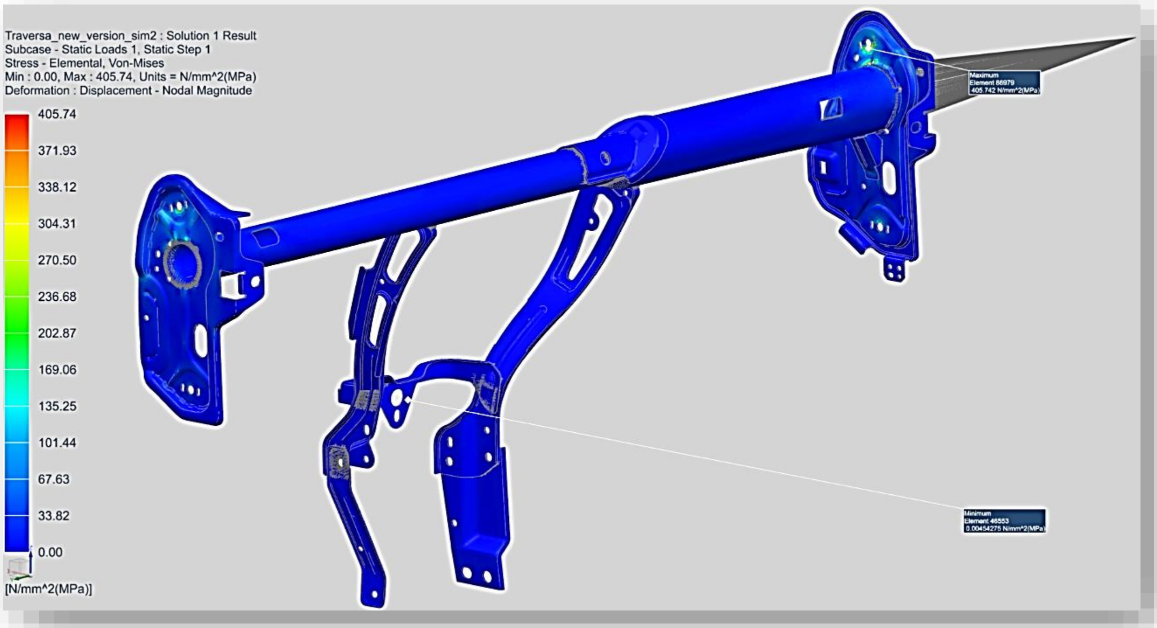

Figure 5.13 Von Mises Stress distribution of the optimized CCB model (back-iso view)

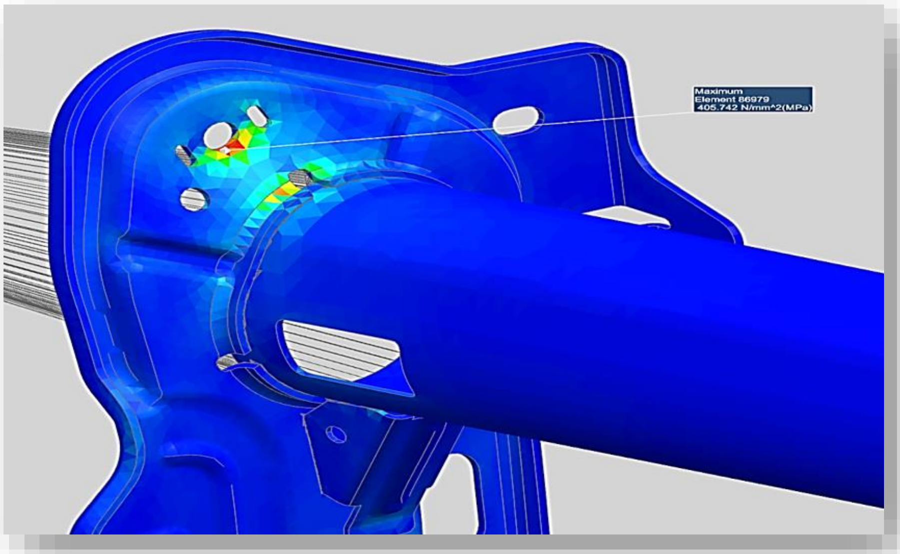

Figure 5.14 Von Mises Stress distribution of the optimized CCB model (detailed view)

Table 5-5 Von Mises stress points and materials of the optimized CCB model

Component	Material	Yield Strength (MPa)	Max Stress (MPa)	Safety Factor (S.F.)
Tube (Main Beam)	FeE420	420 MPa	~110 MPa	3.81
A/B Pillar (General)	FeE340	340 MPa	~270 MPa	1.25
Critical Hotspot	FeE340	340 MPa	**405.74 MPa**	**0.84**

The proposed model produced the lowest maximum stress value, approximately 404.68 MPa. The reinforcement plates increased the local stiffness around the routing windows and promoted a more uniform stress distribution. Consequently, stress concentrations near the modified regions were reduced and load transfer became more efficient. The reinforcement strategy therefore contributed not only to stiffness recovery but also to improved stress management within the structure.

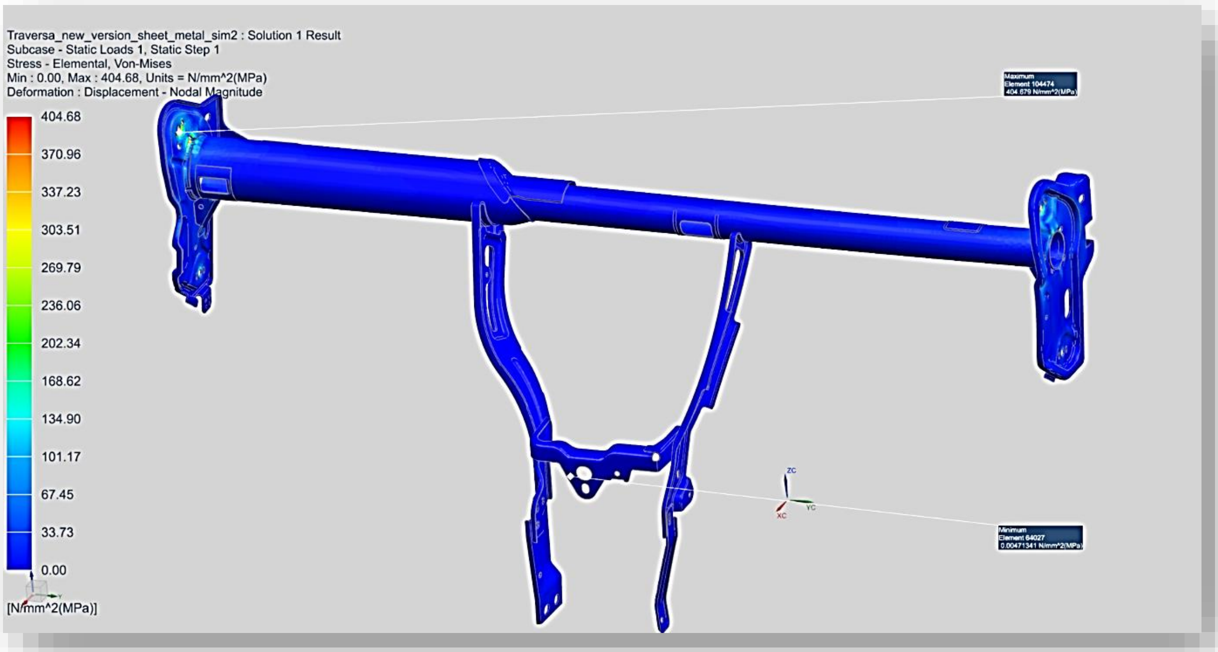

Figure 5.15 Von Mises Stress distribution of the proposed CCB model (front-iso view)

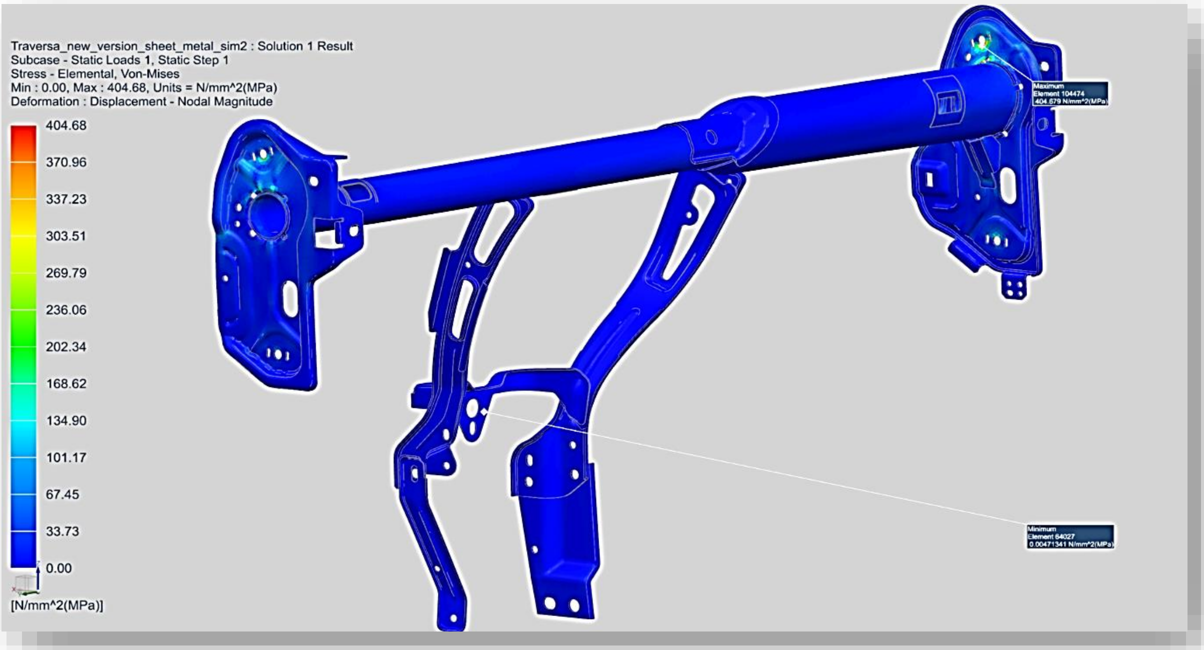

Figure 5.16 Von Mises Stress distribution of the proposed CCB model (back-iso view)

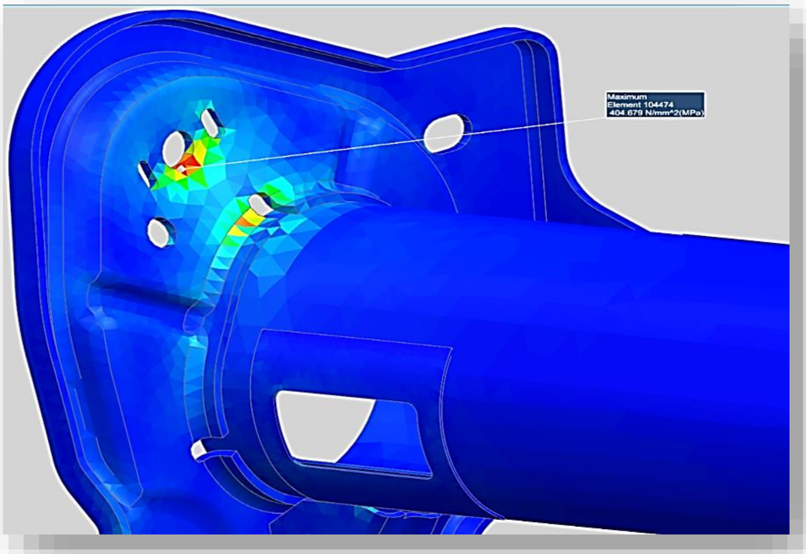

Figure 5.17 Von Mises Stress distribution of the proposed CCB model (detailed view)

Table 5-6 Von Mises stress points and materials of the proposed CCB model

Result Category	Value	Status	Analysis
Max System Stress	**404.68 MPa**	**SAFE**	Located at the side pillar bracket attachment point.
Tube Stress (Windows)	**~30 - 80 MPa**	**EXCELLENT**	The tube is effectively "sleeping" under this load.
Bracket Stress (Base)	**~100 - 150 MPa**	**SAFE**	Far below the **340 MPa** yield limit for FeE340.
Yield Margin (Tube)	**+340 MPa**	**HIGH**	Significant safety factor relative to **420 MPa** limit.

A more detailed investigation of the main tube stresses revealed an even more significant improvement. The maximum local tube stress decreased from 135.30 MPa in the original model to 109.20 MPa in the optimized model and further to 108.89 MPa in the reinforced model. These results demonstrate that the routing modifications did not adversely affect the primary load-carrying component of the Cross-Car Beam. On the contrary, the stress redistribution achieved through the modified geometry reduced local stress levels within the tube itself.

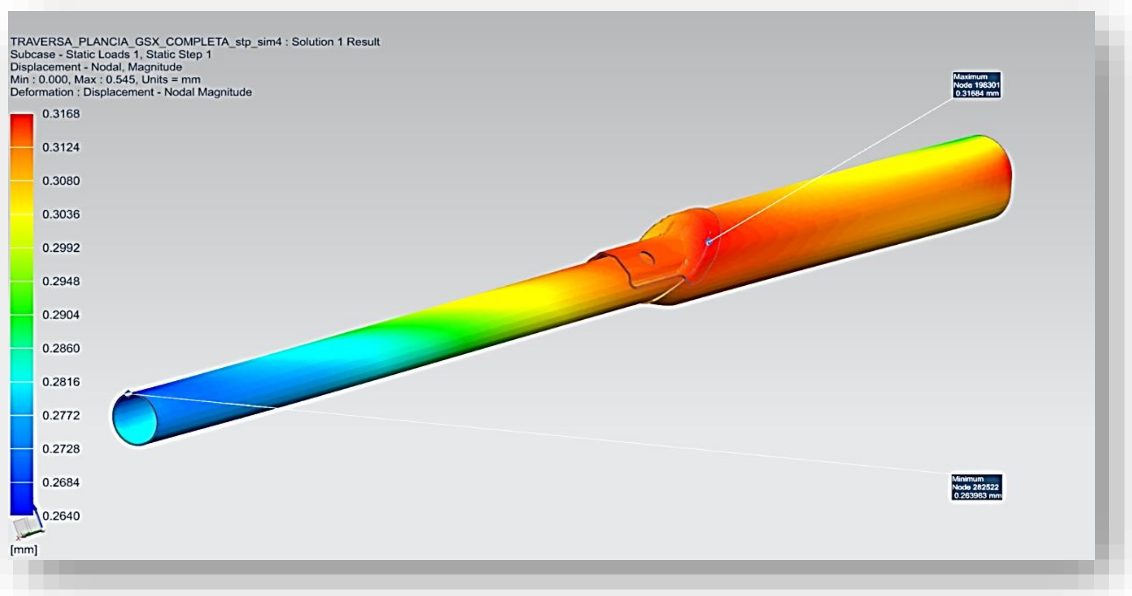

Figure 5.18 Local tube Displacement of the solid CCB model

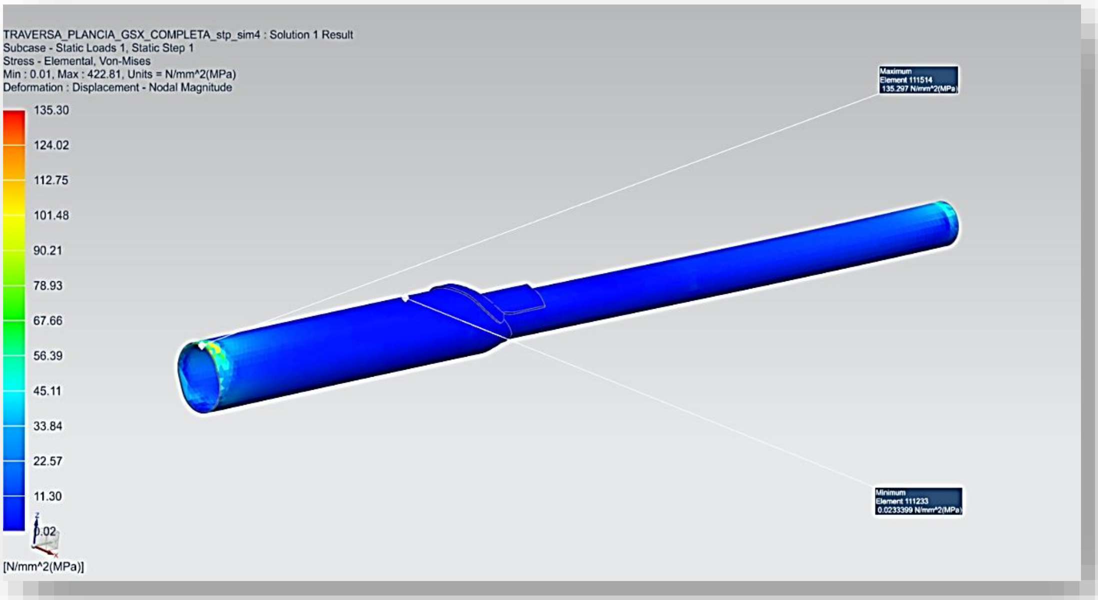

Figure 5.19 Local tube Von Mises stress of the solid CCB model

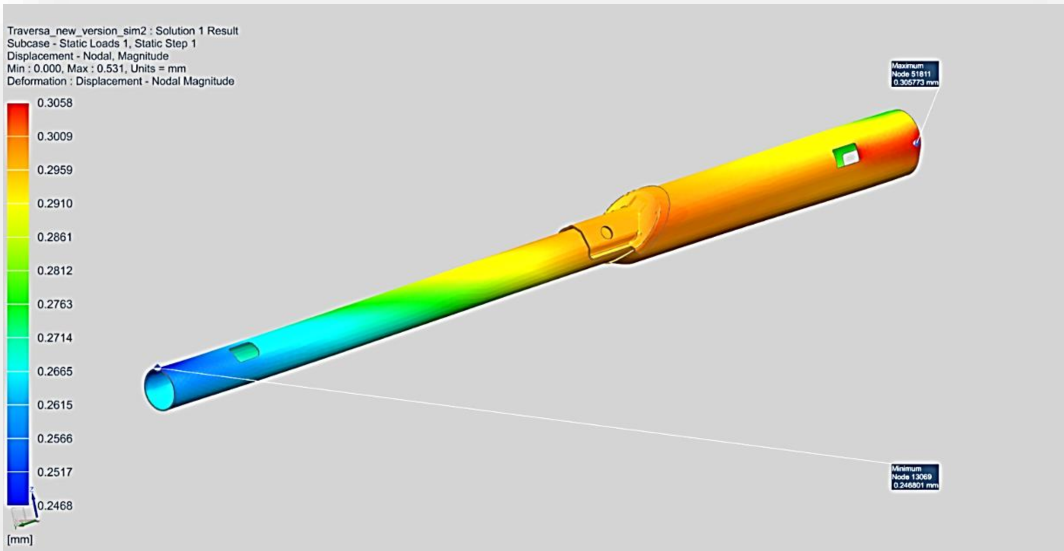

Figure 5.20 Local tube Displacement of the optimized CCB model

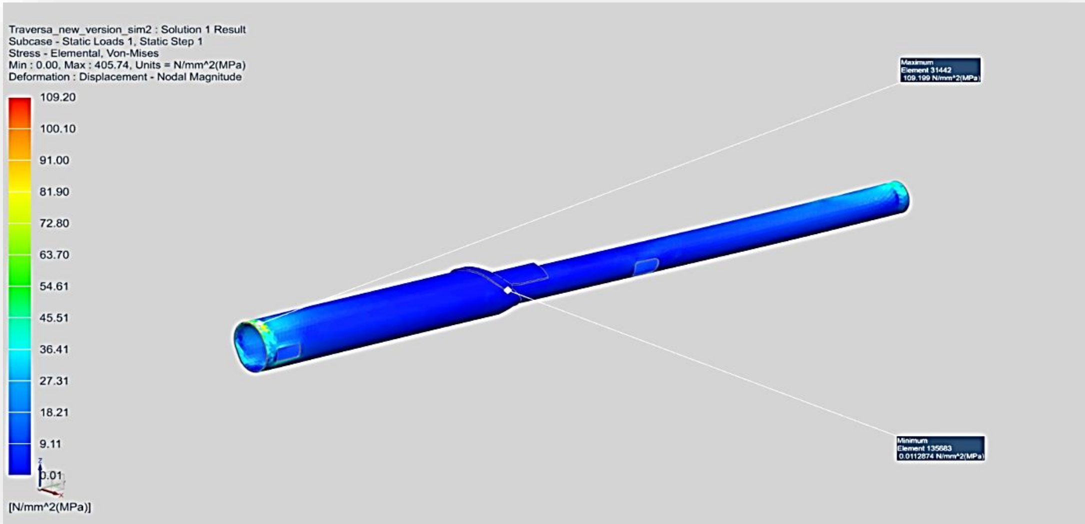

Figure 5.21 Local tube Von Mises stress of the optimized CCB model

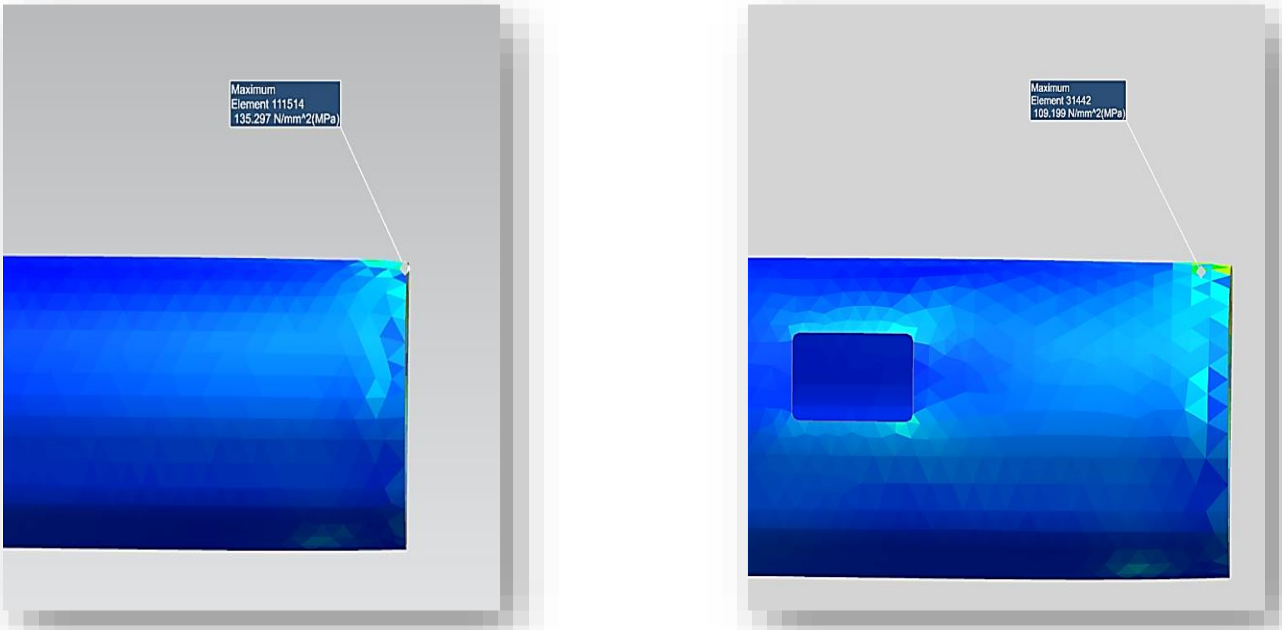

Figure 5.22 Comparison of local tubes solid – optimized CCB model

As can be seen in **Figure 5.22**, in the solid CCB model, the stress is more localized at the edge of the tube with a high stress value, whereas in the optimized model, the stress is more distributed due to the holes, and therefore the edge of the tube has a lower stress value compared to the solid CCB model. This is why max Von Mises stress occurs lower in optimized CCB model

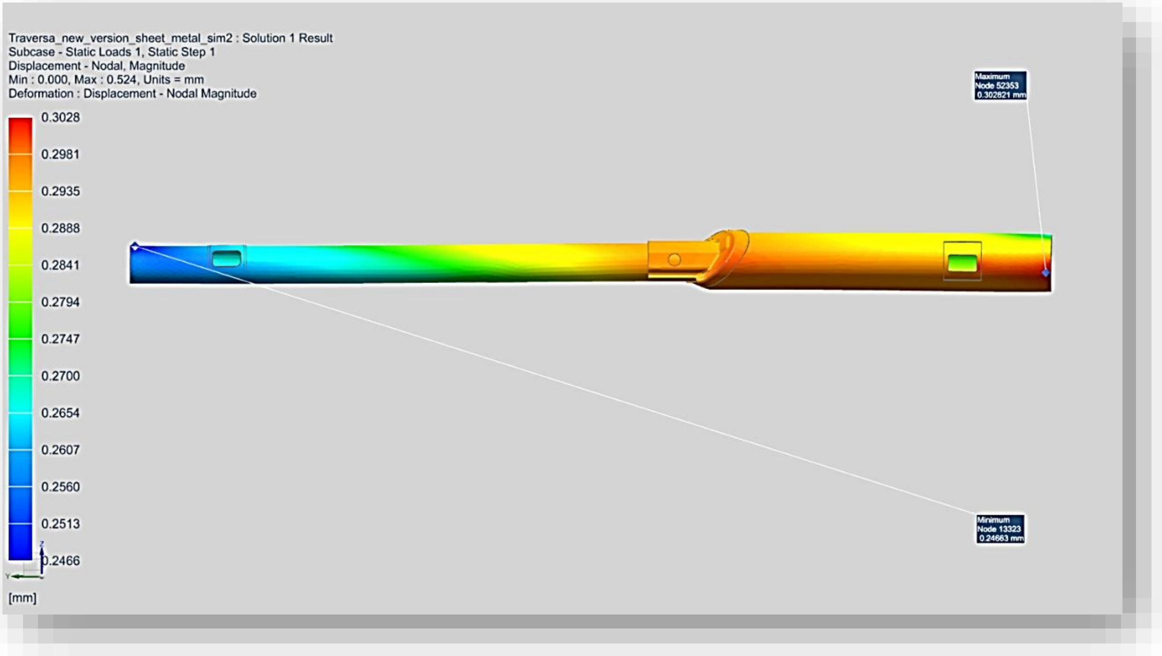

Figure 5.23 Local tube Displacement of the proposed CCB model

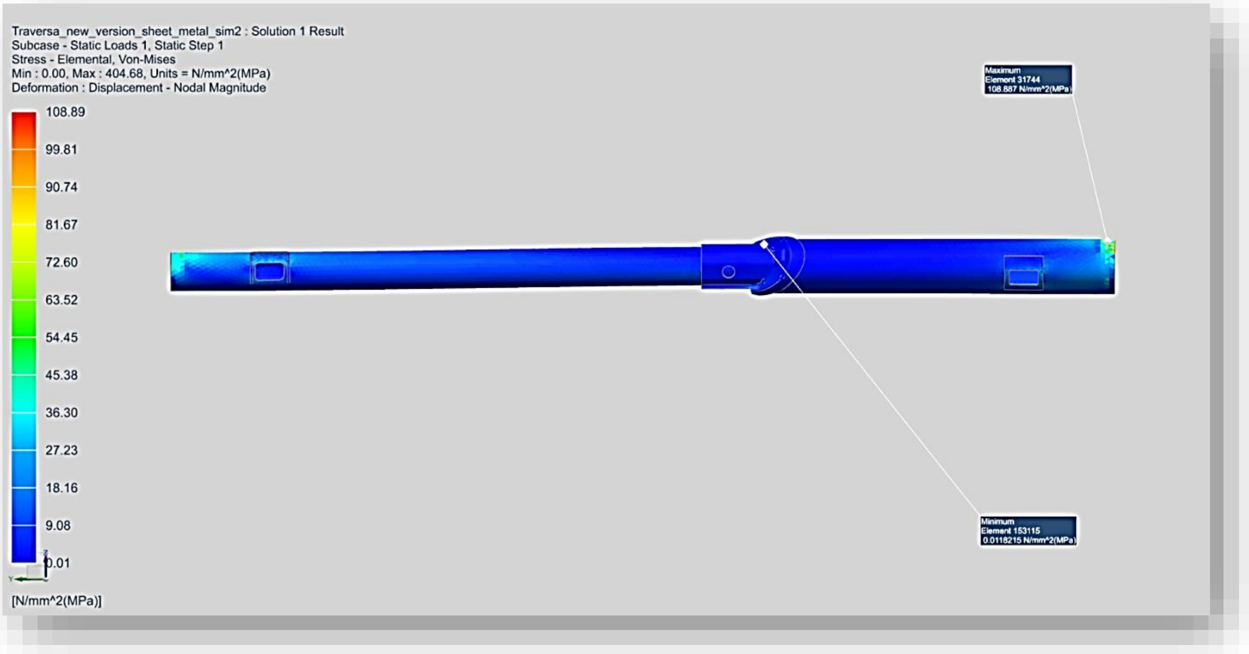

Figure 5.24 Local tube Von Mises stress of the proposed CCB model

Table 5-7 General Comparison of three models (Displacement, Stress)

Metric	Standard (Solid) Model	Optimized CCB Model	Proposed Model (Sheet Metal)
Global Max Displacement	0.545 mm	0.531 mm	0.524 mm
Max Local Tube Displacement	0.317 mm	0.306 mm	0.303 mm
Global Max Stress	422.81 MPa	405.74 MPa	404.68 MPa
Max Local Tube Stress	135.30 MPa	109.20 MPa	108.89 MPa

5.1.2 Additional Crash Loading Sceneroius Results (Steering Wheel, HVAC, Airbag Deployement)

The combined loading analysis produced significantly higher deformation values compared with the 4000 N A-pillar loading case. The deformation distributions obtained from the three Cross-Car Beam configurations are presented in **Figure 5.25, Figure 5.26, Figure 5.27.**

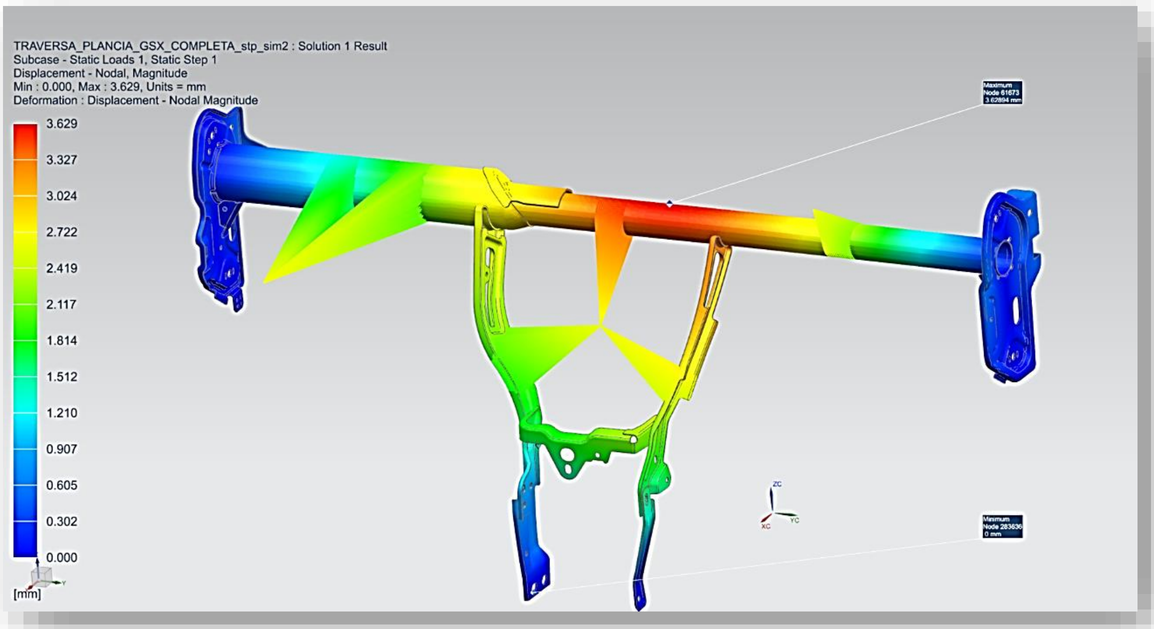

Figure 5.25 Total deformation of the solid CCB model

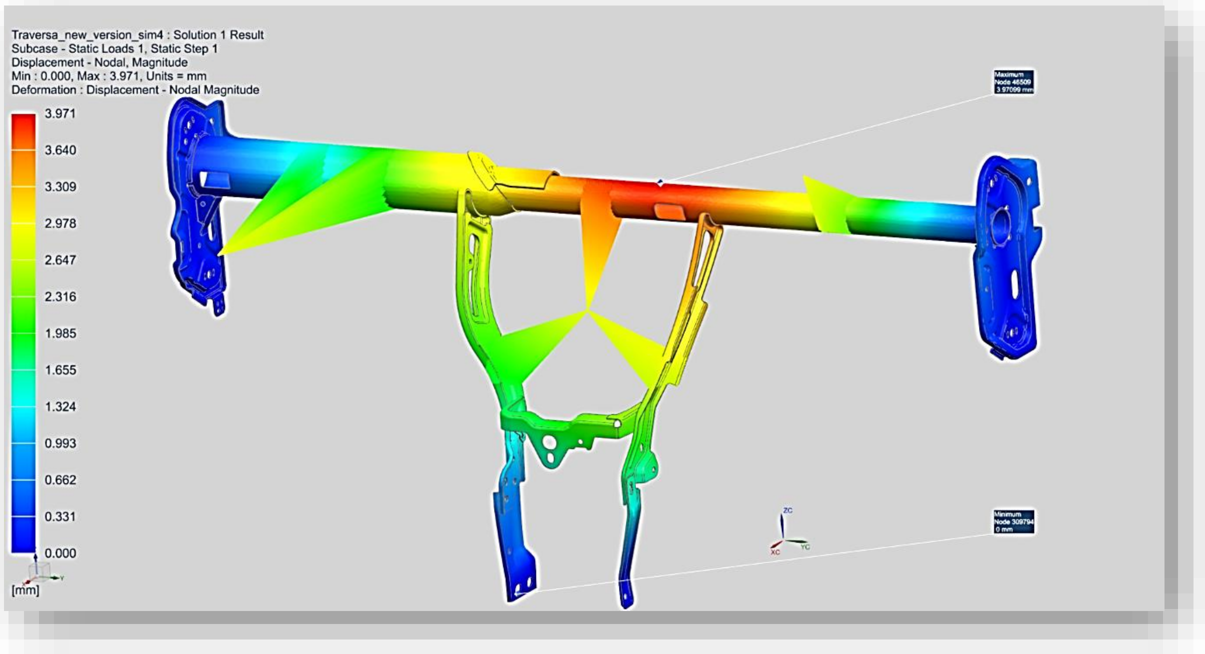

Figure 5.26 Total deformation of the optimized CCB model

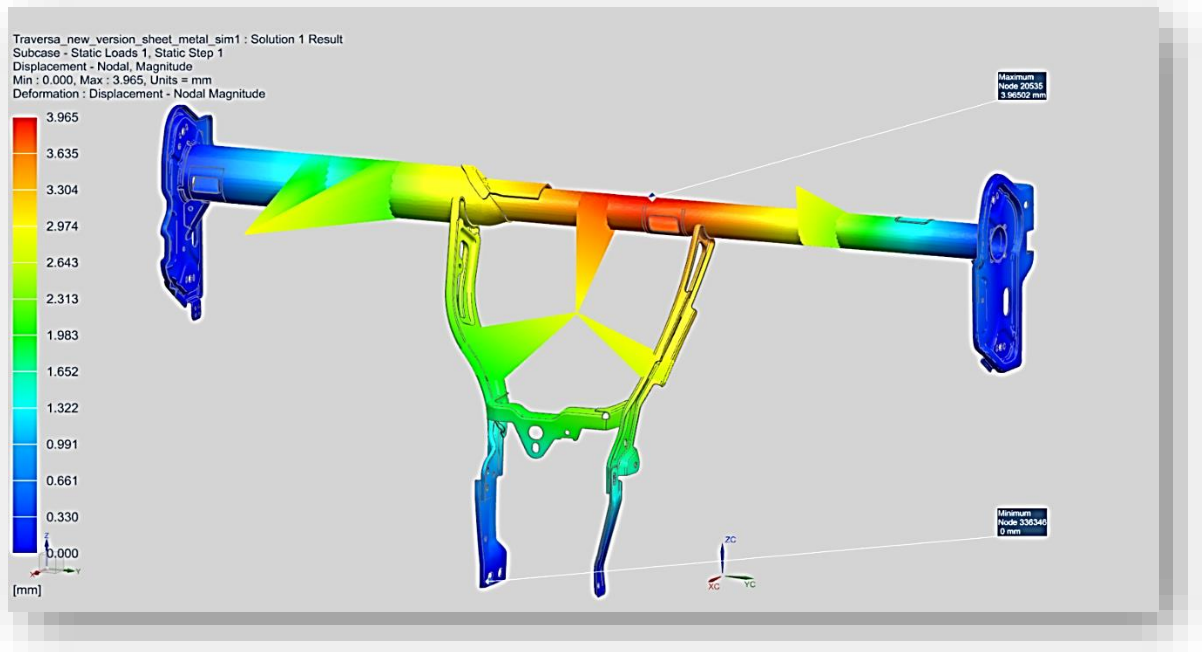

Figure 5.27 Total deformation of the proposed CCB model

The solid model exhibited a maximum displacement of 3.629 mm. The highest deformation occurred in the central region of the Cross-Car Beam where the applied loads generated the largest bending effect. The optimized model produced a maximum displacement of 3.971 mm, representing an increase of approximately 9.4% compared with the original design. This increase indicates that the routing openings reduced the local stiffness of the beam structure and increased its flexibility under loading conditions.

The reinforced model exhibited a maximum displacement of 3.965 mm. Although the reinforcement plates slightly reduced the displacement compared with the optimized configuration, the overall deformation remained relatively similar. This observation suggests that the reinforcement structures primarily improved local stiffness around the modified regions rather than significantly influencing the global deformation behavior of the assembly.

Table 5-8 Results table of the solid CCB model

Result Category	Value	Details / Location
Max Global Displacement	**3.629 mm**	Located at the center of the tube (Red zone)
Min Global Displacement	**0.000 mm**	Located at the pillar mounting points (Blue zone)
Critical Node	**Node 61673**	Point of maximum deflection under combined 35g load
Total Mass on Beam	**20.5 kg**	Steering Wheel (8kg) + HVAC (10kg) + Airbag (2.5kg)
Total Applied Force	**~7,038 N**	Combined forces at 35g acceleration (20.5 kg *35*g)
Tube Material	**FeE420**	Yield Strength: 420 MPa
Bracket Material	**FeE340**	Yield Strength: 340 MPa

Table 5-9 Results and comparison table of the solid - optimized CCB model

Result Category	Standard Model	Optimized Model	Change
Max Displacement	3.629 mm	**3.971 mm**	**+9.4% Increase**
Critical Node	Node 61673	**Node 46509**	Shifted location
Applied Force	~7,038 N	**~7,038 N**	Constant (35g)
Stiffness Status	Stable	**Flexible**	Reduced Rigidity

Table 5-10 Results table of the proposed CCB model

Result Category	Value	Details / Location
Max Global Displacement	**3.965 mm**	Located at **Node 20535** (Center of the tube)
Min Global Displacement	**0.000 mm**	Located at **Node 336346** (Pillar mountings)
Applied Acceleration	**35g**	Static equivalent load for crash safety
Total Assembly Mass	**20.5 kg**	Steering (8kg) + HVAC (10kg) + Airbag (2.5kg)
Tube Material	**FeE420**	Yield Strength: 420 MPa
Reinforcement Material	**FeE420**	Local sheet metal patches on windows
Bracket Material	**FeE340**	Yield Strength: 340 MPa

Following the deformation evaluation, the von Mises stress distributions were examined in order to identify the critical structural regions and evaluate the influence of the routing modifications on the stress transfer mechanism of the Cross-Car Beam assembly.

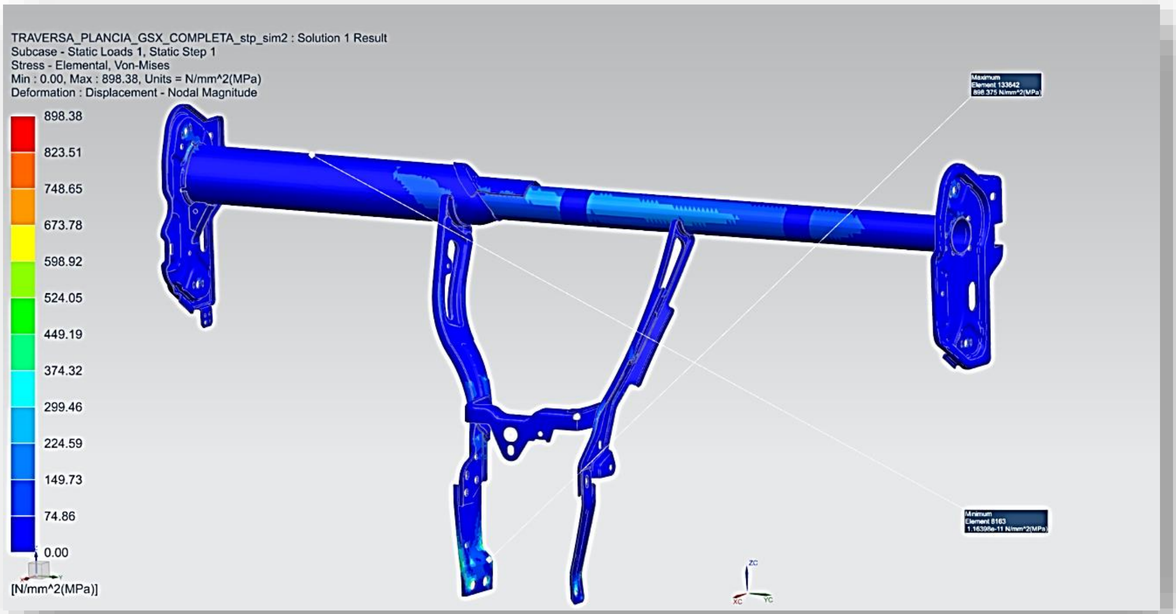

Figure 5.28 Von Mises stress distribution of the solid CCB model

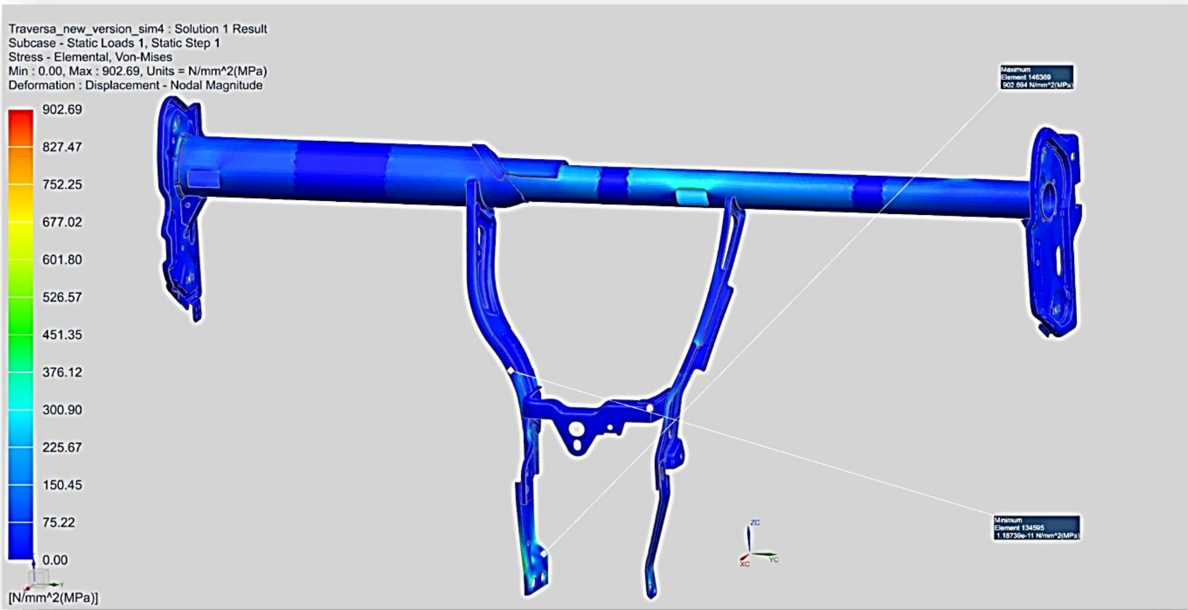

Figure 5.29 Von Mises stress distribution of the optimized CCB model

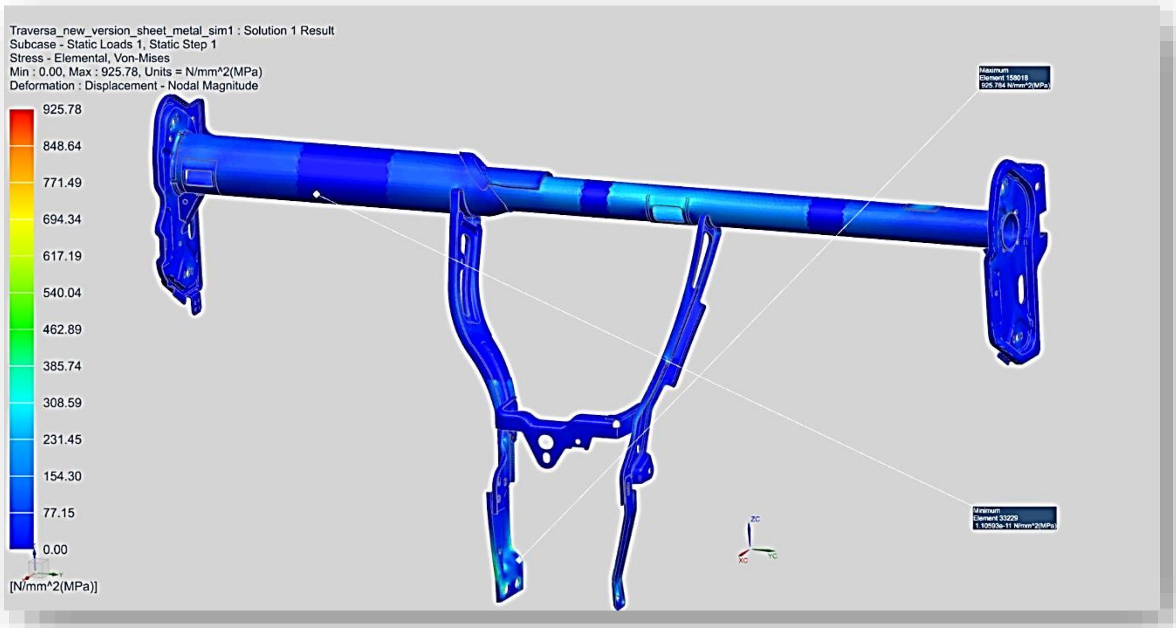

Figure 5.30 Von Mises stress distribution of the proposed CCB model

The solid model exhibited a maximum stress of approximately 898 MPa. The highest stress concentrations were observed around the lower bracket attachment regions, where the loads were transferred into the structure. These locations represented the most critical areas within the original configuration.

After the routing openings were introduced, the stress distribution changed considerably. In the optimized model, the opening boundaries became critical stress concentration regions due to the geometric discontinuities introduced into the tube structure. The maximum tube stress reached approximately 556 MPa, indicating that the modified geometry significantly influenced the local stress behavior of the primary load-carrying member.

Although the routing openings increased local stress concentrations around the opening edges, they also altered the load transfer path within the structure. As a result, the stresses were redistributed through the surrounding structural members rather than remaining concentrated in a limited region of the tube. This redistribution explains the change in the overall stress pattern observed in the optimized configuration.

The reinforced model demonstrated a more favorable stress distribution around the modified regions. The reinforcement plates increased the local stiffness around the routing openings and reduced the severity of the stress concentrations. Consequently, the maximum tube stress decreased from approximately 556 MPa to 464 MPa, corresponding to a reduction of nearly 92 MPa.

Table 5-11 Von mises stress results table of the solid CCB model

Result Category	Value	Details / Location
Max Global Stress	**898.375 MPa**	**Element 133542**: Lower bracket fixation point
Min Global Stress	**~0.000 MPa**	Isolated areas with negligible load
Applied Acceleration	**35g (Combined)**	Static equivalent load for crash scenario
Material Yield (FeE420)	**420 MPa**	**FAIL**: Stress is 213% of yield limit
Material Yield (FeE340)	**340 MPa**	**FAIL**: Stress is 264% of yield limit

Table 5-12 Von mises stress results table of the optimized CCB model

Result Category	Value	Details / Location
Max Global Stress	**902.694 MPa**	**Element 146369**: Lower bracket fixation
Applied Acceleration	**35g (Combined)**	Static equivalent load for crash
Material Yield (FeE420)	**420 MPa**	**FAIL**: Safety Factor 0.46 (Tube Zone)
Material Yield (FeE340)	**340 MPa**	**FAIL**: Safety Factor 0.37 (Bracket Zone)

Table 5-13 Von mises stress results table of the proposed CCB model

Category	Value	Status	Analysis
Max System Stress	**925.78 MPa**	**FAIL**	Located at the bracket foot (**Element 158018**).
Tube Stress (Windows)	**~230 - 310 MPa**	**PASS**	The patches successfully "cured" the tube's stress.
Bracket Yield (FeE340)	**340 MPa**	**FAIL**	Stress is **2.7x** higher than the material limit.
Tube Yield (FeE420)	**420 MPa**	**PASS**	The tube remains well within the elastic zone.

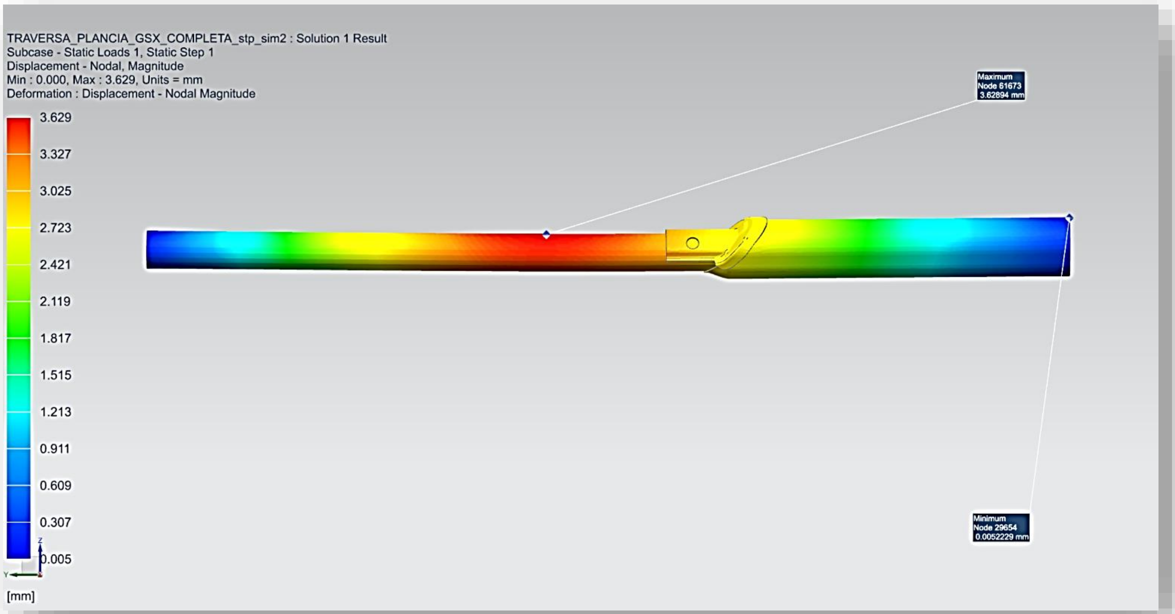

Figure 5.31 Local tube deformation of the solid CCB model

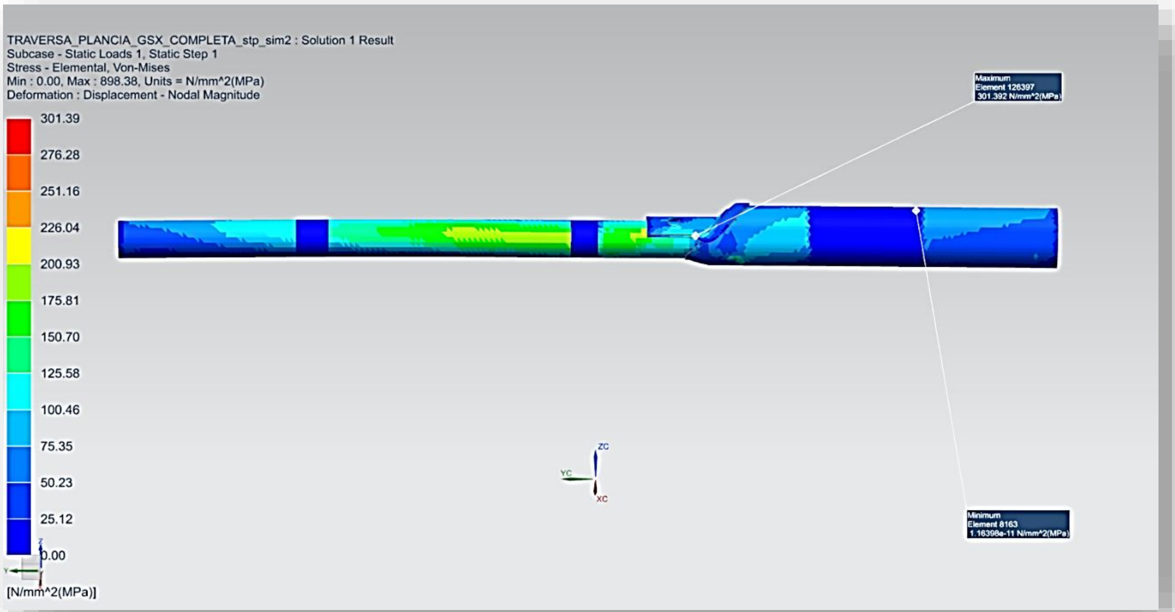

Figure 5.32 Local tube Von mises stress distribution of the solid CCB model

Table 5-14 Local tube Von Mises stress distribution and deformation results of the solid CCB model

Result Category	Value	Details / Location
Material Yield Strength	**420 MPa**	Specific to FeE420 grade
Max Tube Stress	**301.392 MPa**	Located at **Element 126397** (Overlap zone)
Max Displacement	**3.629 mm**	Located at **Node 61673** (Mid-span)
Safety Factor (Tube)	**1.39**	Calculated as 420 / 301.39
Status	**PASS**	Stress is below material yield limit

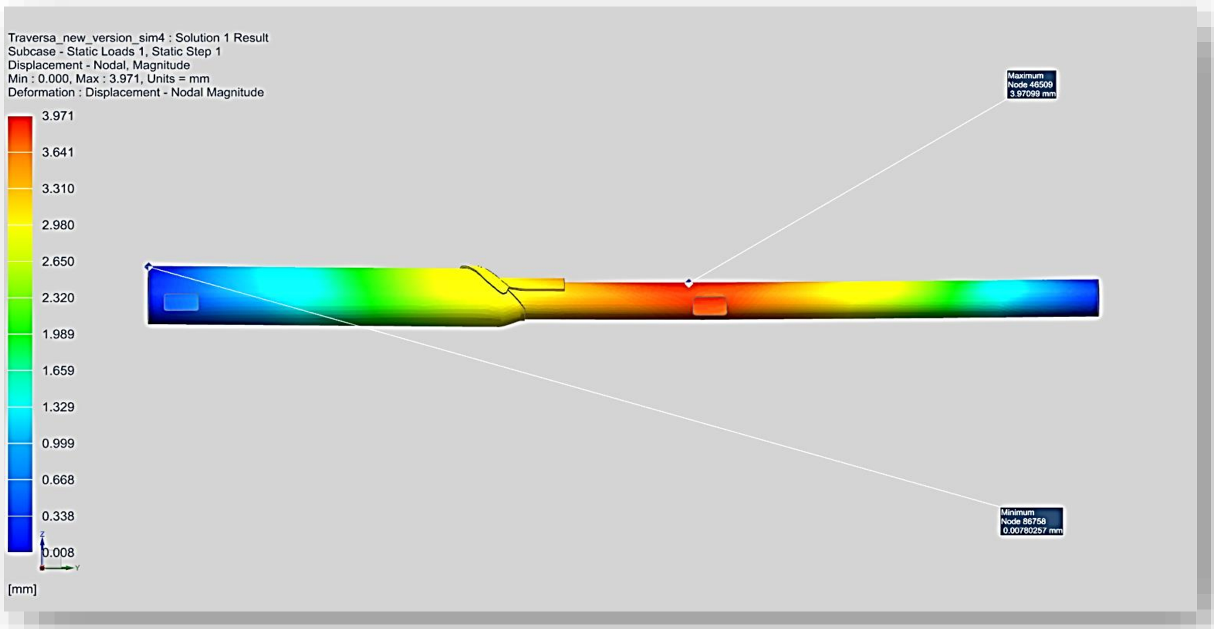

Figure 5.33 Local tube deformation of the optimized CCB model

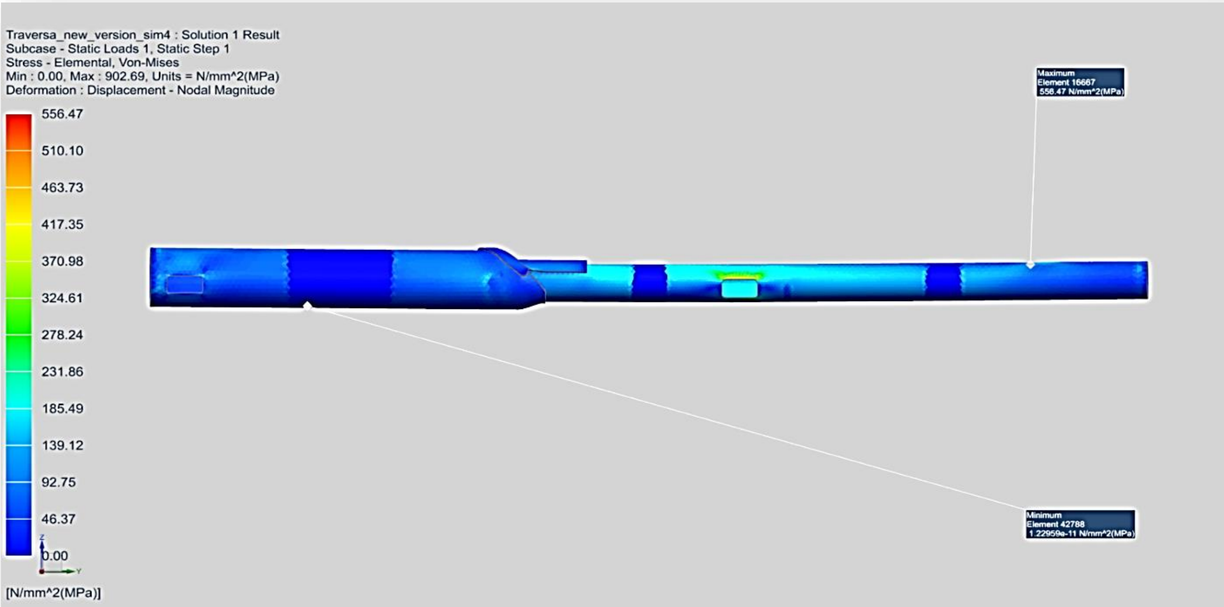

Figure 5.34 Local tube Von mises stress distribution of the optimized CCB model

Table 5-15 Local tube Von mises stress distribution and deformation results of the optimized CCB model

Result Category	**Value**	**Details / Location**
Max Global Displacement	**3.971 mm**	Located at **Node 46509** (Red zone near windows)
Max Beam Stress	**556.47 MPa**	Located at **Element 16667** (Window edge)
Material Yield (FeE420)	**420 MPa**	**FAIL**: Stress is 132% of yield limit
Stress Increase	**+255 MPa**	Jump from 301 MPa (Standard) to 556 MPa
Total Mass on Beam	**20.5 kg**	HVAC (10kg) + Steering (8kg) + Airbag (2.5kg)

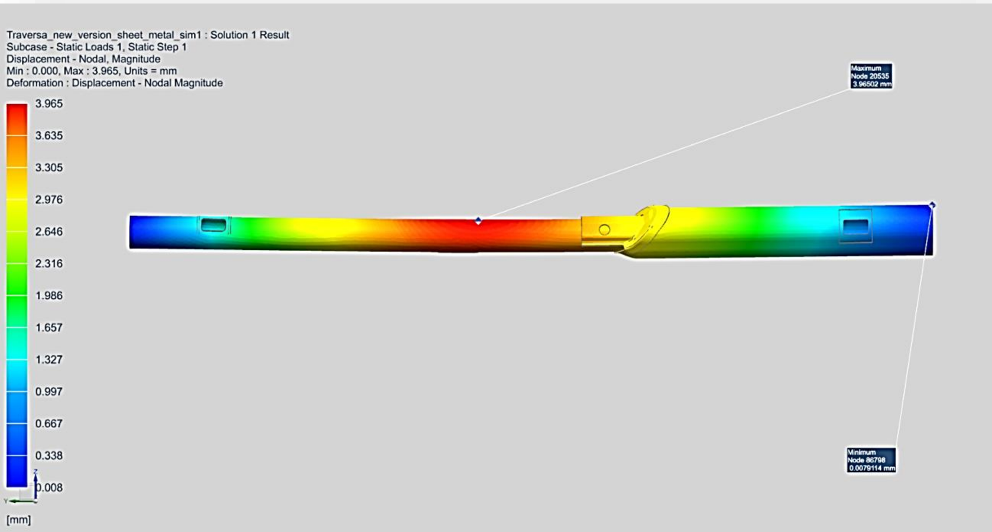

Figure 5.35 Local tube deformation of the proposed CCB model

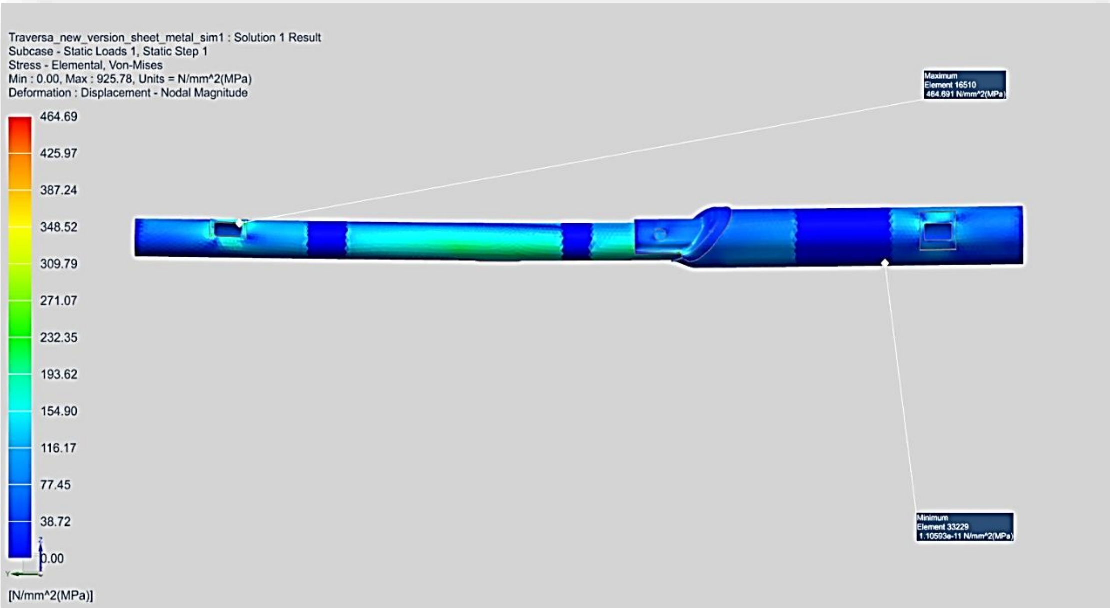

Figure 5.36 Local tube Von mises stress distribution of the proposed CCB model

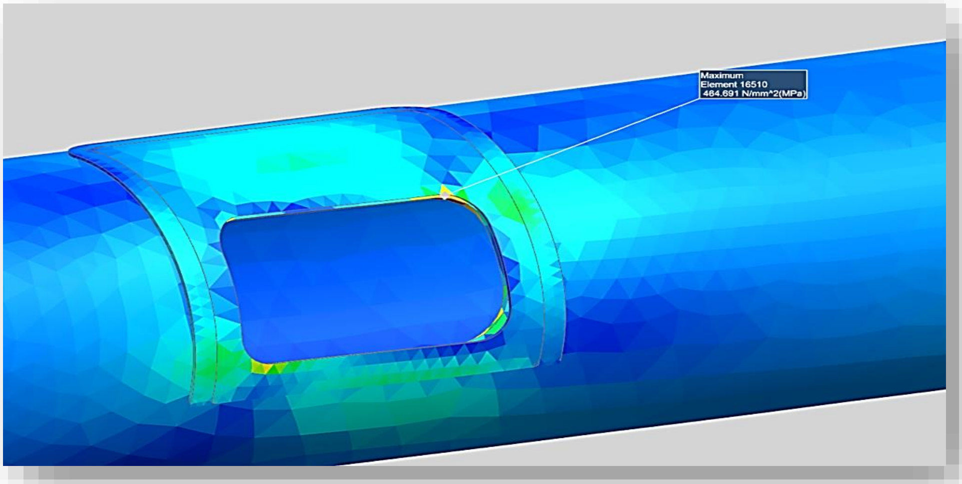

Figure 5.37 Local tube Von mises stress distribution of the proposed CCB model detailed view

Table 5-16 Local tube Von mises stress distribution and deformation results of the proposed CCB model

Category	Value	Status	Analysis
Max Tube Stress	**464.691 MPa**	**Marginal FAIL**	Located at **Element 16510** (Edge of the window reinforcement).
Material Yield (FeE420)	**420 MPa**	**Over-limit**	The stress is approximately **10.6% above** the yield limit.
Max Displacement	**3.965 mm**	**Stable**	Located at **Node 20535** in the center.
Improvement	**-91.7 MPa**	**Significant**	Stress dropped from 556 MPa (unreinforced) to 464 MPa.

The detailed stress contours indicate that the routing openings became the dominant stress concentration locations in the optimized configuration. After the reinforcement plates were introduced, the stress concentrations around the opening boundaries were significantly reduced and the load transfer became more uniform throughout the modified region. As a result, the critical stress locations shifted toward the bracket attachment areas rather than remaining concentrated around the routing openings.

Overall, the combined loading analysis demonstrates that the routing modifications increased structural flexibility and generated local stress concentrations around the opening regions. However, the reinforcement strategy successfully reduced the tube stresses and improved the stress distribution within the Cross-Car Beam assembly. The results indicate that the reinforcement plates effectively compensated for the local stiffness reduction introduced by the routing modifications and improved the structural performance of the optimized design.

5.2 Modal Analysis Results

Modal analysis was conducted to investigate the dynamic behavior of the three Cross-Car Beam configurations and to evaluate the influence of the routing openings and reinforcement structures on the vibration characteristics of the assembly. The evaluation focused on the first three vibration modes because these modes generally have the greatest influence on the structural response and NVH (noise, vibration, harness) performance of automotive dashboard support systems. Natural frequencies, mode shapes, and strain energy distributions were examined for each configuration and compared to assess the dynamic performance of the proposed design.

5.2.1 Solid Model Modal Analysis Results

The modal analysis results obtained for the original solid Cross-Car Beam configuration are presented in this section. The first three vibration modes were evaluated because they represent the most significant dynamic characteristics of the structure within the investigated frequency range. For each mode, the natural frequency, deformation pattern, and strain energy distribution were examined to identify the critical regions contributing to the dynamic behavior of the assembly.

Table 5-17 Natural Frequencies and Strain Energy values of the solid CCB model

Mode No.	Natural Frequency (Hz)	Max Displacement (mm)	Max Strain Energy (N-mm)	Dominant Mode Shape / Character
Mode 1	**61.439 Hz**	0.282 mm	0.0786 N-mm	Vertical bending of the main tube (Right side).
Mode 2	**103.959 Hz**	0.661 mm	0.444 N-mm	Torsional vibration/lateral swaying of the low brackets.
Mode 3	**119.865 Hz**	0.799 mm	2.390 N-mm	Complex high-frequency local vibration.

As shown in **Table 5-17**, the natural frequency increased with increasing vibration mode number. A similar trend was observed for strain energy values, where the third mode exhibited considerably higher strain energy than the first and second modes. This behavior indicates that the higher vibration modes involve more complex deformation patterns and greater energy accumulation within the structure.
The first vibration mode occurred at 61.439 Hz. The corresponding mode shape is presented in **Figure 5.38**. The deformation pattern was characterized primarily by global bending behavior of the Cross-Car Beam assembly. The largest structural motion was observed in the central beam region, while the constrained attachment locations remained relatively stationary.

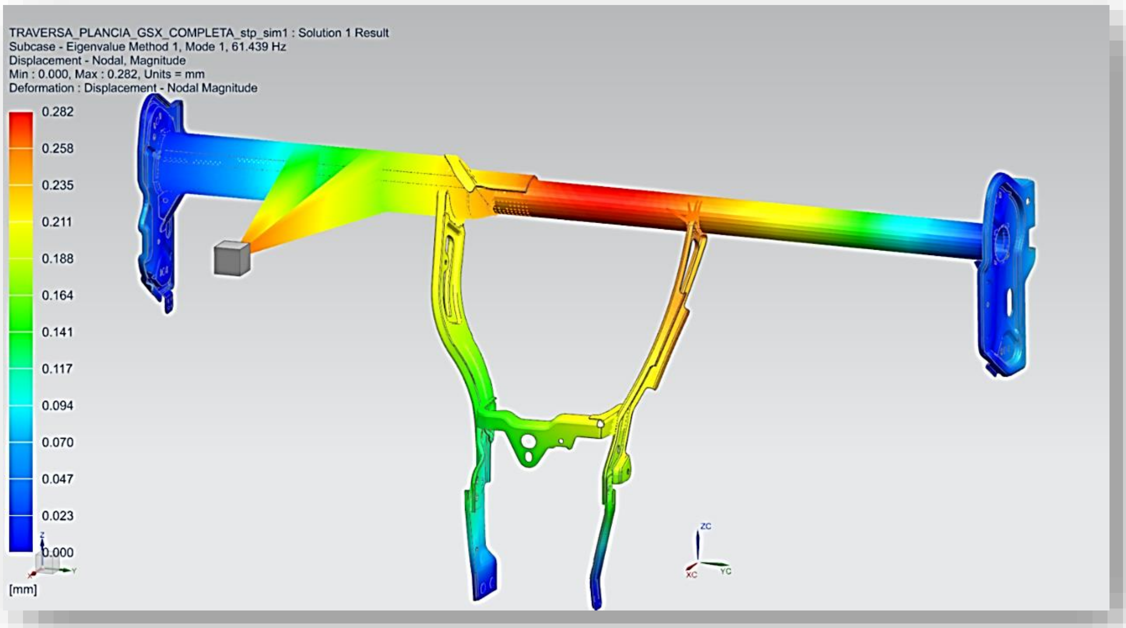

Figure 5.38 First vibration mode shape of the solid CCB model

The strain energy distribution associated with the first mode is presented in **Figure 5.39**. The results indicate that the highest strain energy concentrations occurred around the A-pillar attachment regions and bracket interfaces. These areas therefore contribute significantly to the vibration behavior of the assembly and represent the primary load-carrying regions during dynamic excitation.

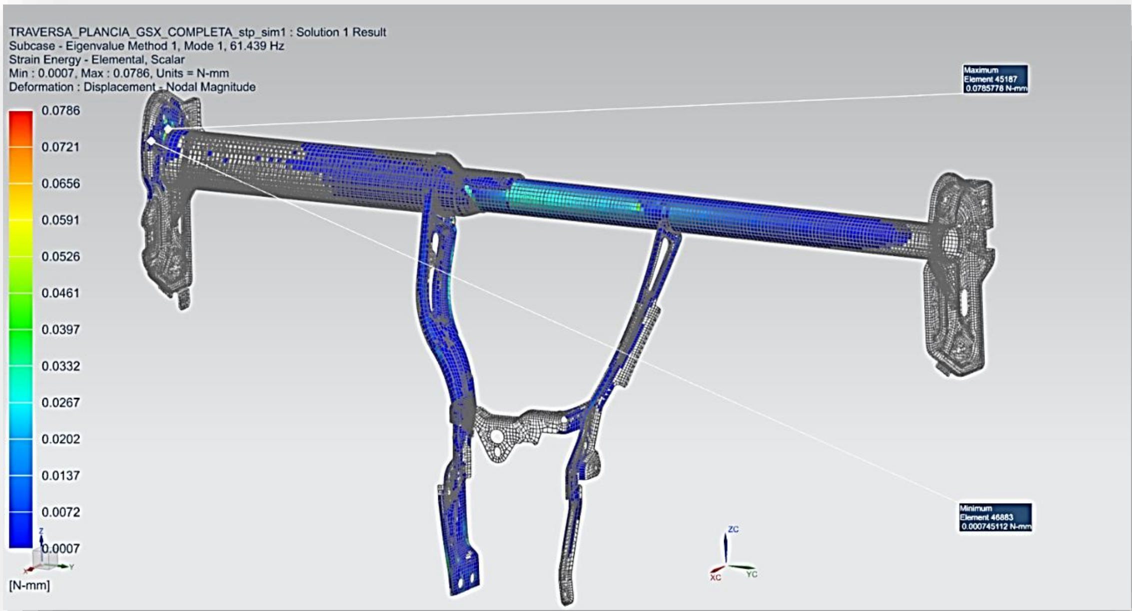

Figure 5.39 Strain energy distribution of mode 1 for the solid CCB model

The second vibration mode was obtained at 103.959 Hz. Compared with the first mode, the deformation pattern exhibited increased torsional behavior along the beam structure. This indicates that the dynamic response of the assembly becomes more complex as the excitation frequency increases.

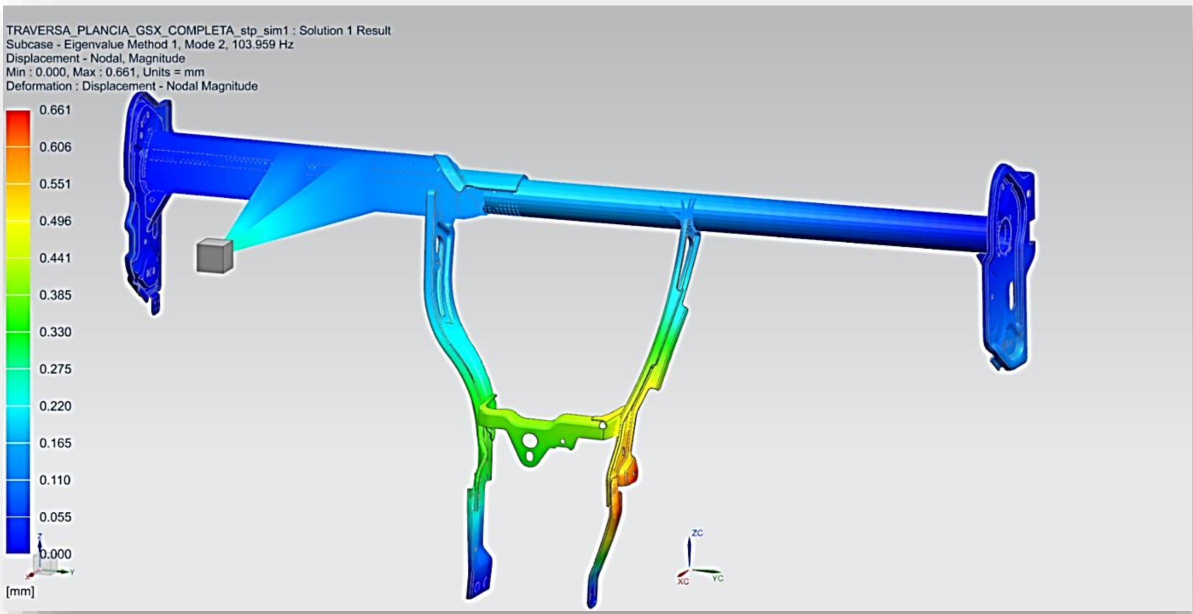

Figure 5.40 Second vibration mode shape of the solid CCB model

The corresponding strain energy distribution is shown in **Figure 5.4**1 Like the first mode, elevated strain energy levels were observed around the attachment interfaces. However, the energy distribution extended over a larger structural region, indicating increased participation of the beam assembly in the vibration response.

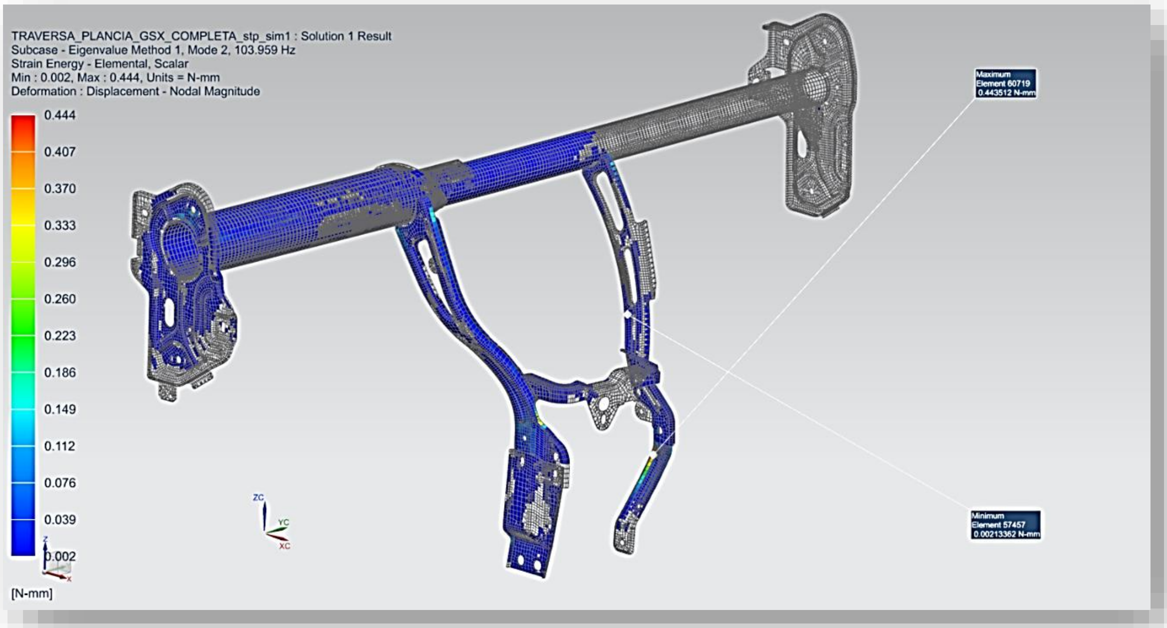

Figure 5.41 Strain energy distribution of mode 2 for the solid CCB model

The third vibration mode occurred at 119.865 Hz and produced the highest strain energy value among the investigated modes. The deformation pattern exhibited more localized structural motion involving both the beam and bracket regions. This behavior suggests that the structure experiences more concentrated dynamic activity at higher frequencies.

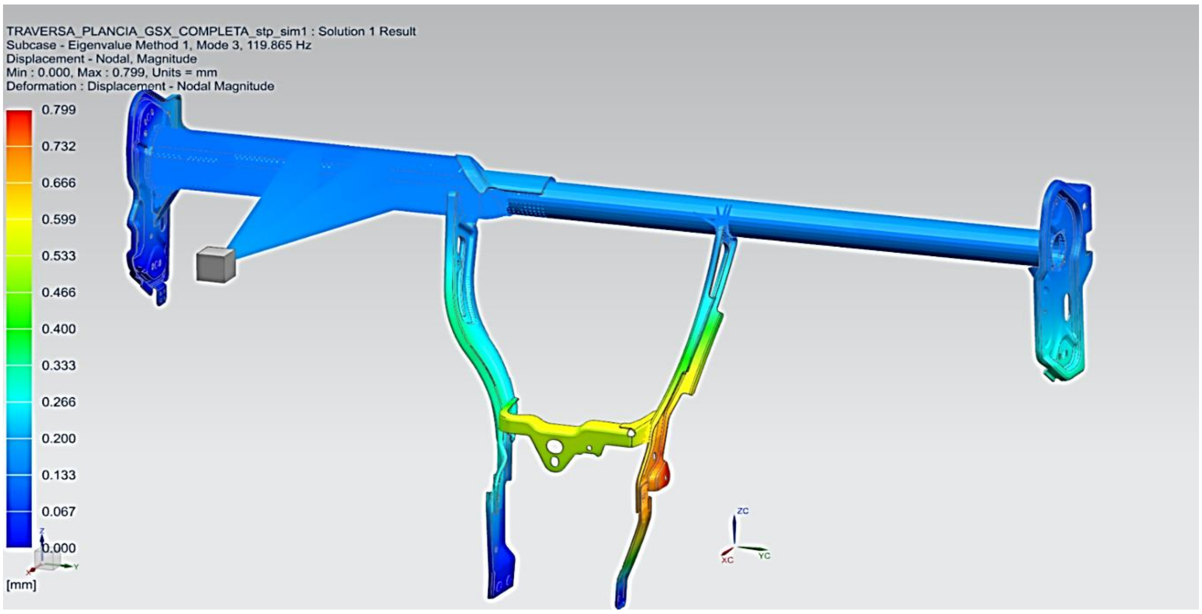

Figure 5.42 Third vibration mode shape of the solid CCB model

The strain energy distribution of the third mode is presented in **Figure 5.43**. A significant increase in energy concentration can be observed around the attachment regions and structural transition zones. The strain energy value of 2.390 N-mm indicates that these locations play a dominant role in the dynamic behavior of the Cross-Car Beam assembly.

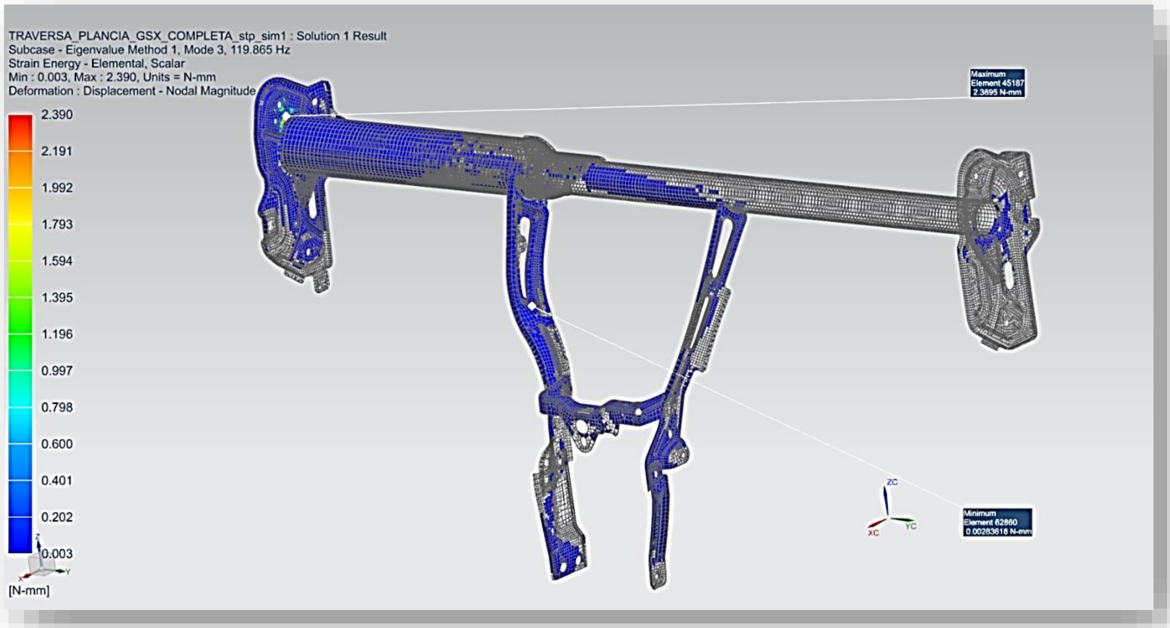

Figure 5.43 Strain energy distribution of mode 3 for the solid CCB model

Overall, the modal analysis results indicate that the attachment interfaces and bracket regions represent the most dynamically sensitive areas of the original Cross-Car Beam configuration. As the vibration mode increases, both the complexity of the deformation pattern and the associated strain energy increase, resulting in greater energy concentration within specific structural regions.

5.2.2 Optimized Model Modal Analysis Results

The modal analysis results obtained for the optimized Cross-Car Beam configuration are presented in this section. Compared with the original solid model, the optimized configuration contains routing openings introduced for internal wiring harness integration. These geometric modifications influence both the stiffness distribution and mass distribution of the structure and therefore affect its dynamic characteristics.

Table 5-18 Natural Frequencies and Strain Energy values of the optimized CCB model

Mode No.	Natural Frequency (Hz)	Max Strain Energy (N-mm)	Improvement / Observation
Mode 1	55.238 Hz	0.177 N-mm	Frequency dropped by ~6 Hz; peak energy is well-managed.
Mode 2	76.546 Hz	0.382 N-mm	Frequency dropped by ~27 Hz; energy is distributed across the brackets.
Mode 3	98.634 Hz	0.662 N-mm	**Critical Success**: Energy dropped from 2.390 to 0.662 N-mm.

As shown in **Table 5-18**, the optimized model exhibited lower natural frequencies than the original solid configuration. This behavior is expected because the routing openings reduce the structural stiffness of the Cross-Car Beam assembly. However, the strain energy distributions indicate that the vibration behavior became more distributed throughout the structure rather than remaining concentrated in specific attachment regions.
The first vibration mode occurred at 55.238 Hz. The corresponding mode shape is presented in **Figure 5.44**. Similar to the solid model, the first mode was characterized primarily by global bending behavior of the beam structure. However, a larger deformation amplitude was observed due to the reduction in stiffness introduced by the routing openings.

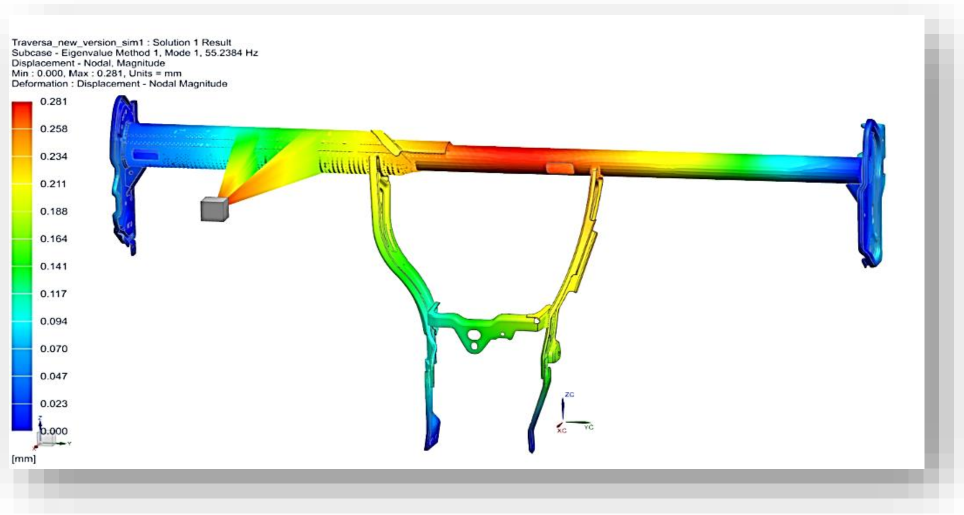

Figure 5.44 First vibration mode shape of the optimized CCB model

The strain energy distribution associated with the first mode is presented in **Figure 5.45**. Compared with the solid configuration, the strain energy became more evenly distributed throughout the beam structure. Instead of being concentrated mainly around the attachment interfaces, a larger portion of the structure participated in the vibration response.

Figure 5.45 Strain energy distribution of mode 1 for the optimized CCB model

The second vibration mode was obtained at 76.546 Hz. The deformation pattern exhibited combined bending and torsional behavior along the beam structure. Compared with the first mode, the vibration response involved a greater portion of the central tube section and surrounding structural components.

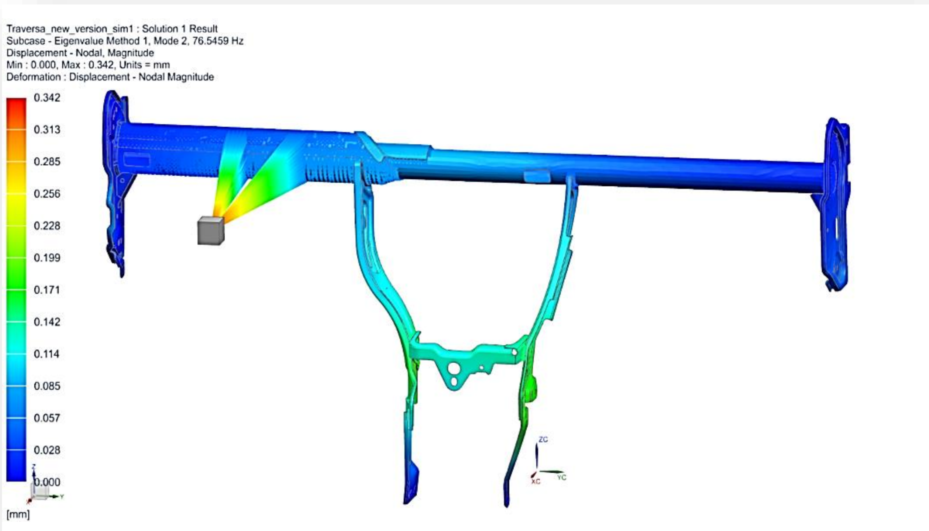

Figure 5.46 Second vibration mode shape of the optimized CCB model

The corresponding strain energy distribution is shown in **Figure 5.47**. The results indicate that the strain energy was distributed over a wider structural area compared with the solid model. This behavior suggests that the routing openings modified the dynamic load transfer path and reduced the severity of localized energy concentrations.

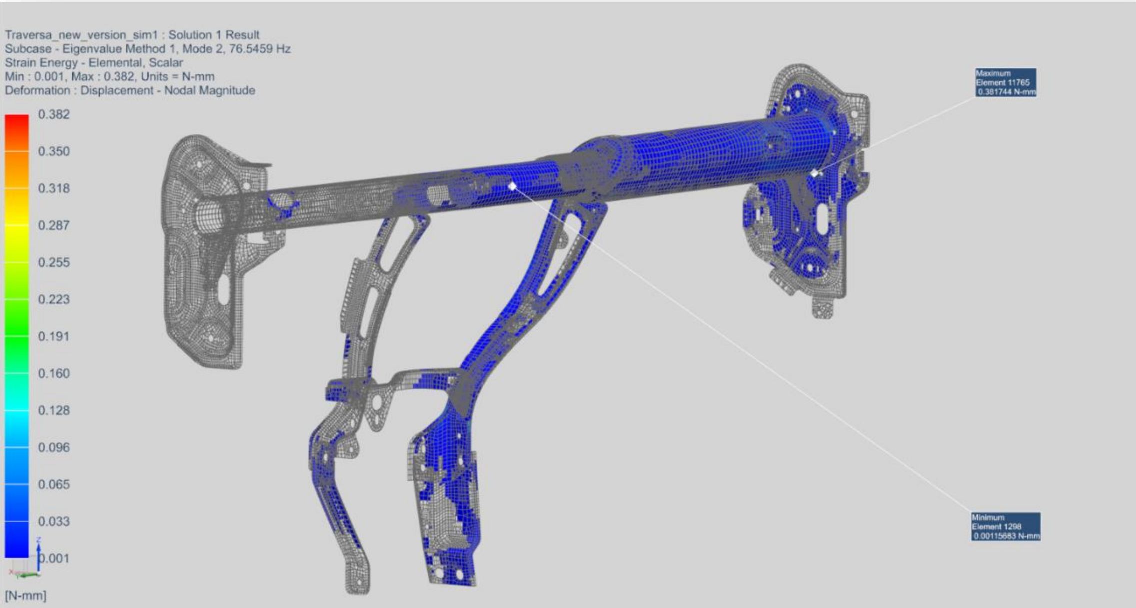

Figure 5.47 Strain energy distribution of mode 2 for the optimized CCB model

The third vibration mode occurred at 98.634 Hz and exhibited a more complex deformation pattern involving local motion of the beam and attachment regions. Compared with the solid configuration, the natural frequency was reduced, indicating the influence of the routing openings on the overall stiffness characteristics of the structure.

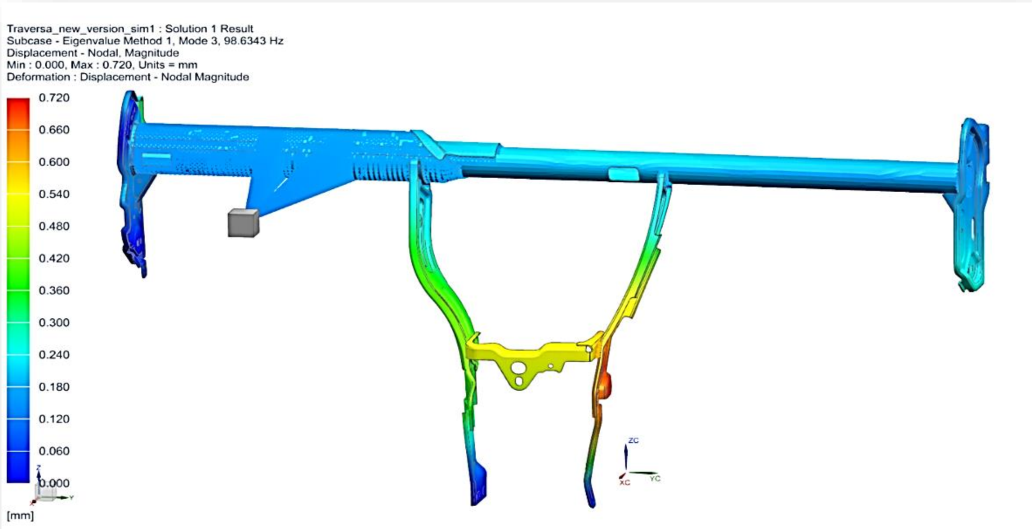

Figure 5.48 Third vibration mode shape of the optimized CCB model

The strain energy distribution associated with the third mode is presented in **Figure 5.49**. Unlike the solid model, where significant energy concentrations were observed around the attachment interfaces, the optimized model exhibited a more uniform strain energy distribution. This indicates that the vibration energy was transferred through a larger portion of the structure rather than accumulating within a limited number of regions.

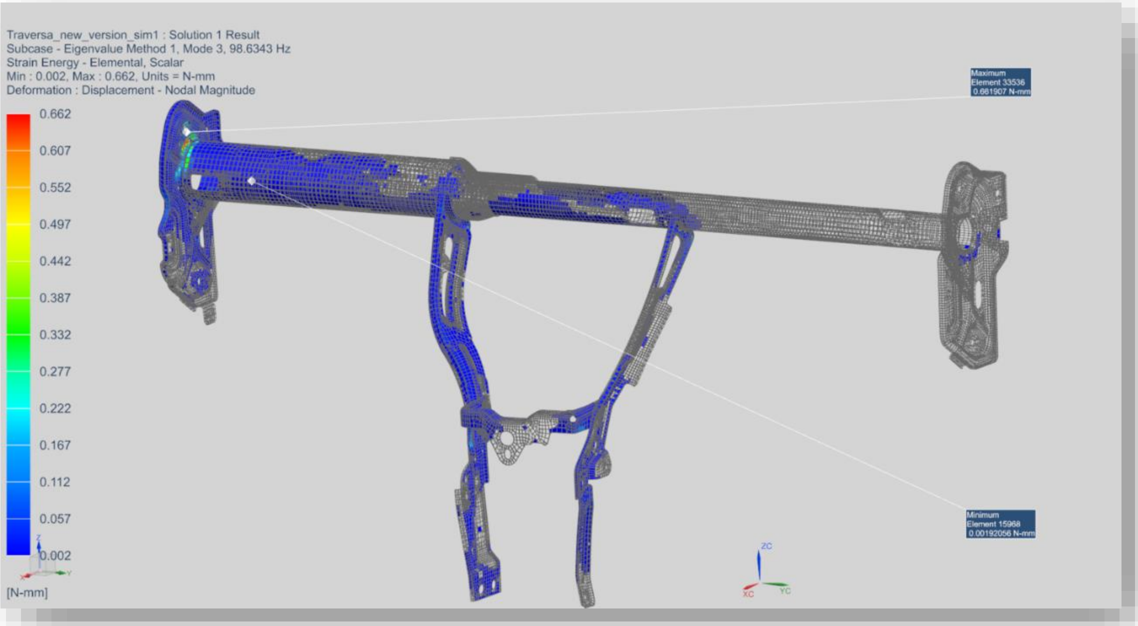

Figure 5.49 Strain energy distribution of mode 3 for the optimized CCB model

Overall, the modal analysis results indicate that the routing openings reduced the natural frequencies of the Cross-Car Beam assembly due to the associated reduction in structural stiffness. However, the strain energy distributions became more balanced and less concentrated within specific structural regions. The optimized configuration therefore exhibited a more distributed dynamic response compared with the original solid model, although at lower natural frequency levels.

5.2.3 Proposed Model Modal Analysis Results

The modal analysis results obtained for the proposed Cross-Car Beam configuration are presented in this section. The proposed model incorporates the routing openings developed for internal wiring harness integration together with FeE420 reinforcement structures designed to improve the stiffness of the modified regions. The objective of this analysis was to evaluate the influence of the proposed design on the dynamic behavior of the Cross-Car Beam assembly and to compare its vibration characteristics with those of the solid and optimized configurations.

Table 5-19 Natural Frequencies and Strain Energy values of the proposed CCB model

Mode No.	Natural Frequency (Hz)	Max Strain Energy (N-mm)	Key Location of Energy
Mode 1	**59.387 Hz**	**0.0908**	Main tube / Central span
Mode 2	**87.286 Hz**	**0.2796**	A-Pillar flange interface
Mode 3	**103.593 Hz**	**0.6925**	A-Pillar mounting holes

As shown in **Table 5-19**, the proposed model exhibited higher natural frequencies than the optimized configuration. This behavior indicates that the additional reinforcement structures increased the stiffness of the modified regions and partially compensated for the stiffness reduction introduced by the routing openings. The strain energy values also indicate a more stable vibration response compared with the optimized model.
The first vibration mode occurred at 59.387 Hz. The corresponding mode shape is presented in **Figure 5.50**. Similar to the previous configurations, the first mode was characterized primarily by global bending deformation of the Cross-Car Beam assembly. However, the deformation amplitude was reduced compared with the optimized model due to the increased stiffness provided by the reinforcement structures.

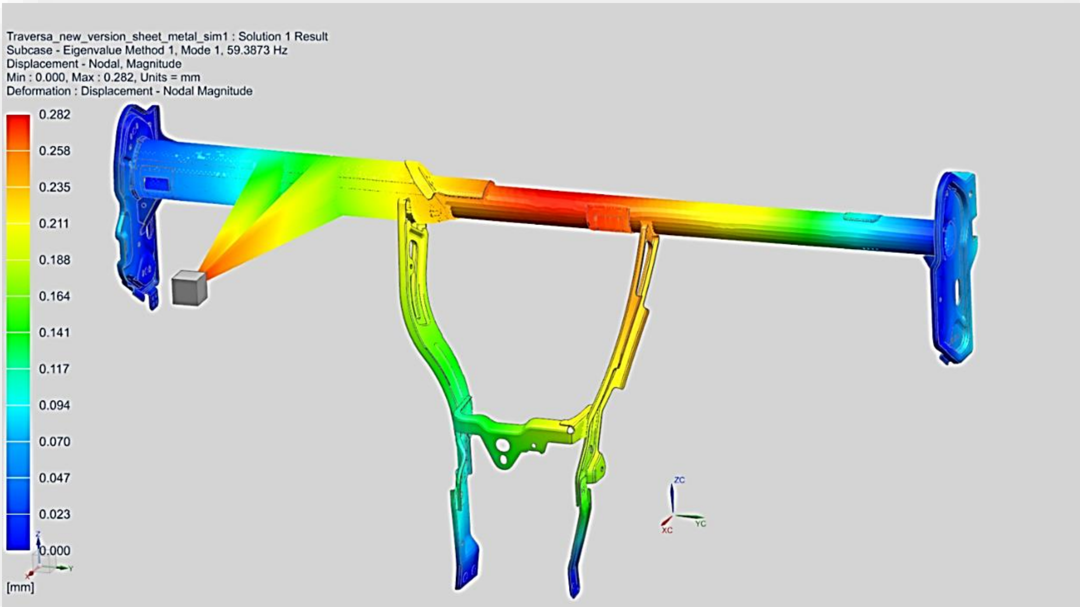

Figure 5.50 First vibration mode shape of the proposed CCB model

The strain energy distribution associated with the first mode is presented in **Figure 5.51**. The results indicate that the proposed design reduced the concentration of vibration energy around the routing opening regions and promoted a more balanced energy distribution throughout the structure.

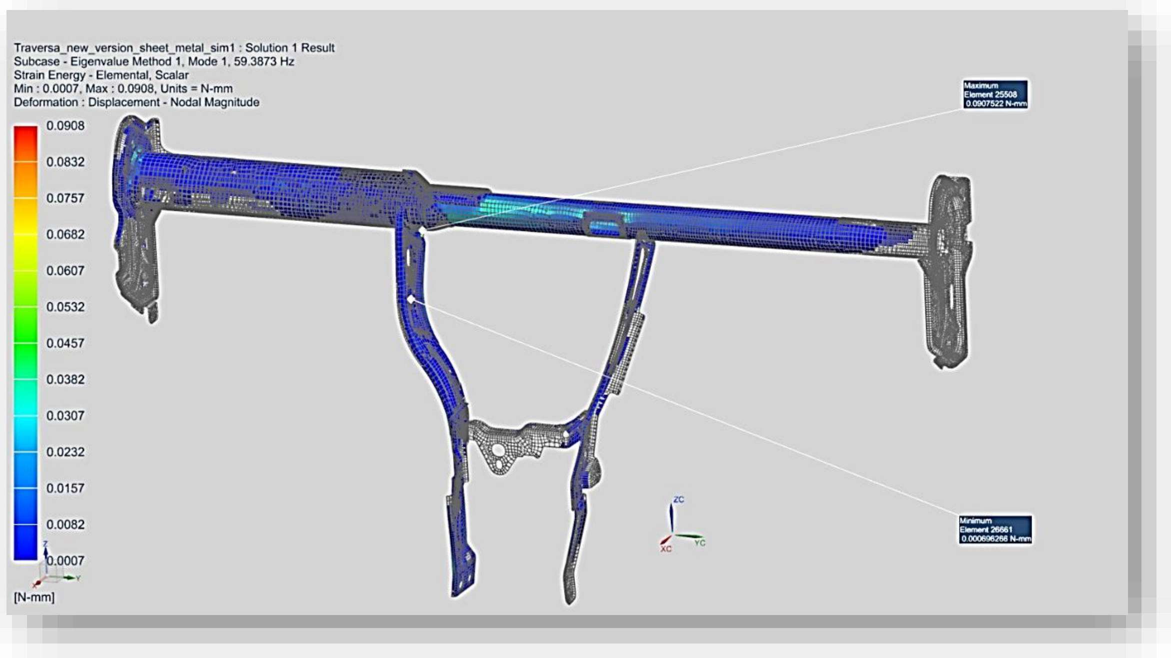

Figure 5.51 Strain energy distribution of mode 1 for the proposed CCB model

The second vibration mode was obtained at 87.286 Hz. The deformation pattern exhibited combined bending and torsional characteristics similar to those observed in the optimized configuration. However, the increased natural frequency demonstrates that the proposed design improved the dynamic stiffness of the assembly.

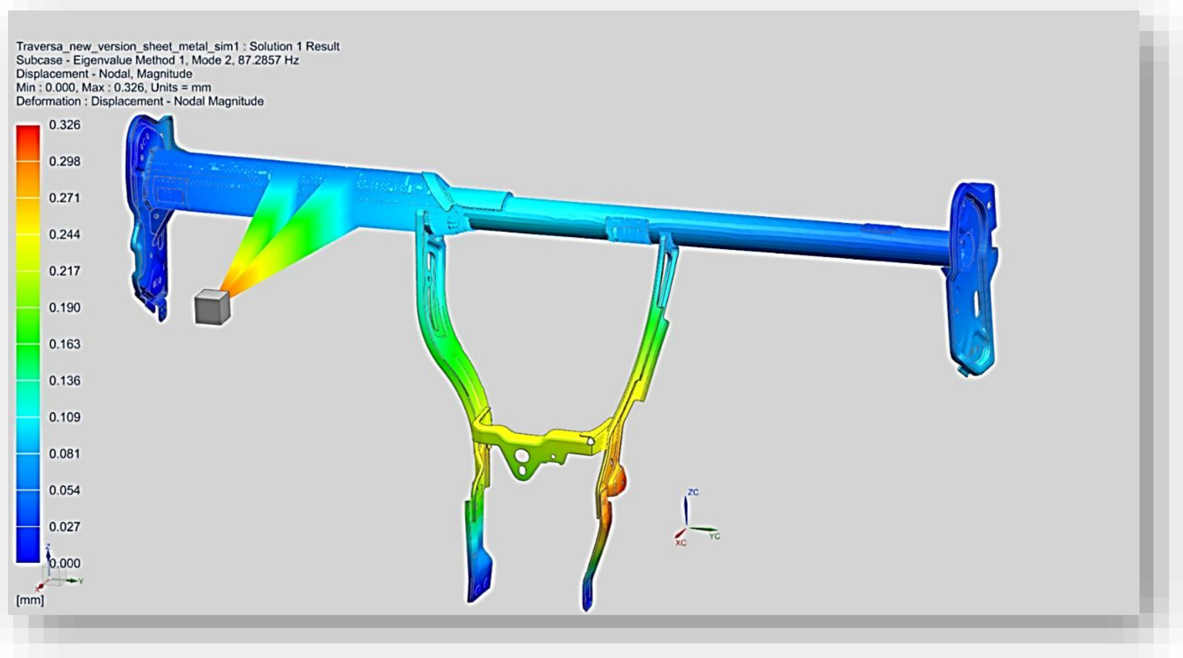

Figure 5.52 Second vibration mode shape of the proposed CCB model

The corresponding strain energy distribution is shown in **Figure 5.53**. Compared with the optimized configuration, a more uniform energy distribution was observed throughout the structure. The reinforcement structures contributed to a reduction in localized strain energy concentrations around the modified regions.

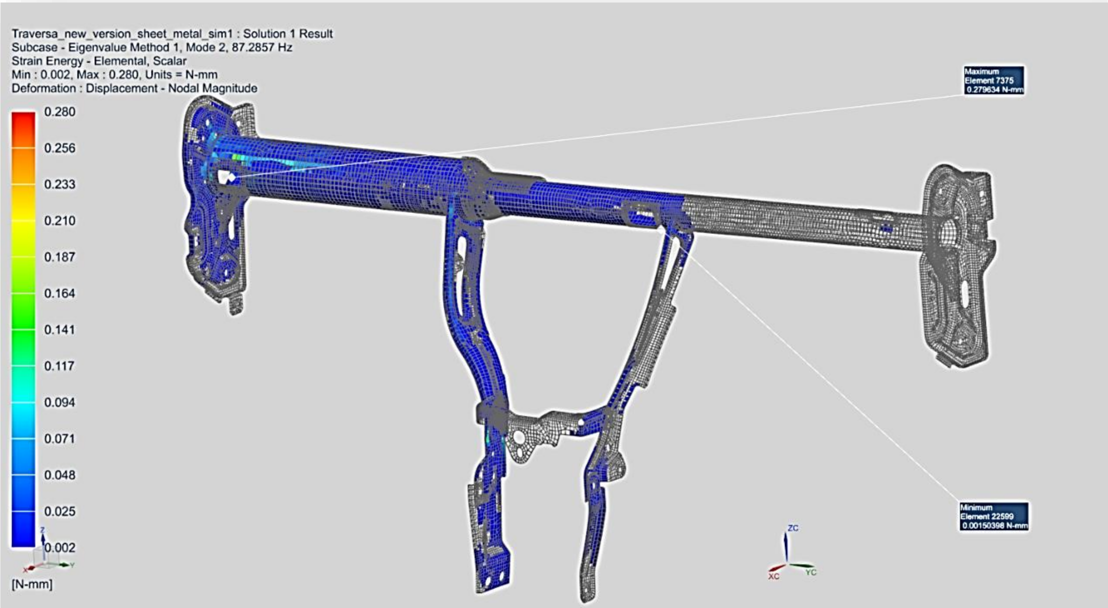

Figure 5.53 Strain energy distribution of mode 2 for the proposed CCB model

The third vibration mode occurred at 103.593 Hz and exhibited a more complex deformation pattern involving both the beam structure and attachment regions. The increase in natural frequency compared with the optimized configuration indicates that the proposed design improved the overall dynamic stiffness of the assembly.

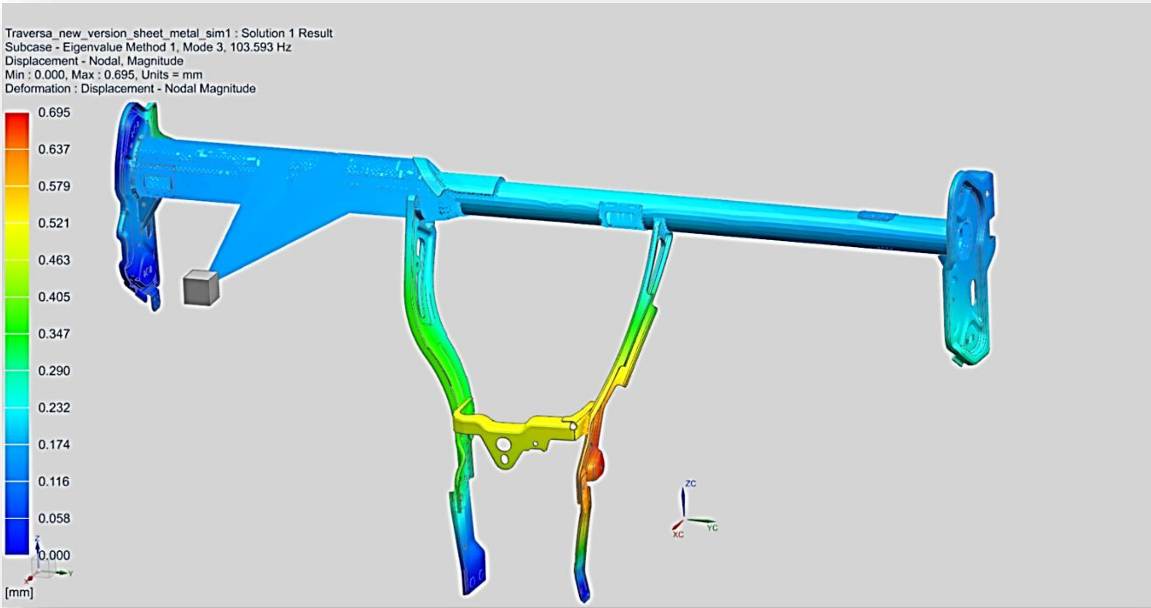

Figure 5.54 Third vibration mode shape of the proposed CCB model

The strain energy distribution associated with the third mode is presented in **Figure 5.55**. The results demonstrate that the proposed design effectively reduced the influence of the routing openings on the vibration response of the structure. The strain energy remained more evenly distributed and no severe concentrations were observed around the opening boundaries.

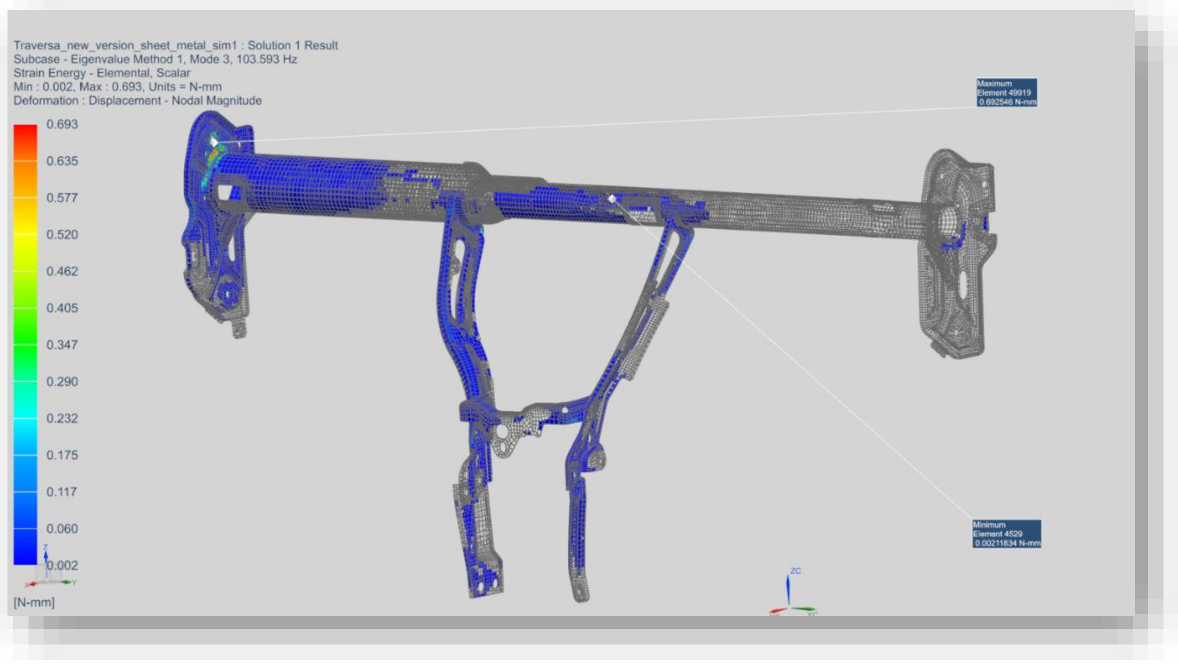

Figure 5.55 Strain energy distribution of mode 3 for the proposed CCB model

Overall, the modal analysis results indicate that the proposed design successfully improved the dynamic characteristics of the optimized Cross-Car Beam configuration. The reinforcement structures increased the natural frequencies and contributed to a more balanced strain energy distribution throughout the structure. As a result, the proposed model exhibited a dynamic response that was closer to the original solid configuration while preserving the packaging advantages introduced by the internal routing concept.

5.2.4 Comparison of Modal Analysis Results

A comparison of the modal analysis results obtained from the solid, optimized, and proposed Cross-Car Beam configurations was performed for evaluating the influence of the routing modifications and reinforcement structures on the dynamic behavior of the assembly. The comparison focused on the first three vibration modes because these modes represent the dominant dynamic characteristics of the structure and are most relevant for automotive vibration performance.

Table 5-20 Natural Frequencies and Strain Energy values of the proposed CCB model

Mode	Solid Model (Hz)	Optimized Model (Hz)	Proposed Model (Hz)
Mode 1	61.439	55.238	59.387
Mode 2	103.959	76.546	87.286
Mode 3	119.865	98.634	103.593

As shown in **Table 5.20**, the introduction of routing openings resulted in a reduction in the natural frequencies of all vibration modes. The optimized model exhibited the lowest frequencies among the three configurations, indicating a reduction in structural stiffness

caused by the material removed from the tube section. This behavior was particularly noticeable in the second vibration mode, where the natural frequency decreased from 103.959 Hz to 76.546 Hz.
The proposed model exhibited higher natural frequencies than the optimized configuration for all investigated modes. The increase in frequency indicates that the reinforcement structures successfully improved the stiffness of the modified regions and partially compensated for the stiffness reduction introduced by the routing openings. Although the frequencies did not fully return to the values observed in the original solid model, a significant recovery in dynamic stiffness was achieved.

Table 5-21 Comparison of Strain Energy Values

Mode	Solid Model (N-mm)	Optimized Model (N-mm)	Proposed Model (N-mm)
Mode 1	0.0786	0.1770	0.0908
Mode 2	0.4440	0.3820	0.2796
Mode 3	2.3900	0.6620	0.6925

The strain energy results indicate significant differences in the dynamic behavior of the three configurations. The solid model exhibited the highest strain energy value in the third vibration mode, where energy was strongly concentrated around the attachment interfaces and structural transition regions. Such localized energy concentrations may contribute to increased dynamic stresses and potential fatigue-related concerns during long-term operation.
After the routing openings were introduced, the strain energy became more evenly distributed throughout the structure. The optimized model exhibited considerably lower strain energy values in the higher vibration modes, indicating that vibration energy was transferred through a larger portion of the assembly rather than accumulating within a limited number of regions. This behavior suggests a more distributed dynamic response.
The proposed model maintained the improved energy distribution characteristics observed in the optimized configuration while simultaneously increasing the natural frequencies of the structure. As a result, the proposed design achieved a more balanced dynamic response by combining improved stiffness with a more uniform vibration energy distribution.
Overall, the modal analysis comparison demonstrates that the routing openings reduced the natural frequencies of the Cross-Car Beam assembly due to the associated reduction in structural stiffness. However, the same modifications also contributed to a more distributed strain energy pattern throughout the structure. The proposed design successfully compensated for a significant portion of the stiffness reduction while preserving the improved strain energy distribution characteristics. Consequently, the proposed configuration provided the most balanced dynamic performance among the evaluated designs and demonstrated the effectiveness of the reinforcement strategy developed in this study.

Chapter 6 - Conclusions

The objective of this study was to develop an optimized Cross-Car Beam (CCB) design capable of supporting internal wiring harness routing while maintaining acceptable structural and dynamic performance. The original Cross-Car Beam configuration relied on externally routed wiring harnesses, which occupied valuable packaging space within the dashboard assembly and increased the complexity of cable management. To address these limitations, a new internal routing concept was developed by introducing routing openings into the beam structure and integrating cable guidance components, WAGO carrier mounting locations, and reinforcement structures.
The packaging analysis demonstrated that the proposed internal routing concept provided a more organized cable management system and improved the utilization of available dashboard space. By routing the wiring harnesses through the Cross-Car Beam structure, the available volume around the dashboard assembly was increased and the cable layout became more compact. The integration of cable guides and WAGO carrier mounting locations further improved the accessibility and organization of the electrical system.
Static structural analyses were performed to evaluate the mechanical performance of the modified design under crash-related loading conditions. The results of the 4000 N A-pillar loading analysis indicated that the routing modifications did not significantly reduce the structural performance of the assembly. The optimized and proposed models exhibited stress and displacement values comparable to those of the original design, demonstrating that the routing openings could be implemented without causing critical structural weaknesses.
A second loading scenario representing the combined effects of the steering wheel, HVAC unit, and passenger airbag system was also investigated. The results showed that the routing openings increased local deformation and generated stress concentrations around the modified regions. However, the proposed design successfully reduced these stress concentrations through the incorporation of FeE420 reinforcement structures. The reinforcement plates improved load distribution around the routing openings and reduced the tube stress levels compared with the optimized configuration.
Modal analyses were conducted to evaluate the vibration characteristics of the three Cross-Car Beam configurations. The introduction of routing openings reduced the natural frequencies of the structure due to the associated reduction in stiffness. Nevertheless, the modal results also indicated a more distributed strain energy pattern throughout the assembly. The proposed model partially recovered the lost stiffness while preserving the improved strain energy distribution characteristics. As a result, the proposed design achieved a balanced dynamic response and maintained acceptable vibration performance.
Overall, the results obtained in this study demonstrate that the proposed Cross-Car Beam design provides a practical solution for integrating internal wiring harness routing without introducing critical structural or dynamic disadvantages. The combination of routing openings, reinforcement structures, cable guidance components, and WAGO carrier integration successfully improved packaging efficiency while maintaining the structural integrity and vibration performance of the assembly. Therefore, the proposed design can be considered a feasible alternative to conventional externally routed Cross-Car Beam configurations for future automotive applications.

6.1 Contributions of the Study

The main contributions of this study can be summarized as follows:

- Development of an internal wiring harness routing concept for the Cross-Car Beam assembly.

- Design and optimization of routing openings for harness integration.
- Development of a reinforcement structure using FeE420 steel to improve local stiffness around modified regions.
- Integration of cable guide and WAGO carrier mounting concepts into the Cross-Car Beam design.
- Evaluation of the structural performance of the proposed design through static finite element analyses.
- Investigation of the dynamic characteristics of the proposed design through modal analysis.
- Comparison of solid, optimized, and proposed Cross-Car Beam configurations to assess the influence of routing modifications on structural and vibration behavior.

6.2 Recommendations for Future Work

Although the proposed design demonstrated satisfactory structural and dynamic performance, several areas remain open for further investigation.

Future studies may focus on experimental validation of the numerical results through physical testing of a prototype Cross-Car Beam assembly. Such testing would provide additional verification of the finite element models and improve confidence in the predicted structural behavior.

Fatigue and durability analyses may also be performed to investigate the long-term effects of vibration loading on the routing openings, reinforcement structures, and cable attachment components. Since automotive structures are exposed to repeated loading throughout their service life, durability assessment would provide valuable information regarding the long-term reliability of the proposed design.

In addition, future work may investigate the vibration behavior of the complete Cross-Car Beam assembly including the actual wiring harnesses, cable guides, and electrical components. Such studies could provide a more comprehensive assessment of Noise, Vibration, and Harshness (NVH) performance and identify potential vibration-related issues associated with internal harness routing.

Further optimization of the reinforcement geometry may also be considered to reduce weight while maintaining structural performance. Advanced optimization techniques and alternative lightweight materials could be investigated to further improve the efficiency of the proposed design.

Finally, the internal routing concept developed in this study may be adapted and evaluated for different vehicle platforms and dashboard architectures in order to assess its applicability to a broader range of automotive applications.

REFERENCES

[1] R. D. Cook, D. S. Malkus, and M. E. Plesha, *Concepts and Applications of Finite Element Analysis*, 4th ed. Wiley, 2002.

[2] D. L. Logan, *A First Course in the Finite Element Method*, 5th ed. Cengage Learning, 2011.

[3] R. Stone and J. K. Ball, *Automotive Engineering Fundamentals*. SAE International, 2004.

[4] S. S. Rao, *Mechanical Vibrations*, 5th ed. Pearson, 2011.

[5] J. A. Wismans, *Crashworthiness of Vehicle Structures*. CRC Press, 1993.

[6] R. Stone and J. K. Ball, *Automotive Engineering Fundamentals*. SAE International, 2004.

[7] R. M. Kowalick, *Vehicle Packaging*. SAE International, 2008.

[8] T. Denton, *Automobile Electrical and Electronic Systems*, 5th ed. Routledge, 2017

[9] G. S. Chen, *Vehicle Noise, Vibration, and Sound Quality*. SAE International, 2012